INVESTIGATING THE ROLE OF GUT MICROBIOME INTERPERSONAL VARIATION AND SHORT-CHAIN FATTY ACIDS IN CARDIOMETABOLIC DISEASE

By

Evan Roy Hutchison

A dissertation submitted in partial fulfillment of

the requirements for the degree of

Doctor of Philosophy

(Microbiology)

at the

UNIVERSITY OF WISCONSIN-MADISON

2023

Date of final oral examination: 12/12/2023

This dissertation is approved by the following members of the Final Oral Committee:

Federico E. Rey, Associate Professor, Bacteriology
Vanessa A. Leone, Assistant Professor, Animal Biologics and Metabolism
Brian W. Parks, Assistant Professor, Nutritional Sciences
Garret Suen, Professor, Bacteriology
Zhengzheng Tang, Associate Professor, Biostatistics and Medical Informatics

ABSTRACT

The gut microbiome is comprised of trillions of microorganisms that collectively contain an estimated 100 times more genes than the human genome. Multiple lines of evidence implicate gut microbes and their metabolites as important modulators of health and disease. Cardiometabolic diseases, an umbrella term referring to disease states such as metabolic syndrome and type-2 diabetes which arise from metabolic dysregulation, have been linked to the gut microbiome because of its ability to influence inflammation, lipid metabolism, and glucose homeostasis. Gut microbes can also modify the effect of diet and pharmaceutical drugs on host physiology, thereby regulating responses to therapeutics. For example, dietary fiber is fermented by gut microbes which produce short-chain fatty acids (SCFAs) as a byproduct. SCFAs, particularly butyrate, have been found to be protective against cardiometabolic disease, but its production in the gut is dependent on the presence of specific bacterial taxa which often vary across individuals. Indeed, the gut microbiome exhibits a large degree of interpersonal variation and can therefore potentially modulate therapeutic effects in an individualized manner.

Several gaps in our understanding of the relationship between the gut microbiome interpersonal variation, SCFAs, and cardiometabolic disease remain and this thesis attempts to fill some of these gaps. In Chapter 2, I examine the role of the gut microbiome in modifying the atheroprotective effect of dietary fiber through microbiome-dependent variations in butyrate production. In Chapter 3 I show that the gut microbiome alters the impact of a next-generation probiotic, *Anaerobutyricum soehngenii,* on glycemic control in gnotobiotic mice harboring distinct human communities and provide evidence that this effect is linked to differential responses to the SCFA propionate. Finally, Chapter 4 investigates the mechanism behind butyrate-induced atheroprotection by examining the roles of butyrate receptors Gpr41, Gpr43, and Gpr109a using

knockout mice models in the context of hypercholesterolemia. Together, these studies demonstrate the ability of the gut-microbiome-SCFA axis to modulate responses to therapeutics and elucidate the effects of SCFA receptors on cardiometabolic disease and cholesterol metabolism.

For Everett

ACKNOWLEDGEMENTS

I have too many people to thank for their support over the last five and half years to fit into just a few paragraphs, so in the spirit of brevity (which is lacking in this thesis), I'd like to offer a few words of gratitude to those who've been especially impactful to me on my journey.

First, to my family, friends, and colleagues – You have all supported me so much and in so many different ways over the years. I am incredibly lucky to have such an amazing network of people in my life whom I know I can always count on. Truly, this would not have been possible without your kind words, laughter, and reassurances.

To my past mentors Joseph Covi, Xandra Smith, Noah Zimmerman, and Tom Rehberger – Thank you for your encouragement and guidance and for showing me that me that I could be a researcher. I wouldn't be here without each of you.

To my committee members Vanessa Leone, Brian Parks, Garret Suen, and Zhengzheng Tang – I am forever grateful for your support and feedback over these past years. You helped shape not only my research but also my understanding of what it means to conduct thorough and careful research.

To my parents, Deb and Jim Hutchison – let's start with the obvious: thanks for making me. I am honestly not sure if there are more loving and supportive on the planet than you two. Even though, despite what you tell your friends, I'm not the Chancellor of Microbiology at UW-Madison, you've always been so proud of me and my biggest fan. I love you both.

To my advisor Federico Rey. You took a chance on me, and you never ceased in your backing and support of my goals. You shared in my low points and celebrated my achievements.

I will take with me the lessons you have taught me on how to be a supportive and encouraging advisor and a careful researcher.

Finally, to Janel. I never would have made it this far without you. You have supported me every step of the way and I cannot express how grateful I am for the sacrifices that you made for me. You are such a kind, talented, and compassionate person and I truly hope that our little Everett will grow up to be just like his mom. I love you billions and billions.

TABLE OF CONTENTS

CHAPTER 1: INTRODUCTION

BACKGROUND

The gut microbiome consists of trillions of microorganisms spanning all domains of life and constitutes one of the most densely populated ecosystems on the planet. This community of microbiota contains a genetic potential that is estimated to be >100 times that of the human genome. In this way, the gut microbiome is often considered an organ of the human body (Baquero & Nombela, 2012) which preforms critical tasks such as aiding in digestion, modulating immune and enteroendocrine function, vitamin synthesis, and exclusion of microbial pathogens (Lynch & Pedersen, 2016; Neuman et al., 2015; Yatsunenko et al., 2012). An individual's gut microbiome is remarkably unique and is shaped by multiple factors including genetics, and environmental factors such as diet, lifestyle, and maternal transmission (Ferretti et al., 2018; Yatsunenko et al., 2012).

Given the intimate link between the gut microbiome and host physiology, it is not surprising that dysfunction of the gut microbiome is associated with many metabolic disease states, including cardiometabolic diseases (Chakaroun et al., 2023). Early studies investigating the link between the gut microbiome and diseases were limited to associations. But recent advances in the speed and reduced cost of DNA sequencing, along with broader use of gnotobiotic animal models (i.e., colonizing germ-free animals with a known microbiome in a controlled setting), have allowed researchers to begin to examine causation in these relationships (Faith et al., 2014; Turnbaugh, Ridaura, et al., 2009). In particular, many recent studies have revealed microbial metabolites, such as short-chain fatty acids (SCFAs), to be mediators between gut microbes and host health (Campos-Perez & Martinez-Lopez, 2021; Koh et al., 2016).

This chapter summarizes the current evidence that microbially derived SCFAs are key mediators of cardiometabolic disease and describes what is known and unknown about the

mechanisms underpinning their effects. I will start by defining cardiometabolic disease and reviewing its core features which include insulin resistance and inflammation. Next, the evidence linking the gut microbiota and cardiometabolic disease will be covered in greater detail, with a particular focus on SCFAs. The metabolic pathways of SCFA production and SCFA-producing bacteria will be discussed as well as the mammalian receptors that sense SCFAs. I will provide evidence that the gut microbiome is an important modifier of diet and therapeutics which has implications for precision medicine. Finally, I will describe how the research presented in this thesis attempts to address the gaps in knowledge on this topic.

1.1 Cardiometabolic disease

The term "cardiometabolic disease" gained popularity in recent decades as a concept that links the underlying mechanisms between metabolic syndrome (MetS) and cardiovascular disease (CVD) (Pescatello, 1999). MetS itself is not a disease *per se*, but rather a collection of metabolic markers (hyperglycemia, hyperlipidemia, reduced HDL-cholesterol, hypertension, and abdominal obesity) that indicate a dysregulated metabolic state (Eckel et al., 2005). MetS results from the dysfunction of metabolic processes such as lipid and glucose regulation and is clinically defined as having at least three of the following comorbidities: hypertension, hyperglycemia, reduced HDL-cholesterol, elevated triglycerides, or abdominal obesity (Eckel et al., 2005). MetS prevalence is growing at a concerning rate especially in countries that are undergoing a reduction in physical activity and an increase in caloric intake. MetS sits within the cardiometabolic disease umbrella and individuals with MetS are at a higher risk for developing T2D and CVD (Aggoun, 2007).

Consequently, cardiometabolic diseases are cardiovascular diseases that are driven by metabolic dysregulation and are inherently associated with type 2 diabetes mellitus (T2D) and metabolic dysfunction associated steatotic liver disease (formerly known as non-alcoholic fatty liver disease) (Targher & Byrne, 2013). The drivers of cardiometabolic disease can be held somewhat in contrast to the clinical risk factors of CVD that predominated in the twentieth century, namely elevated plasma LDL-cholesterol and smoking. Both risk factors have been significantly reduced in recent decades through the widespread use of statins, which lower LDL-cholesterol and changing behaviors around smoking (Sun & Du, 2017). Today, the growing prevalence of obesity and T2D are emerging as primary risk factors for CVD, therefore the concept of cardiometabolic health and its underling drivers (i.e., MetS, insulin resistance, and inflammation) are useful in developing better therapeutic and public policy strategies (Sattar et al., 2020).

Insulin induces a coordinated signaling cascade in multiple tissues, including muscle, liver, and adipose tissue, which ultimately results in the inhibition of lipolysis, gluconeogenesis, and glycogenolysis while promoting glucose uptake, resulting in a lowering of plasma glucose levels (Cheatham & Kahn, 1995). Insulin resistance (IR) is defined as the inability of insulin to effectively reduce blood glucose levels due to a disruption in the transmission of insulin signaling. IR is thought to be a central driver connecting the various pathologies observed in MetS and cardiometabolic disease (Aggoun, 2007; Bornfeldt & Tabas, 2011). Indeed, IR has been linked to each of the criterions involved in MetS: IR results in impaired lipid metabolism and accumulation of free fatty acids and triglycerides in the plasma (Ormazabal et al., 2018). An excess of fatty acids in circulation is associated with hyperglycemia by inhibiting translocation of GLUT4— the major insulin-responsive glucose transporter, to the cell membranes of skeletal muscle and adipocytes, as well as hypertension since free fatty acids induce vasoconstriction (Petersen & Shulman, 2018).

IR-induced hyperlipidemia promotes triglyceride-scavenging by HDL particles and their subsequent disposal resulting in reduced HDL-cholesterol levels in the blood (Rashid et al., 2003). Finally, IR is associated with increased abdominal adiposity by inducing expansion of visceral fat tissue (Carey et al., 1996).

One of the largest shifts in the understanding of cardiometabolic disease pathology in the last half century is the recognition of CVDs such as atherosclerosis as inflammatory diseases. The connection between inflammation and atherosclerosis was first postulated by Rudolf Virchow in the mid-19th century after observing proliferation of "arterial cells" followed by their death (Virchow, 1860). After the discovery of cholesterol in atherosclerotic plaques, a model of disrupted lipid storage became the primary framework for understanding disease progression. Indeed, markers of inflammation have also gained relevance in recent years as predictors of major adverse cardiovascular events (MACE). For example, plasma C-reactive protein, a blood marker of inflammation, was recently found to be a better clinical predictor of MACE than plasma LDL-cholesterol among patients treated with statins (Ridker et al., 2023).

Inflammation is central to the pathology of atherosclerosis throughout the course of disease progression. First, proinflammatory lipoprotein particles such as oxidized LDL (ox-LDL) can activate endothelial cells causing barrier dysfunction (Björkegren & Lusis, 2022). This allows for translocation of LDL particles into the intima layer resulting in expression of monocyte recruitment factors such as VCAM and ICAM on endothelial cells (Björkegren & Lusis, 2022). Monocytes differentiate into macrophages via activation by macrophage colony stimulation factor (M-CSF), which then engulf and attempt to remove cholesterol-rich deposits (Björkegren & Lusis, 2022). If the debris is being deposited faster than it can be removed, then these macrophages become engorged and form "foam-cells" which themselves become apoptotic and

proinflammatory (Björkegren & Lusis, 2022). This causes a vicious cycle of monocyte recruitment, foam cell formation, and release of proinflammatory cytokines which leads to runaway inflammation progression of advanced fatty plaques (Bobryshev et al., 2016). Additionally, inflammation leads to increased risk of thrombosis through destabilization of the atherosclerotic plaques by immune cells (Bot et al., 2007; Shah, 2009; Shah et al., 1995).

1.2 Cardiometabolic disease and the gut microbiome

There is increasing evidence that the gut microbiome plays an important role in cardiometabolic health. Epidemiological studies have identified differences in the microbiomes of healthy individuals compared to individuals with coronary artery disease (Jie et al., 2017; Kelly et al., 2016; Tang & Hazen, 2017), T2D (Larsen et al., 2010; Qin et al., 2012), and obesity (Ley et al., 2006; Turnbaugh, Hamady, et al., 2009). Importantly, associations do not prove causation, so studies that focus on causal mechanisms are invaluable to our understanding of the relationship between gut microbes and disease.

Early reports showed that gut microbes can modulate host metabolism through its ability to metabolize calorically inert components of our diet (i.e. dietary fiber) and thereby modify caloric availability and energy harvest (Turnbaugh et al., 2006; H. Zhang et al., 2009). Additionally, transplantation of gut microbiota from diseased individuals can transfer disease phenotypes such as obesity and atherosclerosis (Gregory et al., 2015; Kasahara et al., 2023; Turnbaugh et al., 2006). Several microbial metabolites have been found to modulate cardiometabolic health in humans and animal models. Several examples from a rapidly-expanding list include: trimethylamine *N*-oxide, which is derived from bacterial metabolism of choline, carnitine and betaine, is linked to an elevated risk of CVD in humans through promoting expression of CD36 and proinflammatory

cytokines via the MAPK/JNK pathway (Z. Wang et al., 2011; Yu et al., 2020); imidazole propionate, which is derived from fermentation of histidine, causes insulin resistance by disrupting insulin signaling through activation of mTORC1 (Koh et al., 2018; Molinaro et al., 2020); bile acids, which are amphipathic molecules that aide in the absorption of dietary fats and also act as signaling molecules through Farnesoid X Receptor (FXR), can be chemically altered by gut microbiota to form deconjugated and secondary bile acids which can themselves affect host physiology and metabolism (Guzior & Quinn, 2021); and finally, SCFAs, produced via microbial fermentation of dietary fiber and some amino acids, have been shown to protect against atherosclerosis by reducing inflammation and gut permeability (butyrate) and reducing absorption of dietary cholesterol (propionate) (Aguilar et al., 2014; Haghikia et al., 2021; Kasahara et al., 2018).

It has long been established that diet has a major effect on both the exacerbation and protection from atherosclerosis (Kritchevsky, 1978; Torres et al., 2015). For example, foods such as whole-grain cereals and legumes which are rich in dietary fiber, are known to be protective against cardiometabolic disease (Higginson & Pepler, 1954; Threapleton et al., 2013). Despite this, individual responses to various dietary and pharmacological treatments for CVD have shown notable interpersonal variation (Healey et al., 2017; Weeke & Roden, 2013). Most studies connecting dietary fiber to improved cardiovascular health rely on population-level analysis (D. Kirk et al., 2021) and do not consider individual responses. As a result, the reasons for disparate individual responses to these interventions remain underexplored.

1.3 SCFAs and SCFA-producing bacteria.

SCFAs, defined as any saturated fatty acid with five carbons or less, are the primary end-product of dietary fiber fermentation in the gut, the most abundant of which are acetate (C2), propionate (C3), and butyrate (C4). The concentrations of SCFAs vary along the gastrointestinal tract with levels in the cecum and colon being ~10 x higher than the ileum (Cummings et al., 1987). The ratio of acetate to propionate to butyrate in the human colon is roughly 60:20:20, but this can range depending on diet (Dürholz et al., 2020; McOrist et al., 2011). SCFAs are produced by gut bacteria that encounter dietary carbohydrates (and amino acids to a lesser extent) which survive host digestion (Smith & Macfarlane, 1997). The concentrations of SCFAs are highest in the colon and diminish as they are transported through colonocytes to portal blood and then into circulation. This is especially true for butyrate—much of which is oxidized for energy by colonocytes—and for propionate which can be used for gluconeogenesis in the liver (den Besten et al., 2013; Roediger, 1982). Once absorbed, bacterially-produced acetate merges with the host-derived acetate pool resulting in higher levels in circulation (Cummings et al., 1987). The bacteria that produce acetate and propionate span multiple phyla including Bacillota, Bacteriodota, and Pseudamonaota, whereas butyrate producers are primarily confined to Bacillota (Koh et al., 2016). Various metabolic pathways for SCFA production have been described in gut bacteria including pyruvate to acetyl-CoA and the Wood-Ljungdahl pathway (acetate), the acrylate, succinate, and propanediol pathways (propionate), and the butyrate kinase and butyryl-CoA:acetate CoA-transferase routes (butyrate) (Duncan et al., 2002; Koh et al., 2016; Louis et al., 2014; Rey et al., 2010; Scott et al., 2006). Consumption of dietary fibers and resistant starches can modify SCFA levels in the gut as well as the abundances of SCFA-producing bacteria, but the magnitude and

nature of these changes are dependent on the specific structure of the substrate and the metabolic capabilities of the resident microbial communities (Murga-Garrido et al., 2021).

1.4 SCFA receptors

Eukaryotes associated with microbes have evolved means to sense and respond to metabolites produced by their counterparts. SCFA are sensed by four G protein-coupled receptors (i.e., Gpr), Gpr41, Gpr43, Gpr109a, and Olfr78 (Kimura et al., 2011). All these receptors have distinct affinities for each SCFA: Gpr41 (propionate > butyrate >> acetate), Gpr43 (acetate ≈ propionate ≈ butyrate), Gpr109a (butyrate as well as non-SCFA ligands niacin and β-hydroxybutyrate) and Olfr78 (acetate ≈ propionate) (Kimura et al., 2011; Koh et al., 2016; Pluznick et al., 2013). These receptors are expressed in various tissues throughout the mammalian body in distributions that are unique to each receptor. Gpr41 is expressed in enteroendocrine cells, bone marrow, spleen, pancreas, adipose tissues, and various immune cells, while Grpr43 is expressed in small intestine epithelium, spleen, muscle cells and T-cells, and Gpr109a is expressed in small and large intestinal epithelium, macrophages and monocytes, adipocytes, and epididymis cells (Kimura et al., 2020; Koh et al., 2016; Samuel et al., 2008). Olfr87 is expressed in the heart, subcutaneous adipose, kidney, and the colon (Yue et al., 2014).

Previous studies demonstrated that butyrate-sensing Gprs (Gpr41, Gpr43, and Gpr109a) have roles in glucose homeostasis, obesity, and blood pressure, all of which impact atherosclerosis and MetS (Bjursell et al., 2010; Kaye David M. et al., 2020; Samuel et al., 2008; Veprik et al., 2016). Samuel et al. showed that Gpr41 modulates adiposity by regulating secretion of appetite-suppressing leptin and the gut motility hormone PYY in a microbiota-dependent manner (Samuel et al., 2008). Kaye et al. found that both Gpr43 and Gpr109a are linked to blood pressure

homeostasis in mice, highlighting potentially overlapping and complementary effects of butyrate receptors (Kaye David M. et al., 2020). Previous studies have examined the roles of Gpr109a in atherosclerosis, but these studies assessed the effects of non-SCFA agonists of Gpr109a: 3-hydroxybutyrate and niacin (Lukasova et al., 2011; S. Zhang et al., 2021). Gpr109a induces distinct β-arrestin- and G-protein-mediated signaling cascades which are preferentially induced by different agonists. This allows for the possibility that Gpr109a activation by different ligands might have different effects in cardiometabolic disease. Gpr41, Gpr43, and Gpr109a all couple with inhibitory G protein (G_i) which inhibits adenylate cyclase and AMP production (Cresci et al., 2010; Kimura et al., 2020). Gpr43 also couples with G_q which increases cytosolic Ca^{+2} concentrations when activated (Tolhurst et al., 2012). Given the diversity of SCFA receptors, their different affinities to each SCFA, and their distinct tissue localizations, much remains to be elucidated about their roles in cardiometabolic disease.

1.5 Microbiome as a modifier of therapeutic exposures

The gut microbiome is highly individualized and varies widely between individuals and changes as a function of age, genetics, diet, and lifestyle (Goodrich et al., 2014; Yatsunenko et al., 2012). Early functional characterization studies reported that while the gut microbiota taxonomic composition between adults is highly variable, the microbiota functional potential (i.e., the metagenomic functional composition) at a broad level was quite similar (Turnbaugh, Hamady, et al., 2009). However, improvements in the resolution of metagenomics and metatranscriptomics have revealed that the microbiome functional programming is indeed highly interpersonally variable (Abu-Ali et al., 2018; Franzosa et al., 2014). The gut microbiota interacts with components of the host diet and ingested pharmaceutical drugs and there is increasing evidence

that the gut microbiome modulates their effects on host biology. For example, microbial enzymatic modifications of anti-cancer drugs can lead to decreased tolerance or efficacy (Chrysostomou et al., 2023; Spanogiannopoulos et al., 2022). Irinotecan, a drug for colon cancer treatment, can be converted to a toxic form by bacterial β-glucuronidases which causes diarrhea (Chrysostomou et al., 2023). Another study found that SCFA-producing bacteria *Faecalibacterium* are associated with enhanced effectiveness of anti-PD1 checkpoint inhibitors in melanoma patients (Gopalakrishnan et al., 2018). Similarly, gut microbes can inactivate drugs used as interventions for diabetes and CVD (Balaich et al., 2021; Hughes et al., 2019). For example, bacterial kinases can inactivate acarbose, an anti-diabetic drug that blocks the breakdown of dietary starch (Balaich et al., 2021). Digoxin, a plant toxin that is used as a drug to treat heart conditions such as arrhythmia, can be inactivated by the gut bacteria *Eggerthella lenta* (Dobkin et al., 1983). Interestingly the ability of *E. lenta* to metabolize digoxin does not confer a fitness advantage and is hypothesized to perform a protective role to the host by detoxifying phytochemicals (Koppel et al., 2018). There is also evidence that the gut microbiome composition can impact responses to dietary interventions. In another example, a study investigating the interaction between the gut microbiome and the Mediterranean-style diet and its consequences on cardiometabolic health found that non-carriers of *Prevotella copri* receive a greater benefit from dietary intervention that carriers of *P. copri* (D. D. Wang et al., 2021). Additionally, a recent study from our lab showed that mice transplanted with fecal microbiota from different human subjects exhibited disparate SCFA profiles and metabolic responses to various dietary fibers (Murga-Garrido et al., 2021). Finally, a study in humans treated with resistant starch resulted in a wide range of fecal SCFA production which were associated with BMI (McOrist et al., 2011). These studies demonstrate the

capacity of the gut microbiome to modify the efficacy of certain therapeutics while also emphasizing the individualized aspect of these interactions.

1.6 The gut microbiome and precision medicine

The personalized nature of the gut microbiome and its modulatory effects on dietary and therapeutic responses have underscored gut microbiota as an important factor in precision medicine and precision nutrition. Precision medicine is a medical model that stratifies patients by their personal attributes (genetics, immune status, metabolic phenotypes, etc.) and tailors intervention strategies at the level of the individual. Similarly, precision nutrition uses personal attributes to shape nutritional treatment with the aim of treating and preventing disease (Kirk et al., 2021). Central to these approaches is the notion that individuals respond differently to the same therapeutic as a function of one or many of these attributes (Ashley, 2016). The microbiome is emerging as a key component to developing precision strategies (Kolodziejczyk et al., 2019). Studies assessing the role of the gut microbiome and anti-PD1 checkpoint inhibitors found that responders to the drug were colonized with higher abundances of *Akkermanisa muciniphila* relative to non-responders (Cani et al., 2022). A seminal study in this field incorporated microbiome characterization information into a precision medicine platform to successfully predict optimal post-prandial glycemic responses to various diets in patients with T2D (Zeevi et al., 2015). The authors found that the microbiome helps explain the variability observed in the interpersonal glycemic responses to the same foods so they used microbiome data along with questionnaires and clinical data to develop a predictive algorithm that generated dietary recommendations. In a validation cohort, the predicted dietary recommendations were more effective at reducing postprandial glycemic responses than expert recommendations from a clinical

dietitian demonstrating the utility and promise of precision medicine approaches (Zeevi et al., 2015). However, precision medicine studies are costly and logistically complex, therefore the development of accurate, low-cost tools to assess the personalized functional capacities and modulatory effect of the gut microbiome are warranted. Together, these studies demonstrate that the microbiome is an important modulator of dietary and pharmacological therapeutics, but more research is needed to better understand the underlying dynamics to optimize precision medicine and nutrition strategies.

CONCLUSION

In summary, this introductory chapter has provided evidence that cardiometabolic diseases are modified by the gut microbiome and that SCFAs, particularly butyrate and propionate, are potential mediators of disease prevention, but the roles of SCFA receptors in this effect remain understudied. I also discussed the gut microbiome as a key modulator of therapeutics exposures but highlighted the need to further characterize microbiota-by-therapeutic interactions. The chapters below will attempt address some of these gaps in knowledge: Chapter 2 focuses on the modulatory effect of the gut microbiome the the atheroprotection of dietary fiber by utilizing humanized gnotobiotic mouse model. I describe how fermentable fiber diet impacts SCFA production and atherosclerosis in a microbiome-dependent manner. Next, in Chapter 3 I address the question of whether the gut microbiome dictates the glycemic control response patterns of MetS patients to a probiotic *Anaerobutyricum soehngenii* by using gnotobiotic mice colonized with fecal microbiota from responders and non-responders. I found that the microbiome differentially influences the efficacy of *A. soehngenii* describe how improved glycemic control is linked to the host response to propionate. Finally, Chapter 4 investigates the roles of SCFA

receptors Gpr41, Gpr43, and Gpr109a in atherosclerosis and hypercholesterolemia using genetic knockout mouse models. I found that Gpr41 is plays a significant role in regulating cholesterol absorption and composition of the gut microbiome. The body of work presented below provides new insights into the relationship between gut microbiome interpersonal variation and SCFAs and its effect on cardiometabolic disease.

REFERENCES

Abbott, B. (2022). Unhelpful microbes inactivate diabetes drug. Communications Medicine, 2(1), Article 1. https://doi.org/10.1038/s43856-021-00068-2

Abu-Ali, G. S., Mehta, R. S., Lloyd-Price, J., Mallick, H., Branck, T., Ivey, K. L., Drew, D. A., DuLong, C., Rimm, E., Izard, J., Chan, A. T., & Huttenhower, C. (2018). Metatranscriptome of human faecal microbial communities in a cohort of adult men. Nature Microbiology, 3(3), Article 3. https://doi.org/10.1038/s41564-017-0084-4

Aggoun, Y. (2007). Obesity, Metabolic Syndrome, and Cardiovascular Disease. Pediatric Research, 61(6), Article 6. https://doi.org/10.1203/pdr.0b013e31805d8a8c

Aguilar, E. C., Leonel, A. J., Teixeira, L. G., Silva, A. R., Silva, J. F., Pelaez, J. M. N., Capettini, L. S. A., Lemos, V. S., Santos, R. A. S., & Alvarez-Leite, J. I. (2014). Butyrate impairs atherogenesis by reducing plaque inflammation and vulnerability and decreasing NFκB activation. Nutrition, Metabolism and Cardiovascular Diseases, 24(6), 606–613. https://doi.org/10.1016/j.numecd.2014.01.002

Ashley, E. A. (2016). Towards precision medicine. Nature Reviews Genetics, 17(9), Article 9. https://doi.org/10.1038/nrg.2016.86

Balaich, J., Estrella, M., Wu, G., Jeffrey, P. D., Biswas, A., Zhao, L., Korennykh, A., & Donia, M. S. (2021). The human microbiome encodes resistance to the antidiabetic drug acarbose. Nature, 600(7887), 110–115. https://doi.org/10.1038/s41586-021-04091-0

Baquero, F., & Nombela, C. (2012). The microbiome as a human organ. Clinical Microbiology and Infection, 18(s4), 2–4. https://doi.org/10.1111/j.1469-0691.2012.03916.x

Björkegren, J. L. M., & Lusis, A. J. (2022). Atherosclerosis: Recent developments. Cell, 185(10), 1630–1645. https://doi.org/10.1016/j.cell.2022.04.004

Bjursell, M., Admyre, T., Göransson, M., Marley, A. E., Smith, D. M., Oscarsson, J., & Bohlooly-Y, M. (2010). Improved glucose control and reduced body fat mass in free fatty acid receptor 2-deficient mice fed a high-fat diet. American Journal of Physiology-Endocrinology and Metabolism, 300(1), E211–E220. https://doi.org/10.1152/ajpendo.00229.2010

Bobryshev, Y. V., Ivanova, E. A., Chistiakov, D. A., Nikiforov, N. G., & Orekhov, A. N. (2016). Macrophages and Their Role in Atherosclerosis: Pathophysiology and Transcriptome Analysis. BioMed Research International, 2016, e9582430. https://doi.org/10.1155/2016/9582430

Bornfeldt, K. E., & Tabas, I. (2011). Insulin Resistance, Hyperglycemia, and Atherosclerosis. Cell Metabolism, 14(5), 575–585. https://doi.org/10.1016/j.cmet.2011.07.015

Bot, I., de Jager, S. C. A., Zernecke, A., Lindstedt, K. A., van Berkel, T. J. C., Weber, C., & Biessen, E. A. L. (2007). Perivascular Mast Cells Promote Atherogenesis and Induce Plaque Destabilization in Apolipoprotein E–Deficient Mice. Circulation, 115(19), 2516–2525. https://doi.org/10.1161/CIRCULATIONAHA.106.660472

Campos-Perez, W., & Martinez-Lopez, E. (2021). Effects of short chain fatty acids on metabolic and inflammatory processes in human health. Biochimica et Biophysica Acta (BBA) - Molecular and Cell Biology of Lipids, 1866(5), 158900. https://doi.org/10.1016/j.bbalip.2021.158900

Cani, P. D., Depommier, C., Derrien, M., Everard, A., & de Vos, W. M. (2022). Akkermansia muciniphila: Paradigm for next-generation beneficial microorganisms. Nature Reviews Gastroenterology & Hepatology. https://doi.org/10.1038/s41575-022-00631-9

Carey, D. G., Jenkins, A. B., Campbell, L. V., Freund, J., & Chisholm, D. J. (1996). Abdominal Fat and Insulin Resistance in Normal and Overweight Women: Direct Measurements Reveal a Strong Relationship in Subjects at Both Low and High Risk of NIDDM. Diabetes, 45(5), 633–638. https://doi.org/10.2337/diab.45.5.633

Chakaroun, R. M., Olsson, L. M., & Bäckhed, F. (2023). The potential of tailoring the gut microbiome to prevent and treat cardiometabolic disease. Nature Reviews Cardiology, 20(4), Article 4. https://doi.org/10.1038/s41569-022-00771-0

Cheatham, B., & Kahn, C. R. (1995). Insulin Action and the Insulin Signaling Network*. Endocrine Reviews, 16(2), 117–142. https://doi.org/10.1210/edrv-16-2-117

Chrysostomou, D., Roberts, L. A., Marchesi, J. R., & Kinross, J. M. (2023). Gut Microbiota Modulation of Efficacy and Toxicity of Cancer Chemotherapy and Immunotherapy. Gastroenterology, 164(2), 198–213. https://doi.org/10.1053/j.gastro.2022.10.018

Cresci, G. A., Thangaraju, M., Mellinger, J. D., Liu, K., & Ganapathy, V. (2010). Colonic Gene Expression in Conventional and Germ-Free Mice with a Focus on the Butyrate Receptor GPR109A and the Butyrate Transporter SLC5A8. Journal of Gastrointestinal Surgery, 14(3), 449–461. https://doi.org/10.1007/s11605-009-1045-x

Cummings, J. H., Pomare, E. W., Branch, W. J., Naylor, C. P., & Macfarlane, G. T. (1987). Short chain fatty acids in human large intestine, portal, hepatic and venous blood. Gut, 28(10), 1221–1227. https://doi.org/10.1136/gut.28.10.1221

den Besten, G., Lange, K., Havinga, R., van Dijk, T. H., Gerding, A., van Eunen, K., Müller, M., Groen, A. K., Hooiveld, G. J., Bakker, B. M., & Reijngoud, D.-J. (2013). Gut-derived short-chain fatty acids are vividly assimilated into host carbohydrates and lipids. American

Journal of Physiology-Gastrointestinal and Liver Physiology, 305(12), G900–G910. https://doi.org/10.1152/ajpgi.00265.2013

Dobkin, J. F., Saha, J. R., Butler, V. P., Neu, H. C., & Lindenbaum, J. (1983). Digoxin-Inactivating Bacteria: Identification in Human Gut Flora. Science, 220(4594), 325–327. https://doi.org/10.1126/science.6836275

Duncan, S. H., Barcenilla, A., Stewart, C. S., Pryde, S. E., & Flint, H. J. (2002). Acetate Utilization and Butyryl Coenzyme A (CoA):Acetate-CoA Transferase in Butyrate-Producing Bacteria from the Human Large Intestine. Applied and Environmental Microbiology, 68(10), 5186–5190. https://doi.org/10.1128/AEM.68.10.5186-5190.2002

Dürholz, K., Hofmann, J., Iljazovic, A., Häger, J., Lucas, S., Sarter, K., Strowig, T., Bang, H., Rech, J., Schett, G., & Zaiss, M. M. (2020). Dietary Short-Term Fiber Interventions in Arthritis Patients Increase Systemic SCFA Levels and Regulate Inflammation. Nutrients, 12(10), Article 10. https://doi.org/10.3390/nu12103207

Eckel, R. H., Grundy, S. M., & Zimmet, P. Z. (2005). The metabolic syndrome. The Lancet, 365(9468), 1415–1428. https://doi.org/10.1016/S0140-6736(05)66378-7

Faith, J. J., Ahern, P. P., Ridaura, V. K., Cheng, J., & Gordon, J. I. (2014). Identifying Gut Microbe-Host Phenotype Relationships Using Combinatorial Communities in Gnotobiotic Mice. Science Translational Medicine, 6(220), 220ra11-220ra11. https://doi.org/10.1126/scitranslmed.3008051

Ferretti, P., Pasolli, E., Tett, A., Asnicar, F., Gorfer, V., Fedi, S., Armanini, F., Truong, D. T., Manara, S., Zolfo, M., Beghini, F., Bertorelli, R., Sanctis, V. D., Bariletti, I., Canto, R., Clementi, R., Cologna, M., Crifò, T., Cusumano, G., … Segata, N. (2018). Mother-to-Infant Microbial Transmission from Different Body Sites Shapes the Developing Infant

Gut Microbiome. Cell Host & Microbe, 24(1), 133-145.e5. https://doi.org/10.1016/j.chom.2018.06.005

Franzosa, E. A., Morgan, X. C., Segata, N., Waldron, L., Reyes, J., Earl, A. M., Giannoukos, G., Boylan, M. R., Ciulla, D., Gevers, D., Izard, J., Garrett, W. S., Chan, A. T., & Huttenhower, C. (2014). Relating the metatranscriptome and metagenome of the human gut. Proceedings of the National Academy of Sciences, 111(22), E2329–E2338. https://doi.org/10.1073/pnas.1319284111

Goodrich, J. K., Waters, J. L., Poole, A. C., Sutter, J. L., Koren, O., Blekhman, R., Beaumont, M., Van Treuren, W., Knight, R., Bell, J. T., Spector, T. D., Clark, A. G., & Ley, R. E. (2014). Human Genetics Shape the Gut Microbiome. Cell, 159(4), 789–799. https://doi.org/10.1016/j.cell.2014.09.053

Gopalakrishnan, V., Spencer, C. N., Nezi, L., Reuben, A., Andrews, M. C., Karpinets, T. V., Prieto, P. A., Vicente, D., Hoffman, K., Wei, S. C., Cogdill, A. P., Zhao, L., Hudgens, C. W., Hutchinson, D. S., Manzo, T., Petaccia de Macedo, M., Cotechini, T., Kumar, T., Chen, W. S., … Wargo, J. A. (2018). Gut microbiome modulates response to anti–PD-1 immunotherapy in melanoma patients. Science, 359(6371), 97–103. https://doi.org/10.1126/science.aan4236

Gregory, J. C., Buffa, J. A., Org, E., Wang, Z., Levison, B. S., Zhu, W., Wagner, M. A., Bennett, B. J., Li, L., DiDonato, J. A., Lusis, A. J., & Hazen, S. L. (2015). Transmission of Atherosclerosis Susceptibility with Gut Microbial Transplantation. Journal of Biological Chemistry, 290(9), 5647–5660. https://doi.org/10.1074/jbc.M114.618249

Guzior, D. V., & Quinn, R. A. (2021). Review: Microbial transformations of human bile acids. Microbiome, 9(1), 140. https://doi.org/10.1186/s40168-021-01101-1

Haghikia, A., Zimmermann, F., Schumann, P., Jasina, A., Roessler, J., Schmidt, D., Heinze, P., Kaisler, J., Nageswaran, V., Aigner, A., Ceglarek, U., Cineus, R., Hegazy, A. N., van der Vorst, E. P. C., Döring, Y., Strauch, C. M., Nemet, I., Tremaroli, V., Dwibedi, C., … Landmesser, U. (2021). Propionate attenuates atherosclerosis by immune-dependent regulation of intestinal cholesterol metabolism. European Heart Journal, ehab644. https://doi.org/10.1093/eurheartj/ehab644

Healey, G. R., Murphy, R., Brough, L., Butts, C. A., & Coad, J. (2017). Interindividual variability in gut microbiota and host response to dietary interventions. Nutrition Reviews, 75(12), 1059–1080. https://doi.org/10.1093/nutrit/nux062

Higginson, J., & Pepler, W. J. (1954). Fat Intake, Serum Cholesterol Concentration, and Atherosclerosis in the South African Bantu. Part II. Atherosclerosis and Coronary Artery Disease. The Journal of Clinical Investigation, 33(10), 1366–1371. https://doi.org/10.1172/JCI103013

Hughes, R. L., Marco, M. L., Hughes, J. P., Keim, N. L., & Kable, M. E. (2019). The Role of the Gut Microbiome in Predicting Response to Diet and the Development of Precision Nutrition Models—Part I: Overview of Current Methods. Advances in Nutrition, 10(6), 953–978. https://doi.org/10.1093/advances/nmz022

Jie, Z., Xia, H., Zhong, S.-L., Feng, Q., Li, S., Liang, S., Zhong, H., Liu, Z., Gao, Y., Zhao, H., Zhang, D., Su, Z., Fang, Z., Lan, Z., Li, J., Xiao, L., Li, J., Li, R., Li, X., … Kristiansen, K. (2017). The gut microbiome in atherosclerotic cardiovascular disease. Nature Communications, 8(1), Article 1. https://doi.org/10.1038/s41467-017-00900-1

Kasahara, K., Kerby, R. L., Zhang, Q., Pradhan, M., Mehrabian, M., Lusis, A. J., Bergström, G., Bäckhed, F., & Rey, F. E. (2023). Gut bacterial metabolism contributes to host global

purine homeostasis. Cell Host & Microbe, 31(6), 1038-1053.e10. https://doi.org/10.1016/j.chom.2023.05.011

Kasahara, K., Krautkramer, K. A., Org, E., Romano, K. A., Kerby, R. L., Vivas, E. I., Mehrabian, M., Denu, J. M., Bäckhed, F., Lusis, A. J., & Rey, F. E. (2018). Interactions between Roseburia intestinalis and diet modulate atherogenesis in a murine model. Nature Microbiology, 3(12), 1461. https://doi.org/10.1038/s41564-018-0272-x

Kaye David M., Shihata Waled A., Jama Hamdi A., Tsyganov Kirill, Ziemann Mark, Kiriazis Helen, Horlock Duncan, Vijay Amrita, Giam Beverly, Vinh Antony, Johnson Chad, Fiedler April, Donner Daniel, Snelson Matthew, Coughlan Melinda T., Phillips Sarah, Du Xiao-Jun, El-Osta Assam, Drummond Grant, … Marques Francine Z. (2020). Deficiency of Prebiotic Fiber and Insufficient Signaling Through Gut Metabolite-Sensing Receptors Leads to Cardiovascular Disease. Circulation, 141(17), 1393–1403. https://doi.org/10.1161/CIRCULATIONAHA.119.043081

Kelly, T. N., Bazzano, L. A., Ajami, N. J., He, H., Zhao, J., Petrosino, J. F., Correa, A., & He, J. (2016). Gut Microbiome Associates With Lifetime Cardiovascular Disease Risk Profile Among Bogalusa Heart Study Participants. Circulation Research, 119(8), 956–964. https://doi.org/10.1161/CIRCRESAHA.116.309219

Kimura, I., Ichimura, A., Ohue-Kitano, R., & Igarashi, M. (2020). Free Fatty Acid Receptors in Health and Disease. Physiol Rev, 100, 41.

Kimura, I., Inoue, D., Maeda, T., Hara, T., Ichimura, A., Miyauchi, S., Kobayashi, M., Hirasawa, A., & Tsujimoto, G. (2011). Short-chain fatty acids and ketones directly regulate sympathetic nervous system via G protein-coupled receptor 41 (GPR41). Proceedings of

the National Academy of Sciences, 108(19), 8030–8035. https://doi.org/10.1073/pnas.1016088108

Kirk, D., Catal, C., & Tekinerdogan, B. (2021). Precision nutrition: A systematic literature review. Computers in Biology and Medicine, 133, 104365. https://doi.org/10.1016/j.compbiomed.2021.104365

Koh, A., De Vadder, F., Kovatcheva-Datchary, P., & Bäckhed, F. (2016). From Dietary Fiber to Host Physiology: Short-Chain Fatty Acids as Key Bacterial Metabolites. Cell, 165(6), 1332–1345. https://doi.org/10.1016/j.cell.2016.05.041

Koh, A., Molinaro, A., Ståhlman, M., Khan, M. T., Schmidt, C., Mannerås-Holm, L., Wu, H., Carreras, A., Jeong, H., Olofsson, L. E., Bergh, P.-O., Gerdes, V., Hartstra, A., De Brauw, M., Perkins, R., Nieuwdorp, M., Bergström, G., & Bäckhed, F. (2018). Microbially Produced Imidazole Propionate Impairs Insulin Signaling through mTORC1. Cell, 175(4), 947-961.e17. https://doi.org/10.1016/j.cell.2018.09.055

Kolodziejczyk, A. A., Zheng, D., & Elinav, E. (2019). Diet–microbiota interactions and personalized nutrition. Nature Reviews Microbiology, 17(12), Article 12. https://doi.org/10.1038/s41579-019-0256-8

Koppel, N., Bisanz, J. E., Pandelia, M.-E., Turnbaugh, P. J., & Balskus, E. P. (2018). Discovery and characterization of a prevalent human gut bacterial enzyme sufficient for the inactivation of a family of plant toxins. eLife, 7, e33953. https://doi.org/10.7554/eLife.33953

Kritchevsky, D. (1978). Fiber, lipids, and atherosclerosis. The American Journal of Clinical Nutrition, 31(10), S65–S74. https://doi.org/10.1093/ajcn/31.10.S65

Larsen, N., Vogensen, F. K., Berg, F. W. J. van den, Nielsen, D. S., Andreasen, A. S., Pedersen, B. K., Al-Soud, W. A., Sørensen, S. J., Hansen, L. H., & Jakobsen, M. (2010). Gut Microbiota in Human Adults with Type 2 Diabetes Differs from Non-Diabetic Adults. PLOS ONE, 5(2), e9085. https://doi.org/10.1371/journal.pone.0009085

Ley, R. E., Turnbaugh, P. J., Klein, S., & Gordon, J. I. (2006). Human gut microbes associated with obesity. Nature, 444(7122), Article 7122. https://doi.org/10.1038/4441022a

Louis, P., Hold, G. L., & Flint, H. J. (2014). The gut microbiota, bacterial metabolites and colorectal cancer. Nature Reviews Microbiology, 12(10), Article 10. https://doi.org/10.1038/nrmicro3344

Lukasova, M., Malaval, C., Gille, A., Kero, J., & Offermanns, S. (2011). Nicotinic acid inhibits progression of atherosclerosis in mice through its receptor GPR109A expressed by immune cells. The Journal of Clinical Investigation, 121(3), 1163–1173. https://doi.org/10.1172/JCI41651

Lynch, S. V., & Pedersen, O. (2016). The Human Intestinal Microbiome in Health and Disease. New England Journal of Medicine, 375(24), 2369–2379. https://doi.org/10.1056/NEJMra1600266

McOrist, A. L., Miller, R. B., Bird, A. R., Keogh, J. B., Noakes, M., Topping, D. L., & Conlon, M. A. (2011). Fecal Butyrate Levels Vary Widely among Individuals but Are Usually Increased by a Diet High in Resistant Starch. The Journal of Nutrition, 141(5), 883–889. https://doi.org/10.3945/jn.110.128504

Molinaro, A., Bel Lassen, P., Henricsson, M., Wu, H., Adriouch, S., Belda, E., Chakaroun, R., Nielsen, T., Bergh, P.-O., Rouault, C., André, S., Marquet, F., Andreelli, F., Salem, J.-E., Assmann, K., Bastard, J.-P., Forslund, S., Le Chatelier, E., Falony, G., … Bäckhed, F.

(2020). Imidazole propionate is increased in diabetes and associated with dietary patterns and altered microbial ecology. Nature Communications, 11(1), Article 1. https://doi.org/10.1038/s41467-020-19589-w

Murga-Garrido, S. M., Hong, Q., Cross, T.-W. L., Hutchison, E. R., Han, J., Thomas, S. P., Vivas, E. I., Denu, J., Ceschin, D. G., Tang, Z.-Z., & Rey, F. E. (2021). Gut microbiome variation modulates the effects of dietary fiber on host metabolism. Microbiome, 9(1), 117. https://doi.org/10.1186/s40168-021-01061-6

Neuman, H., Debelius, J. W., Knight, R., & Koren, O. (2015). Microbial endocrinology: The interplay between the microbiota and the endocrine system. FEMS Microbiology Reviews, 39(4), 509–521. https://doi.org/10.1093/femsre/fuu010

Ormazabal, V., Nair, S., Elfeky, O., Aguayo, C., Salomon, C., & Zuñiga, F. A. (2018). Association between insulin resistance and the development of cardiovascular disease. Cardiovascular Diabetology, 17, 122. https://doi.org/10.1186/s12933-018-0762-4

Pescatello, L. S. (1999). Physical Activity, Cardiometabolic Health and Older Adults: Recent Findings. Sports Medicine, 28(5), 315–323. https://doi.org/10.2165/00007256-199928050-00003

Petersen, M. C., & Shulman, G. I. (2018). Mechanisms of Insulin Action and Insulin Resistance. Physiological Reviews, 98(4), 2133–2223. https://doi.org/10.1152/physrev.00063.2017

Pluznick, J. L., Protzko, R. J., Gevorgyan, H., Peterlin, Z., Sipos, A., Han, J., Brunet, I., Wan, L.-X., Rey, F., Wang, T., Firestein, S. J., Yanagisawa, M., Gordon, J. I., Eichmann, A., Peti-Peterdi, J., & Caplan, M. J. (2013). Olfactory receptor responding to gut microbiota-derived signals plays a role in renin secretion and blood pressure regulation. Proceedings

of the National Academy of Sciences, 110(11), 4410–4415. https://doi.org/10.1073/pnas.1215927110

Qin, J., Li, Y., Cai, Z., Li, S., Zhu, J., Zhang, F., Liang, S., Zhang, W., Guan, Y., Shen, D., Peng, Y., Zhang, D., Jie, Z., Wu, W., Qin, Y., Xue, W., Li, J., Han, L., Lu, D., … Wang, J. (2012). A metagenome-wide association study of gut microbiota in type 2 diabetes. Nature, 490(7418), Article 7418. https://doi.org/10.1038/nature11450

Rashid, S., Watanabe, T., Sakaue, T., & Lewis, G. F. (2003). Mechanisms of HDL lowering in insulin resistant, hypertriglyceridemic states: The combined effect of HDL triglyceride enrichment and elevated hepatic lipase activity. Clinical Biochemistry, 36(6), 421–429. https://doi.org/10.1016/S0009-9120(03)00078-X

Rey, F. E., Faith, J. J., Bain, J., Muehlbauer, M. J., Stevens, R. D., Newgard, C. B., & Gordon, J. I. (2010). Dissecting the in vivo metabolic potential of two human gut acetogens. The Journal of Biological Chemistry, 285(29), 22082–22090. https://doi.org/10.1074/jbc.M110.117713

Ridker, P. M., Bhatt, D. L., Pradhan, A. D., Glynn, R. J., MacFadyen, J. G., & Nissen, S. E. (2023). Inflammation and cholesterol as predictors of cardiovascular events among patients receiving statin therapy: A collaborative analysis of three randomised trials. The Lancet, 0(0). https://doi.org/10.1016/S0140-6736(23)00215-5

Roediger, W. E. W. (1982). Utilization of Nutrients by Isolated Epithelial Cells of the Rat Colon. Gastroenterology, 83(2), 424–429. https://doi.org/10.1016/S0016-5085(82)80339-9

Samuel, B. S., Shaito, A., Motoike, T., Rey, F. E., Backhed, F., Manchester, J. K., Hammer, R. E., Williams, S. C., Crowley, J., Yanagisawa, M., & Gordon, J. I. (2008). Effects of the gut microbiota on host adiposity are modulated by the short-chain fatty-acid binding G protein-

coupled receptor, Gpr41. Proceedings of the National Academy of Sciences, 105(43), 16767–16772. https://doi.org/10.1073/pnas.0808567105

Sattar, N., Gill, J. M. R., & Alazawi, W. (2020). Improving prevention strategies for cardiometabolic disease. Nature Medicine, 26(3), Article 3. https://doi.org/10.1038/s41591-020-0786-7

Scott, K. P., Martin, J. C., Campbell, G., Mayer, C.-D., & Flint, H. J. (2006). Whole-Genome Transcription Profiling Reveals Genes Up-Regulated by Growth on Fucose in the Human Gut Bacterium "Roseburia inulinivorans." Journal of Bacteriology, 188(12), 4340–4349. https://doi.org/10.1128/jb.00137-06

Shah, P. K. (2009). Inflammation and Plaque Vulnerability. Cardiovascular Drugs and Therapy, 23(1), 31–40. https://doi.org/10.1007/s10557-008-6147-2

Shah, P. K., Falk, E., Badimon, J. J., Fernandez-Ortiz, A., Mailhac, A., Villareal-Levy, G., Fallon, J. T., Regnstrom, J., & Fuster, V. (1995). Human monocyte-derived macrophages induce collagen breakdown in fibrous caps of atherosclerotic plaques. Potential role of matrix-degrading metalloproteinases and implications for plaque rupture. Circulation, 92(6), 1565–1569.

Smith, E. A., & Macfarlane, G. T. (1997). Dissimilatory Amino Acid Metabolism in Human Colonic Bacteria. Anaerobe, 3(5), 327–337. https://doi.org/10.1006/anae.1997.0121

Spanogiannopoulos, P., Kyaw, T. S., Guthrie, B. G. H., Bradley, P. H., Lee, J. V., Melamed, J., Malig, Y. N. A., Lam, K. N., Gempis, D., Sandy, M., Kidder, W., Van Blarigan, E. L., Atreya, C. E., Venook, A., Gerona, R. R., Goga, A., Pollard, K. S., & Turnbaugh, P. J. (2022). Host and gut bacteria share metabolic pathways for anti-cancer drug metabolism. Nature Microbiology, 7(10), Article 10. https://doi.org/10.1038/s41564-022-01226-5

Sun, X., & Du, T. (2017). Trends in cardiovascular risk factors among U.S. men and women with and without diabetes, 1988–2014. BMC Public Health, 17(1), 893. https://doi.org/10.1186/s12889-017-4921-4

Tang, W. H. W., & Hazen, S. L. (2017). The Gut Microbiome and Its Role in Cardiovascular Diseases. Circulation, 135(11), 1008–1010. https://doi.org/10.1161/CIRCULATIONAHA.116.024251

Targher, G., & Byrne, C. D. (2013). Nonalcoholic Fatty Liver Disease: A Novel Cardiometabolic Risk Factor for Type 2 Diabetes and Its Complications. The Journal of Clinical Endocrinology & Metabolism, 98(2), 483–495. https://doi.org/10.1210/jc.2012-3093

Threapleton, D. E., Greenwood, D. C., Evans, C. E. L., Cleghorn, C. L., Nykjaer, C., Woodhead, C., Cade, J. E., Gale, C. P., & Burley, V. J. (2013). Dietary fibre intake and risk of cardiovascular disease: Systematic review and meta-analysis. BMJ, 347, f6879. https://doi.org/10.1136/bmj.f6879

Tolhurst, G., Heffron, H., Lam, Y. S., Parker, H. E., Habib, A. M., Diakogiannaki, E., Cameron, J., Grosse, J., Reimann, F., & Gribble, F. M. (2012). Short-Chain Fatty Acids Stimulate Glucagon-Like Peptide-1 Secretion via the G-Protein–Coupled Receptor FFAR2. Diabetes, 61(2), 364–371. https://doi.org/10.2337/db11-1019

Torres, N., Guevara-Cruz, M., Velázquez-Villegas, L. A., & Tovar, A. R. (2015). Nutrition and Atherosclerosis. Archives of Medical Research, 46(5), 408–426. https://doi.org/10.1016/j.arcmed.2015.05.010

Turnbaugh, P. J., Hamady, M., Yatsunenko, T., Cantarel, B. L., Duncan, A., Ley, R. E., Sogin, M. L., Jones, W. J., Roe, B. A., Affourtit, J. P., Egholm, M., Henrissat, B., Heath, A. C.,

Knight, R., & Gordon, J. I. (2009). A core gut microbiome in obese and lean twins. Nature, 457(7228), Article 7228. https://doi.org/10.1038/nature07540

Turnbaugh, P. J., Ley, R. E., Mahowald, M. A., Magrini, V., Mardis, E. R., & Gordon, J. I. (2006). An obesity-associated gut microbiome with increased capacity for energy harvest. Nature, 444(7122), 1027–1031. https://doi.org/10.1038/nature05414

Turnbaugh, P. J., Ridaura, V. K., Faith, J. J., Rey, F. E., Knight, R., & Gordon, J. I. (2009). The Effect of Diet on the Human Gut Microbiome: A Metagenomic Analysis in Humanized Gnotobiotic Mice. Science Translational Medicine, 1(6), 6ra14-6ra14. https://doi.org/10.1126/scitranslmed.3000322

Veprik, A., Laufer, D., Weiss, S., Rubins, N., & Walker, M. D. (2016). GPR41 modulates insulin secretion and gene expression in pancreatic β-cells and modifies metabolic homeostasis in fed and fasting states. The FASEB Journal, 30(11), 3860–3869. https://doi.org/10.1096/fj.201500030R

Virchow, R. (1860). Cellular Pathology as based upon physiological and pathological histology. Twenty lectures delivered in ... 1858. Translated from the second edition of the original by F. Chance. With notes and numerous emendations principally from MS. notes of the author, and illustrated by ... Engravings on wood.

Wang, D. D., Nguyen, L. H., Li, Y., Yan, Y., Ma, W., Rinott, E., Ivey, K. L., Shai, I., Willett, W. C., Hu, F. B., Rimm, E. B., Stampfer, M. J., Chan, A. T., & Huttenhower, C. (2021). The gut microbiome modulates the protective association between a Mediterranean diet and cardiometabolic disease risk. Nature Medicine, 27(2), Article 2. https://doi.org/10.1038/s41591-020-01223-3

Wang, Z., Klipfell, E., Bennett, B. J., Koeth, R., Levison, B. S., DuGar, B., Feldstein, A. E., Britt, E. B., Fu, X., Chung, Y.-M., Wu, Y., Schauer, P., Smith, J. D., Allayee, H., Tang, W. H. W., DiDonato, J. A., Lusis, A. J., & Hazen, S. L. (2011). Gut flora metabolism of phosphatidylcholine promotes cardiovascular disease. Nature, 472(7341), Article 7341. https://doi.org/10.1038/nature09922

Weeke, P., & Roden, D. M. (2013). Pharmacogenomics and Cardiovascular Disease. Current Cardiology Reports, 15(7), 376. https://doi.org/10.1007/s11886-013-0376-0

Yatsunenko, T., Rey, F. E., Manary, M. J., Trehan, I., Dominguez-Bello, M. G., Contreras, M., Magris, M., Hidalgo, G., Baldassano, R. N., Anokhin, A. P., Heath, A. C., Warner, B., Reeder, J., Kuczynski, J., Caporaso, J. G., Lozupone, C. A., Lauber, C., Clemente, J. C., Knights, D., … Gordon, J. I. (2012). Human gut microbiome viewed across age and geography. Nature, 486(7402), 222–227. https://doi.org/10.1038/nature11053

Yu, Z.-L., Zhang, L.-Y., Jiang, X.-M., Xue, C.-H., Chi, N., Zhang, T.-T., & Wang, Y.-M. (2020). Effects of dietary choline, betaine, and L-carnitine on the generation of trimethylamine-N-oxide in healthy mice. Journal of Food Science, 85(7), 2207–2215. https://doi.org/10.1111/1750-3841.15186

Yue, F., Cheng, Y., Breschi, A., Vierstra, J., Wu, W., Ryba, T., Sandstrom, R., Ma, Z., Davis, C., Pope, B. D., Shen, Y., Pervouchine, D. D., Djebali, S., Thurman, R. E., Kaul, R., Rynes, E., Kirilusha, A., Marinov, G. K., Williams, B. A., … Mouse ENCODE Consortium. (2014). A comparative encyclopedia of DNA elements in the mouse genome. Nature, 515(7527), 355–364. https://doi.org/10.1038/nature13992

Zeevi, D., Korem, T., Zmora, N., Israeli, D., Rothschild, D., Weinberger, A., Ben-Yacov, O., Lador, D., Avnit-Sagi, T., Lotan-Pompan, M., Suez, J., Mahdi, J. A., Matot, E., Malka, G.,

Kosower, N., Rein, M., Zilberman-Schapira, G., Dohnalová, L., Pevsner-Fischer, M., … Segal, E. (2015). Personalized Nutrition by Prediction of Glycemic Responses. Cell, 163(5), 1079–1094. https://doi.org/10.1016/j.cell.2015.11.001

Zhang, H., DiBaise, J. K., Zuccolo, A., Kudrna, D., Braidotti, M., Yu, Y., Parameswaran, P., Crowell, M. D., Wing, R., Rittmann, B. E., & Krajmalnik-Brown, R. (2009). Human gut microbiota in obesity and after gastric bypass. Proceedings of the National Academy of Sciences, 106(7), 2365–2370. https://doi.org/10.1073/pnas.0812600106

Zhang, S., Li, Z., Zhang, Y., Chen, J., Li, Y., Wu, F., Wang, W., Cui, Z. J., & Chen, G. (2021). Ketone Body 3-Hydroxybutyrate Ameliorates Atherosclerosis via Receptor Gpr109a-Mediated Calcium Influx. Advanced Science, 8(9), 2003410. https://doi.org/10.1002/advs.202003410

CHAPTER 2: Dissecting the impact of dietary fiber type on atherosclerosis in mice colonized with different gut microbial communities

The work presented in this chapter has been published.

Evan R. Hutchison[+]*, Kazuyuki Kasahara, Qijun Zhang, Eugenio I. Vivas, Tzu-Wen L. Cross, Federico E. Rey**

[+]Lead author

*Corresponding author

AUTHOR CONTRIBUTIONS

ERH, T-WLC, and FER conceived of the study. ERH, KK, and EIV performed the mouse experiments and collected tissues. ERH conducted analysis of atherosclerosis phenotype. ERH and QZ conducted gut metagenomic analysis. ERH and FER prepared the manuscript. This manuscript was approved by all authors.

ABSTRACT

Dietary fiber consumption has been linked with improved cardiometabolic health, however human studies have reported large interindividual variations in the observed benefits. We tested whether the effects of dietary fiber on atherosclerosis are influenced by the gut microbiome. We colonized germ-free *Apoe*$^{-/-}$ mice with fecal samples from three human donors (DonA, DonB, and DonC) and fed them diets supplemented with either a mix of 5 fermentable fibers (FF) or non-fermentable cellulose control (CC) diet. We found that DonA-colonized mice had reduced atherosclerosis burden with FF feeding compared to their CC-fed counterparts, whereas the type of fiber did not affect atherosclerosis in mice colonized with microbiota from the other donors. Microbial shifts associated with FF feeding in DonA mice were characterized by higher relative abundances of butyrate-producing taxa, higher butyrate levels, and enrichment of genes involved in synthesis of B vitamins. Our results suggest that atheroprotection in response to FF is not universal and is influenced by the gut microbiome.

INTRODUCTION

Individual responses to the same diet or therapeutic drugs are often inconsistent and not universal. This notion is a fundamental principle of precision medicine and nutrition (Denson et al., 2019; Ordovas & Berciano, 2020). Many factors influence how a subject responds to a given treatment including genetics, diet, and sex. Recently, it has become apparent that the gut microbiome is a major contributor to the observed interpersonal variation in responsiveness (Deehan et al., 2020; Hughes et al., 2019; Leshem et al., 2020; Zeevi et al., 2015). It is now widely recognized that the gut microbiome plays a significant role in health and that human-associated microbial communities are highly variable among individuals (Turnbaugh et al., 2007). Dietary components, from foodstuffs to orally administered drugs, come in close contact with resident microbes along the gastrointestinal tract. The gut microbiome collectively encodes >100-fold more genes than the human genome, including a rich array of enzymes with the potential to metabolize these ingested compounds and modulate their bioavailability, activity, and ultimately their effects on the host (Javdan et al., 2020; Zimmermann et al., 2019a, 2019b). Indeed, gut microbes have received considerable attention in recent years for their capacity to modulate responses to bioactive compounds (Kolodziejczyk et al., 2019) ranging from antihypertensive drugs to immunosuppressants for organ transplants (Koppel et al., 2018; Lee et al., 2015). Gaining a better understanding of which interventions are most sensitive to variation in the microbiome is critical for the effective implementation of precision medicine.

Cardiovascular disease (CVD) is the leading cause of death in the United States and accounts for over a third of all deaths globally (Ahmad, 2021; Mathers et al., 2017). Atherosclerosis is the most common manifestation of CVD and is driven by inflammatory processes that result in the formation of macrophage-dense, fatty plaques within the arterial wall

(Ross, 1999). There is increasing evidence that the gut microbiome plays an important role in modulating atherosclerosis development. Epidemiological studies have identified differences in the microbiomes of individuals with coronary artery disease (Jie et al., 2017; Kelly et al., 2016; Tang & Hazen, 2017). Furthermore, several microbial metabolites arising from specific dietary components have been shown to modulate atherosclerosis progression in humans and animal models through a variety of mechanisms. For example trimethylamine *N*-oxide, a microbial derivative of choline, is associated with increased risk of major cardiovascular events in humans (Wang et al., 2011); the microbial metabolite indole-3-propionic acid, which is derived from tryptophan, protects against atherosclerosis progression by promoting cholesterol efflux (Xue et al., 2022); and short-chain fatty acids (SCFAs), which are produced via fermentation of dietary fiber, have been shown to ameliorate atherosclerosis by limiting dietary cholesterol absorption (propionate) and reducing inflammation and gut permeability (butyrate) (Aguilar et al., 2014; Haghikia et al., 2021; Kasahara et al., 2018). Indeed, diet has long been known to play a major role in both the promotion and prevention of atherosclerosis (Kritchevsky, 1978; Torres et al., 2015). For example, it is well-established that foods such as whole-grain cereals and legumes which are rich in dietary fiber, are protective against CVD (Higginson & Pepler, 1954; Threapleton et al., 2013). However, inconsistent responses to a number of dietary and pharmacological interventions for CVD have been observed between individuals (Healey et al., 2017; Weeke & Roden, 2013). Most studies linking dietary fiber to improved cardiovascular health are assessed using population averages (Kirk et al., 2021) and do not account for individual characteristics. Therefore, the causes behind these inconsistencies are understudied.

Dietary fibers are oligo- or polysaccharides that resist degradation by host enzymes and are available to be metabolized by microbes in the distal gut. Dietary fibers vary widely in structure

and composition and are often subdivided according to their biochemical properties. One such division is drawn by whether they can be fermented by gut microbes. Thus, fermentable fibers are dietary fibers that can be metabolized by intestinal microbes, while non-fermentable fibers resist intestinal fermentation (Cummings, 1984). By this definition, fermentability is not a static or inherent property of any given fiber since it is context-dependent and is contingent on the presence of specific microbes that can degrade the fiber in question and the host environment (e.g., transit time, rumination). Fermentation of dietary fiber in the gastrointestinal tract results in the production of SCFAs, the most abundant of which are acetate, propionate, and butyrate. SCFAs have been linked to improved cardiometabolic health (Haghikia et al., 2021; Kasahara et al., 2018) and are hypothesized to mediate some of the atheroprotective effects associated with dietary fiber consumption (Ohira et al., 2017). However, multiple studies have shown that SCFA production is dependent on microbiome structure and is highly variable among individuals. For example, McOrist et al. found individualized responses in butyrate production to a resistant starch (RS) dietary supplement (McOrist et al., 2011). Additionally, we recently found that various fermentable fibers (pectin, inulin, fructo-oligosaccharide (FOS), RS-2, and RS-4) elicited disparate responses in SCFA production when fed to mice colonized with different microbial communities (Murga-Garrido et al., 2021).

Given the personalized nature of the gut microbiome and the fact that gut microbes are necessary for metabolizing dietary fiber, we hypothesized that the atheroprotective effects attained in response to a given dietary fiber are modulated by the gut microbiome composition of the consumer. To test this, we colonized groups of germ-free (GF) *apolipoprotein E* deficient (*Apoe*$^{-/-}$) mice with fecal microbial communities from one of three human donors, each of which exhibited divergent microbial compositions and SCFA-producing capacities. Colonized mice were fed a diet

containing either a mixture of fermentable fibers (FF) or a non-fermentable cellulose control diet (CC). We found that protection from atherosclerosis by FF consumption was not universal, but instead modulated by the resident microbiome. We also observed that atheroprotection was associated with increased butyrate production and enrichment for bacterial genes involved in pathways for carbohydrate metabolism and vitamin synthesis.

RESULTS AND DISCUSSION

Engraftment of donor communities prior to dietary treatment.

Germ-free (GF) Female *Apoe*$^{-/-}$ mice were colonized with fecal samples from one of three human donors (Supplementary Fig. 2.1). These samples were selected from a repository of fecal specimens previously collected from adults in their mid-seventies (Herd et al., 2014) and were chosen based on i) their divergent community structure as assessed by unweighted UniFrac distances of 16S rRNA profiles and ii) their capacity to generate differing levels of SCFAs when engrafted in GF mice consuming a semi-purified diet containing an assortment of fibers (Murga-Garrido et al., 2021) . After colonization, mice were maintained on the FF diet for two weeks to allow for stabilization of engrafted communities before the dietary treatment phase (Supplementary Fig. 2.1). Fecal samples were collected at this point to assess bacterial engraftment via 16S rRNA v4 amplicon sequencing. The engraftment efficiency (genus level) was 64% in DonA-, 65% DonB-, and 72% DonC-colonized mice, respectively (Supplementary Fig. 2.2f). When calculated as the percentage of donor genera detected in at least one of the recipient mice, efficiencies were 90, 88, and 87% in DonA-, DonB-, and DonC-colonized mice, respectively (Supplementary Fig. 2.2c-e). These engraftment efficiencies are in line with previous studies (Goodman et al., 2011; Turnbaugh, Ridaura, et al., 2009). Physiological, anatomical, and

behavioral differences between human donors and recipient mice along with differences in diet likely explain why only a fraction of the donor bacteria engrafted.

A few genera were only detected in the recipient mice but were unique to each of the three donor groups, suggesting that these taxa may have been present in low abundance in the human donor samples rather than the result of contamination. Principal coordinate analysis (PCoA) of weighted UniFrac distances of fecal samples collected prior to dietary treatment showed uniform engraftment between mice bound for the two diets (FF-bound and CC-bound) within all treatment groups (all pairwise PERMANOVA adjusted *P*-values >0.1, Supplementary Fig. 2.2a). However, comparisons using unweighted UniFrac distances (sensitive to presence/absence of taxa) showed a significant difference in community structure in DonA-colonized mice between FF-bound and CC-bound communities (adjusted *P*-value = 0.0012, Supplementary Fig. 2.2b). This was driven by 9 genera that were detected in one diet-bound group but not the other (Supplementary Fig. 2.2c). Eleven weeks after dietary treatment, cecal samples were collected and used to assess terminal microbial communities. By the end of the experiment, 5 of the 9 missing genera were no longer detected in cecal contents of mice on either diet, while 4 genera (*Clostridium*, *Faecalibacterium*, *Gemmiger*, and an undetermined *Ruminococcus* genus) were found only in FF-fed mice (Supplementary Fig. 2.2c). This introduces the possibility that the differences observed in the assembled communities between dietary groups for DonA mice are the result of inconsistent engraftment rather than an effect of diet. Alternatively, since microbial communities undergo considerable fluctuations in the period after colonization (Chung et al., 2012), it is possible that these missing taxa were present in the CC-bound mice, but below detectable levels. The latter scenario is supported by the fact that i) all of the missing taxa were detected in the human donor sample used to inoculate all DonA mice, and ii) similar FF-diet-driven patterns were observed with

Faecalibacterium and *Gemmiger* abundances in a previous study (Murga-Garrido et al., 2021) that used the same donor feces and the same diets. These findings highlight the importance of reporting pre-treatment engraftment data in mouse transplant studies such that the conclusions can be appropriately contextualized.

Diet-induced shifts in microbiota composition are largely community-specific.

Two weeks after colonization, mice were placed into their dietary treatment groups and were maintained on their respective diets for 11 weeks. PCoA analysis of weighted and unweighted UniFrac distances (Fig. 2.1a-b) of cecal bacterial communities assessed at the completion of the study shows that mice were highly distinguishable by dietary treatment within each donor group. When using unweighted UniFrac distances, ordination shows that donor group had a stronger effect on community composition than diet (Fig. 2.1a). PCoA of weighted UniFrac distances, which factors in the abundance of each taxon, shows clear distinctions by diet, but more overlap between donor groups (Fig. 2.1b), suggesting that FF consumption elicits distinct changes of some low abundance, phylogenetically related taxa across the three communities. Alpha-diversity (Shannon) was higher in mice colonized with DonA consuming FF relative to CC consumption but was not significantly impacted by diet in DonB- or DonC-colonized mice (Fig. 2.1f). Similarly, observed amplicon sequence variant (ASV) richness was significantly increased with the FF diet in DonA mice but was reduced by FF feeding in DonB mice (Fig. 2.1g). FF-consumption resulted in increased fecal DNA yields, a proxy for microbial biomass (Contijoch et al., 2019), compared to CC-fed mice in cecal content (Supplementary Fig. 2.3). This effect was observed in mice colonized with all three communities and suggests that a diet rich in fermentable fiber generally increases microbial biomass.

Bacterial communities were dominated by Firmicutes and Bacteroidetes and had detectable levels of Proteobacteria, and Verrucomicorbia in all treatment groups (Fig. 2.1d). Actinobacteria were detected in FF-fed DonA-colonized mice, CC-fed DonB-colonized mice, and both diets for DonC-colonized mice. FF feeding lowered the Bacteroidetes to Firmicutes ratio for all donor groups (Fig. 2.1e), but the only significant reduction was observed in DonA-colonized mice. There was generally little consistency in the diet-associated enrichment patterns observed across donor groups, even when considering phylum level changes, suggesting a lack of a universal response to dietary treatment (Fig. 2.1c-g).

We used the Microbiome Multivariable Association with Linear Models (MaAsLin 2) (Mallick et al., 2021) to analyze enrichment patterns at the genus level caused by diet for each donor group. Most genera that were significantly different (adjusted *P*-value <0.1) were unique to each donor group: *Blautia* was the only genus that was significantly enriched by FF-consumption across all donor groups, while *Eggerthella, Butyricimonas,* and *Parabacteroides* were the only genera to exhibit universal enrichment in response to the CC diet (Fig. 2.1c). One obvious explanation for the lack of universality is the fact that each donor group possess different collections of microbes. However, even in the cases of genera that were present across multiple donors, the directionality in response to diet tended to vary by community ([Lachn] *Clostridium*, *Bacteroides*, *Akkermansia*, [Lachn] Undetermined, [Rumin] *Clostridium*, *Oscillospira*, [Erysi] *Clostridium*, [Lachn] *Ruminococcus*). For example, the *Bacteroides* genus was significantly enriched by CC feeding in DonC-colonized mice, by FF feeding in DonB-colonized mice and unaffected by diet in DonA-colonized animals (Fig. 2.1c). Interestingly, the relative abundance of *Akkermansia* was significantly increased by CC feeding in DonB mice, by the FF diet in DonC mice, and was not affected by diet in DonA-colonized mice. *Akkermansia muciniphila*, the most

common species in this genus, feeds on host mucins which can be glycosylated by fiber-degrading bacteria thereby influencing *Akkermansia* levels (Earley et al., 2019; Zhang et al., 2022). Although *Akkermansia* has been reported to thrive on diets poor in fermentable fiber (Kim et al., 2020), our data indicates that microbiota composition can influence *Akkermansia* response to specific fiber sources. It is also possible that the different donor groups possess distinct strains of *Akkermansia muciniphilia* that are themselves differentially affected by diet. Together, these results suggest that microbial responses to dietary fiber are context-dependent and are likely impacted by composition and metabolic capabilities of the broader community.

Fermentable fiber impacts atherosclerosis progression in a donor-dependent manner.

FF-fed mice colonized with DonA had significantly reduced lipid deposition in atherosclerotic plaques and a trend towards reduced plaque area (*P*-value = 0.070) compared to their CC-fed counterparts, while there were no differences observed between diets in either DonB- or DonC-colonized mice (Fig. 2.2a-c). To further characterize atherosclerosis disease status, lesions were assessed for macrophage infiltration by immunohistology with MOMA-2 antibodies. There were no statistically significant differences observed between diets in lesion MOMA-2 density in any of the donor groups (Fig. 2.2a,d), but there was a trend of reduced density with FF feeding in DonA mice (*P*-value = 0.11). Previous studies report inconsistent results regarding of the effect of inulin (a component fiber in the FF diet) on atherosclerosis in mice (Hoving et al., 2018; Rault-Nania et al., 2006). Rault-Nania et al. found that inulin ameliorated atherosclerosis in *Apoe*$^{-/-}$ mice, whereas Hoving and colleagues found that inulin exacerbated atherosclerosis in *APOE*3-Leiden* mice. While this discrepancy could be due to the different diets and/or mouse models used in these studies, our results support the notion that the gut microbiome modulates the

atheroprotective effect of fermentable dietary fiber, providing a possible explanation for these conflicting findings.

The atheroprotective effect of the FF diet is not associated with changes in plasma lipids or alterations in the expression of aortic immune markers.

To test whether fermentable fiber consumption altered lipid composition in circulation, we measured lipid levels in the plasma of the mice described above. No statistical differences were observed between diets for any of the donor groups in plasma levels of total cholesterol, HDL cholesterol, or triglycerides (Fig. 2.2e-g). We also assessed aortic expression levels of *Abca1* and *Abcg1* mRNA by RT-qPCR as markers of reverse cholesterol transport but did not observe any statistically significant differences between diets within any of the donor groups (Supplementary Fig. 2.4d,e). These results suggest that the atheroprotective effect of FF consumption observed in DonA mice was not mediated by major alterations in plasma lipids or cholesterol homeostasis. To test whether atheroprotection was associated with changes in vascular inflammation status, we measured aortic expression of the inflammatory markers *Tnf-α*, *Il1-β*, and *Vcam-1*, which are commonly associated with atherosclerosis progression (Kasahara et al., 2018; Libby Peter, 2012). There were no significant differences observed in expression of these markers between diets in any of the donor groups (Supplementary Fig. 2.4a-c). These data suggest that the atheroprotective effect of FF-feeding in DonA mice may be independent of these immune processes and reverse cholesterol transport, although further analyses are needed to fully rule out these factors.

Cecal SCFA profiles are altered by diet in a donor-dependent manner.

Given the variability in microbiome composition between diets, we next tested whether there were differences in fiber fermentation capacities between donor groups. In line with the microbiome composition patterns above, diet-induced shifts in SCFA profiles were highly dependent on donor group (Fig. 2.3a-d). Acetate, the most abundant SCFA, was increased in FF-fed mice colonized with both DonA and DonB communities (Fig. 2.3a). Propionate was increased by FF-feeding only in DonA mice, whereas diet did not affect propionate levels in the other two donor groups (Fig. 2.3b). FF feeding resulted in substantially elevated cecal butyrate levels in DonA mice, but reduced butyrate levels in DonB-colonized mice compared to CC-fed counterparts (Fig. 2.3c). Cecal butyrate concentrations were not different between diets in DonC-colonized mice. The branched-chain fatty acids isobutyrate and isovalerate, which are primarily produced via protein fermentation, were not affected by diet within any of the donor groups (Fig. 2.3e,f). A lack of differences in branched-chain fatty acids is consistent with the fact that the FF and CC diets are isoproteic. Total SCFA concentrations (i.e., the sum of acetate, propionate, and butyrate) within donor groups were increased by FF-feeding in DonA and DonB, but not DonC (Fig. 2.3d). These results reflect the shifts observed in SCFA-producing microbiota. Among the genera that were increased by FF feeding in DonA mice only were *Clostridium*, *Oscillospira*, *Ruminococcus*, *Gemmiger*, and *Faecalibacterium*, (Fig. 2.1c) all of which contain butyrate producing species (Gophna et al., 2017; Vital et al., 2014). Notably, most of these genera were also present in the other donor groups but were not enriched by FF feeding. This could be due to complex, community-level interactions (e.g., competition) influencing responses of individual genera to dietary fiber, or strain-level differences in response to diet, or both.

Our data is consistent with previously reported studies suggesting that butyrate-induced protection against atherosclerosis in mice occurs in the absence of major changes in plasma lipid

levels (Aguilar et al., 2014; Kasahara et al., 2018). Similar to our results, Kasahara et. al. (Kasahara et al., 2018) reported that the introduction of a butyrate-producing microbe in mice colonized with a simplified bacterial community led to reductions in plaque burden and macrophage infiltration in *Apoe*$^{-/-}$ mice without significant changes in cholesterol homeostasis. However, Kasahara et. al. also detected butyrate-induced reductions in aortic expression of inflammatory markers *Tnf-α*, *Il1-β*, and *Vcam-1*, which we did not observe in our study. Additionally, a recent study found that propionate consumption protected against atherosclerosis by inhibiting cholesterol uptake in the intestine (Haghikia et al., 2021). Although we observed increased cecal propionate levels in DonA-colonized mice consuming the FF diet, we did not detect differences in plasma cholesterol levels. The concentration and site within the gastrointestinal tract where propionate accumulates (i.e., greater concentration in the small intestine when consumed orally *vs*. greater concentration in the large intestine when produced via fiber fermentation) may influence its effect on cholesterol absorption. Together, these findings suggest that SCFA-production capacity is dependent on both accessible dietary fiber and microbial community composition. These results also validate the notion that the abundance of butyrate-producing microbes is associated with cecal levels of butyrate.

Bacterial functional profiles were differentially modulated by dietary fiber in a donor-specific manner.

We next sought to identify links between the functional potential of the microbiome and atheroprotection by examining changes in microbial metagenomic profiles. We performed shotgun sequencing of DNA isolated from cecal contents (average of 29.4 ± 7.7 million paired-end reads/sample; n=5/diet-donor group). Sequence data was analyzed with HUMAnN3 to generate

metagenomic functional profiles that included KEGG orthology (KO) abundances for each mouse. Hierarchical clustering of KO profiles using Bray-Curtis dissimilarity shows that the treatment groups are different from one another, but the effect of diet on clustering patterns varied by donor (Fig. 2.4a). Mice colonized with DonA and DonC clustered closer by diet than by donor group, suggesting a significant level of FF-influenced overlap in KO profiles between these two donor groups. DonB mice on the other hand, clustered separately from all other mice but sub-clustered by diet (Fig. 2.4a). Differential abundances of individual KOs between FF- and CC-fed mice within each donor group were calculated with MaAsLin 2. This analysis revealed that 2,676 KOs that were significantly different (adjusted *P*-value <0.05) between diets in at least one donor group (DonA=971; DonB=1964; DonC=1419). Of these, only 67 (2.5%) were enriched by FF-feeding across all donor groups, whereas 79 (3%) were enriched by CC-feeding across all donor groups, suggesting that most of the diet-induced changes in functional profiles were donor-specific. DonA- and DonC-colonized mice shared the most FF-enriched KOs with 326, while DonA- and DonB-colonized mice shared 99, and animals colonized with DonB- and DonC-colonized mice shared 81 KOs.

We next aimed to gain further insight into how dietary treatment affected the metabolic pathways of the cecal microbial communities in each donor group. We were specifically interested in identifying pathways that might help explain the atheroprotection associated with FF feeding in DonA. We used the MicrobiomeAnalyst KEGG pathway tool (Chong et al., 2020) to conduct pathway enrichment analysis in the KOs that were over-represented by FF feeding relative to their counterparts consuming the CC diet. Similar to the taxonomy results discussed above, we observed a lack of universality among the metagenomic changes in response to diet. Of the 38 KEGG pathways that were detected as significantly overrepresented (adjusted *P*-value <0.1) by FF-

feeding in at least one donor group, only three (*Pyruvate metabolism*, *Amino sugar and nucleotide sugar metabolism*, and *Biosynthesis of amino acids*) were observed across all three donor groups (Fig. 2.4b). In DonA-colonized mice, 27 pathways were significantly overrepresented in the FF diet relative to CC diet. These included pathways involved in vitamin synthesis (*Thiamine biosynthesis*; *Folate biosynthesis*; *Porphyrin metabolism* [vitamin B12]), SCFA synthesis (*Butanoate metabolism*; *Propionate metabolism*), and amino acid metabolism (*Lysine biosynthesis*; *Cysteine and methionine metabolism*; *Histidine metabolism*; *Phenylalanine, tyrosine and tryptophan biosynthesis*; *Valine, leucine and isoleucine biosynthesis*; *Glycine, serine and threonine metabolism*; *Biosynthesis of amino acids*) (Fig. 2.4b). Interestingly, the dietary effects on the enrichment of pathways involved the synthesis of acetate (*Carbon metabolism, Glyoxylate and dicarboxylate metabolism*, and *Pyruvate metabolism*), propionate (*Propionate metabolism*), and butyrate (*Butanoate metabolism*) corresponded very closely with the cecal SCFA levels described above (Fig. 2.4b, Fig. 2.3a-c).

Both folate and vitamin B12 are involved in the detoxification of homocysteine, a metabolite of methionine metabolism that has been linked to cardiovascular disease (K. McCully, 2015; K. S. McCully, 1969). A study involving *Apoe*$^{-/-}$ mice with hyperhomocysteinemia found that supplementation with a mixture of folate, vitamin B12, and vitamin B6 protected against atherosclerosis (Hofmann et al., 2001). Moreover, a recent metagenomic study in humans showed that patients with CVD (n=218) had decreased abundance of genes encoding for components of the folate biosynthesis pathway than healthy patients (n=187) (Jie et al., 2017). Interestingly, the authors of that study also found that CVD was associated with lower abundances of propionate and butyrate synthesis genes. To gain a more detailed picture of the metagenomic dynamics of these pathways, we compared the differential abundances of the individual KOs involved in folate

biosynthesis (KEGG map00790) and anaerobic cobalamin (vitamin B12) biosynthesis (KEGG M00924). In agreement with our enrichment analysis, most of the differentially abundant KOs in both pathways were significantly upregulated by FF feeding in DonA-colonized mice, but not in the other groups (Fig. 2.4c). Folate and vitamin B12 were supplied in the FF and CC diets at the same inclusion rate (AIN-93 vitamin mix, Supplementary Table 1), but it is possible that some amount of additional vitamin availability via microbial biosynthesis may have a physiological effect in host homocysteine metabolism. These results suggest that microbial production of vitamins B12 and folate may act as a potential mediator of the atheroprotection associated with FF diet in mice colonized with this community.

To uncover associations between atheroprotection and fiber metabolism, we determined the level and type of carbohydrate-active enzyme (CAZyme) families between dietary treatments within each donor group using cecal metagenomic data. We detected a number of CAZyme families that were highly abundant in all donor groups and largely unaffected by diet (Fig. 2.5a-b, Supplementary Fig. 2.5). Differential abundance analysis revealed that the CAZyme families which were most significantly affected by diet were about 100-fold lower than the highest abundance CAZymes (Fig. 2.5c). Given the differences in cecal SCFA levels between treatment groups, this suggests that these highly differential, low-abundance CAZymes have an outsized impact on the dynamics of SCFA metabolism. To highlight the most differentially abundant CAZyme families, we compared the abundances of the CAZyme families that were most affected by diet (top 10% by MaAsLin 2 effect size within each donor group, Fig. 2.5c). The vast majority of FF-enriched CAZymes in DonA-colonized mice were significantly correlated (Spearman, *P*-value <0.05) with cecal butyrate levels, potentially linking them to butyrate production (Fig. 2.5c). One such CAZyme family, GH59, encompasses β-galactosidases which free terminal β-D-

galactose monomers from galactan side chains of pectin (Cankar et al., 2014). Interestingly, many commonly cited CAZyme families involved in inulin, pectin, RS-2/4, and scFOS were not found among the most highly differentially abundant CAZymes in our dataset. It is possible that the inclusion of multiple fermentable fibers creates competition among microbes that are specialized for each fiber type preventing the detection of expansion of fiber-specific CAZymes.

In summary, we showed that the gut microbiome regulates the effect of dietary fiber on atherosclerosis development in gnotobiotic *Apoe*$^{-/-}$ mice colonized with different human fecal communities. We found that diet-induced shifts in microbial composition, metabolic potential, and metabolic output (SCFAs) varied among the different donor groups. Our results showed that atheroprotection was associated with increased cecal butyrate levels and abundances of butyrate-producing organisms. Additionally, shotgun metagenomic sequencing revealed donor-dependent shifts in genes involved in carbohydrate metabolism, SCFA production, and vitamin synthesis. These data support the notion that diet-associated shifts in the gut microbiota are not solely a function of diet but are instead the result of complex interactions between diet and the larger gut microbial community structure and functional network. These results are also in line with previous work showing that butyrate is atheroprotective without modifying cholesterol metabolism (Aguilar et al., 2014; Kasahara et al., 2018).

The current study has some limitations that should be addressed. First, we observed an imperfect engraftment efficiency from human donor to mouse recipient. As discussed above, we detected differences in the pre-treatment engraftment patterns of DonA mice. Our data suggests that this difference in detection was likely a consequence of the stochasticity of microbial communities shortly (two weeks) after colonization and not a result of differences in inoculation or contamination. Nonetheless, this discrepancy introduces the possibility that the differences

observed in atherosclerosis within DonA mice were due to inconsistent engraftment rather than response to diet. Another limitation is that our study only used three human donors. A much larger and more diverse cohort of donors would be needed to fully appreciate the breadth of cardiometabolic responses to these diets, but the limited group used here is sufficient to demonstrate that the athero-modulatory effect of dietary fiber is microbiota-dependent. This study is additionally limited by the use of only female mice, precluding us from testing the effect of sex. Finally, the CC and FF diets used in this study differed slightly in their starch content, which may contribute to the differences described above.

Despite these limitations, the work presented here suggests that microbiome variation modulates responses to dietary fiber consumption, which can differentially impact the development of atherosclerosis. Together, these results support the notion that dietary interventions are not universally efficacious and should be tailored to individuals. More research is needed to understand the relevant mechanisms and the metabolic and ecological dynamics that govern the microbiome-dependent individual responses to diet.

METHODS

Germ-free animals. All animals in the current study were handled and maintained in accordance with the University of Wisconsin-Madison, standards for animal welfare and all protocols were approved by the university's Animal Care and Use Committee. Germ-free (GF) *Apoe*$^{-/-}$ mice (derived GF from B6.129P2-Apoe^{tm1Unc}/J; Jax 002052) were housed in a controlled environment within gnotobiotic isolators under a 12-h light/dark cycle and received autoclaved water and chow (LabDiet 5021; LabDiet, St. Louis, MO) *ad libitum*. Mice were housed with Alpha-dri® (Shepherd Specialty Papers, Kalamazoo, MI) bedding and were enriched with paper huts (Bio-Huts, Bio-

Serv, Flemington, NJ) and ALPHA-twist™ (Shepherd Specialty Papers). The GF status of GF isolators were evaluated monthly via PCR using universal 16S rRNA primers with fecal DNA as well as a growth test of feces in rich media incubated at 37 °C aerobically and anaerobically for 7 days.

Selection of human donors. Human fecal samples used in this study were collected from participants as part of the Wisconsin Longitudinal Study (WLS) (Herd et al., 2014, 2018) and stored -80°C. WLS data and specimen collection was approved by the UW-Madison Internal Review Board (2014-1066, 2015-0955) and written informed consent was obtained in the original study (Herd et al., 2018). In a previous publication from our group (Murga-Garrido et al., 2021), a subset of candidate WLS specimens were selected based on their distinct bacterial community structures and then subsequently transplanted into GF mice to measure cecal SCFA profiles. In the current study, we used this information to select three human donor samples: microbiota from donor WLS-sample-8 (referred to here as DonA); donor WLS-sample-1 (referred to here as DonB) and donor WLS-sample-5 (referred to here as DonC). In our previous study (Murga-Garrido et al., 2021), we found that gnotobiotic mice consuming a semi-purified diet containing an assortment of fibers that included resistant starch type 2 and 4, short-chain fructo-oligosaccharides, inulin, and pectin colonized with DonA, DonB or DonC accumulated different levels of SCFA. Mice colonized with DonA accumulated the highest levels of cecal butyrate (~1.5 mM) among all of the donors tested, whereas DonB-colonized mice accumulated significantly lower levels of cecal butyrate (~0.6 mM), and mice colonized with DonC showed the highest cecal propionate levels (~10 mM) and intermediate butyrate levels (~1.0 mM) (Murga-Garrido et al., 2021). All of the WLS specimens used in the current study came from subjects that self-reported consuming a

western-style diet, were overweight (BMI>25), and were not diagnosed with diabetes, cancer, or heart disease (Herd et al., 2014; Murga-Garrido et al., 2021). Identifiable information of WLS participants was blinded to the researchers in the current study.

Colonization of gnotobiotic mice with human feces and dietary treatment. At 6 weeks of age, mice were transferred to ventilated cages on an Allentown Sentry SPP IVC rack system (Allentown Inc., Allentown, NJ) and placed on irradiated FF diet which contained 10% total fiber (wt/wt) composed of 5 fermentable fibers (inulin, pectin, short-chain FOS, RS-2 and RS-4; Supplementary Fig. 2.1, Supplementary Table 1). Inclusion rates of each fermentable fiber source were individually adjusted based on purity and ash content to achieve an effective inclusion rate of 2% of dietary fiber from each fiber source. One week later, GF mice were colonized with microbiota from one of the WLS fecal specimens (DonA, DonB, or DonC) by a single oral gavage of a fecal slurry or by cohousing. Slurries were prepared anaerobically by homogenizing ~200 mg of frozen human feces in 5 mL of pre-reduced Mega Media (Murga-Garrido et al., 2021) in an anaerobic chamber, and then were immediately used to gavage recipient mice using syringes flushed with anaerobic atmosphere. A subset of GF mice was colonized by cohousing together with mice that had been gavage-colonized with human feces 4 weeks prior. Cohousing is an effective strategy for colonizing germ-free mice and is similar to gavage in terms of microbiota colonization and phenotype transfer (Bokoliya et al., 2021; Hansen et al., 2012). We were unable to detect differences in cecal microbial profiles, nor did we observe significant differences in phenotypes between cohoused mice and their gavage-colonized counterparts (Supplementary Fig. 2.2a,b, Supplementary Table 2). Therefore, we considered all mice within the same treatment group as biological replicates regardless of colonization method. Operating under the rationale that

a diet with a greater diversity of fiber sources would promote colonization of more microbes, mice were maintained on the FF diet for an additional two weeks to allow colonization to stabilize before the dietary treatment phase. Upon dietary treatment, mice either continued the FF diet or were switched to the CC diet containing 10% cellulose (Supplementary Table 1), a non-fermentable fiber control. All experimental diets in this study were vacuum packed and irradiation-sterilized by the manufacturer. The FF diet and CC diet differed only in their fiber sources. Our experimental design scheme (Supplementary Fig. 2.1) resulted in six treatment groups (three donors and two diets; n = 7-10 mice per treatment group), each of which were conducted in two separately-caged cohorts to account for cage effects. After 11 weeks of dietary treatment, mice were sacrificed at 20 weeks of age after 4 hours of fasting.

Atherosclerotic lesion analysis. Upon sacrifice, the heart was perfused with PBS buffer before being cut laterally from mid heart to the ascending aorta to contain the aortic sinus. This section was embedded in OCT compound, frozen on dry ice, and stored at -80°C until further processing. To characterize atherosclerotic plaques in the aortic sinus, the embedded tissue was sectioned on a cryostat (CM1950, Leica, Deer Park, IL) and collected on slides in 100 μm intervals, moving proximally from the base of the aortic root toward the ascending aorta. This resulted in slides containing eight equidistant sections (10 μm thickness) spanning 700 μm of the aortic sinus (0, 100, 200, 300, 400, 500, 600, 700 μm from the base of the aortic root). Formalin-fixed slides from each mouse were rinsed with 60% isopropanol for 1 minute, stained for lipids using Oil Red O for 15 minutes, and counter-stained with hematoxylin for 1 minute. Macrophage infiltration assessment of atherosclerotic plaques was conducted by incubating formalin-fixed slides (same sectioning pattern as above) overnight with macrophage antibodies (MOMA-2, 1:50; ab33451,

Abcam, Cambridge, UK) followed by incubation with secondary antibodies (1:400; ab6733, Abcam) for 1 hour and streptavidin horseradish peroxidase (1:500; P0397, Agilent, Santa Clara, CA) for 15 minutes. Sections were then washed with PBS and counterstained with DAB for 15 seconds and hematoxylin for 5 seconds. Images of all stained sections were digitally captured and then analyzed on ImageJ (National Institutes of Health, Bethesda, MD) to measure lipid-positive area, total plaque area, and MOMA-2 positive area. Plaque areas and lipid-positive areas for each mouse are expressed as averages across all eight sections. To calculate macrophage infiltration, the three sections with the largest visible lesions were selected from each mouse and their MOMA-2 positive area densities were averaged. One sample was lost during processing, so sample sizes for atherosclerosis characterization ranged from 7-10 samples per treatment group.

Cecal short-chain fatty acids. SCFA levels in cecal contents were measured using headspace gas chromatography. Samples were prepared by adding 20-150 mg of frozen cecal contents to vials (Restek, Bellefonte, PA) containing N μL of water (where N equals 300 minus the mg of cecal content) along with 2 g of NaH_2SO_4 and 1 mL of chilled 60 μM 2-butanol as an internal standard. The preparations were immediately sealed in a GC sampling vial then allowed to sit overnight at RT. Standards for acetate, propionate, isobutyrate, butyrate, isovalerate, valerate and were combined at known concentrations (pH 7.0) and serially diluted to generate a standard curve. Vials were loaded into a HS-20 headspace sampler (Shimadzu, Columbia, OH), shaken for 20 minutes at 80°C and injected onto an SH-Stabilwax 30 m column (227-36246-01, Simadzu) connected to a flame ionization detector on a CG-2010 Plus GC (Shimadzu). Running conditions were as follows: the sample vial was equilibrated at 80 kPa for 3 minutes before injection; injection was performed using a 2 mL injection loop, a 12 second loading period with the transfer line at 150°C,

1:15 split ratio, and a N_2 column flow of 1.2 mL/min; the column temperature was maintained at 40°C for 2 minutes and then increased to 200°C at a rate of 20°C/min, held for 2 minutes, and then reduced to 120°C (-20°C/min), reduced to 40°C (-40°C/min) and held at 40°C for 1 minute. Areas under the curve for each target compound were calculated with Shimadzu Lab Solution software (version 5.92) and normalized by the sample mass and the dilution factor and converted to $\mu mol \cdot g^{-1}$ using a standard curve.

Plasma triglyceride and cholesterol measurements. Blood was collected from mice while under isoflurane-induced anesthesia by cardiac puncture using an EDTA-rinsed syringe. Blood cells were separated by centrifugation then plasma was collected and stored at -80°C. Plasma levels of triglycerides, total cholesterol, and high-density lipoprotein (HDL) cholesterol, were measured using commercially available colorimetric assay kits from Waco Diagnostics (Cat. No. 994-02891, 99902601, 997-01301, respectively; Fujifilm, Tokyo, Japan) in accordance with manufacturer's instructions.

Quantitative real-time PCR. Total RNA was extracted from frozen aorta using TRIzol reagent (Invitrogen/Thermo Fisher Scientific, Waltham, MA) with two-minutes of bead-beating (BioSpec Products, Barlesville, OK) at RT in tubes containing 1.0 g of 1 mm diameter zirconium beads (BioSpec Products) and cleaned with the Qiagen RNeasy mini kit (Qiagen, Hilden, Germany). Template cDNA was synthesized using 125 ng of purified RNA in 20 μL reaction volumes. cDNA was diluted 1:1 with water then 1 μL was mixed with SYBR qPCR Mastermix (Bio-Rad, Hercules, CA) and combined with the appropriate primers (400 nM) and water for a total reaction volume of 10 μL. A list of primers is shown in Supplementary Table 3. The cycling protocol was performed

using Mastercycler® nexus (Eppendorf, Hamburg, Germany) as follows: 30 sec at 95˚C, followed by 35 cycles of 10 sec at 95˚C, 30 sec at 60˚C. A melt curve was conducted form 65˚C to 95˚C at increments of 0.5˚C at 5 sec/step. All reactions were run in duplicate and delta-delta-Ct values were calculated relative to the endogenous control (*Gapdh*).

16S rRNA gene sequencing. DNA was extracted from all mouse cecal content and feces as well as human fecal slurries using a phenol-chloroform extraction method that included a bead-beating step (Turnbaugh, Hamady, et al., 2009). 16S rRNA gene (V4) amplification was done by PCR involving unique barcodes (8-bp) both on the forward and reverse primers what are fused to Illumina adapters . The V4 amplicons from each sample were combined and submitted for sequencing on an Illumina MiSeq run (2x250 bp, Illumina, San Diego, CA) at the University of Wisconsin, Madison Biotechnology Center's DNA Sequencing Facility. Samples with less than 20% of the average sample read count were excluded, resulting in the removal of four samples from further analysis. The remaining samples ranged from 33,869 to 133,538 paired-end reads with an average of 77,704 paired-end reads per sample. Qiime2 (version 2019.10) was used to generate amplicon sequence variant (ASV) tables and taxonomy tables from the 16S rRNA reads. Demultiplexed reads were trimmed and filtered for quality with the Qiime2 DADA2 plug-in (Callahan et al., 2016). ASVs were annotated to the genus level with SILVA reference database (Quast et al., 2013) (version 132) using Naïve Bayes classifier in Qiime2. All subsequent analysis were conducted in R. ASV-level feature counts normalized by converting to relative abundance. ASVs were filtered to include only those with at least 0.0001 average relative abundance across all cecal samples. For genus-level analysis, a cutoff was set at 0.0005 average relative abundance across all samples. These cutoffs were also applied to the fecal sample ASV and genera profiles

(human inoculum fecal slurries and pre-dietary treatment mouse feces). Engraftment efficiency was calculated as the number of features that were detected in the pre-treatment mouse feces of at least one animal per donor- or donor/diet-group divided by the number of features detected in the donor fecal slurry. Positive detection was defined as any feature (ASV or genus) that was found to be greater than 0.0001 relative abundance in a given sample.

Shotgun sequencing. Genomic DNA isolated from the cecal contents of 5 mice per treatment group was used for metagenomic analysis. Libraries were prepared using the Illumina TruSeq PCR-free kit following vendor protocols and sequenced at the University of Wisconsin Biotechnology Center's DNA Sequencing Facility. All samples were run on a single NovaSeq6000 2x150 S4-Flowcell lane. The resulting sequences were trimmed for quality using Trimmomatic (version 0-39) and then aligned against reference host genomes (*Mus musculus* GRCm38_Rel98) with bowtie2 (version 2.3.4) to remove host reads (average host alignment rate was 5.3%) leaving only high-quality, non-host reads. Cleaning ultimately resulted in an average of 29.4 million paired-end reads per sample.

Functional annotation. Reads remaining after trimming and removal of host sequences were concatenated into a single fastq file and fed into HUMAnN3 (version 3.0.0.alpha.4) for functional annotation. This resulted in a UniRef90 (Suzek et al., 2015) gene family abundance table in reads per kilobase, and a relative abundance table of microbial taxa for each mouse. The UniRef90 gene family abundance tables were converted to KO counts per million (CPM) abundance tables with the human_regroup_table and human_renorm_table functions. Differential abundance analysis was conducted on KOs that were present in at least 25% of samples.

CAZyme annotation. CAZyme profiles of each sample were predicted using run_dbcan (version 2.0.11). We assembled cleaned (trimmed, host-free) reads into contigs with metaSPAdes (version 3.14.0) with multiple k-mer sizes (metaspades.py -k 21, 33, 55, 77). Contigs shorter than 500 bp were discarded from further processing. Open reading frames (ORFs; i.e., microbial metagenes), were predicted from assembled contigs via Prodigal (version 2.6.3) using Hidden Markov Model (HMM) with default parameters. All predicted genes shorter than 100 bp were discarded from further processing. Nucleotide ORF sequences were converted amino acid sequences and were used as input for run_dbcan (version 2.0.11) to predict CAZyme profiles. CAZyme annotation was accepted if an ORF was annotated by >= 2 tools (DIAMOND, HMMER, Hotpep). This resulted in a table indicating the presence or absence of each CAZyme family in the CAZyme database. To estimate CAZyme abundance, each CAZyme family was assigned a count-per-million (CPM) value of its associated ORF as predicted by Prodigal. If multiple CAZymes were predicted from the same ORF, they were all assigned the ORF's CPM value.

Microbiome analysis. PCoA plots and diversity measures were generated using 16S rRNA ASV profiles with the phyloseq (version 1.40.0) package in R. All pairwise PERMANOVA tests were conducted between dietary groups within each donor group using the pairwiseAdonis (version 0.4) R package with 9999 permutations. Feature-level differential abundance analysis of 16S rRNA amplicon taxonomy, shotgun metagenomic KO abundances and shotgun metagenomic CAZyme abundances were conducted using the MaAsLin 2 function within the MaAsLin 2 (version 1.10.0) R package with default settings (Mallick et al., 2021). To assess KO pathway enrichment, sets of KOs that were significantly upregulated by FF feeding (MaAsLin 2 differential abundance, adjusted *P*-value <0.1) were generated for each donor group and used as input for the

PerformKOEnrichAnalysis_KO01100 function within the MicrobiomeAnalyistR (version 0.0.0.9000) package in R with default parameters. This resulted in a list of KEGG pathways that were significantly (P-value <0.05) overrepresented in FF-fed mice within each donor group. CAZymes families were considered to be highly differential if they belonged to the top 10% of CAZymes ordered by MaAsLin 2 effect size within each donor group, regardless of direction (absolute value of effect size).

Statistical analysis. Unless otherwise noted, comparisons of means were conducted using a two-sided Wilcoxon rank-sum test between dietary groups within each donor group. Equal variance was determined for all means tests (Levene's test, P-value >0.05) except comparisons of atherosclerotic plaques (size, lipid content, macrophage infiltration) and cecal SCFA levels which were found to have significantly different variances between diets (Levene's test, P-value <0.05). Correlations between CAZymes and cecal SCFA levels were conducted using all mice to calculate Spearman's rank correlation coefficient. P-value adjustment for PERMANOVA was done using the Bonferroni method, while all other adjusted P-values were calculated using the Benjamini-Hochberg method.

DATA AVAILABILITY

Sequencing data reported in this study is available at the European Nucleotide Archive (ENA) under the study accession number PRJEB58699.

CODE AVAILABILITY

The code used in this study is available upon request.

ACKNOWLEDGEMENTS

The authors thank Dr. Barbara Mickelson (Envigo) for assistance with diets. We also thank the University of Wisconsin Biotechnology Center's DNA Sequencing Facility for providing sequencing and support services. We thank the University of Wisconsin Center for High Throughput Computing (CHTC) in the Department of Computer Sciences for providing computational resources, support, and assistance. This work was partly supported by grants from NIH HL144651 (FER, QZ), HL148577 (FER, KK, EIV), and EB030340 (FER, ERH). This work was also supported by a grant from a Transatlantic Networks of Excellence Award from the Leducq Foundation (17CVD01). ERH was supported in part by the Metabolism and Nutrition Training Program NIH T32 (DK007665) and by the University of Wisconsin-Madison Food Research Institute (Robert H. and Carol L. Deibel Distinguished Graduate Fellowship in Probiotic Research). T-WLC was supported by the National Institutes of Health, under Ruth L. Kirschstein National Research Service Award T32 HL007936 from the National Heart Lung and Blood Institute to the University of Wisconsin-Madison Cardiovascular Research Center.

COMPETING INTERESTS

The authors of this study have no financial or non-financial competing interests.

REFERENCES

Aguilar, E. C., Leonel, A. J., Teixeira, L. G., Silva, A. R., Silva, J. F., Pelaez, J. M. N., Capettini, L. S. A., Lemos, V. S., Santos, R. A. S., & Alvarez-Leite, J. I. (2014). Butyrate impairs atherogenesis by reducing plaque inflammation and vulnerability and decreasing NFκB activation. *Nutrition, Metabolism and Cardiovascular Diseases*, *24* (6), 606–613. https://doi.org/10.1016/j.numecd.2014.01.002

Ahmad, F. B. (2021). Provisional Mortality Data—United States, 2020. *MMWR. Morbidity and Mortality Weekly Report*, *70*. https://doi.org/10.15585/mmwr.mm7014e1

Bokoliya, S. C., Dorsett, Y., Panier, H., & Zhou, Y. (2021). Procedures for Fecal Microbiota Transplantation in Murine Microbiome Studies. *Frontiers in Cellular and Infection Microbiology*, *11*. https://www.frontiersin.org/articles/10.3389/fcimb.2021.711055

Callahan, B. J., McMurdie, P. J., Rosen, M. J., Han, A. W., Johnson, A. J. A., & Holmes, S. P. (2016). DADA2: High resolution sample inference from Illumina amplicon data. *Nature Methods*, *13* (7), 581–583. https://doi.org/10.1038/nmeth.3869

Cankar, K., Kortstee, A., Toonen, M. A. J., Wolters-Arts, M., Houbein, R., Mariani, C., Ulvskov, P., Jorgensen, B., Schols, H. A., Visser, R. G. F., & Trindade, L. M. (2014). Pectic arabinan side chains are essential for pollen cell wall integrity during pollen development. *Plant Biotechnology Journal*, *12* (4), 492–502. https://doi.org/10.1111/pbi.12156

Chong, J., Liu, P., Zhou, G., & Xia, J. (2020). Using MicrobiomeAnalyst for comprehensive statistical, functional, and meta-analysis of microbiome data. *Nature Protocols*, *15* (3), Article 3. https://doi.org/10.1038/s41596-019-0264-1

Chung, H., Pamp, S. J., Hill, J. A., Surana, N. K., Edelman, S. M., Troy, E. B., Reading, N. C., Villablanca, E. J., Wang, S., Mora, J. R., Umesaki, Y., Mathis, D., Benoist, C., Relman, D.

A., & Kasper, D. L. (2012). Gut Immune Maturation Depends on Colonization with a Host-Specific Microbiota. *Cell*, *149* (7), 1578–1593. https://doi.org/10.1016/j.cell.2012.04.037

Contijoch, E. J., Britton, G. J., Yang, C., Mogno, I., Li, Z., Ng, R., Llewellyn, S. R., Hira, S., Johnson, C., Rabinowitz, K. M., Barkan, R., Dotan, I., Hirten, R. P., Fu, S.-C., Luo, Y., Yang, N., Luong, T., Labrias, P. R., Lira, S., … Faith, J. J. (2019). Gut microbiota density influences host physiology and is shaped by host and microbial factors. *eLife*, *8*, e40553. https://doi.org/10.7554/eLife.40553

Cummings, J. H. (1984). Cellulose and the human gut. *Gut*, *25* (8), 805–810.

Deehan, E. C., Yang, C., Perez-Muñoz, M. E., Nguyen, N. K., Cheng, C. C., Triador, L., Zhang, Z., Bakal, J. A., & Walter, J. (2020). Precision Microbiome Modulation with Discrete Dietary Fiber Structures Directs Short-Chain Fatty Acid Production. *Cell Host & Microbe*, *27* (3), 389-404.e6. https://doi.org/10.1016/j.chom.2020.01.006

Denson, L. A., Curran, M., McGovern, D. P. B., Koltun, W. A., Duerr, R. H., Kim, S. C., Sartor, R. B., Sylvester, F. A., Abraham, C., de Zoeten, E. F., Siegel, C. A., Burns, R. M., Dobes, A. M., Shtraizent, N., Honig, G., Heller, C. A., Hurtado-Lorenzo, A., & Cho, J. H. (2019). Challenges in IBD Research: Precision Medicine. *Inflammatory Bowel Diseases*, *25* (Suppl 2), S31–S39. https://doi.org/10.1093/ibd/izz078

Earley, H., Lennon, G., Balfe, Á., Coffey, J. C., Winter, D. C., & O'Connell, P. R. (2019). The abundance of Akkermansia muciniphila and its relationship with sulphated colonic mucins in health and ulcerative colitis. *Scientific Reports*, *9* (1), 15683. https://doi.org/10.1038/s41598-019-51878-3

Goodman, A. L., Kallstrom, G., Faith, J. J., Reyes, A., Moore, A., Dantas, G., & Gordon, J. I. (2011). Extensive personal human gut microbiota culture collections characterized and

manipulated in gnotobiotic mice. *Proceedings of the National Academy of Sciences*, *108* (15), 6252–6257. https://doi.org/10.1073/pnas.1102938108

Gophna, U., Konikoff, T., & Nielsen, H. B. (2017). Oscillospira and related bacteria – From metagenomic species to metabolic features. *Environmental Microbiology*, *19* (3), 835–841. https://doi.org/10.1111/1462-2920.13658

Haghikia, A., Zimmermann, F., Schumann, P., Jasina, A., Roessler, J., Schmidt, D., Heinze, P., Kaisler, J., Nageswaran, V., Aigner, A., Ceglarek, U., Cineus, R., Hegazy, A. N., van der Vorst, E. P. C., Döring, Y., Strauch, C. M., Nemet, I., Tremaroli, V., Dwibedi, C., … Landmesser, U. (2021). Propionate attenuates atherosclerosis by immune-dependent regulation of intestinal cholesterol metabolism. *European Heart Journal*, ehab644. https://doi.org/10.1093/eurheartj/ehab644

Hansen, C. H. F., Nielsen, D. S., Kverka, M., Zakostelska, Z., Klimesova, K., Hudcovic, T., Tlaskalova-Hogenova, H., & Hansen, A. K. (2012). Patterns of Early Gut Colonization Shape Future Immune Responses of the Host. *PLOS ONE*, *7* (3), e34043. https://doi.org/10.1371/journal.pone.0034043

Healey, G. R., Murphy, R., Brough, L., Butts, C. A., & Coad, J. (2017). Interindividual variability in gut microbiota and host response to dietary interventions. *Nutrition Reviews*, *75* (12), 1059–1080. https://doi.org/10.1093/nutrit/nux062

Herd, P., Carr, D., & Roan, C. (2014). Cohort Profile: Wisconsin longitudinal study (WLS). *International Journal of Epidemiology*, *43* (1), 34–41. https://doi.org/10.1093/ije/dys194

Herd, P., Schaeffer, N. C., DiLoreto, K., Jacques, K., Stevenson, J., Rey, F., & Roan, C. (2018). The Influence of Social Conditions Across the Life Course on the Human Gut Microbiota:

A Pilot Project With the Wisconsin Longitudinal Study. *The Journals of Gerontology: Series B*, *73* (1), 124–133. https://doi.org/10.1093/geronb/gbx029

Higginson, J., & Pepler, W. J. (1954). Fat Intake, Serum Cholesterol Concentration, and Atherosclerosis in the South African Bantu. Part II. Atherosclerosis and Coronary Artery Disease. *The Journal of Clinical Investigation*, *33* (10), 1366–1371. https://doi.org/10.1172/JCI103013

Hofmann, M. A., Lalla, E., Lu, Y., Gleason, M. R., Wolf, B. M., Tanji, N., Ferran, L. J., Kohl, B., Rao, V., Kisiel, W., Stern, D. M., & Schmidt, A. M. (2001). Hyperhomocysteinemia enhances vascular inflammation and accelerates atherosclerosis in a murine model. *The Journal of Clinical Investigation*, *107* (6), 675–683. https://doi.org/10.1172/JCI10588

Hoving, L. R., De Vries, M. R., De Jong, R. C. M., Katiraei, S., Pronk, A., Quax, P. H. A., Van Harmelen, V., & Willems van Dijk, K. (2018). The Prebiotic Inulin Aggravates Accelerated Atherosclerosis in Hypercholesterolemic APOE*3-Leiden Mice. *Nutrients*, *10* (2), Article 2. https://doi.org/10.3390/nu10020172

Hughes, R. L., Marco, M. L., Hughes, J. P., Keim, N. L., & Kable, M. E. (2019). The Role of the Gut Microbiome in Predicting Response to Diet and the Development of Precision Nutrition Models—Part I: Overview of Current Methods. *Advances in Nutrition*, *10* (6), 953–978. https://doi.org/10.1093/advances/nmz022

Javdan, B., Lopez, J. G., Chankhamjon, P., Lee, Y.-C. J., Hull, R., Wu, Q., Wang, X., Chatterjee, S., & Donia, M. S. (2020). Personalized Mapping of Drug Metabolism by the Human Gut Microbiome. *Cell*, *181* (7), 1661-1679.e22. https://doi.org/10.1016/j.cell.2020.05.001

Jie, Z., Xia, H., Zhong, S.-L., Feng, Q., Li, S., Liang, S., Zhong, H., Liu, Z., Gao, Y., Zhao, H., Zhang, D., Su, Z., Fang, Z., Lan, Z., Li, J., Xiao, L., Li, J., Li, R., Li, X., … Kristiansen,

K. (2017). The gut microbiome in atherosclerotic cardiovascular disease. *Nature Communications*, *8* (1), Article 1. https://doi.org/10.1038/s41467-017-00900-1

Kasahara, K., Krautkramer, K. A., Org, E., Romano, K. A., Kerby, R. L., Vivas, E. I., Mehrabian, M., Denu, J. M., Bäckhed, F., Lusis, A. J., & Rey, F. E. (2018). Interactions between Roseburia intestinalis and diet modulate atherogenesis in a murine model. *Nature Microbiology*, *3* (12), 1461. https://doi.org/10.1038/s41564-018-0272-x

Kelly, T. N., Bazzano, L. A., Ajami, N. J., He, H., Zhao, J., Petrosino, J. F., Correa, A., & He, J. (2016). Gut Microbiome Associates With Lifetime Cardiovascular Disease Risk Profile Among Bogalusa Heart Study Participants. *Circulation Research*, *119* (8), 956–964. https://doi.org/10.1161/CIRCRESAHA.116.309219

Kim, Y., Hwang, S. W., Kim, S., Lee, Y.-S., Kim, T.-Y., Lee, S.-H., Kim, S. J., Yoo, H. J., Kim, E. N., & Kweon, M.-N. (2020). Dietary cellulose prevents gut inflammation by modulating lipid metabolism and gut microbiota. *Gut Microbes*, *11* (4), 944–961. https://doi.org/10.1080/19490976.2020.1730149

Kirk, D., Catal, C., & Tekinerdogan, B. (2021). Precision nutrition: A systematic literature review. *Computers in Biology and Medicine*, *133*, 104365. https://doi.org/10.1016/j.compbiomed.2021.104365

Kolodziejczyk, A. A., Zheng, D., & Elinav, E. (2019). Diet–microbiota interactions and personalized nutrition. *Nature Reviews Microbiology*, *17* (12), Article 12. https://doi.org/10.1038/s41579-019-0256-8

Koppel, N., Bisanz, J. E., Pandelia, M.-E., Turnbaugh, P. J., & Balskus, E. P. (2018). Discovery and characterization of a prevalent human gut bacterial enzyme sufficient for the

inactivation of a family of plant toxins. *eLife*, *7*, e33953. https://doi.org/10.7554/eLife.33953

Kozich, J. J., Westcott, S. L., Baxter, N. T., Highlander, S. K., & Schloss, P. D. (2013). Development of a Dual-Index Sequencing Strategy and Curation Pipeline for Analyzing Amplicon Sequence Data on the MiSeq Illumina Sequencing Platform. *Applied and Environmental Microbiology*, *79* (17), 5112–5120. https://doi.org/10.1128/AEM.01043-13

Kritchevsky, D. (1978). Fiber, lipids, and atherosclerosis. *The American Journal of Clinical Nutrition*, *31* (10), S65–S74. https://doi.org/10.1093/ajcn/31.10.S65

Lee, J. R., Muthukumar, T., Dadhania, D., Taur, Y., Jenq, R. R., Toussaint, N. C., Ling, L., Pamer, E., & Suthanthiran, M. (2015). Gut Microbiota and Tacrolimus Dosing in Kidney Transplantation. *PLOS ONE*, *10* (3), e0122399. https://doi.org/10.1371/journal.pone.0122399

Leshem, A., Segal, E., & Elinav, E. (2020). The Gut Microbiome and Individual-Specific Responses to Diet. *mSystems*, *5* (5), e00665-20. https://doi.org/10.1128/mSystems.00665-20

Libby Peter. (2012). Inflammation in Atherosclerosis. *Arteriosclerosis, Thrombosis, and Vascular Biology*, *32* (9), 2045–2051. https://doi.org/10.1161/ATVBAHA.108.179705

Mallick, H., Rahnavard, A., McIver, L. J., Ma, S., Zhang, Y., Nguyen, L. H., Tickle, T. L., Weingart, G., Ren, B., Schwager, E. H., Chatterjee, S., Thompson, K. N., Wilkinson, J. E., Subramanian, A., Lu, Y., Waldron, L., Paulson, J. N., Franzosa, E. A., Bravo, H. C., & Huttenhower, C. (2021). Multivariable association discovery in population-scale meta-omics studies. *PLOS Computational Biology*, *17* (11), e1009442. https://doi.org/10.1371/journal.pcbi.1009442

Mathers, C., Stevens, G., Hogan, D., Mahanani, W. R., & Ho, J. (2017). Global and Regional Causes of Death: Patterns and Trends, 2000–15. In *Disease Control Priorities: Improving Health and Reducing Poverty. 3rd edition*. The International Bank for Reconstruction and Development / The World Bank. https://doi.org/10.1596/978-1-4648-0527-1_ch4

McCully, K. (2015). Homocysteine and the pathogenesis of atherosclerosis. *Expert Review of Clinical Pharmacology*, *8*, 1–9. https://doi.org/10.1586/17512433.2015.1010516

McCully, K. S. (1969). Vascular pathology of homocysteinemia: Implications for the pathogenesis of arteriosclerosis. *The American Journal of Pathology*, *56* (1), 111–128.

McOrist, A. L., Miller, R. B., Bird, A. R., Keogh, J. B., Noakes, M., Topping, D. L., & Conlon, M. A. (2011). Fecal Butyrate Levels Vary Widely among Individuals but Are Usually Increased by a Diet High in Resistant Starch. *The Journal of Nutrition*, *141* (5), 883–889. https://doi.org/10.3945/jn.110.128504

Murga-Garrido, S. M., Hong, Q., Cross, T.-W. L., Hutchison, E. R., Han, J., Thomas, S. P., Vivas, E. I., Denu, J., Ceschin, D. G., Tang, Z.-Z., & Rey, F. E. (2021). Gut microbiome variation modulates the effects of dietary fiber on host metabolism. *Microbiome*, *9* (1), 117. https://doi.org/10.1186/s40168-021-01061-6

Ohira, H., Tsutsui, W., & Fujioka, Y. (2017). Are Short Chain Fatty Acids in Gut Microbiota Defensive Players for Inflammation and Atherosclerosis? *Journal of Atherosclerosis and Thrombosis*, *24* (7), 660–672. https://doi.org/10.5551/jat.RV17006

Ordovas, J. M., & Berciano, S. (2020). Personalized nutrition and healthy aging. *Nutrition Reviews*, *78* (12 Suppl 2), 58–65. https://doi.org/10.1093/nutrit/nuaa102

Quast, C., Pruesse, E., Yilmaz, P., Gerken, J., Schweer, T., Yarza, P., Peplies, J., & Glöckner, F. O. (2013). The SILVA ribosomal RNA gene database project: Improved data processing

and web-based tools. *Nucleic Acids Research*, *41* (D1), D590–D596. https://doi.org/10.1093/nar/gks1219

Rault-Nania, M.-H., Gueux, E., Demougeot, C., Demigné, C., Rock, E., & Mazur, A. (2006). Inulin attenuates atherosclerosis in apolipoprotein E-deficient mice. *British Journal of Nutrition*, *96* (5), 840–844. https://doi.org/10.1017/BJN20061913

Ross, R. (1999). Atherosclerosis—An Inflammatory Disease. *New England Journal of Medicine*, *340* (2), 115–126. https://doi.org/10.1056/NEJM199901143400207

Suzek, B. E., Wang, Y., Huang, H., McGarvey, P. B., Wu, C. H., & the UniProt Consortium. (2015). UniRef clusters: A comprehensive and scalable alternative for improving sequence similarity searches. *Bioinformatics*, *31* (6), 926–932. https://doi.org/10.1093/bioinformatics/btu739

Tang, W. H. W., & Hazen, S. L. (2017). The Gut Microbiome and Its Role in Cardiovascular Diseases. *Circulation*, *135* (11), 1008–1010. https://doi.org/10.1161/CIRCULATIONAHA.116.024251

Threapleton, D. E., Greenwood, D. C., Evans, C. E. L., Cleghorn, C. L., Nykjaer, C., Woodhead, C., Cade, J. E., Gale, C. P., & Burley, V. J. (2013). Dietary fibre intake and risk of cardiovascular disease: Systematic review and meta-analysis. *BMJ*, *347*, f6879. https://doi.org/10.1136/bmj.f6879

Torres, N., Guevara-Cruz, M., Velázquez-Villegas, L. A., & Tovar, A. R. (2015). Nutrition and Atherosclerosis. *Archives of Medical Research*, *46* (5), 408–426. https://doi.org/10.1016/j.arcmed.2015.05.010

Turnbaugh, P. J., Hamady, M., Yatsunenko, T., Cantarel, B. L., Duncan, A., Ley, R. E., Sogin, M. L., Jones, W. J., Roe, B. A., Affourtit, J. P., Egholm, M., Henrissat, B., Heath, A. C.,

Knight, R., & Gordon, J. I. (2009). A core gut microbiome in obese and lean twins. *Nature*, *457* (7228), Article 7228. https://doi.org/10.1038/nature07540

Turnbaugh, P. J., Ley, R. E., Hamady, M., Fraser-Liggett, C. M., Knight, R., & Gordon, J. I. (2007). The Human Microbiome Project. *Nature*, *449* (7164), 804–810. https://doi.org/10.1038/nature06244

Turnbaugh, P. J., Ridaura, V. K., Faith, J. J., Rey, F. E., Knight, R., & Gordon, J. I. (2009). The Effect of Diet on the Human Gut Microbiome: A Metagenomic Analysis in Humanized Gnotobiotic Mice. *Science Translational Medicine*, *1* (6), 6ra14-6ra14. https://doi.org/10.1126/scitranslmed.3000322

Vital, M., Howe, A. C., & Tiedje, J. M. (2014). Revealing the Bacterial Butyrate Synthesis Pathways by Analyzing (Meta)genomic Data. *mBio*, *5* (2). https://doi.org/10.1128/mBio.00889-14

Wang, Z., Klipfell, E., Bennett, B. J., Koeth, R., Levison, B. S., DuGar, B., Feldstein, A. E., Britt, E. B., Fu, X., Chung, Y.-M., Wu, Y., Schauer, P., Smith, J. D., Allayee, H., Tang, W. H. W., DiDonato, J. A., Lusis, A. J., & Hazen, S. L. (2011). Gut flora metabolism of phosphatidylcholine promotes cardiovascular disease. *Nature*, *472* (7341), Article 7341. https://doi.org/10.1038/nature09922

Weeke, P., & Roden, D. M. (2013). Pharmacogenomics and Cardiovascular Disease. *Current Cardiology Reports*, *15* (7), 376. https://doi.org/10.1007/s11886-013-0376-0

Xue, H., Chen, X., Yu, C., Deng, Y., Zhang, Y., Chen, S., Chen, X., Chen, K., Yang, Y., & Ling, W. (2022). Gut Microbially Produced Indole-3-Propionic Acid Inhibits Atherosclerosis by Promoting Reverse Cholesterol Transport and Its Deficiency Is Causally Related to

Atherosclerotic Cardiovascular Disease. *Circulation Research*, *131* (5), 404–420. https://doi.org/10.1161/CIRCRESAHA.122.321253

Zeevi, D., Korem, T., Zmora, N., Israeli, D., Rothschild, D., Weinberger, A., Ben-Yacov, O., Lador, D., Avnit-Sagi, T., Lotan-Pompan, M., Suez, J., Mahdi, J. A., Matot, E., Malka, G., Kosower, N., Rein, M., Zilberman-Schapira, G., Dohnalová, L., Pevsner-Fischer, M., … Segal, E. (2015). Personalized Nutrition by Prediction of Glycemic Responses. *Cell*, *163* (5), 1079–1094. https://doi.org/10.1016/j.cell.2015.11.001

Zhang, Y., Hu, J., Tan, H., Zhong, Y., & Nie, S. (2022). Akkermansia muciniphila, an important link between dietary fiber and host health. *Current Opinion in Food Science*, 100905. https://doi.org/10.1016/j.cofs.2022.100905

Zimmermann, M., Zimmermann-Kogadeeva, M., Wegmann, R., & Goodman, A. L. (2019a). Mapping human microbiome drug metabolism by gut bacteria and their genes. *Nature*, *570* (7762), 462–467. https://doi.org/10.1038/s41586-019-1291-3

Zimmermann, M., Zimmermann-Kogadeeva, M., Wegmann, R., & Goodman, A. L. (2019b). Separating host and microbiome contributions to drug pharmacokinetics and toxicity. *Science (New York, N.Y.)*, *363* (6427), eaat9931. https://doi.org/10.1126/science.aat9931

FIGURES

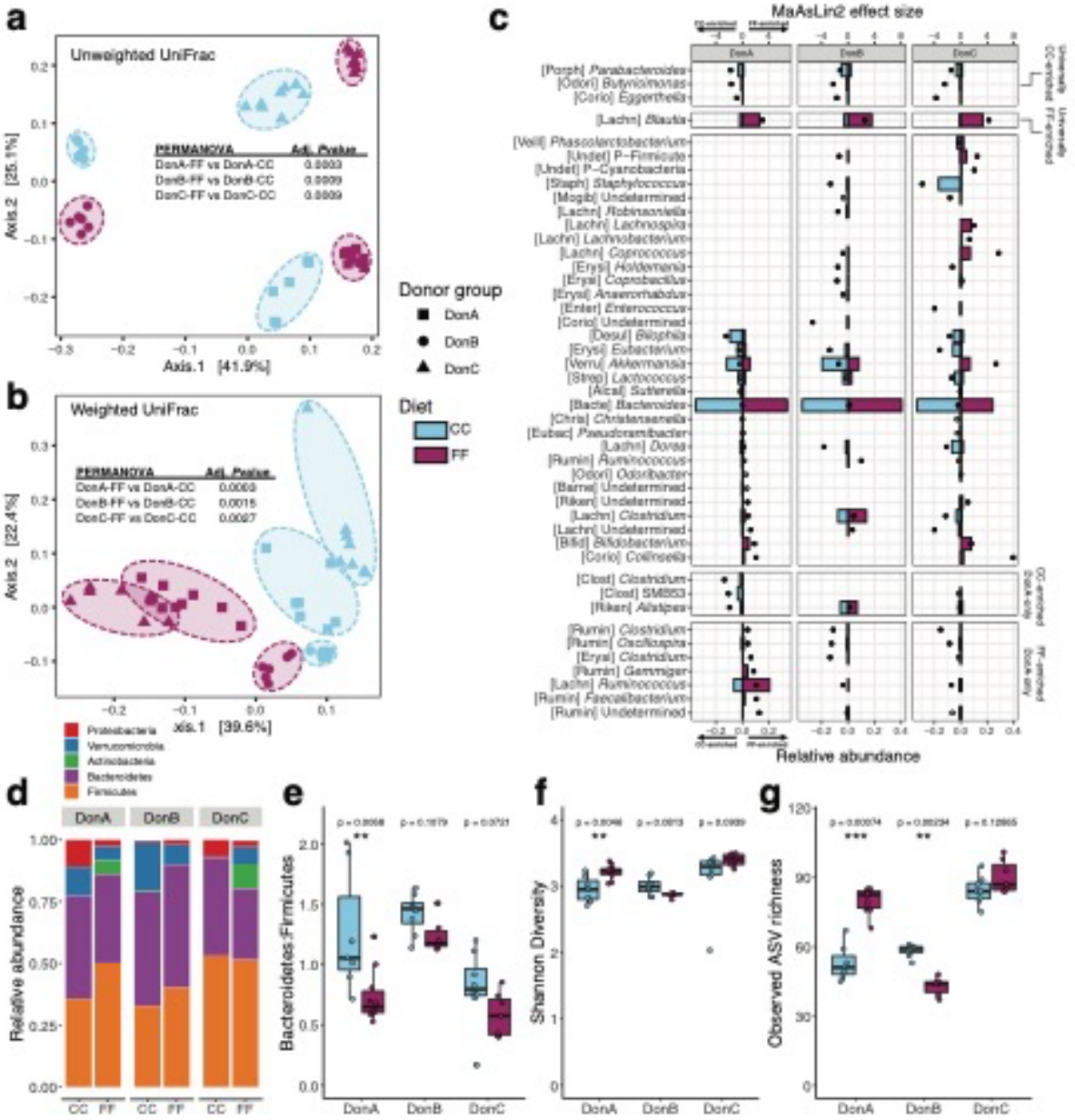

Figure 2.1 Effects of dietary fiber on microbial community structure in gnotobiotic mice colonized with different human communities. **a**, **b** Principal Coordinate Analysis (PCoA) of unweighted and weighted UniFrac distances of 16S rRNA V4 ASVs; magenta = Fermentable Fiber (FF), blue = Cellulose Control (CC). Animals colonized with fecal samples from three different donors: DonA, DonB, and DonC. **c** Relative abundances of genus-level taxa for the two diets (bottom x-axis, colored bars) along with between-diet differential abundance (MaAsLin 2) effect

sizes (top x-axis, dots). Significant differences in abundance for taxa within each donor group are denoted by a solid dot (adjusted *P*-value <0.1) and open circles denote no significant change (adjusted *P*-value >0.1). The dot's orientation relative to the origin represents the effect of diet on the abundance of each taxa (negative values correspond to CC abundances, positive values correspond to FF abundances). The first 5 letters of the family encompassing each taxon is shown in brackets; if the family is undetermined the taxon phylum is listed instead and noted with a "P-". **d** Relative abundance of Phylum-level taxa as a function of diet and donor group. **e** Bacteroidetes to Firmicutes ratio. **f**, **g** Shannon diversity index and observed richness. Box and whisker plots denote the interquartile range, median, and spread of points within 1.5 times the interquartile range along with individual data points. Comparisons on means (n = 7-10/diet/donor group) conducted with Wilcoxon test, * P <0.05, ** P <0.01, *** P <0.001.

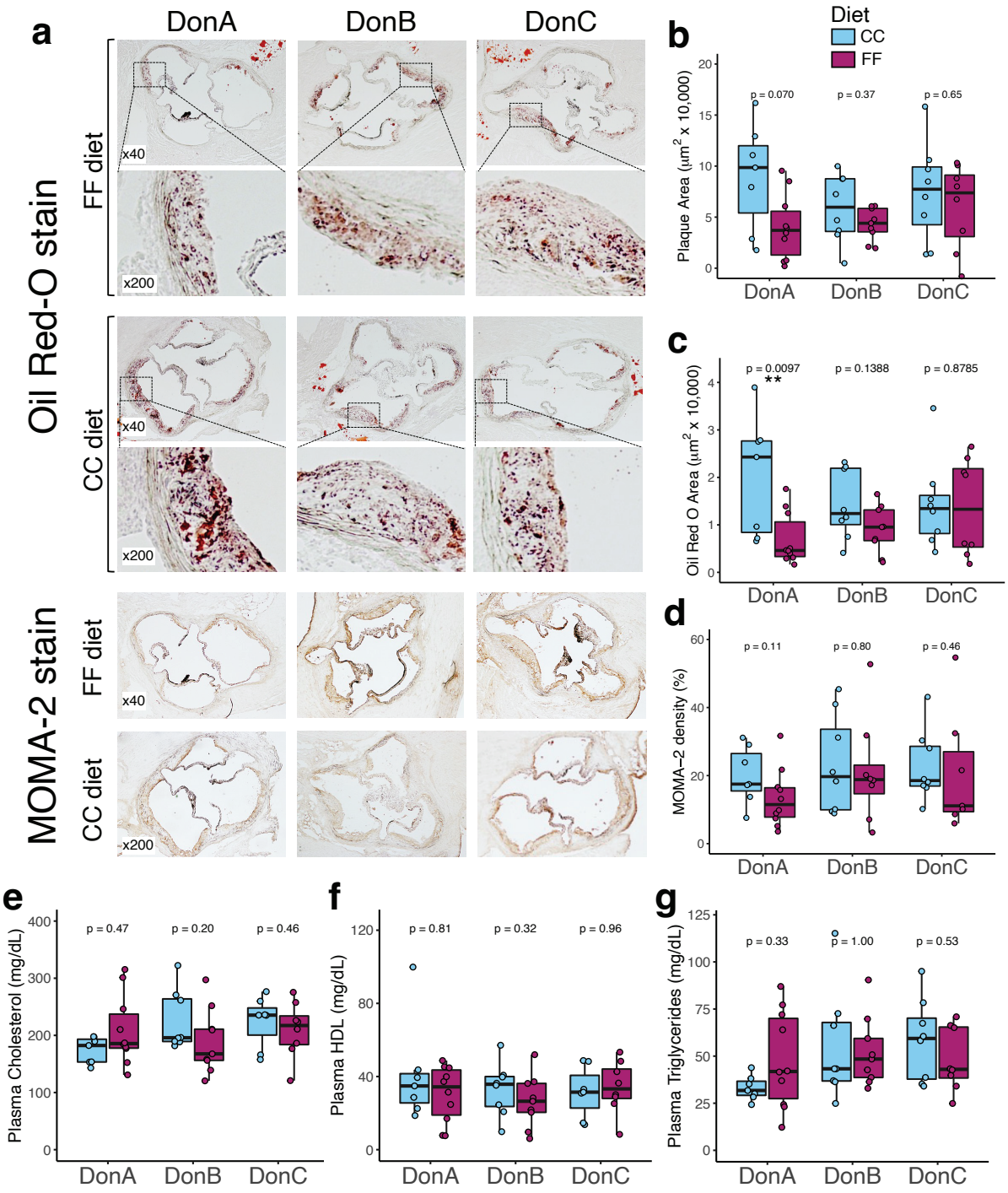

Figure 2.2 Atherosclerosis response to dietary fiber in mice colonized with different human communities. Atherosclerosis was measured in GF *Apoe*$^{-/-}$ mice colonized with human fecal communities DonA, DonB, and DonC and fed either fermentable fiber diet (FF, magenta), or a

cellulose control diet (CC, blue). **a** Representative Oil Red O staining and MOMA-2 antibody staining of aortic sinus cross-sections content. Quantification of plaque average area (**a**), lipid positive area (**b**) or MOMA-2 positive area (**c**). Plasma levels of total cholesterol (**a**), HDL-cholesterol (**b**) and triglycerides (**c**). Box and whisker plots denote the interquartile range, median, and spread of points within 1.5 times the interquartile range along with individual data points. Comparisons of means between diets within each donor group (n = 7-10/diet/donor group) were conducted using a Wilcoxon test with appropriate correction for equal variance assumption (Levenes' test), * $P < 0.05$, ** $P < 0.01$.

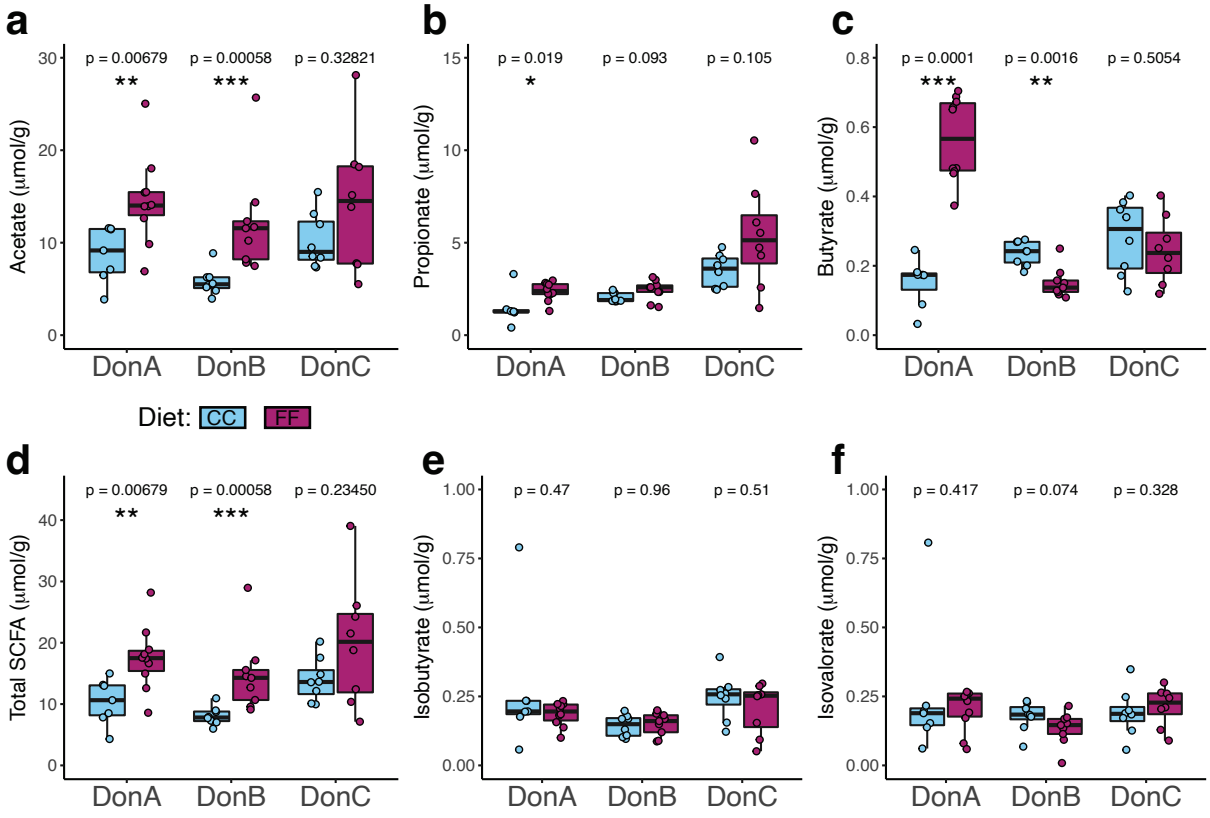

Figure 2.3 Effect of dietary fiber on cecal levels of SCFAs and branched-chain fatty acids. Cecal levels of acetate (**a**), propionate (**b**), butyrate (**c**), total SCFAs (sum of acetate, propionate, and butyrate, **d**), isobutyrate (**e**) and isovalerate (**f**). Data expressed per gram of cecal content wet weight. Box and whisker plots denote the interquartile range, median, and spread of points within 1.5 times the interquartile range along with individual data points. Comparisons of means between diets within each donor group (n = 7-10/diet/donor group) were conducted using a Wilcoxon test, * P <0.05, ** P <0.01, *** P <0.001.

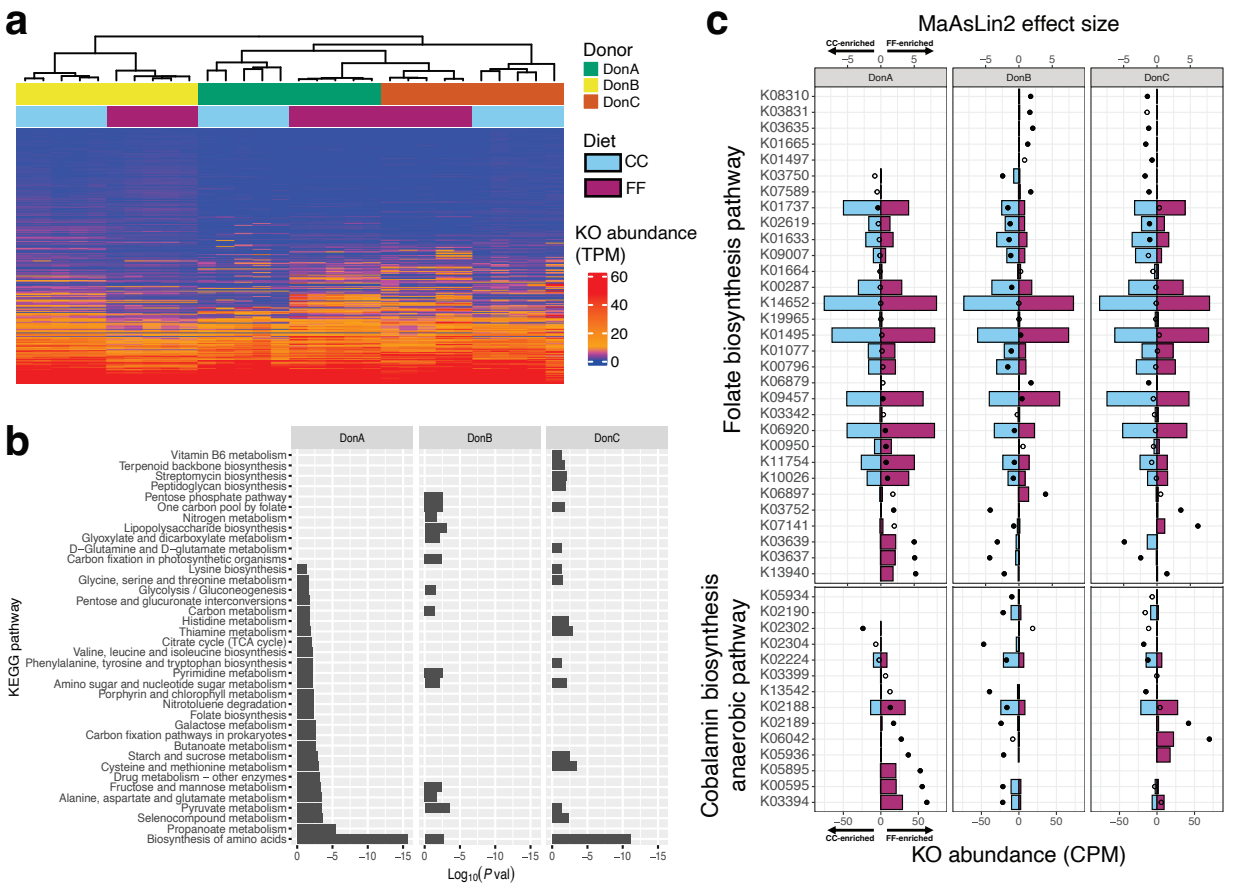

Figure 2.4 Effect of dietary fiber on KEGG orthology profiles and metagenomic pathway enrichment across donor groups. **a** Heatmap of KO profiles expressed in CPM for each mouse. Individual profiles were clustered using the spearman hierarchical clustering method. **b** Overrepresented KEGG pathways and their significance (represented as the $\log_{10}$ of the enrichment *P*-value) identified by pathway enrichment analysis using lists of KOs from each donor group that were significantly upregulated (MaAsLin 2 differential abundance, adjusted *P*-value <0.1). **c** MaAsLin 2 differential abundance (bottom axis, colored bars) and effect size (top axis, solid dot = adjusted *P*-value <0.1, open dot = adjusted *P*-value >0.1) of KOs involved in folate biosynthesis and cobalamin (vitamin B12) biosynthesis. Negative values reflect KO abundance (CPM) in CC-

fed mice and effect sizes (MaAsLin 2 coefficient) favoring the CC condition, while positive values indicate KOs abundances and effect sizes in the FF condition (n = 5/diet/donor group).

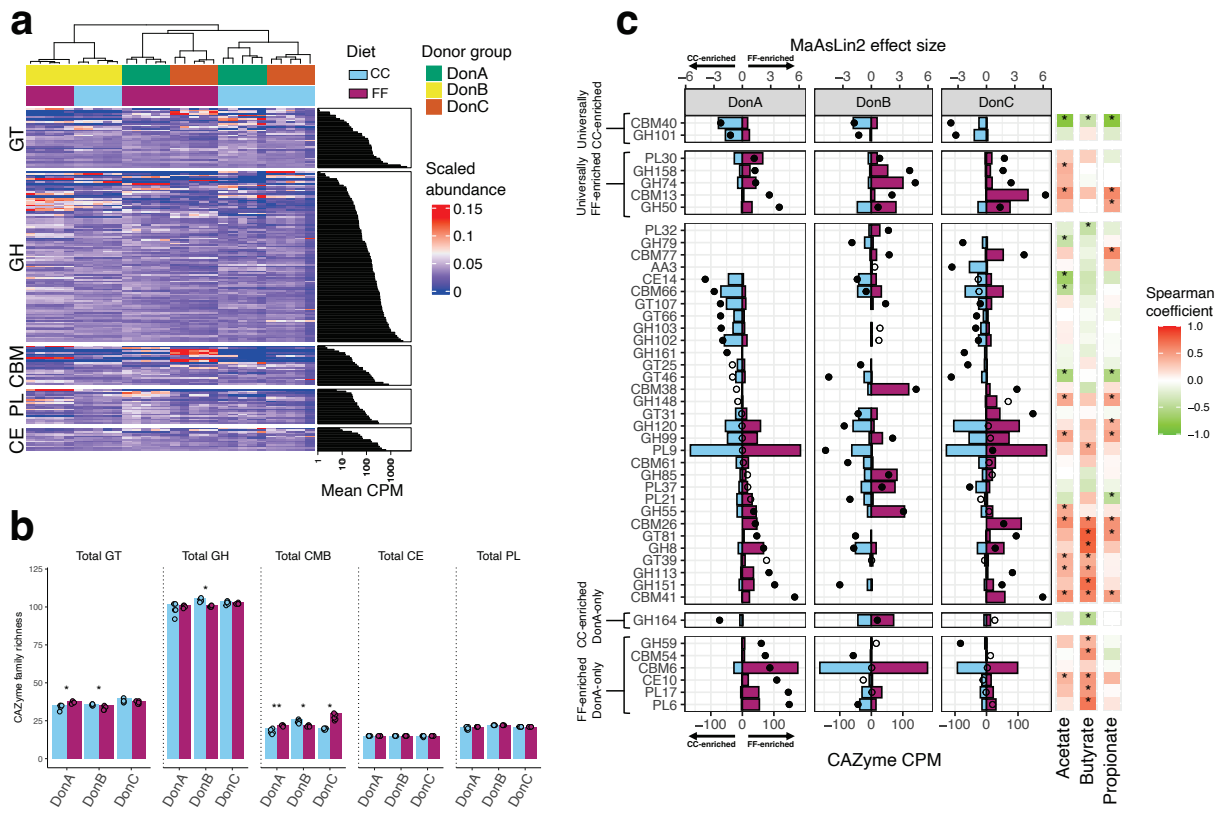

Figure 2.5 Effect of dietary fermentable fiber on microbial Carbohydrate Active EnZyme (CAZyme) profiles. **a** Heatmap of CAZyme family profiles arranged by category (Glycoside hydrolase = GH; glycosyltransferases = GT; carbohydrate binding modules = CBM; carbohydrate esters = CE; and polysaccharide lyases = PL) along with the mean counts for each CAZyme family expressed in counts per million (CPM). Mice profiles were clustered using the spearman hierarchical clustering method. **b** Comparison of CAZyme family richness between diets (total number of CAZyme families detected within each CAZyme category) by donor group. Barplots denote the mean with individual data points; comparisons of means between dietary groups were conducted using the Wilcoxon test;* P <0.05, ** P <0.01. **c** MaAsLin 2 differential abundance (bottom axis, colored bars) and effect size (top axis, solid dot = adjusted P-value <0.1, open dot = adjusted P-value >0.1) of the top 10% most differentially abundant CAZymes (n = 5/diet/donor

group). The right panel depicts a heatmap of spearman correlation coefficients between each corresponding CAZyme family and cecal SCFA levels across all mice, * *P*-value <0.05.

SUPPLEMENTARY FIGURES AND TABLES

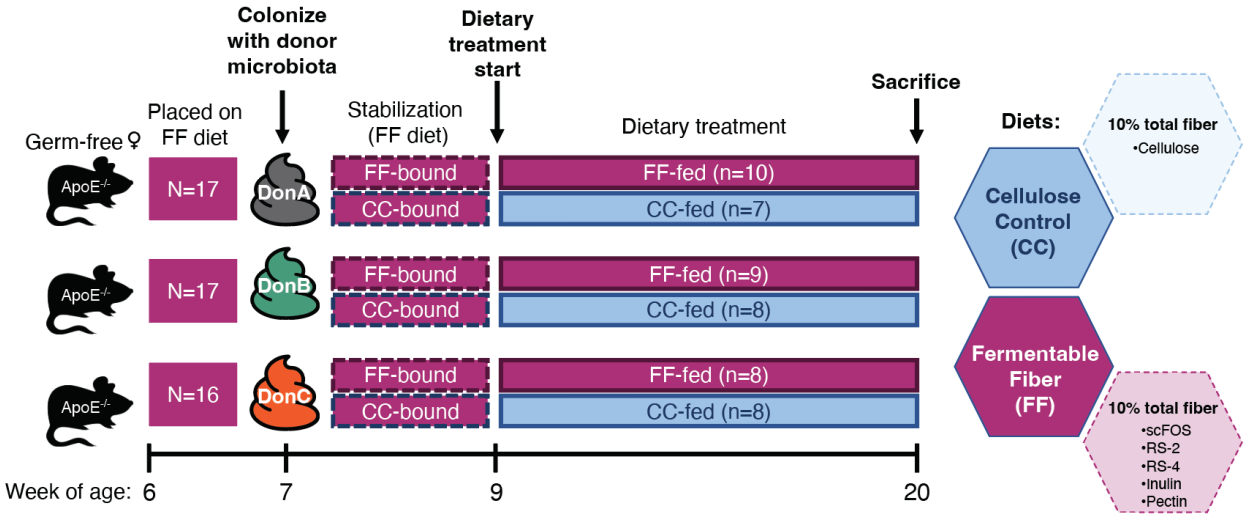

Supplementary Figure 2.1 Schematic of the experimental design used in this study.

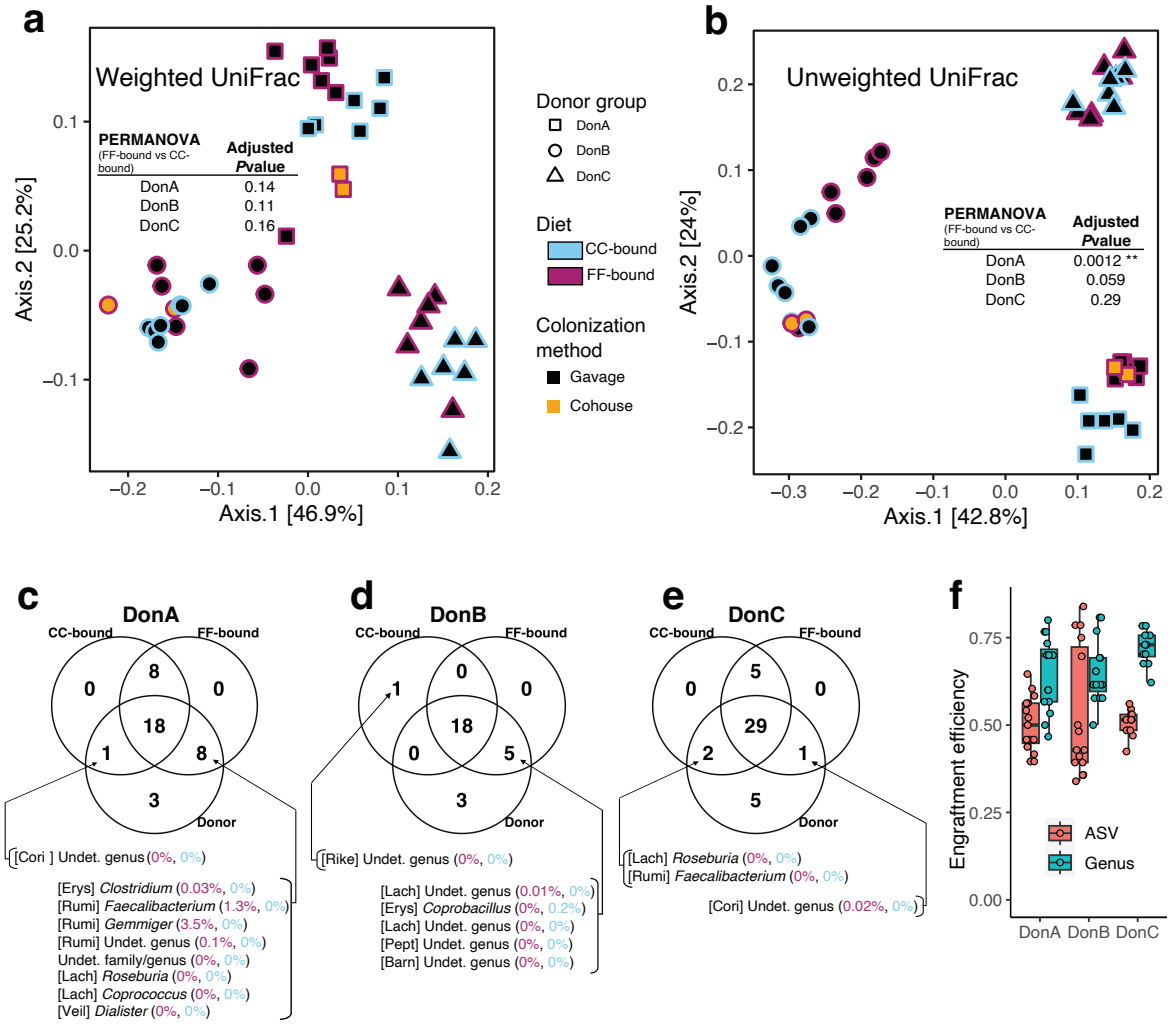

Supplementary Figure 2.2 Engraftment of genera from each donor fecal sample into recipient mice prior to dietary treatment**.** Principal coordinate analysis (PCoA) of pre-treatment fecal samples using weighted (**a**) and unweighted (**b**) UniFrac distances. Colonization method is denoted by the inner color of each point (black = gavage, orange = cohouse) and assigned diet group is denoted by the outer color (FF-bound = magenta, CC-bound = blue). **c-e** Venn diagrams of the genera detected in the donor fecal sample and in at least one mouse belonging to the CC-bound group or the FF-bound group of mice two weeks after colonization and prior to beginning the

dietary treatment phase. The genera listed below the Venn diagrams are denoted by their family (in brackets) and their group-average abundance in the cecal content of mice belong to the CC-fed group (blue text) or the FF-fed group (magenta text) at the end of the study after dietary treatment. Undet. = undetermined. **f** Engraftment efficiency for each mouse is expressed at the of genus level (teal) or at the ASVs level (salmon) two weeks after inoculation, but prior to dietary treatment.

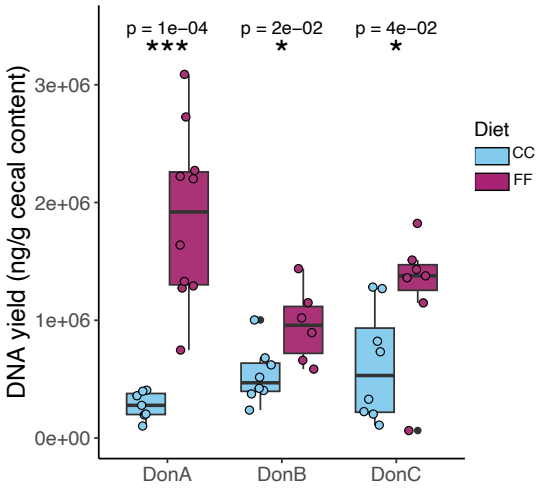

Supplementary Figure 2.3 Fecal DNA yields per gram of cecal content obtained from mice colonized with human fecal communities DonA, DonB, and DonC and fed either fermentable fiber diet (FF, magenta), or a cellulose control diet (CC, blue). Box and whisker plots denote the interquartile range, median, and spread of points within 1.5 times the interquartile range along with individual data points. Comparisons of means between diets within each donor group (n = 7-10/diet/donor group) were conducted using a Wilcoxon test, * P <0.05, *** P <0.001.

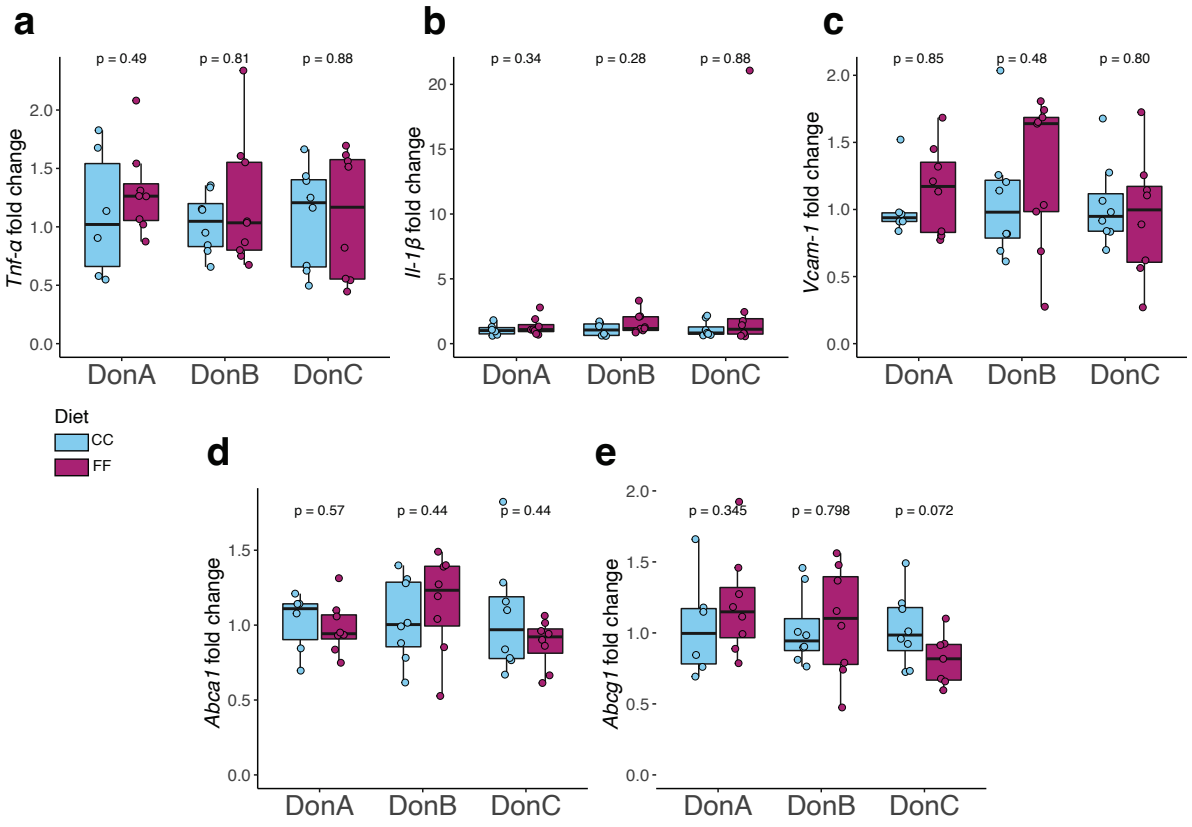

Supplementary Figure 2.4 Quantitative RT-PCR measurements of inflammatory markers and cholesterol efflux genes in aortic samples. **a-c** Log_2 fold-changes of mRNA abundance for inflammatory markers, and **d,e** genes encoding subunits of key cholesterol transporters between mice consuming FF and CC diets. All fold-changes are expressed relative to the donor-matched CC-fed group and were calculated using *Gapdh* as a reference gene. Box and whisker plots denote the interquartile range, median, and spread of points within 1.5 times the interquartile range along with individual data points. Comparisons of means between diets within each donor group were conducted using a Wilcoxon test.

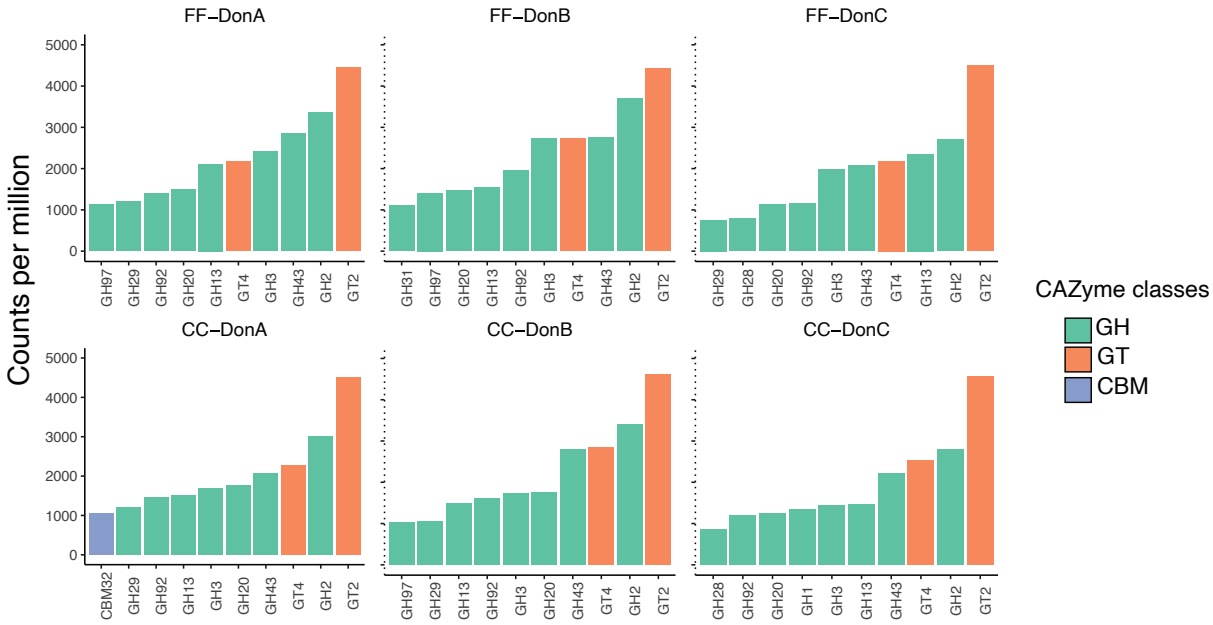

Supplementary Figure 2.5 Average (mean) CPM of the top 10 most abundant CAZyme families within each diet-donor group (FF top, CC bottom). CAZyme classes are indicated by color (Glycoside hydrolase = GH; glycosyltransferases = GT; carbohydrate binding modules = CBM). Values are expressed in counts per million (CPM).

Supplementary Table 1. Composition of diets. Macronutrient composition and ingredient list of the fermentable fiber and cellulose control diets.

Macronutrient	Cellulose diet (CC)	Fermentable fiber diet (FF)
Protein, % by weight	17.7	17.7
Carbohydrate, % by weight	48.4	47.9
Fat, % by weight	15.2	15.2
Protein, % Kcal from	17.7	17.7
Carbohydrate, % Kcal from	48.2	48
Fat, % Kcal from	34.1	34.3
Kcal/g	4	4
Ingredient	*(g/Kg)*	
Casein	200	200
L-Cystine	3	3
AMIOCA	261.22	236.02
Maltodextrin	132	132
Sucrose	100	100
Cellulose	100	0
Soybean Oil	75	75
Lard	75	75
Mineral Mix, AIN-93G-MX	35	35
Vitamin Mix, AIN-93-VX	16	16
Choline Bitartrate	2.75	2.75
TBHQ, antioxidant	0.03	0.03
Inulin	0	23.4
Fructooligosaccharide (FOS)	0	21.5
HI-MAIZE 260 (Resistant starch type 2)	0	33.3
Resistant wheat starch (Resistant starch type 4)	0	23.5
Pectin	0	23.5

Supplementary Table 2. Comparison of phenotypes between gavage- and cohouse-colonozed mice . All mice were colonized with human microbiota via gavage except subset of mice within the FF-fed DonA and DonB groups which were colonized by cohousing with 2 gavage-colonized mice. Statistical comparison of terminal phenotypes between gavage-colonized mice and their cohouse-colonized counterparts within each affected treatment group.

		P-value	
Phenotype	**Statistical test**	**DonA-FF**	**DonB-FF**
Cecal 16S rRNA community profiles (Unweighted UniFrac distances)	PERMANOVA	0.43	0.10
Cecal 16S rRNA community profiles (Weighted UniFrac distances)	PERMANOVA	0.10	0.30
Plaque area	Wilcoxon	0.11	0.70
Oil-Red-O area	Wilcoxon	0.48	0.70
MOMA-2 density	Wilcoxon	1.00	1.00
Cecal acetate	Wilcoxon	0.35	0.70
Cecal propionate	Wilcoxon	1.00	1.00
Cecal isobutyrate	Wilcoxon	0.48	0.10
Cecal butyrate	Wilcoxon	0.61	0.40
Cecal isovalerate	Wilcoxon	0.91	0.10
Plasma triglycerides	Wilcoxon	0.61	1.00
Plasma total cholesterol	Wilcoxon	0.26	0.20
Plasma HDL cholesterol	Wilcoxon	0.17	0.20
Tnf-α fold-change	Wilcoxon	0.79	1.00
Il1-**β** fold-change	Wilcoxon	0.79	0.40
Vcam-1 fold-change	Wilcoxon	0.25	1.00
Abca1 fold-change	Wilcoxon	0.79	0.40
Abcg1 fold-change	Wilcoxon	1.00	0.40

Supplementary Table 3. Primers used for qPCR assays.
Forward primer sequences for each target gene are nedoted by "-F" and reverse sequences are denoted by "-R".

Primer name	Sequence
Abca1-F	GGTTTGGAGATGGTTATACAATAGTTGT
Abca1-R	CCCGGAAACGCAAGTCC
Abcg1-F	TCACCCAGTTCTGCATCCTCTT
Abcg1-R	GCAGATGTGTCAGGACCGAGT
Tnfα-F	ATGAGCACAGAAAGCATGATC
Tnfα-R	TACAGGCTTGTCACTCGAATT
Il-6-F	CCACTTCACAAGTCGGAGGCTTA
Il-6-R	GCAAGTGCATCATCGTTGTTCATAC
Vcam1-F	TGCCGGCATATACGAGTGTGA
Vcam1-R	CCCGATGGCAGGTATTACCAAG
Gapdh-F	TGTGTCCGTGGATCTGA
Gapdh-R	CCTGCTTCACCTTCTTGA

CHAPTER 3: The gut microbiome modulates the impact of *Anaerobutyricum soehngenii* probiotic supplementation in mice

Evan R. Hutchison[+], *Hubert W. Peng, Chris R. Davis, Mei-I Yen, Eugenio I. Vivas, Michael M. Tallon, Thi Phoung Nam Bui, Willem De Vos, Eric Yen, Max Nieuwdorp, Federico E. Rey**

[+]Lead author

*Corresponding author

AUTHOR CONTRIBUTIONS

FER, ERH, and MN conceived of the study. ERH, and EIV performed gnotobiotic mouse studies and collected tissues. ERH, MMT, HWP, CRD, and MIY performed experiments with conventionally-raised mice. NMR measurements were collected by HWP, CRD, MIY, and EY. ERH conducted biochemical tests, prepared 16S rRNA libraries, conducted statistical tests, and analyzed the data. TPMB and WDV provided guidance for AS culturing. The manuscript was written by ERH and FER.

ABSTRACT

The gut microbiome is recognized as a key driver in metabolic syndrome (MetS). Manipulating gut microbiota with the aim of ameliorating MetS is gaining traction through the use of next-generation probiotics such as *Anerobutyricum soehngenii* (AS). However, the effectiveness of AS treatment is mixed as some individuals respond favorably, while others do not. Since the microbiome varies significantly between individuals, we hypothesized that the responsiveness to AS treatment is mediated by structure and function of the gut microbiome. To test this, we assessed glucose homeostasis in mice transplanted with fecal microbiota from two responder subjects (R65 and R55) and two non-responder subjects (N96 and N40) and continuously treated them with either live AS culture or heat-killed culture (HK) via gavage. We found that R65-colonized mice received a benefit in glycemic control (oral glucose tolerance and insulin tolerance) with AS treatment while the other transplanted mice did not. This improvement was associated with higher levels of cecal propionate, which when administered to R65- or N40-colonized mice as the pro-drug tripropionin (5.3% wt/wt), improved insulin sensitivity in a microbiota-dependent manner, suggesting that the effect of propionate on glycemic control is modulated by the gut microbiome. We also observed that feeding tripropionin reduced fat mass and improved glycemic control in conventional mice. Together, these findings highlight the importance of host-by-microbiota interactions and underscore the importance in developing microbiome-targeting therapeutics.

INTRODUCTION

Changes in food production, dietary habits, antibiotic usage, and lifestyle over the last century have greatly impacted health across the globe. In general, populations are experiencing an overall decrease in the prevalence of infectious diseases and an increase in chronic metabolic diseases, including metabolic syndrome (MetS). MetS is a cluster of conditions that it is clinically defined as having at least three of the following comorbidities; hypertension, hyperglycemia, reduced HDL-cholesterol, elevated triglycerides, or abdominal obesity (Eckel et al., 2005; Grundy et al., 2005). The rate of increase in MetS is highly concerning since MetS is a strong risk factor for developing cardiovascular disease and type-2 diabetes (Moore, 2017). Indeed, insulin resistance is thought to be an underlying driver of MetS pathology (Roberts et al., 2013), therefore, therapeutics that improve insulin sensitivity are urgently needed to reduce MetS pervasiveness and prevent disease progression.

The gut microbiome is recognized as an important factor in MetS development (Mazidi et al., 2016). For example, germ-free (GF) are protected from high-fat diet (HFD)-induced obesity and glycemic dysregulation (Backhed et al., 2004). Human studies have shown that MetS features such as obesity are associated with reduced microbial diversity and an overrepresentation of microbial genes involved in carbohydrate metabolism (Turnbaugh et al., 2006; Turnbaugh, Hamady, et al., 2009). The gut microbiome impacts host physiology in multiple ways including through modifying nutrient availability from undigested dietary components (Jumpertz et al., 2011; Turnbaugh et al., 2006) and by the production of metabolites that influence host inflammation and metabolic pathways (Hapfelmeier et al., 2010; Kau et al., 2011; Koh et al., 2018; Maslowski et al., 2009). Short-chain fatty acids (SCFAs) are produced by gut microbes through fermentation of dietary fibers and provide both an energy substrate to the host and act as signaling

molecules that can affect metabolic processes that impact obesity and insulin sensitivity (Canfora et al., 2015). The most abundant SCFAs in the gut are acetate, propionate, and butyrate, each of which have their own metabolic properties. Acetate, in the form of acetyl-CoA, serves as a central metabolite in multiple pathways, while propionate is a precursor for gluconeogenesis, and butyrate is the favored energy source for colonic epithelial cells. These molecules also serve as ligands for the G protein-coupled receptors Gpr41 (propionate > butyrate >> acetate), Gpr43 (acetate ≈ propionate ≈ butyrate), Gpr109a (butyrate) and Olfr78 (acetate ≈ propionate) in the intestine which elicit various immune and metabolic responses in the host (Kimura et al., 2020; Pluznick et al., 2013). However, given the dual roles of SCFAs as both sources of energy and signaling molecules, the effects of SCFAs in MetS are complex and not yet fully understood. Additionally, transplantation of microbiota communities from human donors discordant for obesity into GF mice resulted in a transfer of the obesity phenotype, demonstrating the causal role of microbiota in adiposity (Ridaura et al., 2013). Together, this evidence has prompted the development of microbiome-based therapeutics such as next-generation probiotics for the treatment of MetS.

One such probiotic is *Anaerobutyricum soehngenii* (AS). This bacterium was originally found to be associated with improved insulin sensitivity in MetS patients treated with fecal microbiota transplantation from healthy donors (Vrieze et al., 2012). AS is a strict anaerobe belonging to the Lachnospioraceae family of the Bacillota phylum and produces both propionate and butyrate (Shetty et al., 2018). Administration of AS to *db*/*db* mice was shown to improve insulin sensitivity relative to a heat-killed control (Udayappan et al., 2016). To assess the safety and effectiveness of AS as a therapeutic in humans to improve glycemic control, a clinical trial using oral administration of AS was recently conducted in male MetS patients (Gilijamse et al., 2020). Although AS was shown to be safe, its effects on insulin sensitivity as assessed by a

hyperinsulinemic euglycemic clamp were mixed; while AS treatment improved insulin sensitivity in some patients (responders), it had no effect or even an adverse effect in others (non-responders). Analysis of the baseline fecal bacterial composition of the patients revealed associations between certain bacterial taxa and responsiveness to AS treatment (Gilijamse et al., 2020). This led to the hypothesis that the gut microbiota influences the efficacy of AS on insulin sensitivity.

Here, we use a gnotobiotic mouse model to test whether the effect of AS treatment on glucose homeostasis is modulated by the gut microbiome. We show that mice colonized with donor fecal microbiota from two AS responders or two non-responders exhibit distinct responses to AS treatment versus a heat-killed AS control. We further show that cecal propionate is associated with improved glycemic control in mice colonized with microbiota from one of the donors, but not in mice with the other three donors. Finally, we demonstrate that administration of tripropionin, a prodrug of propionate, improves insulin sensitivity in a microbiota-dependent manner.

RESULTS

Gut microbiota engraftment was consistent across mice within each donor group

Groups of germ-free (GF) C57BL/6J mice were placed on a high-fat diet (HFD, 45% kcal from fat) at 5 weeks of age and colonized via oral gavage with fecal slurries generated from one of four human donor samples (R65, R55, N96, or N40; n = 9-10 mice per donor group). Mice were cohoused in large rat cages to encourage microbiota homogeneity and maintained on the HFD for 8 weeks to promote insulin resistance prior to treatment (Figure. 1a). At this point, we collected fecal samples from the mice and conducted 16S rRNA sequencing to assess microbiota engraftment. Importantly, there were no differences observed in the pre-treatment fecal 16S rRNA community structures within any of the donor groups between mice that went to AS treatment or

HK treatment, indicating that the fecal microbiota between individual mice were sufficiently homogenous prior to treatment (Supp. Fig. 3.1a,b). To assess the engraftment efficiency of the donor fecal microbiota to the recipient mice, we sequenced the feces of mice immediately prior to the AS/HK treatment phase as well as the donor inoculum samples (donor fecal slurry samples were collected after each gavage session). The ASV engraftment efficiencies (the number of ASVs detected in both the recipient mouse feces and the donor samples divided by the total ASVs in the donor sample) for R65, R55, N96, and N40 were 52%, 52%, 49%, and 49%, respectively (Supp. Fig. 3.1c). The engraftment efficiencies at the genus level were 58%, 68%, 66%, and 66%, respectively (Supp. Fig. 3.1c).

Gut microbial community influences the effect of AS treatment on glucose homeostasis

After 8 weeks on HFD, mice were treated with either live AS culture or heat-killed AS culture (HK) by oral gavage three times per week. Four weeks after initiating treatment, mice were subjected to an oral glucose tolerance test (oGTT). Live AS treatment in mice colonized with R65 microbiota had significantly reduced baseline fasting blood glucose levels prior to the oGTT (Supp. Fig. 3.2a) and a significantly reduced oGTT area under the curve (AUC) relative to their HK-treated counterparts (Fig. 3.1b,d). AS treatment did not affect fasting insulin levels measured prior to the oGTT in any donor groups (Fig. 3.1f). Additionally, AS-treated N40- and R55-colonized mice had significantly higher fasting glucose levels than their respective HK-treated control mice prior to the OGTT (Supp. Fig. 3.2a). One week following the oGTT, mice were subjected to an insulin tolerance test (ITT). Consistent with the oGTT results, AS treatment in R65-microbiota-colonized mice had an enhanced response to insulin as determined by a reduced ITT AUC compared to mice receiving the HK treatment (Fig 1c,e). AS treatment in mice colonized

with N40 microbiota caused a significant increase in ITT AUC compared to their HK-treated counterparts (Fig. 3.1c). Consistent with the oGTT results, AS treatment did not affect the ITT response in R55- and N96-colonized mice compared to HK-treated mice (Fig. 3.1c). In contrast to fasting glucose levels measured during the oGTT, there were no significant differences in fasting blood glucose levels between AS and HK treatments in any of the donor groups prior to the ITT (Supp. Fig. 3.2b). Finally, AS treatment did not affect body weight, liver weight, or epididymal fat pad mass in any of the donor groups (Supp. Fig. 3.2c-e).

Anaerobutyricum soehngenii (AS) treatment does not modify cecal bacterial community structure

To determine the effect of live AS treatment on intestinal microbiota composition we conducted 16S rRNA V4 amplicon sequencing of cecal contents across all donor groups. There were no significant differences between mice treated with live AS or HK in any of the four donor groups as determined by weighted and unweighted UniFrac distances (PERMANOVA, adjusted P value > 0.05; Fig. 3.2a-b). To examine if there were donor-specific differences in individual taxa between treatments, we conduct differential abundance analysis with MaAsLin2 for genus-level features between AS- and HK-treated mice within each donor group. Of the genera that were present above 1% average relative abundance in at least one donor group, only 7 were significantly different (P < 0.05) between treatment groups (Fig. 3.2c). AS led to higher levels of *Fusicatenibacter* and *Enterococcus* and lower levels of *Akkermansia* in R65-colonized mice; lower levels of *Runimicoccus torques* group in R55-colonized mice; higher levels of *Subdoligranulum* in N96-colonized mice; and lower levels of *Blautia* and *Collinsella* in N40-colonized mice

compared to HK-treated controls. However, none of these changes were at a large enough magnitude to persist after being subjected multiple comparison adjustment (adjusted $P < 0.1$).

Additionally, AS treatment had little to no effect on within-sample alpha diversity depending on the donor group. Mice colonized with N96 microbiota had significantly lower ASV richness ($P = 0.004$) and a trending decrease in Shannon diversity ($P = 0.074$) following AS treatment compared to their HK-treated counterparts, but there was no difference in Simpson diversity (Fig. 3.2d-f). N40-colonized mice treated with AS had lower inverse Simpson diversity than HK-treated mice ($P = 0.03$), but there was no difference in richness or Shannon diversity. Moreover, there were no differences observed in any of the diversity metrics tested between AS- and HK-treated mice colonized with either R65 or R55 microbiota.

Donor-specific association between propionate and glucose homeostasis improvements

Bacterial-derived SCFAs are known to influence host glycemic control, so we measured levels of acetate, propionate, and butyrate in the cecal content There were no significant differences observed in any of the SCFAs between AS-treated mice and their HK-treated counterparts, although R65-colonized mice treated with AS had a trending increase in propionate levels ($P = 0.11$, Fig. 3.3a-c). We also performed Spearman correlation analysis between individual SCFAs and the AUC values determined for oGTT and ITT within each donor group and observed a significantly negative association between propionate and AUCs for both oGTT ($R = -0.84$, $P = 0.0045$) and ITT ($R = -0.89$, $P = 0.0014$) in R65-colonized mice (Fig. 3.3d). No significant negative associations were observed between propionate and ITT AUC or oGTT AUC for any of the other donor-microbiota groups, although N96-colonized mice and N40 -colonized mice had a trending positive correlation with oGTT ($P = 0.07$) and ITT AUC ($P = 0.08$), respectively (Fig. 3.2e-g). In

addition, cecal levels of butyrate and oGTT AUC were significantly negatively correlated with oGTT AUC ($P = 0.01$) in N40-colonized mice (Supp. Table 3.1). Finally, mice colonized with N40 microbiota had a positive association between acetate and ITT AUC ($P = 0.04$, Supp. Table 3.1). This data shows that propionate is conditionally associated with improved glycemic control, suggesting that the gut microbiota may modify the host's response to propionate.

The effect of tripropionin on insulin sensitivity is conditional upon gut microbiota

Given the opposing effects of AS treatment between R65- and N40-colonized mice and their contrasting associations with cecal propionate, we next tested whether mice colonized with these distinct microbial communities responded differently to exogenous propionate treatment. We colonized GF mice with either R65 or N40 fecal microbiota, fed them a HFD as described above, and then treated them with a HFD supplemented with either 5.3% tripropionin (TP) or 5.3% glycerol as a control (GC) (Fig. 3.4a). Tripropionin is a propylated triglyceride analogous to tributyrin, a prodrug of butyrate. Triacylation of SCFAs delays their absorption compared to administration of a sodium-SCFA salt, as the SCFA moiety needs to first be cleaved by lipases before being absorbed (Egorin et al., 1999). In this way, the TP diet is hypothesized to deliver propionate over a longer timeframe and more-distally in the intestinal tract than sodium propionate, thereby delivering propionate in a fashion more akin to fiber fermentation. We hypothesize that this is important since the concentration of SCFA-sensing cell types, such as enteroendocrine L cells, increases as you move more distally along the gastrointestinal tract (Hansen et al., 2013).

TP had no effect on oGTT response in either R65- or N40-colonized mice (Fig. 3.4b). However, TP treatment significantly reduced the ITT AUC in R65-colonized mice compared to

the GC-fed counterparts, but not in N40-colonized mice (Fig. 3.4c). This diet-by-microbiota interaction was mirrored in the propionate levels observed in cecal contents, with TP leading to higher concentrations of cecal propionate in mice colonized with R65 microbiota, but not in N40-colonized mice (Fig. 3.4e). There were no differences in cecal acetate or butyrate levels between diets in either donor group (Fig. 3.4d,f). TP treatment led to significant and sustained decreases in body weight for both R65- and N40 mice (Fig. 3.4g). The drop in body weight in both donor groups was observed immediately after the dietary switch and persisted for the entire 8-week duration of the experiment.

Due to the risk for contamination as well as configuration of the gnotobiotic cage system, we were unable to accurately assess food consumption in our gnotobiotic animals, we measured the effects of TP on food consumption by treating 11-week-old conventionally raised C57Bl/6J male mice with either the TP or GC diet. We did not observe any evidence of reduced food consumption with the TP diet in at least the first 6 weeks after treatment (Fig 5b). Like the gnotobiotic experiment, TP induced a delayed but significant reduction in body weight compared to glycerol-fed mice (Fig. 3.5c). Interestingly, TP also significantly reduced oGTT and ITT AUCs compared to glycerol fed mice after four and five weeks of treatment, respectively (Fig. 3.5d,e). Additionally, body mass composition via NMR revealed that TP's effect on body mass was due to a reduction fat mass and not lean mass (Fig. 3.5f-h). TP did not elicit any observable signs of toxicity or reduced animal fitness after 13 weeks on diet. These results indicate that TP does not induce differences in consumption patterns compared to the GC-fed controls, however, a reduction in fat mass is observed, driving reduced body weight. We also show that TP improves glycemic control in conventionally raised male mice.

DISCUSSION

In the current study, we tested the role of the gut microbiome in modulating the effects of AS on glycemic control by colonizing mice with microbiota from human MetS subjects who were either responsive or non-responsive to AS treatment in a clinical trial. The responsiveness of the mice only partially mirrored that of their human donors, but the effects of AS were indeed dependent on the gut microbiota. In a previous study using *db*/*db* mice on a chow diet, Udayappan et al. showed that AS treatment led to improved insulin responsiveness compared to glycerol-treated control mice (Udayappan et al., 2016) in conventionally-raised animals. Our findings mirror this result, but only in one group (R65-colonized) of gnotobiotic mice, indicating that the gut microbiome modifies the effectiveness of AS treatment. Although the current study differs in both genetics and diet, our results suggest that the resident microbiome of the *db*/*db* mice used in the Udayappan et al. study (the combination of diet, maternal inheritance, facility environment, etc.) may have contributed the observed outcomes. Indeed, it is known that facility-associated variations within the gut microbiome can influence disease outcomes and treatment effects in mice (Laukens et al., 2016; Parker et al., 2018). Taken together, our results indicate that the efficacy of AS treatment is partly dependent on the microbiome, suggesting that the basal, inherent gut microbial communities are an important differentiating factor in this context.

We observed a partial recapitulation of the human insulin sensitivity phenotypes in recipient mice; non-responsiveness to AS was observed in the non-responder groups (N96- and N40-colonized mice), but only one of the two responder groups (R65-colonized mice) received a benefit from AS treatment. It is possible that the FMT from human donors to recipient mice maintained specific microbial conformations which imparted their respective AS-treatment response patterns. However, we cannot unambiguously conclude this for multiple reasons; First,

the transplantation of fecal microbiota from human feces to the mouse intestine results in incomplete engraftment resulting in altered community structures (Hutchison et al., 2023; Turnbaugh, Ridaura, et al., 2009). Second, responses of the patients to AS treatment was likely influenced by many factors other than their gut microbiome (exercise, diet, genetics, etc.). Finally, the physiology of mice is different than that of humans, thus a mouse can never fully recapitulate the disease or microbiome dynamics of humans. The current study was not designed to address these limitations, but previous studies have shown that human phenotypes are nonetheless transferrable to mice (Ridaura et al., 2013) indicating that it is possible to maintain some level of functional microbial programming in humanized gnotobiotic mice. Regardless, the results reported here demonstrate that the microbiome modulates the effect of AS on insulin sensitivity.

AS is reported to produce propionate and butyrate *in vitro* (Shetty et al., 2018), but multiple studies have reported a lack of major differences in fecal SCFA levels associated with AS treatment in mice (Udayappan et al., 2016) and humans (Gilijamse et al., 2020; Koopen et al., 2021). Here, we similarly report that AS failed to significantly alter cecal SCFA levels within mice in any of the donor groups. This may be attributed to the fact that AS is known to colonize the small intestine where it may only partially contribute to SCFA levels in the distal gut. We observed a significant association between cecal propionate levels and improved glycemic control in R65-colonized mice only suggesting that the gut microbiota modulates the effect of propionate on the host. This was confirmed by treating mice with propionate via TP and observing similar microbiome-dependent effects in insulin sensitivity. These results echo the inconsistent effects of propionate on glucose homeostasis reported in previous studies. Studies in mice have reported that propionate has either a protective (Lin et al., 2012), detrimental (Tirosh et al., 2019), or no effect (Li et al., 2012) on glucose homeostasis. These studies differed in diet, dosage, and design, each

of which likely contributed to the variations in the outcomes, but our results implicate the microbiome as an additional factor that may be complicating the picture as to whether propionate is beneficial or harmful for glucose control.

Interestingly, TP raised levels of cecal propionate only in R65 mice. This could be due to the R65 microbiota's ability to hydrolyze tripropionin and liberate free propionate with greater efficiency that N40 microbiota. But given that N40-colonized mice had higher levels of propionate than R65-colonized mice, we suspect that the N40-microbiota is efficient at propionate production, and the ceca of these mice are reaching an environmental maximum. In this scenario, propionate production by microorganisms and/or hydrolysis of TP may be less thermodynamically favorable than in R65-colonized mice which have lower basal propionate levels. In this way, we hypothesize that TP has a blunted effect in N40-colonized mice since it is effectively unable to deliver more propionate to an already saturated system. This is supported by a recent finding that exogenous butyrate can inhibit the production of coenzyme A intermediates within the butyrate synthesis pathway (Pensinger et al., 2023). Whether this is true for propionate, however, requires further study.

TP treatment also led to microbiome-independent reductions in body mass, likely through a reduction in adipose tissue as demonstrated in conventional mice. Differences in body mass are associated with altered insulin sensitivity, but the reduction in body mass in TP-treated N40 colonized mice did not improve glycemic control. This indicates that the microbiome modulates TP's effect through a mechanism that supersedes or is independent of body mass. Finally, TP's anti-adiposity and improvements in glycemic control in conventional mice point to TP's potential as a possible therapeutic. However, as stated above, our results with gnotobiotic mice suggest that the TP-associated benefits observed in conventional mice may be a consequence of the facility-

specific microbiome present in the mice in our laboratory. This should be examined further and could be a useful model to explore the causative organism and/or functions by comparing with mice from other facilities.

The current study has some limitations that should be addressed. First, our treatment groups had a small sample size (n= 4-5 per treatment group) which may have limited the sensitivity of our analysis. This was a result of our experimental design in which we cohoused all mice within a single donor group (n= 9-10 per donor group) to maximize microbial homogeneity prior to splitting the mice into treatment groups. This approach is advantageous because it eliminates the cage effect prior to treatment, but it comes at the expense of sample size. Second, we used a heat-killed culture of AS as a negative control which may contain components that influence glycemic control (e.g., signaling proteins, small molecules, cell wall components, etc.). The addition of a blank and conditioned media-control groups would be necessary to rule out this possibility, but this fell outside the scope of the current study and was not feasible given the design. Third, we only used male mice because the donor specimens were from male subjects, but this nonetheless limits our interpretation. Finally, we were unable to detect differences in AS qPCR signal between the AS and HK treatment groups in the cecum or the jejunum. These results are consistent with Udayappan et al. in which dosing mice with up to $1x10^{10}$ CFU of AS did not result in significantly different abundance from the placebo group in the cecum (Udayappan et al., 2016). This suggests that live AS was unable to colonize the intestine. Even if this is the case, it does not preclude live AS from having a biological, albeit transient, effect.

While this study does not capture the breadth of functional capacities or microbial diversity present in human or mouse gut microbiota, it clearly demonstrates the modulatory role of the gut microbiome in the effectiveness and metabolic consequences of microbial therapeutics.

Ultimately, this study underscores the importance in characterizing and understanding the host-by-microbiota dynamics that influence responses to specific therapeutics to develop and improve precision medicine strategies.

METHODS

Germ-free animals

All animals used in this study were handled in accordance with the University of Wisconsin-Madison's animal welfare policies and all experiments were conduction under an Animal Care and Use Committee-approved protocol. Germ-free (GF) C57BL/6 mice were housed in sterile isolators and maintained on autoclaved chow (LabDiet 5021; LabDiet, St. Louis, MO) and sterile water *ad libitum*. GF cages contained Alpha-dri® (Shepherd Specialty Papers, Kalamazoo, MI) bedding along with paper huts (Bio-Huts, Bio-Serv, Flemington, NJ) and ALPHA-twist™ (Shepherd Specialty Papers) for enrichment. Monthly tests were conducted in each isolator to confirm GF status of the mice. These included a growth test of feces in rich media for 7 days at 37 °C and checking for amplification of the 16S rRNA gene using universal primers.

Human donor samples

Fecal samples were collected from human participants in a previous study (Gilijamse et al., 2020) examining the effectiveness and safety of AS treatment in male subjects with unmedicated metabolic syndrome (Grundy et al., 2005). The fecal specimens used in this study were collected from subjects prior to AS treatment and were immediately frozen and maintained at -80 °C (Gilijamse et al., 2020). All subjects provided written informed consent as participants of the

clinical trial which was approved by the Amsterdam University Medical Center's IRB and registered at the Dutch Trial registry (NTR4913, https://www.trialregister.nl/trial/4775).

Selection of human donors.

The primary outcome of the AS clinical trial was insulin sensitivity as measured by glucose disposal rate (Rd) during a hyperinsulinemic euglycemic stable isotope-based clamp (Gilijamse et al., 2020). Subjects who had an improvement in Rd from baseline (increased by at least 4 μmol/kg/min) were categorized as "Responders", while those had a decrease in Rd from baseline (decreased by at least 4 μmol/kg/min) were classified as "Non-responders". For colonization of gnotobiotic mice in the current study, we selected the top two subjects who underwent the largest magnitude of change in Rd in each category; responder subject 65 (R65, ΔRd = +11), responder subject 55 (R55, ΔRd = +12.1), non-responder 96 (N96, ΔRd = -8.6), non-responder 40 (R40, ΔRd = -8.5).

Colonization of GF mice with human fecal microbiota

Groups of male GF C57BL/6J mice (n = 9-10) were moved from isolators to autoclaved rat cages (1 rat cage per donor group) on an Allentown Sentry SPP IVC rack system (Allentown Inc., Allentown, NJ) at 5 weeks of age and place on an irradiated HFD (Supp. Table 3.2, TD.08811; Envigo, Madison, WI) for one week before colonization with human microbiota. Human fecal samples were prepared for gavage by mixing 200-500 mg of frozen fecal content into 2-5 mL (100 mg/mL) of anaerobic Mega Media (Murga-Garrido et al., 2021) in an anaerobic chamber. The fecal slurry was vortexed for 1 min and placed on ice and then used to gavage mice no longer that 1 hour after preparation. Each mouse was gavaged with 100 μL of fecal slurry and after all mice

were gavaged, 500 μL of the slurry was collected and frozen for microbial composition analysis. Mice were gavaged for a second time with freshly prepared fecal slurries one week later using the same procedure described above. All mice within a single donor group were housed together and maintained on the HFD for 8 weeks before being split into treatment groups.

AS treatment experiments

AS culture was prepared by growing *Anaerobutyricum shoengenii* L2-7 (DSM 17630) anaerobically in a single 2 L batch using YCFA media at 37 °C for 24 h when the culture reached stationary phase. The culture was spun down for 20 min at 4,000 g and washed in sterile anaerobic PBS, spun down again, and then resuspended in anaerobic PBS 10% glycerol. The suspension was distributed into 1.2 mL aliquots (enough to gavage 10 mice) in hungate tubes and frozen and stored at -80 °C. Culture purity was confirmed by microscopic examination and amplification of the full length 16S rRNA gene using universal 16S primers (27-F: AGAGTTTGATCMTGGCTCAG, 1492-R: GGWTACCTTGTTACGACTT) followed by sanger sequencing. The resulting sequences were unambiguous across the entire amplicon, being consistent with a pure culture. Thawed aliquots of culture were determined to possess $1.5x10^9$ cfu/mL (as estimated using the MPN method in YCFA media) and remained viable for the duration of the study (cultures were viable for at least 18 months after freezing). Eight weeks after the initial colonization with human microbiota, mice within a single donor-group rat cage were split into two smaller Allentown IVC mouse cages (n= 4-5/cage), and gavaged with 100 μL of either live AS culture or 100 μL of heat-killed AS culture. Heat-killed cultures were heat-shocked in a water bath at 80°C for 15 min and did not yield any growth after direct inoculation of YCFA broth. All mice were gavaged 3 times per week (over a period of no less than four days) and maintained on the HFD for the duration of

the treatment-phase of the experiment. Mice were sacrificed 6 weeks after start of AS/HK treatment.

Tripropionin experiments with gnotobiotic mice

Separate groups of 6-week-old male C57BL/6J GF mice were placed on the HFD and colonized with either R65 microbiota or N40 microbiome using the same procedures as described above. Eight weeks after colonization, mice in donor-group (9 mice in a single rat cage) were split into two smaller Allentown IVC mouse cages (n= 4-5/cage), and a HFD supplemented with either 5.3% tripropionin (TD.220540, Inotiv) or 5.3% glycerol (TD.220540, Inotiv, Supp. Table 3.2). Mice were maintained on these diets and subjected to oGTT and ITT as described above at 4 and 5 weeks after diet change, respectively.

Tripropionin experiments with conventional mice

Male C57BL/6J mice were ordered from Jackson Laboratories (strain 000664, Bar Harbor, ME) and maintained in a ventilated rack system (Alternative Design, Siloam Springs, AR) with chlorinated water with corn husk bedding with *ad libitum* access to chlorinated water and a chow diet (Teklad 8604, Inotiv, Madison, WI). At 11 weeks of age, the mice were placed on either the 5.3% tripropionin or glycerol treatment diets. Per-cage food consumption (2 mice per cage) and body weights were monitored for 6 weeks. Mice were subjected to oGTT and ITT at 4 and 5 weeks after dietary treatment, respectively. After an additional 6 weeks on the experimental diet, body weight and fat vs lean mass were monitored using nuclear magnetic resonance (NMR) machine fitted for mice (LF90 Body Composition Analyzer, Bruker Corporation, Billerica, MA).

Sacrifice

All mice were fasted for 4 hours prior to euthanasia. Upon sacrifice, mice were anesthetized using isoflurane and blood was collected via heart puncture. Mice were then immediately euthanized via cervical dislocation and various tissues including epididymal fat pads, cecal content, colon, liver were dissected and flash-frozen using liquid nitrogen.

OGTT

Four weeks after treatment initiation mice were placed in fresh cages fasted for 4 hours. Baseline blood glucose measurements were taken using a AlphaTrak2 glucometer (Zoetis, Parsippany, NJ) a drop of blood from a tail snip. After the baseline measurement, mice were immediately dosed with 2 g of glucose per Kg of body weight. Subsequent blood glucose measurements were taken 15, 30, 45, 60, 90, and 120 minutes after the baseline measurement. Plasma samples were collected at baseline as well as the 30-minute and 60-minute time points for insulin measurements.

ITT

One week after the OGTT mice were placed in new cages and fasted for 4 hours. A baseline blood glucose measurement was taken as described above and freshly prepared insulin (Gibco, ThermoFisher Scientific, Waltham, MA) was immediately dosed at 0.75 IU per Kg of body weight via IP injection. Subsequent blood glucose measurements were taken 15, 30, 45, 60, 90, and 120 minutes after the baseline measurement. ITT blood glucose measurements for each timepoint are expressed as a percent change from baseline.

Cecal SCFA measurement

Cecal levels of SCFAs were measured by headspace gas chromatography as previously described (Hutchison et al., 2023). Briefly, frozen cecal content (20-50 mg) was weighed and added to vials (Restek, Bellefonte, PA) containing 2.0 g of H_2SO_4 and a volume a water such that the total volume was equal to 300 µL (Cecal content [mg] + water [µL] = 300). An additional 1 mL of 60 mM 2-butanol was added to each vial as in internal control. The prepared vials were loaded run on a HS20 headspace sampler (Shimadzu, Columbia, OH) and loaded onto a column (30 m SH-Stabilwax, 227-36246-01, Shimadzu) connected to a flame ionization detector on a CG-2010 Plus GC (Shimadzu). The initialization and running conditions used were published previsously (Hutchison et al., 2023). Chromatogram peak areas were quantified using Shimadzu Lab Solution software (version 5.92) and each SCFA peak converted to µmol/g of cecal content using standard curves and normalizing for sample input mass.

16S rRNA sequencing

DNA and microbiome characterization from human fecal slurries, mouse cecal content, and mouse feces was extracted using a phenol:chloroform plus bead-beating protocol followed by 16S rRNA gene amplicon sequencing as previously described (Hutchison et al., 2023). Briefly, feces or cecal contents were mixed by bead-beating twice for 3 minutes in the presence of phenol:cholraphorm:isoamyl. alcohol (UltraPure™ [25:24:1, v/v], ThermoFisher Scientific) and SDS. The aqueous phase was collected and DNA was precipitated by the addition of 1 M sodium acetate and 100% isopropanol. The DNA was then cleaned with the Neucleospin cleanup kit (Macherey-Nagel, Düren, Nordrhein-Westfalen, Germany) and the purified DNA was subjected to 16S rRNA gene amplicon sequencing. 16S rRNA amplicon libraries were prepared using V3-V4 universal primer sets with Illumina adapters and barcodes (Murga-Garrido et al., 2021). The

resulting libraries were loaded onto a single Illumina MiSeq lane (Illumina, San Diego, CA) at the University of Wisconsin Next Generation Sequencing Core (Madison, WI) which produced an average sampling depth of 36,196 ±11,225 reads per sample. DADA2 (Callahan et al., 2016) quality control and clean-up was conducted with QIIME2 (Bolyen et al., 2019) (version 2022.2). Taxonomy was classified using the SILVA database (Quast et al., 2013) (version 132).d

Microbiome analysis

The phyloseq (version 1.40.0) package in R was used to generate UniFrac distance matrices. The pairwiseAdonis (version 0.4) R package with 9999 permutations was used to conduct PERMANOVA tests to compare ASV profiles between treatment groups within each donor group. Differential abundance analysis of genus-level features was conducted using the MaAsLin2 (version 1.10.0) package in R (Mallick et al., 2021). For differential abundance analysis, genus-level features were filtered to only include those that were above 1% average relative abundance in at least one donor group. Engraftment efficiencies were assessed using ASV and genus-level feature data from the donor fecal sample and feces collected from mice 2 weeks after colonization but prior to AS/HK treatment. Efficiencies were calculated as C/D, where C is the number of common features that were detected in both the donor and at least one recipient mouse, and D is the total number of features detected in the donor. Detection was defined as any feature that was present at 0.05% relative abundance or higher.

Statistics

All comparisons of means were conducted via Student's T test between treatment groups within each donor group and at each timepoint unless otherwise stated. Correlations between ITT and

oGTT AUCs and cecal SCFA levels were conducted using Spearman's rank correlation method. *P*-value adjustment for PERMANOVA was done using the Bonferroni method and the Holm-Bonferroni method was used to adjust correlation *P*-values. All box and whisker plots represent the interquartile range (IR), median, and 1.5 times the IR overlayed with individual data points from each mouse. Line plots depict the mean of each group at each timepoint with error bars representing the standard error.

ACKNOWLEDGEMENTS

Our sincerest thanks to Dr. Barb Mickelson for her expertise in designing the diets used in the current study. Also, we would like to acknowledge the University of Wisconsin Next Generation Sequencing Core for providing sequencing and subject area expertise.

DATA AVAILABILITY

The data from this study is available upon request.

REFERENCES

Backhed, F., Ding, H., Wang, T., Hooper, L. V., Koh, G. Y., Nagy, A., Semenkovich, C. F., & Gordon, J. I. (2004). The gut microbiota as an environmental factor that regulates fat storage. *Proceedings of the National Academy of Sciences*, *101* (44), 15718–15723. https://doi.org/10.1073/pnas.0407076101

Bolyen, E., Rideout, J. R., Dillon, M. R., Bokulich, N. A., Abnet, C. C., Al-Ghalith, G. A., Alexander, H., Alm, E. J., Arumugam, M., Asnicar, F., Bai, Y., Bisanz, J. E., Bittinger, K., Brejnrod, A., Brislawn, C. J., Brown, C. T., Callahan, B. J., Caraballo-Rodríguez, A. M., Chase, J., … Caporaso, J. G. (2019). Reproducible, interactive, scalable and extensible microbiome data science using QIIME 2. *Nature Biotechnology*, *37* (8), Article 8. https://doi.org/10.1038/s41587-019-0209-9

Callahan, B. J., McMurdie, P. J., Rosen, M. J., Han, A. W., Johnson, A. J. A., & Holmes, S. P. (2016). DADA2: High resolution sample inference from Illumina amplicon data. *Nature Methods*, *13* (7), 581–583. https://doi.org/10.1038/nmeth.3869

Canfora, E. E., Jocken, J. W., & Blaak, E. E. (2015). Short-chain fatty acids in control of body weight and insulin sensitivity. *Nature Reviews Endocrinology*, *11* (10), Article 10. https://doi.org/10.1038/nrendo.2015.128

Eckel, R. H., Grundy, S. M., & Zimmet, P. Z. (2005). The metabolic syndrome. *The Lancet*, *365* (9468), 1415–1428. https://doi.org/10.1016/S0140-6736 (05)66378-7

Egorin, M. J., Yuan, Z.-M., Sentz, D. L., Plaisance, K., & Eiseman, J. L. (1999). Plasma pharmacokinetics of butyrate after intravenous administration of sodium butyrate or oral administration of tributyrin or sodium butyrate to mice and rats. *Cancer Chemotherapy and Pharmacology*, *43* (6), 445–453. https://doi.org/10.1007/s002800050922

Gilijamse, P. W., Hartstra, A. V., Levin, E., Wortelboer, K., Serlie, M. J., Ackermans, M. T., Herrema, H., Nederveen, A. J., Imangaliyev, S., Aalvink, S., Sommer, M., Levels, H., Stroes, E. S. G., Groen, A. K., Kemper, M., de Vos, W. M., Nieuwdorp, M., & Prodan, A. (2020). Treatment with Anaerobutyricum soehngenii: A pilot study of safety and dose–response effects on glucose metabolism in human subjects with metabolic syndrome. *Npj Biofilms and Microbiomes*, *6* (1). https://doi.org/10.1038/s41522-020-0127-0

Grundy, S. M., Cleeman, J. I., Daniels, S. R., Donato, K. A., Eckel, R. H., Franklin, B. A., Gordon, D. J., Krauss, R. M., Savage, P. J., Smith, S. C., Spertus, J. A., Costa, F., American Heart Association, & National Heart, Lung, and Blood Institute. (2005). Diagnosis and management of the metabolic syndrome: An American Heart Association/National Heart, Lung, and Blood Institute Scientific Statement. *Circulation*, *112* (17), 2735–2752. https://doi.org/10.1161/CIRCULATIONAHA.105.169404

Hansen, C. F., Vrang, N., Sangild, P. T., & Jelsing, J. (2013). Novel insight into the distribution of L-cells in the rat intestinal tract. *American Journal of Translational Research*, *5* (3), 347–358.

Hapfelmeier, S., Lawson, M. A. E., Slack, E., Kirundi, J. K., Stoel, M., Heikenwalder, M., Cahenzli, J., Velykoredko, Y., Balmer, M. L., Endt, K., Geuking, M. B., Curtiss, R., McCoy, K. D., & Macpherson, A. J. (2010). Reversible Microbial Colonization of Germ-Free Mice Reveals the Dynamics of IgA Immune Responses. *Science*, *328* (5986), 1705–1709. https://doi.org/10.1126/science.1188454

Hutchison, E. R., Kasahara, K., Zhang, Q., Vivas, E. I., Cross, T.-W. L., & Rey, F. E. (2023). Dissecting the impact of dietary fiber type on atherosclerosis in mice colonized with

different gut microbial communities. *Npj Biofilms and Microbiomes*, *9* (1), Article 1. https://doi.org/10.1038/s41522-023-00402-7

Jumpertz, R., Le, D. S., Turnbaugh, P. J., Trinidad, C., Bogardus, C., Gordon, J. I., & Krakoff, J. (2011). Energy-balance studies reveal associations between gut microbes, caloric load, and nutrient absorption in humans. *The American Journal of Clinical Nutrition*, *94* (1), 58–65. https://doi.org/10.3945/ajcn.110.010132

Kau, A. L., Ahern, P. P., Griffin, N. W., Goodman, A. L., & Gordon, J. I. (2011). Human nutrition, the gut microbiome and the immune system. *Nature*, *474* (7351), Article 7351. https://doi.org/10.1038/nature10213

Kimura, I., Ichimura, A., Ohue-Kitano, R., & Igarashi, M. (2020). Free Fatty Acid Receptors in Health and Disease. *Physiol Rev*, *100*, 41.

Koh, A., Molinaro, A., Ståhlman, M., Khan, M. T., Schmidt, C., Mannerås-Holm, L., Wu, H., Carreras, A., Jeong, H., Olofsson, L. E., Bergh, P.-O., Gerdes, V., Hartstra, A., De Brauw, M., Perkins, R., Nieuwdorp, M., Bergström, G., & Bäckhed, F. (2018). Microbially Produced Imidazole Propionate Impairs Insulin Signaling through mTORC1. *Cell*, *175* (4), 947-961.e17. https://doi.org/10.1016/j.cell.2018.09.055

Koopen, A., Witjes, J., Wortelboer, K., Majait, S., Prodan, A., Levin, E., Herrema, H., Winkelmeijer, M., Aalvink, S., Bergman, J. J. G. H. M., Havik, S., Hartmann, B., Levels, H., Bergh, P.-O., Son, J. van, Balvers, M., Bastos, D. M., Stroes, E., Groen, A. K., … Rampanelli, E. (2021). Duodenal Anaerobutyricum soehngenii infusion stimulates GLP-1 production, ameliorates glycaemic control and beneficially shapes the duodenal transcriptome in metabolic syndrome subjects: A randomised double-blind placebo-controlled cross-over study. *Gut*. https://doi.org/10.1136/gutjnl-2020-323297

Laukens, D., Brinkman, B. M., Raes, J., De Vos, M., & Vandenabeele, P. (2016). Heterogeneity of the gut microbiome in mice: Guidelines for optimizing experimental design. *FEMS Microbiology Reviews*, *40* (1), 117–132. https://doi.org/10.1093/femsre/fuv036

Li, L., Hua, Y., & Ren, J. (2012). Short-Chain Fatty Acid Propionate Alleviates Akt2 Knockout-Induced Myocardial Contractile Dysfunction. *Experimental Diabetes Research*, *2012*, 1–10. https://doi.org/10.1155/2012/851717

Lin, H. V., Frassetto, A., Jr, E. J. K., Nawrocki, A. R., Lu, M. M., Kosinski, J. R., Hubert, J. A., Szeto, D., Yao, X., Forrest, G., & Marsh, D. J. (2012). Butyrate and Propionate Protect against Diet-Induced Obesity and Regulate Gut Hormones via Free Fatty Acid Receptor 3-Independent Mechanisms. *PLOS ONE*, *7* (4), e35240. https://doi.org/10.1371/journal.pone.0035240

Mallick, H., Rahnavard, A., McIver, L. J., Ma, S., Zhang, Y., Nguyen, L. H., Tickle, T. L., Weingart, G., Ren, B., Schwager, E. H., Chatterjee, S., Thompson, K. N., Wilkinson, J. E., Subramanian, A., Lu, Y., Waldron, L., Paulson, J. N., Franzosa, E. A., Bravo, H. C., & Huttenhower, C. (2021). *Multivariable Association Discovery in Population-scale Meta-omics Studies* [Preprint]. Microbiology. https://doi.org/10.1101/2021.01.20.427420

Maslowski, K. M., Vieira, A. T., Ng, A., Kranich, J., Sierro, F., Yu, D., Schilter, H. C., Rolph, M. S., Mackay, F., Artis, D., Xavier, R. J., Teixeira, M. M., & Mackay, C. R. (2009). Regulation of inflammatory responses by gut microbiota and chemoattractant receptor GPR43. *Nature*, *461* (7268), 1282–1286. https://doi.org/10.1038/nature08530

Mazidi, M., Rezaie, P., Kengne, A. P., Mobarhan, M. G., & Ferns, G. A. (2016). Gut microbiome and metabolic syndrome. *Diabetes & Metabolic Syndrome: Clinical Research & Reviews*, *10* (2, Supplement 1), S150–S157. https://doi.org/10.1016/j.dsx.2016.01.024

Moore, J. X. (2017). Metabolic Syndrome Prevalence by Race/Ethnicity and Sex in the United States, National Health and Nutrition Examination Survey, 1988–2012. *Preventing Chronic Disease*, *14*. https://doi.org/10.5888/pcd14.160287

Murga-Garrido, S. M., Hong, Q., Cross, T.-W. L., Hutchison, E. R., Han, J., Thomas, S. P., Vivas, E. I., Denu, J., Ceschin, D. G., Tang, Z.-Z., & Rey, F. E. (2021). Gut microbiome variation modulates the effects of dietary fiber on host metabolism. *Microbiome*, *9* (1), 117. https://doi.org/10.1186/s40168-021-01061-6

Parker, K. D., Albeke, S. E., Gigley, J. P., Goldstein, A. M., & Ward, N. L. (2018). Microbiome Composition in Both Wild-Type and Disease Model Mice Is Heavily Influenced by Mouse Facility. *Frontiers in Microbiology*, *9*. https://www.frontiersin.org/articles/10.3389/fmicb.2018.01598

Pensinger, D. A., Dobrila, H. A., Stevenson, D. M., Davis, N. M., Amador-Noguez, D., & Hryckowian, A. J. (2023). *Exogenous butyrate inhibits butyrogenic metabolism and alters expression of virulence genes in Clostridioides difficile* (p. 2023.07.06.548018). bioRxiv. https://doi.org/10.1101/2023.07.06.548018

Pluznick, J. L., Protzko, R. J., Gevorgyan, H., Peterlin, Z., Sipos, A., Han, J., Brunet, I., Wan, L.-X., Rey, F., Wang, T., Firestein, S. J., Yanagisawa, M., Gordon, J. I., Eichmann, A., Peti-Peterdi, J., & Caplan, M. J. (2013). Olfactory receptor responding to gut microbiota-derived signals plays a role in renin secretion and blood pressure regulation. *Proceedings of the National Academy of Sciences*, *110* (11), 4410–4415. https://doi.org/10.1073/pnas.1215927110

Quast, C., Pruesse, E., Yilmaz, P., Gerken, J., Schweer, T., Yarza, P., Peplies, J., & Glöckner, F. O. (2013). The SILVA ribosomal RNA gene database project: Improved data processing

and web-based tools. *Nucleic Acids Research*, *41* (D1), D590–D596. https://doi.org/10.1093/nar/gks1219

Ridaura, V. K., Faith, J. J., Rey, F. E., Cheng, J., Duncan, A. E., Kau, A. L., Griffin, N. W., Lombard, V., Henrissat, B., Bain, J. R., Muehlbauer, M. J., Ilkayeva, O., Semenkovich, C. F., Funai, K., Hayashi, D. K., Lyle, B. J., Martini, M. C., Ursell, L. K., Clemente, J. C., … Gordon, J. I. (2013). Gut Microbiota from Twins Discordant for Obesity Modulate Metabolism in Mice. *Science*, *341* (6150), 1241214–1241214. https://doi.org/10.1126/science.1241214

Roberts, C. K., Hevener, A. L., & Barnard, R. J. (2013). Metabolic Syndrome and Insulin Resistance: Underlying Causes and Modification by Exercise Training. *Comprehensive Physiology*, *3* (1), 1–58. https://doi.org/10.1002/cphy.c110062

Shetty, S. A., Zuffa, S., Bui, T. P. N., Aalvink, S., Smidt, H., & De Vos, W. M. (2018). Reclassification of Eubacterium hallii as Anaerobutyricum hallii gen. Nov., comb. Nov., and description of Anaerobutyricum soehngenii sp. Nov., a butyrate and propionate-producing bacterium from infant faeces. *International Journal of Systematic and Evolutionary Microbiology*, *68* (12), 3741–3746. https://doi.org/10.1099/ijsem.0.003041

Tirosh, A., Calay, E. S., Tuncman, G., Claiborn, K. C., Inouye, K. E., Eguchi, K., Alcala, M., Rathaus, M., Hollander, K. S., Ron, I., Livne, R., Heianza, Y., Qi, L., Shai, I., Garg, R., & Hotamisligil, G. S. (2019). The short-chain fatty acid propionate increases glucagon and FABP4 production, impairing insulin action in mice and humans. *Science Translational Medicine*, *11* (489), eaav0120. https://doi.org/10.1126/scitranslmed.aav0120

Turnbaugh, P. J., Hamady, M., Yatsunenko, T., Cantarel, B. L., Duncan, A., Ley, R. E., Sogin, M. L., Jones, W. J., Roe, B. A., Affourtit, J. P., Egholm, M., Henrissat, B., Heath, A. C.,

Knight, R., & Gordon, J. I. (2009). A core gut microbiome in obese and lean twins. *Nature*, *457* (7228), Article 7228. https://doi.org/10.1038/nature07540

Turnbaugh, P. J., Ley, R. E., Mahowald, M. A., Magrini, V., Mardis, E. R., & Gordon, J. I. (2006). An obesity-associated gut microbiome with increased capacity for energy harvest. *Nature*, *444* (7122), 1027–1031. https://doi.org/10.1038/nature05414

Turnbaugh, P. J., Ridaura, V. K., Faith, J. J., Rey, F. E., Knight, R., & Gordon, J. I. (2009). The Effect of Diet on the Human Gut Microbiome: A Metagenomic Analysis in Humanized Gnotobiotic Mice. *Science Translational Medicine*, *1* (6), 6ra14-6ra14. https://doi.org/10.1126/scitranslmed.3000322

Udayappan, S., Manneras-Holm, L., Chaplin-Scott, A., Belzer, C., Herrema, H., Dallinga-Thie, G. M., Duncan, S. H., Stroes, E. S. G., Groen, A. K., Flint, H. J., Backhed, F., de Vos, W. M., & Nieuwdorp, M. (2016). Oral treatment with Eubacterium hallii improves insulin sensitivity in db/db mice. *Npj Biofilms and Microbiomes*, *2* (1). https://doi.org/10.1038/npjbiofilms.2016.9

Vrieze, A., Van Nood, E., Holleman, F., Salojärvi, J., Kootte, R. S., Bartelsman, J. F. W. M., Dallinga–Thie, G. M., Ackermans, M. T., Serlie, M. J., Oozeer, R., Derrien, M., Druesne, A., Van Hylckama Vlieg, J. E. T., Bloks, V. W., Groen, A. K., Heilig, H. G. H. J., Zoetendal, E. G., Stroes, E. S., de Vos, W. M., … Nieuwdorp, M. (2012). Transfer of Intestinal Microbiota From Lean Donors Increases Insulin Sensitivity in Individuals With Metabolic Syndrome. *Gastroenterology*, *143* (4), 913-916.e7. https://doi.org/10.1053/j.gastro.2012.06.031

FIGURES

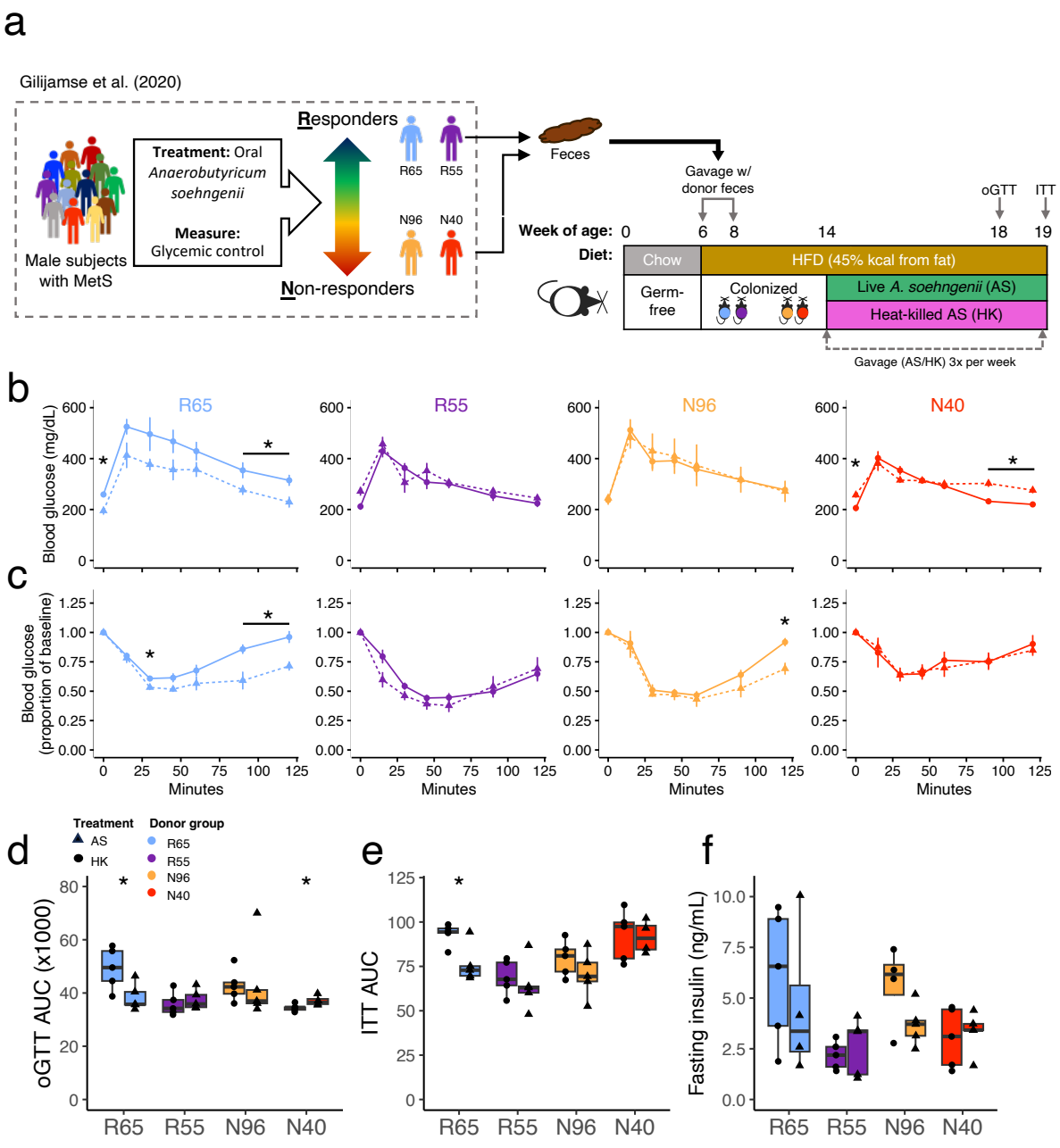

Figure 3.1. As treatment impacts glycemic control in a microbiota-dependent manner. Schematic (**a**) of the experimental design. Fecal samples from responders (R65, R55) and non-responders (N96, N40) were collected from participants of a clinical trial measuring glycemic control in subjects with metabolic syndrome orally treated with AS (Gilijamse et al., 2020). These fecal samples were used to colonize mice in the current study. Results of the oGTT (**b,d**) and ITT

(**c,e**) for AS and HK treated mice in each donor group along with fasting plasma insulin (**f**) measured at the start of the oGTT. Comparisons of means were conducted using Student's T-test between treatment groups within each donor group. Significance is indicated by * ($P < 0.05$). Sample size = 4-5/group.

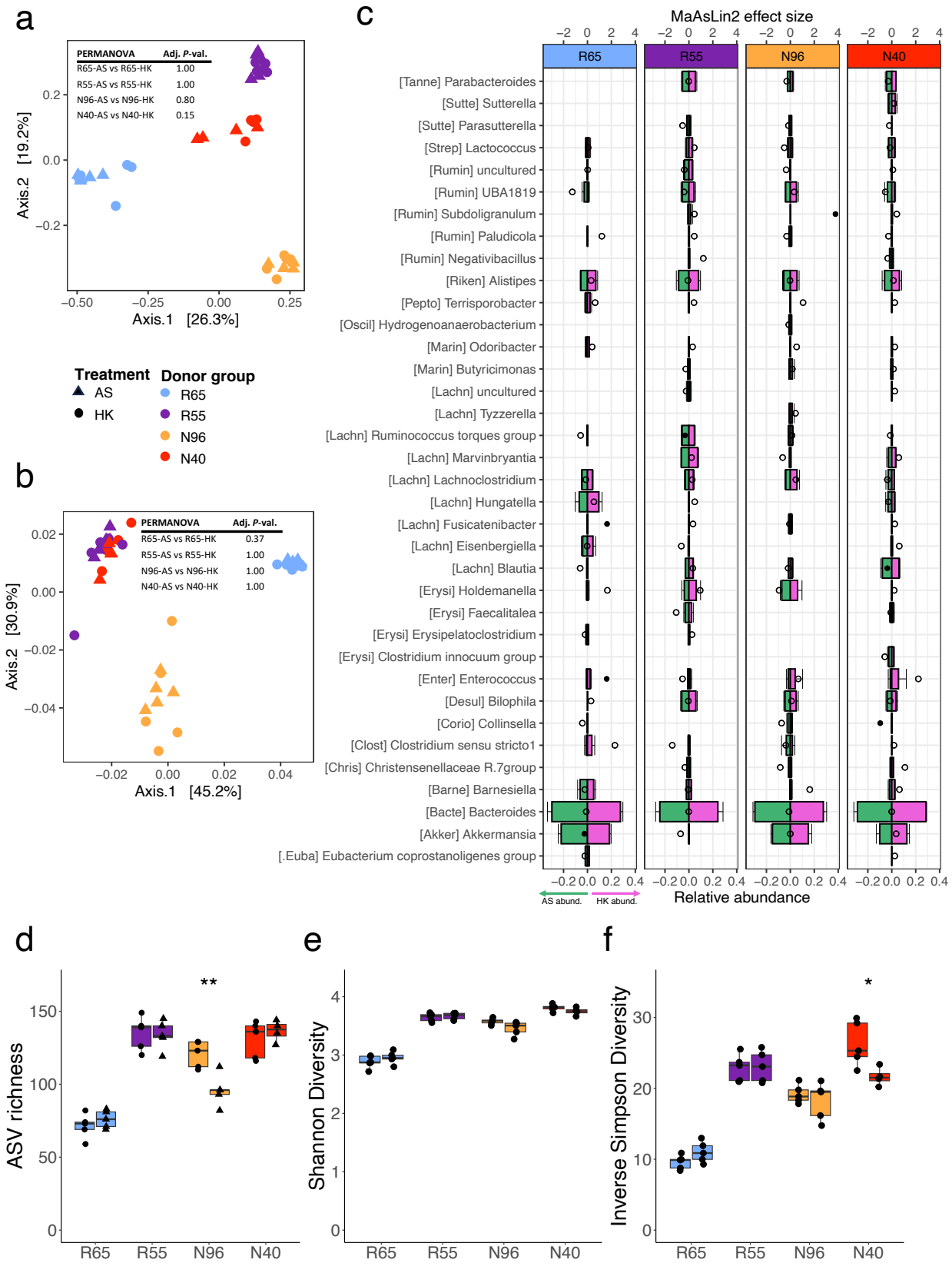
a
PERMANOVA Adj. P-val.
R65-AS vs R65-HK 1.00
R55-AS vs R55-HK 1.00
N96-AS vs N96-HK 0.80
N40-AS vs N40-HK 0.15
Axis.2 [19.2%]
Axis.1 [26.3%]
Treatment
AS
HK
Donor group
R65
R55
N96
N40
b
PERMANOVA Adj. P-val.
R65-AS vs R65-HK 0.37
R55-AS vs R55-HK 1.00
N96-AS vs N96-HK 1.00
N40-AS vs N40-HK 1.00
Axis.2 [30.9%]
Axis.1 [45.2%]
c
MaAsLin2 effect size
R65
R55
N96
N40
[Tanne] Parabacteroides
[Sutte] Sutterella
[Sutte] Parasutterella
[Strep] Lactococcus
[Rumin] uncultured
[Rumin] UBA1819
[Rumin] Subdoligranulum
[Rumin] Paludicola
[Rumin] Negativibacillus
[Riken] Alistipes
[Pepto] Terrisporobacter
[Oscil] Hydrogenoanaerobacterium
[Marin] Odoribacter
[Marin] Butyricimonas
[Lachn] uncultured
[Lachn] Tyzzerella
[Lachn] Ruminococcus torques group
[Lachn] Marvinbryantia
[Lachn] Lachnoclostridium
[Lachn] Hungatella
[Lachn] Fusicatenibacter
[Lachn] Eisenbergiella
[Lachn] Blautia
[Erysi] Holdemanella
[Erysi] Faecalitalea
[Erysi] Erysipelatoclostridium
[Erysi] Clostridium innocuum group
[Enter] Enterococcus
[Desul] Bilophila
[Corio] Collinsella
[Clost] Clostridium sensu stricto1
[Chris] Christensenellaceae R.7group
[Barne] Barnesiella
[Bacte] Bacteroides
[Akker] Akkermansia
[.Euba] Eubacterium coprostanoligenes group
AS abund.
HK abund.
Relative abundance
d
ASV richness
e
Shannon Diversity
f
Inverse Simpson Diversity
R65
R55
N96
N40

Figure 3.2. AS treatment did not drastically alter cecal bacterial composition. PCoA plots of unweighted (**a**) and weighted (**b**) UniFrac distances. **c** MaAsLin2 differential-abundance effect size (top axis, dots) of genus-level features between AS- and HK-treated mice within each donor group. The position of the dot relative to the origin represents the direction and magnitude of the effect (left of origin = higher abundance in AS-treated mice; right of origin = higher abundance in HK-treated mice). The significance of effect size is indicated by a solid dot ($P < 0.05$) or open dot ($P > 0.05$). Relative abundances of each genus (bottom axis) are indicated by the bars (green = abundance in AS group, pink = abundance in HK group). The first five letters of the family name for each genus are shown in brackets (Supp. Table 3.3). **d-f** Alpha diversity metrics for each group. Comparisons of means were conducted using Student's T-test between treatment groups within each donor group. Significance is indicated by * ($P < 0.05$), ** ($P < 0.01$). Sample size = 4-5/group.

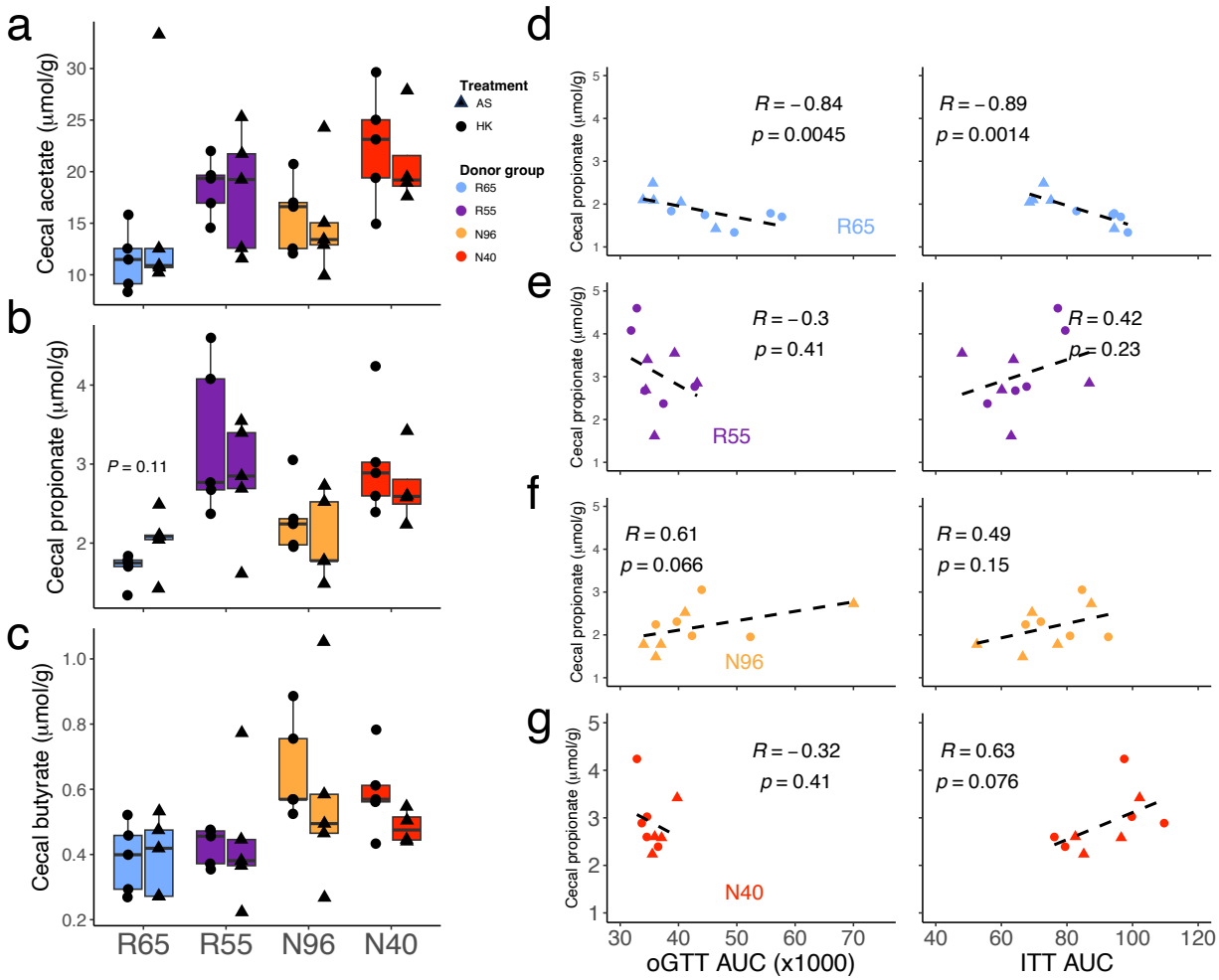

Figure 3.3. Cecal propionate is associated with improved glycemic control in a microbiota-dependent manner. Cecal levels of acetate (**a**), propionate (**b**) and butyrate (**c**) expressed in μmol per gram of wet-weight cecal content. Comparisons of means were conducted using Student's T-test between treatment groups within each donor group. Sample size = 4-5/group. (**d-g**) Scatter plots of cecal propionate levels and the AUCs for oGTT and ITT within each donor group along with the spearman's rho ("R") and *P*-value for each correlation. Mice from both treatment groups (AS and HK) were used in the correlation analysis for each donor group (n = 9-10/donor group).

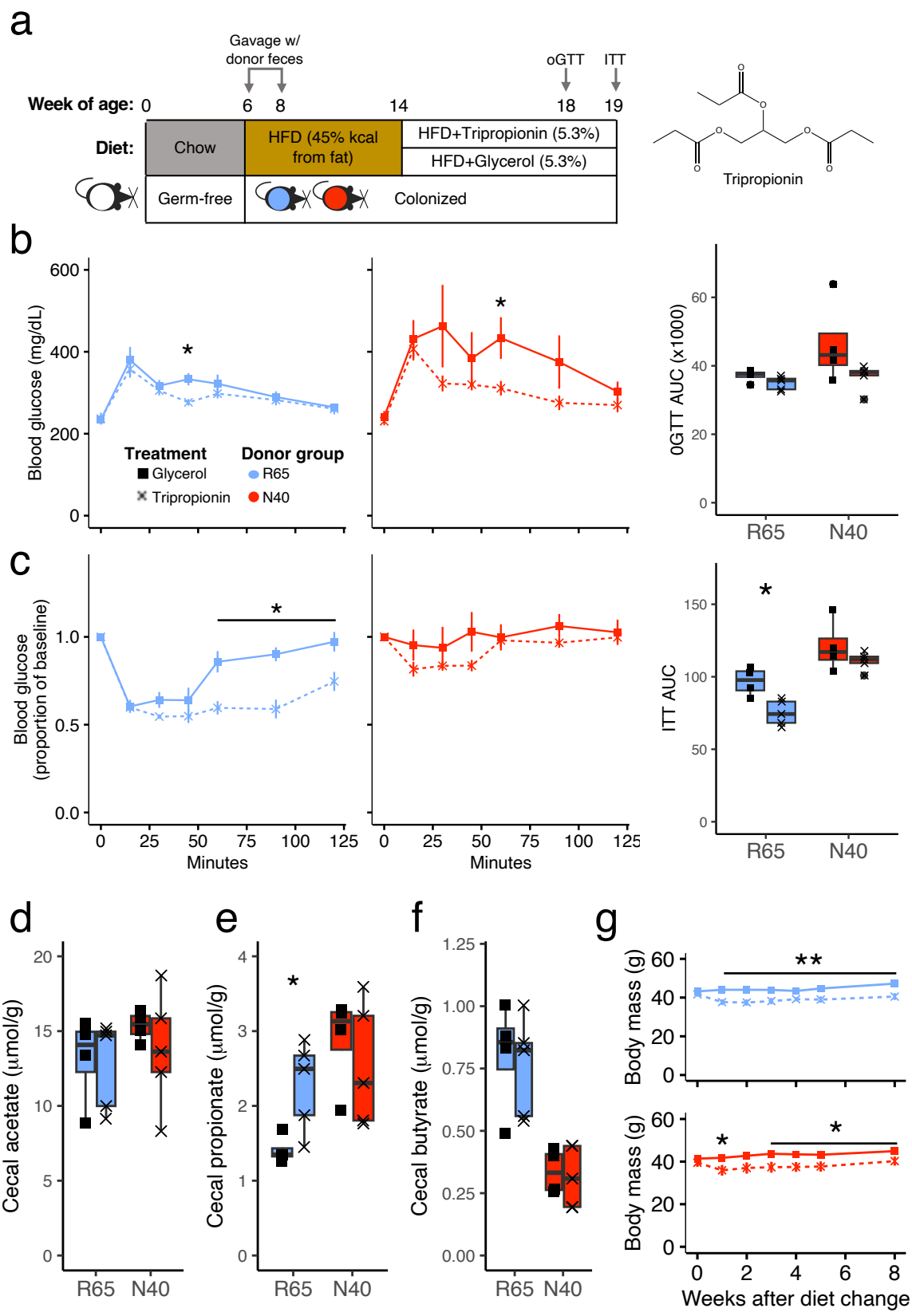
a
Gavage w/ donor feces
oGTT
ITT
Week of age: 0
6
8
14
18
19
Diet:
Chow
HFD (45% kcal from fat)
HFD+Tripropionin (5.3%)
HFD+Glycerol (5.3%)
Germ-free
Colonized
Tripropionin
b
Blood glucose (mg/dL)
Treatment
Glycerol
Tripropionin
Donor group
R65
N40
0GTT AUC (x1000)
c
Blood glucose (proportion of baseline)
Minutes
ITT AUC
d
Cecal acetate (µmol/g)
e
Cecal propionate (µmol/g)
f
Cecal butyrate (µmol/g)
g
Body mass (g)
Weeks after diet change

Figure 3.4. The gut microbiota modulates tripropionin's effect on insulin sensitivity and cecal propionate levels. Schematic (**a**) of the experimental design and the chemical structure of tripropionin. Glucose curves of oGTT (**b**) and relative change in blood glucose curves for ITT (**c**) of R65-colonized mice (left, light blue) and N-40 colonized mice (middle, red) along with their respective AUCs (right). Cecal levels of acetate (**d**), propionate (**e**) and butyrate (**f**) expressed in μmol per gram of wet-weight cecal content. (**g**) Body weight measurements of R65-colonized mice (upper, light blue) and N-40 colonized mice (lower, red) during the course of the treatment phase of the experiment. Comparisons of means were conducted using Student's T-test between treatment groups within each donor group and at each timepoint. Significance is indicated by * ($P < 0.05$), ** ($P < 0.01$). Sample size = 4-5/group.

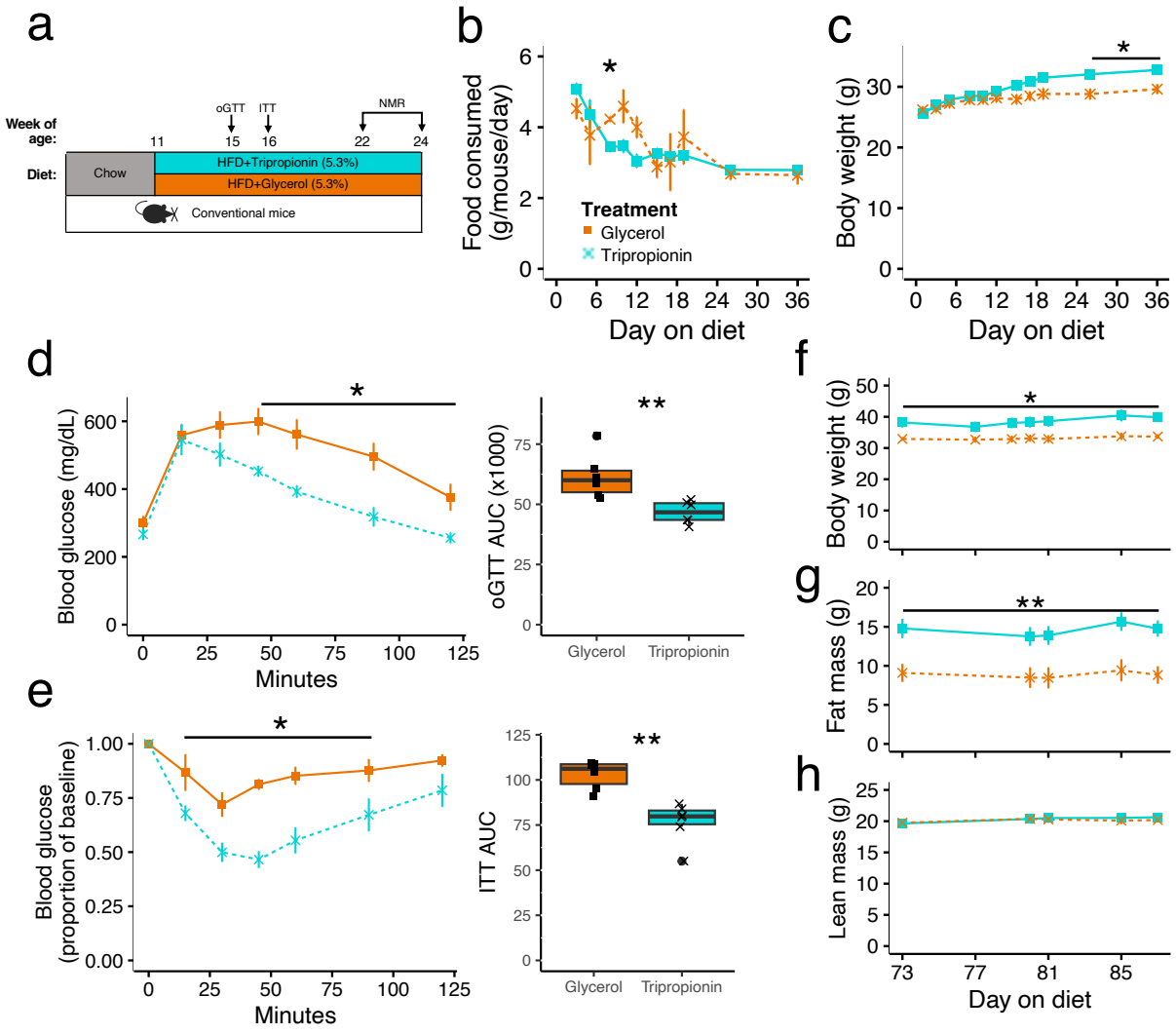

Figure 3.5. Tripropionin improves glycemic control and reduces adiposity in conventionally raised mice. Schematic (**a**) of the experimental design. Per-cage food consumption (**b**) and body weight (**c**) during the first 6 weeks of treatment. Blood glucose curve (left) and AUC (right) for oGTT (**d**) and ITT (e). Body weight (**f**) and NMR measurements of fat mass (**g**) and lean mass (**h**) collected 10 to 12 weeks after the start of dietary treatment. Comparisons of means were conducted using Student's T-test between treatment groups within each donor group and at each timepoint. Significance is indicated by * ($P < 0.05$), ** ($P < 0.01$). Sample size = 4-5/group.

SUPPLEMENTARY FIGURES AND TABLES

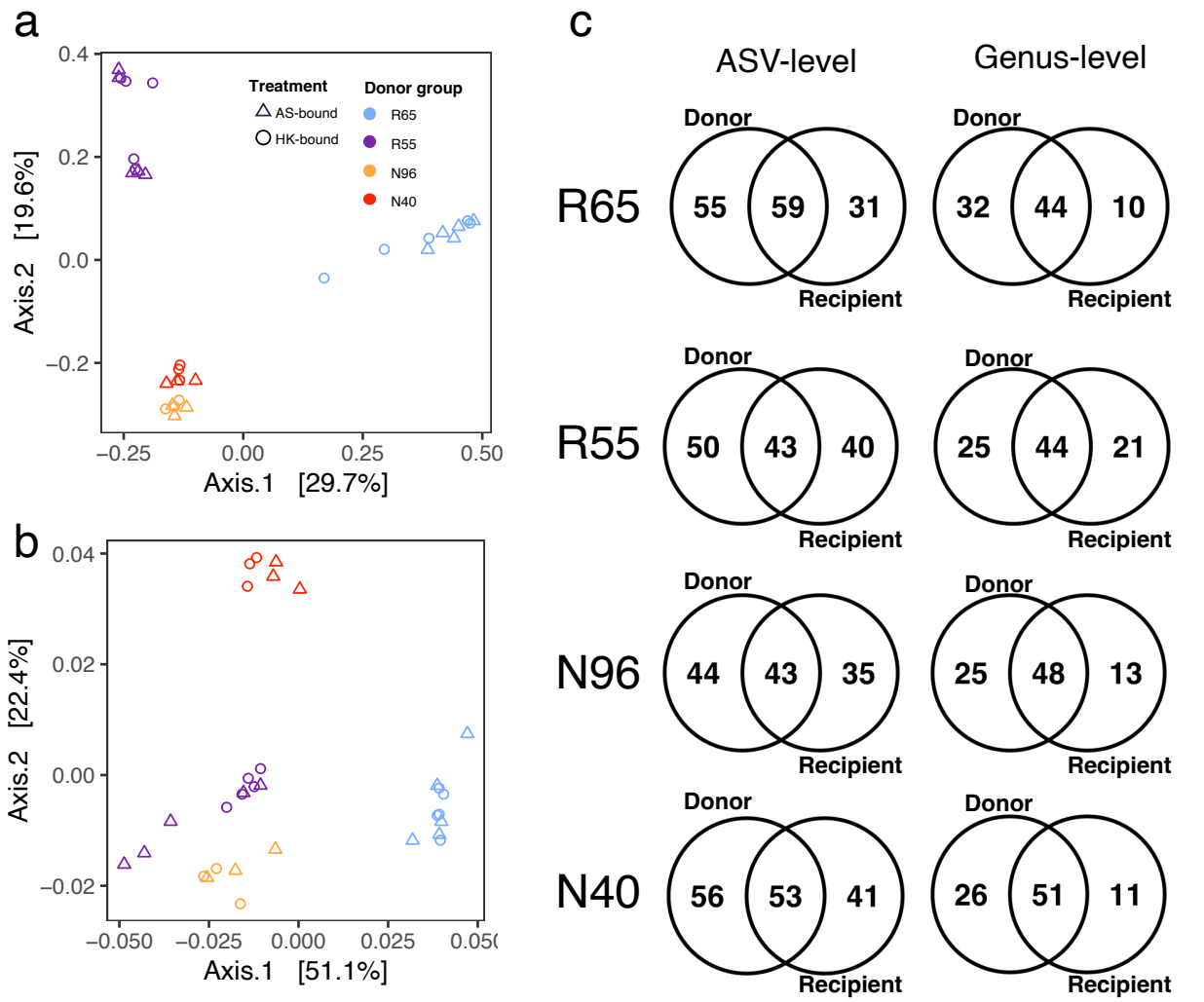

Supplementary Figure 3.1. Bacterial community beta diversity and engraftment of donor microbiota in recipient mice prior to AS/HK treatment. PCoA plots of unweighted (**a**) and weighted (**b**) UniFrac distances of 16S rRNA sequencing profiles of feces collected immediately prior to initializing treatment with AS or HK. At the time of feces collection, all mice were housed in the same cage (n = 9-10 per cage) but had been randomly assigned to go to the AS treatment group (AS-bound) or the HK treatment group (HK-bound). **c** ASV-level and genus level features detected in the donor samples, the recipient mice feces prior to AS/HK treatment or both from mice in each donor group.

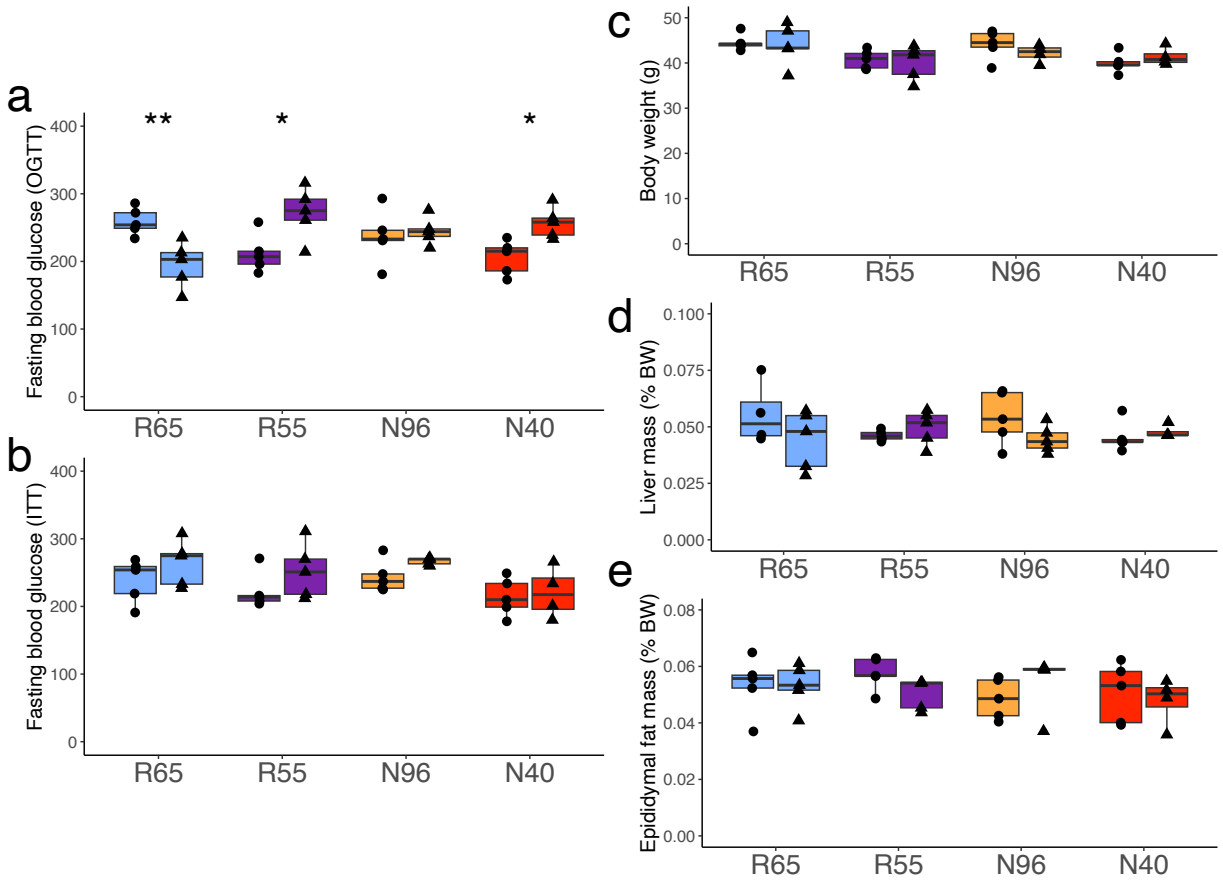

Supplementary Figure 3.2. Fasting blood glucose and other metabolic phenotype measurements. Fasting blood glucose levels at the start of the oGTT (**a**) and the ITT (**b**) one week later. Measurements of body weight (**c**), liver mass (**d**), and epididymal fat mass (**e**) collected upon sacrifice, one week after ITT. Comparisons of means were conducted using Student's T-test between treatment groups within each donor group. Significance is indicated by * ($P < 0.05$), ** ($P < 0.01$). Sample size = 4-5/group.

Supplementary Table 3.1. Spearman correlation rho (**ϱ**) coefficients, *P*-values, and adjusted *P*-values (fdr) of cecal SCFA levels vs AUCs for oGTT and ITT within each donor group.

		R65			R55			N96			N40		
SCFA	**Response variable**	**ϱ**	***P*val**	**fdr**	**ϱ**	***P*val**	**fdr**	**ϱ**	***P*val**	**fdr**	**ϱ**	***P*val**	**fdr**
Acetate	ITT AUC	-0.42	0.23	0.57	0.68	*0.04*	0.21	0.20	0.58	0.90	0.70	*0.04*	0.22
Acetate	OGTT AUC	-0.21	0.56	0.57	0.15	0.68	1.0	0.27	0.45	0.90	-0.20	0.61	1.0
Propionate	ITT AUC	-0.89	*0.001*	0.01	0.42	0.23	1.0	0.49	0.15	0.57	0.63	0.08	0.30
Propionate	OGTT AUC	-0.84	*0.005*	0.02	-0.30	0.41	1.0	0.61	0.07	0.40	-0.32	0.41	1.0
Butyrate	ITT AUC	-0.67	*0.04*	0.16	0.30	0.41	1.0	0.50	0.14	0.57	0.32	0.41	1.0
Butyrate	OGTT AUC	-0.45	0.19	0.57	0.12	0.76	1.0	0.59	0.08	0.40	-0.82	*0.01*	0.06

Supplementary Table 3.2. Composition of diets. All diets were irradiated and vacuum-packed.

Ingredient (g/Kg)	High-fat diet (TD.08811)	5.3% Tripropionin diet (TD.220540)	5.3% Glycerol diet (TD.220541)
Casein	195	195	195
L-Cystine	3	3	3
Sucrose	340	287	287
Corn Starch	56.86	56.86	56.86
Maltodextrin	60	60	60
Anhydrous Milkfat	210	210	210
Soybean Oil	20	20	20
Cellulose	50	50	50
Mineral Mix AIN-93G-MX (94046)	43	43	43
Vitamin Mix AIN-93-VX (94047)	19	19	19
Choline Bitartrate	3	3	3
TBHQ antioxidant	0.04	0.04	0.04
Tripropionin	-	53	-
Glycerol	-	-	53
Kcal/g	4.7	4.5	4.6

Supplemental Table 3.3. List of family-level abbreviations of bacterial classifications used in Figure 2.

Family name	Truncated name
Enterococcaceae	[Enter]
Lachnospiraceae	[Lachn]
Akkermansiaceae	[Akker]
Ruminococcaceae	[Rumin]
Rikenellaceae	[Riken]
Clostridiaceae	[Clost]
Erysipelotrichaceae	[Erysi]
Bacteroidaceae	[Bacte]
Barnesiellaceae	[Barne]
Coriobacteriaceae	[Corio]
Peptostreptococcaceae	[Pepto]
[Eubacterium]	[.Euba]
Marinifilaceae	[Marin]
Christensenellaceae	[Chris]
Desulfovibrionaceae	[Desul]
Streptococcaceae	[Strep]
Sutterellaceae	[Sutte]
Tannerellaceae	[Tanne]
Oscillospirales	[Oscil]

CHAPTER 4: *Gpr41* deficiency alters the gut microbiota-bile acid axis and attenuates hypercholesterolemia through inhibition of ileal *Npc1l1* expression.

Evan R. Hutchison[+]*, Jung-Ha Byun, Lauren Lucas, Kazuyuki Kasahara, Ruben Aquino Martinez, Michael Tallon, Qijun Zhang, Mallikarjun Jillella, Daniel Amador-Nuguez, Yongjun Liu, Vanessa A. Leone, Brian Parks, Federico E. Rey**

[+]Lead author

*Corresponding author

AUTHOR CONTRIBUTIONS

ERH and FER conceived of and designed the study. ERH JHB, and MMT bred the mice and conducted the mouse experiments. ERH collected tissues with assistance from MMT, JHB, KK, and RAM. LL and DAN analyzed bile acids. YL conducted histological analysis of the livers. ERH and BP conducted FPLC analysis and VAL provided resources for atherosclerosis assessment. ERH conducted all statical analyses with assistance from MJ and QZ. The manuscript was written by ERH and FER and approved by all co-authors.

ABSTRACT

More than 20% of the US population is estimated to have hypercholesterolemia which is a major risk factor for cardiovascular diseases (CVD) such as atherosclerosis. The gut microbiome modulates hypercholesterolemia through the production of the short-chain fatty acids (SCFA) acetate, propionate, and butyrate through fermentation of dietary fiber. SCFAs are sensed by multiple G protein-coupled receptors (Gpr) including Gpr41, Gpr43, and Gpr109a. Here, we aim to elucidate their individual roles in hypercholesterolemia and CVD by assessing atherosclerosis progression and lipid metabolism in knockout (KO) mice deficient in *Gpr41*, *Gpr43*, or *Gpr109a* under a proprotein convertase subtilisin/kexin type 9 adeno-associated virus (PCSK9-AAV) model for hypercholesterolemia. We found that none of the KO strains had significantly altered atherosclerotic plaque area compared to their wildtype littermates. Unexpectedly, *Gpr41*$^{-/-}$ males had reduced levels of plasma triacylglycerol and low-density lipoprotein cholesterol compared to WT littermates. This was associated with downregulated expression of *Npc1l1,* a key transporter involved in cholesterol absorption as well as reduced expression of transporters for other macronutrients. Moreover, male *Gpr41*$^{-/-}$ mice had altered gut microbiota composition and bile acid profiles relative to their WT counterparts. Transplantation of *Gpr41*$^{-/-}$ microbiota into germ-free mice did not recapitulate the cholesterol phenotype, suggesting that the effect of Gpr41 on cholesterol absorption is not mediated through alteration of the gut microbiota. Together these findings suggest that Gpr41, through activation by SCFAs, acts as an intestinal chemo-sensor that coordinates the expression of proteins involved in nutrient uptake.

INTRODUCTION

Cardiovascular disease (CVD) is the leading cause of death worldwide and is expected to rise as individuals with elevated risk factors increase in populous countries such as India and China (Celermajer et al., 2012). Atherosclerosis is an inflammatory disease resulting from dysregulation of lipid metabolism and chronic inflammation (Anogeianaki et al., 2011). Major advances in atherosclerosis treatment and prevention like statins and stents have had substantial impact on CVD, but despite these advances, this disease remains a major cause of mortality and morbidity highlighting the need for additional treatment options. Moreover, some patients experience side effects with statin treatment, with emerging evidence that these drugs may increase the risk of type 2 diabetes in some patients (Galicia-Garcia et al., 2020). Therefore, alternative strategies to address atherosclerosis and hypercholesterolemia are warranted.

One promising target for new CVD therapies is the gut microbiome. Intestinal microbes influence the host in part via production of a vast array of metabolites. Recent evidence suggests that gut-microbiome-derived metabolites such as SCFAs improve cardiometabolic health (Ahmad et al., 2019; Ohira et al., 2017). SCFAs are end-products of bacterial fermentation of dietary fibers and resistant starches. Acetate, propionate, and butyrate are the most abundant SCFAs in the intestine of humans and mice. Butyrate in particular has been shown to elicit beneficial metabolic effects including reduction of inflammation and atherosclerosis, as well as promotion of gut-barrier function (Arpaia et al., 2013; Jonsson & Bäckhed, 2017; Kasahara et al., 2018). Propionate has been shown to ameliorate atherosclerosis in mice by reducing plasma cholesterol levels through regulation of cholesterol absorption (Haghikia et al., 2021). Moreover, a lack of SCFA-producing bacteria is associated with higher risk for atherosclerosis (Karlsson et al., 2012). However, the mechanisms behind the atheroprotective effects of SCFAs are not fully understood.

SCFAs are sensed by G-protein coupled receptors (Gpr) including Gpr41, Gpr43, and Gpr109a. Each receptor has unique tissue expression profiles, but all three are expressed in intestinal tissue, adipose tissues, and immune cells (dendritic cells, Tregs (Gpr41); Tregs, macrophages, neutrophils (Gpr43); macrophages, neutrophils, Tregs (Gpr109a) (Kimura et al., 2020; Lukasova et al., 2011). Moreover, all three receptors have distinct affinities for each SCFA; Gpr41 (propionate > butyrate >> acetate), Gpr43 (acetate ≈ propionate ≈ butyrate), Gpr109a (butyrate only as well as non-SCFA ligands niacin and β-hydroxybutyrate) (Kimura et al., 2020). Previous studies have demonstrated that butyrate-sensing Gprs have roles in insulin sensitivity, obesity, and hypertension, all of which are known to impact atherosclerosis (Bjursell et al., 2010; Kaye David M. et al., 2020; Samuel et al., 2008; Veprik et al., 2016). Additionally, Gpr43 and Gpr109a also have roles in regulatory T cell differentiation which is relevant to atherosclerosis progression (Singh et al., 2014; Smith et al., 2013). These studies show that SCFA receptors are involved in physiological processes which impact atherosclerosis, but their involvement in SCFA-induced atheroprotection has not been systematically tested.

Here we examine the roles of Gpr41, Gpr43, and Gpr109a in atherosclerosis development and hyperlipidemia using individual strains of mice deficient in each receptor. Unexpectedly, we observed that *Gpr41* deficiency attenuated hypercholesterolemia, which was associated with an altered cecal microbial community structure and function as well as reduced ileal expression of the cholesterol transporter *Npc1l1*. Together, we show that Gpr41 plays an important role in shaping the gut microbiome and regulating nutrient absorbance.

RESULTS

Deficiency in *Gpr41, Gpr43,* or *Gpr109a* does not alter atherosclerotic plaque progression

We tested the roles of Gpr41, Gpr43, and Gpr109a in atherosclerosis development in individual strains of mice (male and female) deficient in each of these receptors relative to their respective wild-type (WT) littermates. Cholesterol levels – i.e., a major driver of atherosclerosis progression – were increased by administering an adeno-associated virus serotype 8 (AAV) carrying proprotein convertase subtilisin/kexin (PCSK9) payload (PCSK9-AAV) via retro-orbital injection at 6 weeks of age (Fig. 4.1a). We chose to maintain these mice on a high plant polysaccharide (HPP) diet supplemented with 1.5% cholesterol (wt/wt) to increase blood cholesterol in C57BL/6J mice infected with PCSK9-AAV while supporting high levels of SCFAs (Supp. Fig.1a-d). After 12 weeks on diet, no differences in aortic sinus plaque area between WT and any of the SCFA receptor KO mice were evident regardless of sex (Fig. 4.1b). There were also no differences in plaque oil red O (ORO) positive area between *Gpr41*$^{-/-}$ or *Gpr43*$^{-/-}$ mice compared to their WT counterparts (Fig. 4.1c); however, a significant reduction in plaque ORO area was evident in both male and female *Gpr109a*$^{-/-}$ mice compared their WT littermates (Fig. 4.1c). Further analysis of *Gpr109a*$^{-/-}$ mice revealed no significant difference in MOMA2 positive area between WT and KO mice, indicating that the difference in plaque lipid content was not due to differences in macrophage infiltration (Supp. Fig. 4.2a). Interestingly, *Gpr109a*$^{-/-}$ females showed increased plasma PCSK9; this was surprising, since increased plasma PCSK9 would presumably result in more advanced atherosclerosis (Supp. Fig.2b). There was no difference in plasma PCSK9 levels between KO and WT mice in any of the other SCFA receptor groups (Supp. Fig. 4.2b). *Gpr41*$^{-/-}$ males and females as well as *Gpr43*$^{-/-}$ males had reduced plasma total cholesterol relative to their respective WT littermates (Fig. 4.1d). Reduced liver mass was observed in *Gpr41*$^{-/-}$ males and females compared to their WT counterparts (Fig. 4.1e). *Gpr41*$^{-/-}$ males also had reduced gonadal adiposity, while *Gpr109a*$^{-/-}$ females had increased gonadal fat mass compared to their WT

littermates (Fig. 4.1f). Together these results indicate that whole-body deficiency of either *Gpr41*, *Gpr43*, and *Gpr109a* had little to no effect on atherosclerotic lesion development. However, these data also suggest that these receptors, particularly Gpr41, may be involved in lipid metabolism and adiposity in a sex-dependent manner.

Male *Gpr41*$^{-/-}$ mice have reduced plasma LDL cholesterol and TAG

Given the various metabolic phenotypes affected by *Gpr41*-deficiency in male mice, we next further characterized plasma lipids and liver phenotypes in male *Gpr41*$^{-/-}$ and their WT littermates. Fast protein liquid chromatography (FPLC) of pooled plasma samples revealed the reduced cholesterol content in *Gpr41*$^{-/-}$ males was primarily due to a reduction in the LDL-cholesterol fraction (Fig. 4.2a). There was no difference observed in plasma HDL-cholesterol between genotypes (Supp. Fig. 4.2c), which was also reflected in the FPLC HDL-cholesterol fraction (Fig. 4.2a). Male *Gpr41*$^{-/-}$ mice had reduced plasma triacylglycerol (TAG) levels relative to WT mice (Fig. 4.2b). We next assessed lipid content and inflammatory status in the liver. There was no difference in liver total cholesterol or TAG content (Fig. 4.2c,d) nor did we observe any differences in histological scores for steatosis, ballooning, or lobular inflammation between WT and *Gpr41*$^{-/-}$ males (Fig. 4.2e-h). These results show that WT mice have elevated plasma lipids, specifically TAG- and cholesterol-rich LDL particles relative to *Gpr41*$^{-/-}$ mice, while no accumulation of TAG or cholesterol was observed in the liver.

Secondary bile acid profiles and cecal propionate levels are altered in male *Gpr41*$^{-/-}$ mice

Enterohepatic circulation of bile acids plays an important role in whole-body sterol flux. To assess how bile acid metabolism might be altered between genotypes, we assessed bile acid

profiles of male WT and *Gpr41*$^{-/-}$ mice. We measured plasma and cecal levels of bile salts (bile acids conjugated a taurine or glycine) and unconjugated bile acids by uHPLC/MS/MS. In the plasma, deoxycholic acid (DCA), tauro-conjugated DCA (TDCA) as well as tauro-conjugated hyodeoxycholic acid (THDCA) were significantly reduced (P <0.05) in plasma of *Gpr41*$^{-/-}$ mice compared to their WT counterparts (Fig. 4.3a). There were no significant differences in either conjugated or unconjugated primary bile acid levels (Fig. 4.3a). In the cecum, four primary unconjugated bile acids were detected; chenodeoxycholic acid (CDCA), cholic acid (CA), and β- and ω-muricholic acids, and one primary conjugated bile acid, β-muricholic acid (T-β-MCA, Fig. 4.3b). Among these, ω-muricholic acid and CDCA tended to be lower in *Gpr41*$^{-/-}$ cecal contents (P = 0.08 and P = 0.06, respectively) compared to their WT counterparts (Fig. 4.3b). Eight major secondary bile acid species were detected, among which 6 were significantly reduced in *Gpr41*$^{-/-}$ mice, specifically lithocholic acid (LCA), 12-oxo-LCA, 3-oxo-DCA, ursodeoxycholic acid (UDCA), hyodeoxycholic acid (HDCA), and DCA (Fig. 4.3b). Notably, all of the detected bile acid species except 7-oxo-DCA were significantly reduced in *Gpr41*$^{-/-}$ mice. Only two conjugated bile acids were above the detection limit (TCA, and TDCA), neither of which were significantly altered between genotypes. These results show a reduction of circulating and intestinal bile acids – especially secondary bile acids – in *Gpr41*$^{-/-}$ mice with a lack of a substantial differences in primary bile acid levels. Together this evidence suggests *Gpr41* deficiency induces alterations in the bile acid pool that are driven primarily by microbially-produced secondary bile acids rather than alterations in host bile acid synthesis.

We also measured SCFA levels in the cecal contents of these mice. No differences in acetate, butyrate, or branched-chain fatty acid levels were detected between genotypes, however, *Gpr41*$^{-/-}$ mice had increased concentration of propionate compared to WT mice (Fig. 4.3c-g). These

results, along with the differences in secondary bile acid profiles, strongly suggest *Gpr41* deficiency may impact the membership and functional capacity of the intestinal microbiota.

Gpr41 regulates cecal microbiota composition

We next assessed the cecal microbiome composition and function in male *Gpr41*$^{-/-}$ mice relative to their WT littermates. To do this, we first characterized the cecal bacterial community composition via 16S rRNA gene amplicon sequencing. Principal coordinate analysis (PCoA) of weighted UniFrac distances showed the cecal community membership between WT and *Gpr41*$^{-/-}$ mice were distinct (Fig. 4.4a). Interestingly, genotype-associated differences in bacterial community membership were not observed between *Gpr43*$^{-/-}$ or *Gpr109a*$^{-/-}$ mice and their respective WT littermates (Supp. Fig. 4.3a) suggesting that, among the SCFA receptors, Gpr41 elicits the largest influence on cecal bacterial community membership, at least in the context of the diet used in this study. Compared to their WT littermates, *Gpr41*$^{-/-}$ mice had a significant reduction in ASV richness and Shannon diversity index (Fig. 4.4b-c). Differential abundance analysis showed the major differences in community membership between *Gpr41*$^{-/-}$ and WT mice were due to differences in relative abundances of specific taxa rather than their presence or absence (Fig.4d). For example, all the differentially abundant genera were detected in both genotypes, suggesting Gpr41 regulates the level of colonization of specific taxa rather than gatekeeping which taxa can colonize. *Gpr41*-deficiency led to lower relative abundances of 17 genera belonging to the families Lachnospiraceae, Oscillospiraceae, Ruminococcaceae, Erysipelotrichaceae, Butyricicoccaceae, Rikenellaceae, Deferribacteraceae, and Clostridiales (Fig. 4.4d). In contrast, only three genera, *Bacteroides*, *Lactobacillus*, and *Streptococcus,* were significantly higher in *Gpr41*$^{-/-}$ mice (Fig. 4.4d).

We searched for genera that were correlated with plasma TAG and total cholesterol levels. To do this, we included all male WT littermates from each SCFA-receptor group in our analysis (n = 32) which, despite all being on a C57BL/6J background, exhibited distinct microbial signatures – likely a remnant from their vivarium of origin (Fig. 4.4e). The rationale behind this analysis was to capture as many mice and as much microbial diversity as possible to increase the robustness of the associations, but without the confounding influence of genotype. Spearman correlation analysis resulted in 7 genera that were significantly (P <0.01) and positively correlated with plasma cholesterol and/or TAG (Fig. 4.4f). We found that *Bifidobacterium,* Xylanophylum group, "uncultured" Lachnospiraceae genus, and Clostridia VadinBB60 exhibited positive correlations with plasma cholesterol, *Roseburia* was positively associated with plasma TAG, whereas Lachnospiraceae A2, UCG-006, and *Lachnoclostridium* were positively correlated with both plasma cholesterol and TAG (Fig. 4.4g). *Odoribacter* was negatively correlated with plasma cholesterol (Fig. 4.4g). Of the taxa that were positively associated with plasma lipids in all male WT mice, five (Lachnospiraceae A2 genus, "uncultured" Lachnospiraceae genus, *Roseburia*, Lachnospiraceae UCG-006, and Clostridia VadinBB60) were downregulated in *Gpr41*$^{-/-}$ mice compared to their WT littermates (Fig. 4.4e). This suggests that Gpr41 selects for taxa that are associated with increased circulating levels of lipid.

We then conducted metagenomic analysis to assess differences in microbial function, specifically abundance of bile-modifying genes, in *Gpr41*$^{-/-}$ mice and their WT counterparts. The first step of bile salt modification by intestinal microbes is hydrolysis of the amino acid to form unconjugated primary bile acids. This reaction is catalyzed by bile salt hydrolase (*bsh*) which is present in many gut microbiota. The subsequent modifications that produce DCA and LCA rely on the bile acid 7α-dehydroxylation operon (*bai*) (Heinken et al., 2019). While this pathway has

been extensively researched in human microbiota such as *Clostridium scindens* and *Clostridium hylemonae*, assessing the abundances of homologous genes in mouse metagenomes is understudied. To do this, we used hidden Markov models (HMM) profiles of *bsh* and the genes in the *bai* operon (*baiA2, baiB, baiCD, baiE, baiF, baiG, baiH, baiI, baiN*) to search for homologs within the Mouse Gastrointestinal Bacteria Catalogue (MGBC) (Beresford-Jones et al., 2022) genome database. We used these homologs as reference sequences upon which we mapped the cecal metagenomic reads, enabling us to quantify their abundances. The abundance of *bsh* trended higher in *Gpr41*$^{-/-}$ mice compared to WT mice ($P = 0.093$, Fig. 4.5a). In contrast, *Gpr41*$^{-/-}$ mice had significantly fewer *baiCD, baiE, baiF, baiI,* and *baiH* than their WT counterparts (Fig. 4.5b). Nearly all the *bai* genes detected in these metagenomes belonged to the genus *Dorea* in the Lachnospirales family (Supp Fig. 4.2b). Interestingly, the detected *bai* gene hits were highly distinct from those of the human strains *C. scindens* and *C. hylemonae*, suggesting that *Dorea* instead of *Clostridium* may occupy the 7α-dehydroxylation niche in mouse-specific genomes. The *bsh* gene, on the other hand, was detected from a diverse collection of taxa across 6 phyla (Supp. Fig. 4.3b). These findings suggest that *Gpr41*$^{-/-}$ microbiota potentially has reduced capacity to synthesize DCA and LCA via the *bai* pathway, which may explain the reduced concentration of these secondary bile acids in the cecum and plasma.

Gpr41 deficiency reduces expression of ileal *Npc1l1* and other nutrient transporters

To compare the effects of *Gpr41* deficiency on intestinal and liver gene expression, we assessed the transcriptomic profiles of the liver and ileum of WT and *Gpr41*$^{-/-}$ male mice using RNA-seq, using DSEeq2 to detect differentially expressed genes (DEGs). We observed 645 DEGs (unadjusted $P < 0.01$) in the liver, with 445 upregulated in WT and 200 upregulated in *Gpr41*$^{-/-}$

livers. Pathway enrichment analysis of liver DEGs using Enrichr showed that 44 KEGG pathways were significantly enriched ($P < 0.01$) in the WT livers, while two (*Retinol metabolism* and *Steroid hormone biosynthesis*) were upregulated in *Gpr41*$^{-/-}$ livers (Supp. Fig. 4.4a). The pathways enriched in WT included various immune and inflammatory signaling processes, the most significant of which were the *Chemokine signaling pathway, Cytokine-cytokine receptor interaction,* and *TNF signaling pathway* (Supp. Fig. 4.4a). A subset of DEGs were present in multiple WT-enriched pathways, of which the most frequently represented DEGs were *Nfkbia* (NFKB inhibitor α), *Fos* (Fos proto-oncogene), *Ccl2* (monocyte chemoattractant protein-1), *Icam1* (intercellular adhesion molecule 1), *Tlr2* (Toll-like receptor 2), all of which are involved in immune signaling (Supp. Fig. 4.4b). We also examined expression of the rate-limiting genes involved in cholesterol synthesis (*Hmgcr*, *Sqle*) and their regulators (*Srepf1*, *Srebf2*), however, no differences were detected ($P<0.05$), although a trend toward reduction of *Hmgcr* mRNA was observed in the livers of *Gpr41*$^{-/-}$ mice ($P = 0.053$, Supp. Fig.4c). This suggests the elevated LDL-cholesterol observed in WT mice is likely not due to differences in hepatic cholesterol synthesis. Together, these results indicate the vast majority of DEGs in the liver are downregulated in *Gpr41*$^{-/-}$ mice and these genes are overrepresented in immune processes.

In the ileum, we detected 486 DEGs ($P <0.01$) with 354 upregulated in WT mice and 132 upregulated in *Gpr41*$^{-/-}$ mice. KEGG pathway enrichment analysis revealed that WT-enriched DEGs were overrepresented in 12 pathways (Fig. 4.6a). Interestingly, two pathways, *Cholesterol metabolism* and *Fat digestion and absorption* pathways were enriched in both the WT and *Gpr41*$^{-/-}$ small intestine (Fig. 4.6a). Upon further examination of the DEGs that contributed to *Cholesterol metabolism* pathway enrichment in both genotypes, we observed overexpression of genes involved in cholesterol uptake and lipoprotein formation in WT mice (*Cyp27a1*, *Abca1*, *Abcg8*, *Abcg5*,

Npc1, and *Apoe*), and genes involved in lipase activity and lipoprotein uptake in *Gpr41*$^{-/-}$ mice (*Lipg*, *Pcsk9*, and *Ldlr*) (Fig. 4.6b). Importantly (in the context of the PCSK9-AAV model), there was no difference in expression in the liver or circulating PCSK9 protein (Supp. Fig. 4.2b). The DEGs that contributed to *Fat digestion and absorption* pathway enrichment between genotypes similarly centered around overexpression of lipid transport genes in WT mice (*Abca1*, *Abcg8*, *Abcg5*, and *Npc1l1*) and lipase genes in the *Gpr41*$^{-/-}$ mice (*Pnliprp2*, *Clps*, and *Acat2*) (Fig. 4.6d). NPC1L1 is the primary transporter of cholesterol in the intestine and can influence plasma cholesterol levels. Given that these mice were fed a high cholesterol diet, the results reported here suggest that downregulation of *Npc1l1* in the small intestine of *Gpr41*$^{-/-}$ mice could contribute to the observed reduction in circulating cholesterol levels. Ileal expression of bile acid transporters *Ost-α* and *Asbt* were also reduced in *Gpr41*$^{-/-}$ mice suggesting that Gpr41 deficiency results in a general reduction of sterol uptake (Fig. 4.6e). Interestingly, various pathways that were enriched in the ileum of WT mice are linked by their involvement in temporal (*Circadian rhythm*) as well as nutrient uptake processes (*Protein digestion and absorption, Retinol metabolism, Cholesterol metabolism, Vitamin digestion and absorption, Mineral absorption, Fat digestion and absorption*) indicating that Gpr41 may play a role in sensing nutrient availability and coordinating nutrient harvest (Fig. 4.6a).

Additionally, we noticed that a disproportionate number of DEGs in the ileum belonged to the solute carrier (*Slc*) family of genes which code for membrane transport proteins. Given the observation that WT mice had enriched expression of genes in the *Protein digestion and absorption* pathway, we compared the expression of *Slc* genes belonging to gene classes that are involved in amino acid and peptide transport (*Slc1a, Slc6a, Slc7a, Slc16a, Slc36a, Slc38a, Slc43a, and Slc15*). Out of a total of 44 AA transport genes that were detected in the ileum (above a

detection threshold of 100 TPM), seven (16%) were significantly differentially expressed (P <0.05) between WT and *Gpr41*$^{-/-}$ mice, all of which were upregulated in under WT conditions (Fig. 4.6c). This further supports the hypothesis that *Gpr41*$^{-/-}$ mice have an impaired response to nutrient availability, which may lead to differences in nitrogen availability in the luminal content between WT and *Gpr41*$^{-/-}$ mice.

Gpr41 deficiency alters expression of FXR gene targets

Consistent with the reductions in bile acids within *Gpr41*$^{-/-}$ mice, we also observed reduction in genes regulated by the transcription factor farnesoid X receptor (FXR) which is activated by bile acids (Matsubara et al., 2013). We observed significant (unadjusted $P < 0.05$) downregulation of the FXR gene targets (Wang et al., 2008) *Shp*, *Fabp6*, *Baat, Ostα*, *Apoc3*, *Apoa1*, *Apoe,* and *Abcc2* in *Gpr41*$^{-/-}$ mice in the ileum (Supp. Fig. 4.5b). We also observed differences in liver expression of the FXR gene targets *Vldlr, Abcb11, Insig2, Shp, Slc10a2, Apoc2, Pltp, and Sdc1* (Supp. Fig. 4.5a). This may signify reduced FXR activation by bile acids in these mice, however the expression patterns of these genes do not match the classically reported FXR regulatory effect. For example, according to previous studies (Wang et al., 2008), reduced FXR activity would lead to a reduction in *Shp*, *Fabp6*, *Baat, Ostα*, *Apoe,* and *Abcc2,* but it should lead to an increase in *Apoa1* and *Apoc3* expression, which is opposite of our findings (Supp. Fig. 4.5b). Similarly, the recognized effects of FXR activation would predict that *Abcv11* and *Insig2*, and *Apoc2* would be downregulated in the livers of *Gpr41*$^{-/-}$ mice, not an upregulation as we observed (Supp. Fig. 4.5a). This discrepancy may be the result of differing activation of a complex network of multiple regulatory elements between *Gpr41*$^{-/-}$ mice and their WT littermates.

Transplantation of WT and *Gpr41*$^{-/-}$ cecal microbiota did not result in distinct microbial communities or transfer cholesterol phenotypes.

To test whether *Gpr41*$^{-/-}$-induced alterations in the gut microbiota caused the differences in plasma cholesterol levels between genotypes, we conducted a cecal microbiota transplant (CMT) from male *Gpr41*$^{-/-}$ mice and their WT littermates into GF C57BL/6J male mice fed the same high-cholesterol HPP diet described in the previous experiment (Supp. Fig. 4.6a). The recipient mice were injected with PCSK9-AAV two weeks after colonization to induce hyperlipidemia. Eight weeks after transplantation we tested plasma levels of total cholesterol but did not observe a significant difference between WT-CMT and *Gpr41*$^{-/-}$-CMT mice (Supp. Fig. 6b). Moreover, 16S rRNA community compositions were indistinguishable between WT-CMT and *Gpr41*$^{-/-}$-CMT recipient mice at both 4 weeks (fecal communities) and 8 weeks (cecal communities) post-transplant (Supp. Fig. 4.6c,d). The bacterial communities of the gnotobiotic recipient mice converged to a common conformation regardless of the source their inoculum, suggesting that *Gpr41* deficiency is required to maintain the distinct community structures observed between *Gpr41*$^{-/-}$ mice and their WT littermates.

DISCUSSION

SCFAs, particularly butyrate and propionate, have been shown to protect against CVD and atherosclerosis (Aguilar et al., 2014; Bartolomaeus et al., 2019; Haghikia et al., 2021; Kasahara et al., 2018). Various mechanisms explaining this phenomenon have been described, but whether SCFA-sensing receptors are involved in these mechanisms remains an outstanding question. Previous studies have examined the roles of Gpr109a in atherosclerosis, but these studies assessed the effects of non-SCFA agonists of Gpr109a: 3-hydroxybutyrate and niacin (Lukasova et al.,

2011; Zhang et al., 2021). Gpr109a induces distinct β-arrestin- and G-protein-mediated signaling cascades which are preferentially induced by different agonists. SCFA signaling via Gpr109a might therefore have a distinct effect in atherosclerosis but had not been tested previously.

The aim of the current study was to assess whether any of the SCFA receptors Gpr41, Gpr43, or Gpr109a mediate butyrate- or propionate-induced protection against atherogenesis. Surprisingly, SCFA receptor deficiency did not result in exacerbated atherosclerosis compared to WT littermates in either males or females. Moreover, we observed male and female *Gpr41*$^{-/-}$, and male *Gpr43*$^{-/-}$ mice were protected against hypercholesterolemia compared to WT littermates in our model. Interestingly, these reductions in non-HDL cholesterol did not protect against atherogenesis, suggesting that whole-body ablation of *Gpr41* and *Gpr43* have counteracting effects on atherosclerosis progression. Additionally, we observed several significant and at least initially, counterintuitive phenotypes within *Gpr41*$^{-/-}$ male mice relative to their WT littermates, including reduced plasma TAG and LDL cholesterol, reduced fat mass, and reduced liver weight. Previous studies involving *Gpr41*$^{-/-}$ males have described opposing observations in fat mass, but differences in plasma TAG and cholesterol have not previously been detected (Bellahcene et al., 2012; Samuel et al., 2008). These discrepancies could be explained by the different diets used in the various experiments, furthermore, our PCSK9-AAV-induced hyperlipidemia model in the absence of a western-style diet may reveal novel underlying mechanisms that are independent of the typical metabolic dysregulation associated with high-fat/high-sugar diets.

Initially, these observations led us to suspect that *Gpr41*$^{-/-}$ mice would have reduced lipid content burden and therefore reduced inflammation, but we subsequently failed to detect differences in liver inflammation or lipid content. Liver transcriptional analyses did not reveal major changes in the expression of cholesterol synthesis genes suggesting that the differences in

cholesterol were not due to changes in hepatic cholesterol production. In the ileum, however, we detected a significant reduction in *Npl1l1* expression in *Gpr41*$^{-/-}$ mice. NPC1L1 is the primary intestinal transporter responsible for dietary cholesterol absorption (Altmann et al., 2004); it was recently found that intestinal *Npc1l1* expression is negatively regulated by propionate (Haghikia et al., 2021). Interestingly, the decrease in *Npc1l1* expression in *Gpr41*$^{-/-}$ mice corresponded with an increase in cecal propionate.

Male *Gpr41*$^{-/-}$ mice had significantly lower relative abundances of taxa belonging primarily to Rummincoccaceae, Lachnospiraceae, and Oscillospiraceae families of the Bacillota family, whereas higher relative abundances of *Bacteroides* genus within the phylum Bacteroidota were observed. Among the three most abundant SCFAs in the gut, Gpr41 senses propionate with the highest affinity. Notably, propionate producers are found in both Bacillota (Lachnospiraceae and Ruminococcaceae) and Bacteroidota (*Bacteroides spp*.) phyla (Reichardt et al., 2014). Since higher levels of cecal propionate were detected in *Gpr41*$^{-/-}$ mice, it is possible that the *Bacteroides* members may have an outsized influence over propionate production than those of Lachnospiraceae and Ruminococcaceae. It is possible Gpr41 regulates the abundance of propionate producers in the intestine through a negative-feedback mechanism, however, further research would be needed to test this hypothesis. Together, these findings indicate a potential mechanism behind the differences in plasma cholesterol, whereby Gpr41 regulates intestinal microbiota colonization and composition leading to differences in propionate production, which in turn regulates intestinal *Npc1l1* expression and cholesterol absorption.

We tested this hypothesis by transplanting of *Gpr41*$^{-/-}$ and WT cecal microbiota into hyperlipidemic germ-free mice, however, we were not able to recapitulate the plasma cholesterol phenotype through microbes alone. However, monitoring of the fecal microbiome composition of

the transplanted mice revealed that recipients of *Gpr41*$^{-/-}$ or WT microbiota were indistinguishable after transplantation, indicating that *Gpr41* deficiency is necessary to maintain the distinct microbiota configuration. Therefore, while this indicates that the *Gpr41*-regulated microbial community membership is not entirely responsible for the changes in plasma cholesterol, the convergence of the recipient microbiomes prevents us from definitively concluding that the microbiome is not causal.

Gpr41$^{-/-}$ mice had altered secondary bile acid profiles in both the plasma and cecum. Secondary bile acids are the result of microbial modulation of deconjugated primary bile acids and can have downstream signaling effects which can affect host metabolism. Bile acids, including secondary bile acids, are agonists of FXR, which is a key regulator of enterohepatic bile acid homeostasis. While we did not observe differences in ileal expression of the classic FXR-regulated gene *Fgf15*, we did detect reductions in mRNA of other FXR target genes in the ileum and livers of *Gpr41*$^{-/-}$ mice. This is consistent with the reduction of the global bile acid pool in *Gpr41*$^{-/-}$ mice, but discrepancies in the direction of regulation (up- or down-regulated) between the published effects of FXR activation and the expression patterns observed in our mice indicates a more complex picture that suggests that multiple counter-acting transcription factors are affected by *Gpr41* deficiency. Additionally, we observed reductions in multiple intestinal amino acid transporters in the ileum of *Gpr41*$^{-/-}$ mice, consistent with the theme of altered absorptive programming in *Gpr41*-deficiency.

Our study has a few limitations that should be noted. First, the use of whole-body KO mice prevents us from testing tissue-level effects of these receptors. Indeed, each receptor is expressed in various tissue types (Kimura et al., 2020), which may have counter-acting effects on atherosclerosis. This could be further tested through the use of tissue-specific conditional

knockouts. Additionally, this study was limited to the context of PCSK9-AAV-induced hypercholesterolemia. Diet alone is insufficient to induce hypercholesterolemia in C75BL/6J mice, so a physiological perturbation is required to study atherosclerosis in these animals. This is usually done by genetic manipulation (*Apoe*$^{-/-}$, or *Ldlr*$^{-/-}$), however, PCSK9-AAV offers an important alternative that avoids complicated and laborious double-KO breeding schemes. Nonetheless, his introduces the possibility of confounding effects related to overexpression of PCSK9 since it has been reported that *Pcsk9* interacts with other surface receptors besides the LDL-receptor (Bai et al., 2018).

In summary, our findings indicate that neither Gpr41, Gpr43, nor Gpr109a are major mediators of SCFA-induce atheroprotection, although we cannot rule out their role at the tissue-level. We also provide evidence that Gpr41 coordinates intestinal expression of nutrient transporters under hyperlipidemic conditions, in line with the notion of SCFAs and their receptors as key regulators of intestinal physiology. Finally, we also provide evidence that Gpr41 induces enhanced cholesterol absorption, which may have implications for CVD therapeutic strategies.

METHODS

Gpr-KO Animals and Diets

Gpr41$^{-/-}$, *Gpr43*$^{-/-}$, and *Gpr109a*$^{-/-}$ mice were generated as previously described and generously donated by Karen Ho, Northwestern University (*Gpr41*$^{-/-}$ and *Gpr43*$^{-/-}$) and Pamela Martin, Augusta University (*Gpr109a*$^{-/-}$). All knockout (KO) strains had previously been backcrossed with C57BL/6J mice for multiple generations. Within each strain, KO mice were paired with C75BL/6J (Jackson Laboratories, Bar Harbor, ME) breeding mates to produce a heterozygous (Het) F_1 generation for each strain. The Hets were then paired for breeding to produce a F_2 generation

consisting of WT, HET and KO littermates. Genotyping was conducted to select the WT and KO pups for use in subsequent experiments. All mice were housed in a ventilated cage system (Alternative Design, Siloam Springs, AR) with corn husk bedding with access to chlorinated water and chow (Teklad 8604, Inotiv, Madison, WI) *ad libitum*. All animal experiments were conducted in accordance with the University of Wisconsin Madison's animal welfare standards and were approved by the university's Animal Care and Use Committee.

Gpr-KO experimental design

At 6 weeks of age, male and female WT and KO littermates were injected with $1.5x10^{11}$ particles of PCSK9-AAV8 (AAV8-D377Y-mPCSK9, Vector Biolabs, Malvern, PA) via retroorbital injection under isoflurane-induced anesthesia. Mice were also switched to a high-plant polysaccharide, high-cholesterol (1.5% wt/wt) diet supplemented with cocoa butter (6.5% wt/wt) (TD.210423, Inotiv) after injection. Mice were maintained on this diet for 12 weeks at which point they were sacrificed for tissue collection.

Atherosclerosis analysis

Atherosclerotic plaque area was measured in the aortic sinus as previously described (Hutchison et al., 2023). Briefly, 10 μm sections of the aortic sinus were systemically collected such that each slide set contained sections from 0, 100, 200, 300, 400, 600, 700, and 800 μm ascendant from the base of the aortic sinus where the aortic valve leaflets first appear. Slides containing these sections were fixed with formalin and stained with ORO and imaged on an inverted light microscope. Digitally captured images were analyzed using ImageJ (National Institutes of Health, Bethesda, MD) to measure lipid content (ORO-positive area) and total plaque area. The mean of the values

across all sections were used to calculate average lipid content and average plaque area for each mouse. Sections that were damaged were removed from the mean calculation. The aortas from three mice were damaged during collection and could therefore not be analyzed.

Analysis of plasma markers

Blood was obtained via heart puncture of anesthetized mice just prior to euthanasia with 0.5 M EDTA and plasma was collected after centrifugation. Colorimetric assay kits were used to acquire plasma levels of total cholesterol, HDL-cholesterol, TAG and ALT. Plasma levels of PCSK9 were determined using an ELISA assay kit (ab215538, abcam, Cambridge, UK).

Plasma FPLC analysis

Plasma from 7 male WT and 7 male *Gpr41*$^{-/-}$ mice were evenly pooled based on genotype and mixed. A volume of 165 μL of each pool was diluted in 835 μL of PBS and the entire mixture (1 mL total) was loaded onto a AKTA fast protein liquid chromatography (Amersham Pharmacia Biotech, Amersham, UK) fitted with a Superose 6 column (Cytiva, Marlborough, MA) in tandem with a Superdex 200 column (Cytiva) using a mobile phase consisting of 10 mM PBS (pH 7.4) and 0.02% sodium azide. After the first 11 minutes, 0.5 mL fractions were collected every minute into 48 separate elution tubes. Each fraction was analyzed for TAG and cholesterol content using the colorimetric assay kits described above.

Liver lipid content

Lipids were extracted from the liver by bead-beating 20-50 mg of frozen liver tissue with three 2.8 mm ceramic beads in the presence of lipid extraction buffer from the abcam Liquid Extraction Kit

(ab211044, abcam) for 2x30 seconds followed by agitation for 20 minutes. The extraction slurry was spun down at 10,000 x g for 5 minutes at 4°C and the supernatant was transferred to a new tube and allowed to dry overnight. The resulting residue was dissolved in 50 µL of the kit resuspension buffer plus 350 µL of 10% Triton X-100 (X-100, Sigma-Aldrich, Burlington, MA) and heated (37°C) sonication for 30-45 minutes. The lipid extract was used in the TAG and total cholesterol colorimetric kits described above to determine lipid content per gram of tissue.

Bile acid measurements by uHPLC-MS/MS

Cecal sample prep. Lipids were extracted from ~30 mg of frozen cecal contents using the same lipid extraction method for liver tissue described above, except that after drying overnight, extracts were dissolved in 80% methanol and stored at room temperature (RT). *Plasma sample prep*. 20 μL of plasma was diluted in 80 μL of 100% methanol, vortexed for 30 seconds, spun down at 14,000 x g for 5 minutes at 4°C, and the supernatant was collected. Cecal and plasma lipid extracts were further diluted 1:10 using ultrahigh-pressure liquid chromatography (uHPLC)-grade H_2O, and 100 µl was transferred to an HPLC vial for analysis. Samples were analyzed using an ultrahigh-pressure liquid chromatography-tandem mass spectrometry (uHPLC-MS/MS) system consisting of a Thermo Scientific Vanquish uHPLC system coupled to a heated electrospray ionization (HESI; using negative polarity) and hybrid quadrupole high-resolution mass spectrometer (Q Exactive Orbitrap; Thermo Scientific). Settings for the ion source were as follows: auxiliary gas flow rate of 10, sheath gas flow rate of 30, sweep gas flowrate of 1, 2.5-kV spray voltage, 320°C capillary temperature, 300°C heater temperature, and S-lens radiofrequency (RF) level of 50%. Nitrogen was used as nebulizing gas by the ion trap source. Liquid chromatography (LC) separation was achieved using a Waters Acquity UPLC BEH C18 column with 1.7-µm

particle size, 2.1 by 100 mm in length. Solvent A was water with 10 mM ammonium acetate adjusted to pH 6.0 with acetic acid. Solvent B was 100% methanol. The total run time was 31.5 min with the following gradient: a 0- to 24-min gradient from 30% solvent B (initial condition) to 100% solvent B; hold 5 min at 100% solvent B; drop to 30% solvent B for 2.5-min reequilibration to initial condition. The flow rate was 200 µl/min throughout. Other LC parameters were as follows: autosampler temperature, 4°C; injection volume, 10 µl; column temperature, 50°C. The MS method performed a full MS1 full scan (290 to 1,000 m/z) from 3- to 20-min. Scans used a resolution value of 17,500, an automatic gain control (ACG) target value of 1E6, and a maximum injection time (IT) of 40 ms. Experimental MS data were converted to the mzXML format and used for bile acid identification. Bile acid peaks were identified using MAVEN (metabolomics analysis and visualization engine). Bile acids in which half of the mice had peak areas less than 10,000 were removed from further analysis. Each bile acid was quantified and converted to μM (plasma) or mmol/g of cecal content by using standard curves and normalizing by sample input mass. Standards for each bile acid species were loaded on the same run as the samples except ω-muricholic acid, tauroursodeoxycholic acid, taurohyodeoxycholic acid and tauro-β-muricholic acid which were loaded on a separate run. Slopes for these standards were adjusted to account for run-to-run variation. We were unable to obtain a standard for tauro-α-muricholic acid, so the tauro-β-muricholic slope was used for conversion in its place.

Short-chain fatty acid analysis of cecal content

Frozen cecal content was added to vial containing 1 mL of 60 mM 2-butanol as an internal control, 2 g of H_2SO_4, and n µL of water, where n = 300-mg of cecal content added. The vial was immediately sealed and allowed to dissociate at RT for 2-3 days. Prepared vials were loaded onto

headspace sampler (HS20, Shimadzu, Columbia, OH) and gas chromatograph (CG-2010 Plus GC, Shimadzu) under previously described conditions (Hutchison et al., 2023). The resulting chromatograms were analyzed using Shimadzu Lab Solution software (version 5.92) and areas under the curve (AUC) were calculated for acetate, butyrate, and propionate. Concentrations of each SCFA per g of cecal content were determined by converting the AUCs to μM and then adjusting for sample input mass.

Microbiome sequencing

DNA from flash-frozen cecal or fecal content was extracted via bead-beating with phenol-chloroform and cleaned as described previously (Hutchison et al., 2023). Purified DNA was subjected to 16S rRNA V4 library prep and sequencing via Illumina MiSeq as described previsously (Hutchison et al., 2023) and sequenced at the UW-Madison Next Generation Sequencing Core. The resulting 16S rRNA amplicon sequences were demultiplexed and cleaned using Qiime2's (Bolyen et al., 2019) plugin for the DADA2 (Callahan et al., 2016) package. Once sample was removed from analysis due to low read count (>1000). QC and removal of chimeric reads resulted in an average of 57,815 reads per sample of the *Gpr KO* experiment and 28,309 reads per sample from the CMT experiment.

Microbiome 16S analysis

Prior to analysis, ASV tables were cleaned to remove spurious ASVs that had less than a total of 20 reads across all samples. Weighted and unweighted UniFrac distances were calculated using ASV relative abundance tables with phylogenetic trees and used to generate principal coordinate analysis (PCoA) ordination plots for the removal of low-abundance ASVs (below 0.1% in all

samples). ASV taxonomy was assigned using a pre-trained SILVA (Quast et al., 2013) classifier (silva-138-99-515-806-nb-classifier) in Qiime2. Differential abundance of cecal genus-level features of male *Gpr41*$^{-/-}$ mice and their WT littermates was determined using MaAslin2 (Mallick et al., 2021) package (version 1.10.0) in R after removal of genera that were below an average relative abundance cutoff of 0.05%.

Cecal metagenomic analysis

DNA samples from the cecal contents of five Gpr41$^{-/-}$ and five WT males were submitted to the University of Wisconsin-Madison Biotechnology Center. DNA concentration was verified using the Qubit® dsDNA HS Assay Kit (Life Technologies, Grand Island, NY). Samples were prepared according to the QIAGEN FX DNA Library Preparation Kit (QIAGEN). Quality and quantity of the finished libraries were assessed using an Agilent Tapestation (Agilent, Santa Clara, CA) and Qubit® dsDNA HS Assay Kit, respectively. Paired end, 150 bp sequencing was performed using the Illumina NovaSeq X Plus (Illumina, San Diego, CA). Host DNA was removed from the resulting reads (bowtie2, version 2.3.4) and were trimmed with trimmomatic (version 0.39). To quantify *bsh* and *bai* genes, we collected the hidden Markov model (HMM) profiles of each gene from KOfamKOALA (Aramaki et al., 2020) (version 2023-10-02) and conducted a hmmsearch using HMMER (version 3.3.2) against the Mouse Gastrointestinal Bacterial Catalog (Beresford-Jones et al., 2022) (MGBC). After removing all redundant sequences, the final reference database consisted of 1,435 genes, the vast majority of which were *bsh*. We quantified each gene by mapping the cleaned metagenomic reads to the reference database using RSEM (version 1.3.1) with the --bowtie2 and --very-sensitive parameters. The resulting FPKM count table was filtered based on the hmmsearch score. We initially chose the score threshold for each individual gene

recommended by KOfamKOALA, or – when not available, used the hmm score generated after hmmsearch the hmm profile against the *C. scindens* genome ASM2089211v1 (Supp. Table 4.1). However, this resulted in zero detection of *baiA*, *baiE*, and *baiF* in any mice. We reasoned that the *bai* genes present in mice may be significantly distinct from those in the literature which are primarily found in human indigenous strains. Therefore, we reduced the score threshold by half (Supp. Table 4.1). Taxonomy contributions were assigned by tracing the each hit back to its genome of origin in MGBC.

RNA Isolation and Construction of RNA-Seq Libraries

Total RNA from liver and ileum of five Gpr41$^{-/-}$ and five WT males was extracted using the following procedure: Frozen tissue (20-100 mg) was added to 1 mL Trizol (Cat #15596026, Thermo Fisher Scientific, Waltham, MA) and immediately bead-beated for 2 minutes in a screwcap tube with 0.5 g 1 mm diameter zirconium beads (Cat. #11079110ZX, Biospec Products, Bartlesville, OK). Homogenates incubated at room temperature (RT) for five minutes followed by addition of 0.2 mL of chloroform and shaken by hand for 15 seconds and placed at RT for 3 minutes. Samples were then centrifuged at 12,000 x g for 15 minutes at 4°C. 500 μL of the aqueous phase was collected and mixed with 318 μL of chilled 100% ethanol. The entire volume was then added to the Qiagen RNeasy Mini kit (Cat. # 74004, Qiagen, Germantown MD) and processed according to the manufacturer's instructions. RNA extracts were submitted to the University of Wisconsin-Madison Biotechnology Center for service. Each RNA extract was assayed on a NanoDrop One Spectrophotometer and an Agilent 4200 Tapestaion to assess RNA purity and integrity. RNA samples that met Illumina's TruSeq Stranded mRNA Reference Guide (Document# 1000000040498 v00, October 2017) quality criteria were prepared for sequencing.

Briefly, 1 ug total RNA sample was enriched for mRNA by oligo (dT) selection followed by fragmentation using divalent cations under elevated temperature. Double-stranded cDNA was synthesized using SuperScript II RT (Invitrogen, Carlsbad, California) and random primers for first strand cDNA synthesis followed by second strand synthesis using DNA Polymerase I and RNAse H for removal of mRNA. Double-stranded cDNA was purified with SPRI beads (Beckman Coulter Genomics, CA), followed by incubation with Klenow DNA Polymerase and Adenine to add an 'A' base (Adenine) to the 3' end of the blunt phosphorylated DNA fragments. DNA fragments were ligated to Illumina unique molecular index (UMI) adapters, which have a single 'T' base (Thymine) overhang at their 3'end. Following ligation, cDNA was purified with SPRI beads, and PCR-amplified (10 cycles) with PhusionTM DNA Polymerase using Illumina's genomic DNA primer set and purified with SPRI beads. Quality and quantity of the finished libraries were assayed on an Agilent 4200Tapestation using D1000 Screentape and the Qubit HS Quantification Kit (Invitrogen, Carlsbad, CA), respectively.

Liver and ileum RNA-seq analysis

Paired end 150bp sequencing was carried out on a single Illumina NovaSeq6000 run. The resulting PE reads were demultiplexed and cleaned with trimmomatic, which yielded an average of 34.8 million PE reads per sample. Cleaned reads were then annotated against the Genome Reference Consortium (GRC) build 38 *Mus musculus* genome using RSEM. This resulted in a table of transcripts per million reads (TPM) counts for genes assigned with a Ensembl gene ID. Transcripts that summed to less than 10 TPM were removed from further analysis. One *Gpr41*$^{-/-}$ liver sample, which exhibited signs of contamination as it had a highly distinct expression profile from all other liver samples, was removed from further analysis. Differential expression analysis was conducted

using the DESeq2 (version 1.36.0) R package. DEGs were considered significantly if they had *P*-values < 0.01. All significantly up- or downregulate DEGs were used as input to the Enrichr package (version 3.2) to assess KEGG ("KEGG_2019_Mouse" database) pathway enrichment in WT (upregulated DEGs) and *Gpr41*$^{-/-}$ (downregulated DEGs) in R, which generated a *P*-value for each KEGG pathway.

Liver histology

After sacrifice, liver samples were fixed using either 10% formalin at room temperature for 48 hours, followed by storage in 80% alcohol at 4 °C. The fixed samples were embedded in paraffin, sectioned, and stained with hematoxylin and eosin (H&E), Masson's trichrome, and picrosirius red. For histopathological analysis, sections were examined under light microscopy by a board-certified liver pathologist (YJL), who was blinded to the treatment groups. Hepatic steatosis was graded based on the percentage of the liver section occupied by fat vacuoles (grade 0 = < 5%; grade 1 = 5 to 33%; grade 2 = 34 to 66%; grade 3 =>66%). Lobular inflammation (clusters of recruited immune cells in the lobules) was graded based on the foci of chronic inflammatory cells (grade 0 = none; grade 1 = 1-2 foci per 20x field; grade 2 = 2-4 foci per 20x field; grade 3 = >4 foci per 20x field). Hepatocyte ballooning degeneration was graded based on the number of ballooned hepatocytes present in the sections (grade 0 = none; grade 1 = few; grade 2 = many). The stage of hepatic fibrosis was assessed using Masson's trichrome and picrosirius red staining (stage 0 = no fibrosis; stage 1a = zone 3 mild perisinusoidal fibrosis; stage 1b = zone 3 moderate perisinusoidal fibrosis; stage 1c = periportal/portal fibrosis only; stage 2 = zone 3 plus periportal/portal fibrosis; stage 3 = bridging fibrosis; stage 4 = cirrhosis). The grade and stage

scoring system adopted here mimics the Non-alcoholic Fatty Liver Disease Scoring System (NAS) that was designed for the evaluation of steatohepatitis and fibrosis in humans (Kleiner et al., 2005)

Experiment testing cholesterol content in diet

We supplemented a standard natural ingredient base-formula diet (2018 global 18% protein diet, Inotiv) with 0, 1.5, or 2% cholesterol (wt/wt). This diet was fed to PCSK9-AAV-infected C57BL/6J male mice for three weeks (n = 3-4 mice/group). After three weeks, plasma was collected and to assess total cholesterol and collected fresh fecal samples to determine SCFA profiles as described above.

Cecal transplant experiment

Flash-frozen cecal contents from male *Gpr41*$^{-/-}$ mice and their WT littermates was pooled from 4-5 mice, mixed with Mega Media (1 mL per 100 mg), and vortexed to make a slurry. This was used to gavage male GF mice (0.1 mL per mouse). The slurry preparation and gavage was repeated one week later. Mice were then injected with $1.5x10^{11}$ particles of PCSK9-AAV8 as by RI as described above. The mice were sacrificed 8 weeks post injection at which point plasma was collected for cholesterol measurement, and cecal content was flash-frozen for microbiome analysis. Fresh feces was also collected 4 weeks post injection for microbiome analysis.

Statistics

The Student's T-test was used to compare means between genotypes within each strain and sex unless otherwise stated. Similarities of microbiome profiles were assessed by PERMANOVA using the adonis function in the vegan R package (version 2.6-4). *P*-values or the comparison of

means between genotypes of individual gene transcripts (liver and ileum) were generated by DESeq2.

DATA AVAILABILITY

All data in the current study is available upon request.

ACKNOWLEDGMENTS

We would like to thank Dr. Karen Ho at Northwestern University and Dr. Pamela Martin at Augusta University for generously donating the mice used for this study and Drs. Bar Mickelson and Jake Lusis for their expertise on the diet formulation. We would also like to that the University of Wisconsin-Madison's Biotechnology Center's DNA Sequencing Facility (Research Resource Identifier – RRID:SCR_017759) and the Gene Expression Center for providing expertise and recourses. Our thanks to the University of Wisconsin-Madison's Experimental Animal Pathology Lab and the Medical Sciences Center vivarium staff for their assistance with this study.

REFERENCES

Aguilar, E. C., Leonel, A. J., Teixeira, L. G., Silva, A. R., Silva, J. F., Pelaez, J. M. N., Capettini, L. S. A., Lemos, V. S., Santos, R. A. S., & Alvarez-Leite, J. I. (2014). Butyrate impairs atherogenesis by reducing plaque inflammation and vulnerability and decreasing NFκB activation. *Nutrition, Metabolism and Cardiovascular Diseases*, *24*(6), 606–613. https://doi.org/10.1016/j.numecd.2014.01.002

Ahmad, A. F., Dwivedi, G., O'Gara, F., Caparros-Martin, J., & Ward, N. C. (2019). The gut microbiome and cardiovascular disease: Current knowledge and clinical potential. *American Journal of Physiology-Heart and Circulatory Physiology*, *317*(5), H923–H938. https://doi.org/10.1152/ajpheart.00376.2019

Altmann, S. W., Davis, H. R., Zhu, L., Yao, X., Hoos, L. M., Tetzloff, G., Iyer, S. P. N., Maguire, M., Golovko, A., Zeng, M., Wang, L., Murgolo, N., & Graziano, M. P. (2004). Niemann-Pick C1 Like 1 Protein Is Critical for Intestinal Cholesterol Absorption. *Science*, *303*(5661), 1201–1204. https://doi.org/10.1126/science.1093131

Anogeianaki, A., Angelucci, D., Cianchetti, E., D'alessandro, M., Maccauro, G., Saggini, A., Salini, V., Caraffa, A., Teté, S., Conti, F., Tripodi, D., & Shaik-Dasthagirisaheb, Y. B. (2011). Atherosclerosis: A Classic Inflammatory Disease. *International Journal of Immunopathology and Pharmacology*, *24*(4), 817–825. https://doi.org/10.1177/039463201102400401

Aramaki, T., Blanc-Mathieu, R., Endo, H., Ohkubo, K., Kanehisa, M., Goto, S., & Ogata, H. (2020). KofamKOALA: KEGG Ortholog assignment based on profile HMM and adaptive score threshold. *Bioinformatics*, *36*(7), 2251–2252. https://doi.org/10.1093/bioinformatics/btz859

Arpaia, N., Campbell, C., Fan, X., Dikiy, S., van der Veeken, J., deRoos, P., Liu, H., Cross, J. R., Pfeffer, K., Coffer, P. J., & Rudensky, A. Y. (2013). Metabolites produced by commensal bacteria promote peripheral regulatory T-cell generation. *Nature*, *504*(7480), 451–455. https://doi.org/10.1038/nature12726

Bai, X., Peng, J., Wang, M., Xiao, J., Xiang, Q., Ren, Z., Wen, H., Jiang, Z., Tang, Z., & Liu, L. (2018). PCSK9: A potential regulator of apoE/apoER2 against inflammation in atherosclerosis? *Clinica Chimica Acta*, *483*, 192–196. https://doi.org/10.1016/j.cca.2018.04.040

Bartolomaeus, H., Balogh, A., Yakoub, M., Homann, S., Markó, L., Höges, S., Tsvetkov, D., Krannich, A., Wundersitz, S., Avery, E. G., Haase, N., Kräker, K., Hering, L., Maase, M., Kusche-Vihrog, K., Grandoch, M., Fielitz, J., Kempa, S., Gollasch, M., … Wilck, N. (2019). Short-Chain Fatty Acid Propionate Protects From Hypertensive Cardiovascular Damage. *Circulation*, *139*(11), 1407–1421. https://doi.org/10.1161/CIRCULATIONAHA.118.036652

Bellahcene, M., O'Dowd, J., Wargent, E., Zaibi, M., Hislop, D. C., Ngala, R., Smith, D. M., Cawthorne, M., Stocker, C., & Arch, J. (2012). Male mice that lack the G-protein-coupled receptor GPR41 have low energy expenditure and increased body fat content. *British Journal of Nutrition*. https://doi.org/10.1017/S0007114512003923

Beresford-Jones, B. S., Forster, S. C., Stares, M. D., Notley, G., Viciani, E., Browne, H. P., Boehmler, D. J., Soderholm, A. T., Kumar, N., Vervier, K., Cross, J. R., Almeida, A., Lawley, T. D., & Pedicord, V. A. (2022). The Mouse Gastrointestinal Bacteria Catalogue enables translation between the mouse and human gut microbiotas via functional mapping. *Cell Host & Microbe*, *30*(1), 124-138.e8. https://doi.org/10.1016/j.chom.2021.12.003

Bjursell, M., Admyre, T., Göransson, M., Marley, A. E., Smith, D. M., Oscarsson, J., & Bohlooly-Y, M. (2010). Improved glucose control and reduced body fat mass in free fatty acid receptor 2-deficient mice fed a high-fat diet. *American Journal of Physiology-Endocrinology and Metabolism*, *300*(1), E211–E220. https://doi.org/10.1152/ajpendo.00229.2010

Bolyen, E., Rideout, J. R., Dillon, M. R., Bokulich, N. A., Abnet, C. C., Al-Ghalith, G. A., Alexander, H., Alm, E. J., Arumugam, M., Asnicar, F., Bai, Y., Bisanz, J. E., Bittinger, K., Brejnrod, A., Brislawn, C. J., Brown, C. T., Callahan, B. J., Caraballo-Rodríguez, A. M., Chase, J., … Caporaso, J. G. (2019). Reproducible, interactive, scalable and extensible microbiome data science using QIIME 2. *Nature Biotechnology*, *37*(8), Article 8. https://doi.org/10.1038/s41587-019-0209-9

Callahan, B. J., McMurdie, P. J., Rosen, M. J., Han, A. W., Johnson, A. J. A., & Holmes, S. P. (2016). DADA2: High resolution sample inference from Illumina amplicon data. *Nature Methods*, *13*(7), 581–583. https://doi.org/10.1038/nmeth.3869

Celermajer, D. S., Chow, C. K., Marijon, E., Anstey, N. M., & Woo, K. S. (2012). Cardiovascular Disease in the Developing World. *Journal of the American College of Cardiology*, *60*(14), 1207–1216. https://doi.org/10.1016/j.jacc.2012.03.074

Galicia-Garcia, U., Jebari, S., Larrea-Sebal, A., Uribe, K. B., Siddiqi, H., Ostolaza, H., Benito-Vicente, A., & Martín, C. (2020). Statin Treatment-Induced Development of Type 2 Diabetes: From Clinical Evidence to Mechanistic Insights. *International Journal of Molecular Sciences*, *21*(13), E4725. https://doi.org/10.3390/ijms21134725

Haghikia, A., Zimmermann, F., Schumann, P., Jasina, A., Roessler, J., Schmidt, D., Heinze, P., Kaisler, J., Nageswaran, V., Aigner, A., Ceglarek, U., Cineus, R., Hegazy, A. N., van der

Vorst, E. P. C., Döring, Y., Strauch, C. M., Nemet, I., Tremaroli, V., Dwibedi, C., … Landmesser, U. (2021). Propionate attenuates atherosclerosis by immune-dependent regulation of intestinal cholesterol metabolism. *European Heart Journal*, ehab644. https://doi.org/10.1093/eurheartj/ehab644

Heinken, A., Ravcheev, D. A., Baldini, F., Heirendt, L., Fleming, R. M. T., & Thiele, I. (2019). Systematic assessment of secondary bile acid metabolism in gut microbes reveals distinct metabolic capabilities in inflammatory bowel disease. *Microbiome*, *7*(1), 75. https://doi.org/10.1186/s40168-019-0689-3

Hutchison, E. R., Kasahara, K., Zhang, Q., Vivas, E. I., Cross, T.-W. L., & Rey, F. E. (2023). Dissecting the impact of dietary fiber type on atherosclerosis in mice colonized with different gut microbial communities. *Npj Biofilms and Microbiomes*, *9*(1), Article 1. https://doi.org/10.1038/s41522-023-00402-7

Jonsson, A. L., & Bäckhed, F. (2017). Role of gut microbiota in atherosclerosis. *Nature Reviews Cardiology*, *14*(2), 79–87. https://doi.org/10.1038/nrcardio.2016.183

Karlsson, F. H., Fåk, F., Nookaew, I., Tremaroli, V., Fagerberg, B., Petranovic, D., Bäckhed, F., & Nielsen, J. (2012). Symptomatic atherosclerosis is associated with an altered gut metagenome. *Nature Communications*, *3*(1), Article 1. https://doi.org/10.1038/ncomms2266

Kasahara, K., Krautkramer, K. A., Org, E., Romano, K. A., Kerby, R. L., Vivas, E. I., Mehrabian, M., Denu, J. M., Bäckhed, F., Lusis, A. J., & Rey, F. E. (2018). Interactions between Roseburia intestinalis and diet modulate atherogenesis in a murine model. *Nature Microbiology*, *3*(12), 1461. https://doi.org/10.1038/s41564-018-0272-x

Kaye David M., Shihata Waled A., Jama Hamdi A., Tsyganov Kirill, Ziemann Mark, Kiriazis Helen, Horlock Duncan, Vijay Amrita, Giam Beverly, Vinh Antony, Johnson Chad, Fiedler April, Donner Daniel, Snelson Matthew, Coughlan Melinda T., Phillips Sarah, Du Xiao-Jun, El-Osta Assam, Drummond Grant, … Marques Francine Z. (2020). Deficiency of Prebiotic Fiber and Insufficient Signaling Through Gut Metabolite-Sensing Receptors Leads to Cardiovascular Disease. *Circulation*, *141*(17), 1393–1403. https://doi.org/10.1161/CIRCULATIONAHA.119.043081

Kimura, I., Ichimura, A., Ohue-Kitano, R., & Igarashi, M. (2020). Free Fatty Acid Receptors in Health and Disease. *Physiol Rev*, *100*, 41.

Kleiner, D. E., Brunt, E. M., Van Natta, M., Behling, C., Contos, M. J., Cummings, O. W., Ferrell, L. D., Liu, Y.-C., Torbenson, M. S., Unalp-Arida, A., Yeh, M., McCullough, A. J., Sanyal, A. J., & Network, N. S. C. R. (2005). Design and validation of a histological scoring system for nonalcoholic fatty liver disease. *Hepatology*, *41*(6), 1313–1321. https://doi.org/10.1002/hep.20701

Lukasova, M., Malaval, C., Gille, A., Kero, J., & Offermanns, S. (2011). Nicotinic acid inhibits progression of atherosclerosis in mice through its receptor GPR109A expressed by immune cells. *The Journal of Clinical Investigation*, *121*(3), 1163–1173. https://doi.org/10.1172/JCI41651

Mallick, H., Rahnavard, A., McIver, L. J., Ma, S., Zhang, Y., Nguyen, L. H., Tickle, T. L., Weingart, G., Ren, B., Schwager, E. H., Chatterjee, S., Thompson, K. N., Wilkinson, J. E., Subramanian, A., Lu, Y., Waldron, L., Paulson, J. N., Franzosa, E. A., Bravo, H. C., & Huttenhower, C. (2021). Multivariable association discovery in population-scale meta-

omics studies. *PLOS Computational Biology*, *17*(11), e1009442. https://doi.org/10.1371/journal.pcbi.1009442

Matsubara, T., Li, F., & Gonzalez, F. J. (2013). FXR signaling in the enterohepatic system. *Molecular and Cellular Endocrinology*, *368*(1), 17–29. https://doi.org/10.1016/j.mce.2012.05.004

Ohira, H., Tsutsui, W., & Fujioka, Y. (2017). Are Short Chain Fatty Acids in Gut Microbiota Defensive Players for Inflammation and Atherosclerosis? *Journal of Atherosclerosis and Thrombosis*, *24*(7), 660–672. https://doi.org/10.5551/jat.RV17006

Quast, C., Pruesse, E., Yilmaz, P., Gerken, J., Schweer, T., Yarza, P., Peplies, J., & Glöckner, F. O. (2013). The SILVA ribosomal RNA gene database project: Improved data processing and web-based tools. *Nucleic Acids Research*, *41*(D1), D590–D596. https://doi.org/10.1093/nar/gks1219

Reichardt, N., Duncan, S. H., Young, P., Belenguer, A., McWilliam Leitch, C., Scott, K. P., Flint, H. J., & Louis, P. (2014). Phylogenetic distribution of three pathways for propionate production within the human gut microbiota. *The ISME Journal*, *8*(6), Article 6. https://doi.org/10.1038/ismej.2014.14

Samuel, B. S., Shaito, A., Motoike, T., Rey, F. E., Backhed, F., Manchester, J. K., Hammer, R. E., Williams, S. C., Crowley, J., Yanagisawa, M., & Gordon, J. I. (2008). Effects of the gut microbiota on host adiposity are modulated by the short-chain fatty-acid binding G protein-coupled receptor, Gpr41. *Proceedings of the National Academy of Sciences*, *105*(43), 16767–16772. https://doi.org/10.1073/pnas.0808567105

Singh, N., Gurav, A., Sivaprakasam, S., Brady, E., Padia, R., Shi, H., Thangaraju, M., Prasad, P. D., Manicassamy, S., Munn, D. H., Lee, J. R., Offermanns, S., & Ganapathy, V. (2014).

Activation of Gpr109a, Receptor for Niacin and the Commensal Metabolite Butyrate, Suppresses Colonic Inflammation and Carcinogenesis. *Immunity*, *40*(1), 128–139. https://doi.org/10.1016/j.immuni.2013.12.007

Smith, P. M., Howitt, M. R., Panikov, N., Michaud, M., Gallini, C. A., Bohlooly-Y, M., Glickman, J. N., & Garrett, W. S. (2013). The Microbial Metabolites, Short-Chain Fatty Acids, Regulate Colonic Treg Cell Homeostasis. *Science*, *341*(6145), 569–573. https://doi.org/10.1126/science.1241165

Veprik, A., Laufer, D., Weiss, S., Rubins, N., & Walker, M. D. (2016). GPR41 modulates insulin secretion and gene expression in pancreatic β-cells and modifies metabolic homeostasis in fed and fasting states. *The FASEB Journal*, *30*(11), 3860–3869. https://doi.org/10.1096/fj.201500030R

Wang, Y.-D., Chen, W.-D., Moore, D. D., & Huang, W. (2008). FXR: A metabolic regulator and cell protector. *Cell Research*, *18*(11), Article 11. https://doi.org/10.1038/cr.2008.289

Zhang, S., Li, Z., Zhang, Y., Chen, J., Li, Y., Wu, F., Wang, W., Cui, Z. J., & Chen, G. (2021). Ketone Body 3-Hydroxybutyrate Ameliorates Atherosclerosis via Receptor Gpr109a-Mediated Calcium Influx. *Advanced Science*, *8*(9), 2003410. https://doi.org/10.1002/advs.202003410

FIGURES

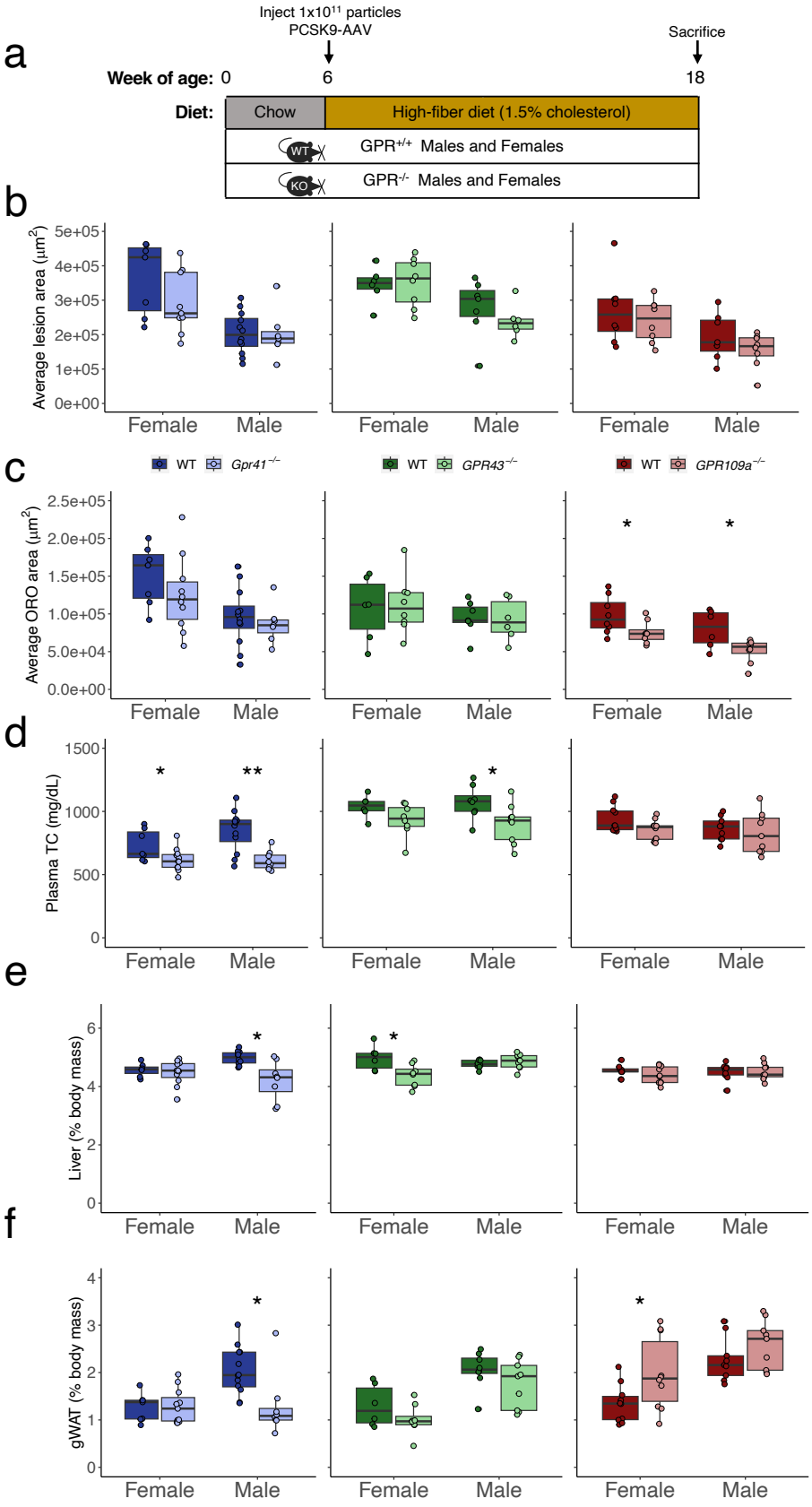
a
Inject 1x10^11 particles
PCSK9-AAV
Sacrifice
Week of age: 0
6
18
Diet:
Chow
High-fiber diet (1.5% cholesterol)
WT
GPR+/+ Males and Females
KO
GPR-/- Males and Females
b
Average lesion area (µm2)
5e+05
4e+05
3e+05
2e+05
1e+05
0e+00
Female
Male
c
WT
Gpr41-/-
WT
GPR43-/-
WT
GPR109a-/-
Average ORO area (µm2)
2.5e+05
2.0e+05
1.5e+05
1.0e+05
5.0e+04
0.0e+00
*
*
d
Plasma TC (mg/dL)
1500
1000
500
0
*
**
*
e
Liver (% body mass)
6
4
2
0
*
*
f
gWAT (% body mass)
4
3
2
1
0
*
*

Figure 4.1. Atherosclerotic and metabolic phenotypes of SCFA-receptor KO mice. (**a**) Schematic of the experimental design. Atherosclerotic plaque area (**b**) and lipid content (**c**) measurements by sex and genotype. Total cholesterol (**d**) liver mass (**e**) and gonadal white adipose tissue mass (**f**) as a proportion of body weight. Comparisons of means were conducted via T-test (*P* value between genotypes within each sex and SCFA-receptor group (n = 6-12/group). The level of significance is indicated with (*) $P < 0.05$ and (**) $P < 0.01$. SCFA, short-chain fatty acids; TC, total cholesterol

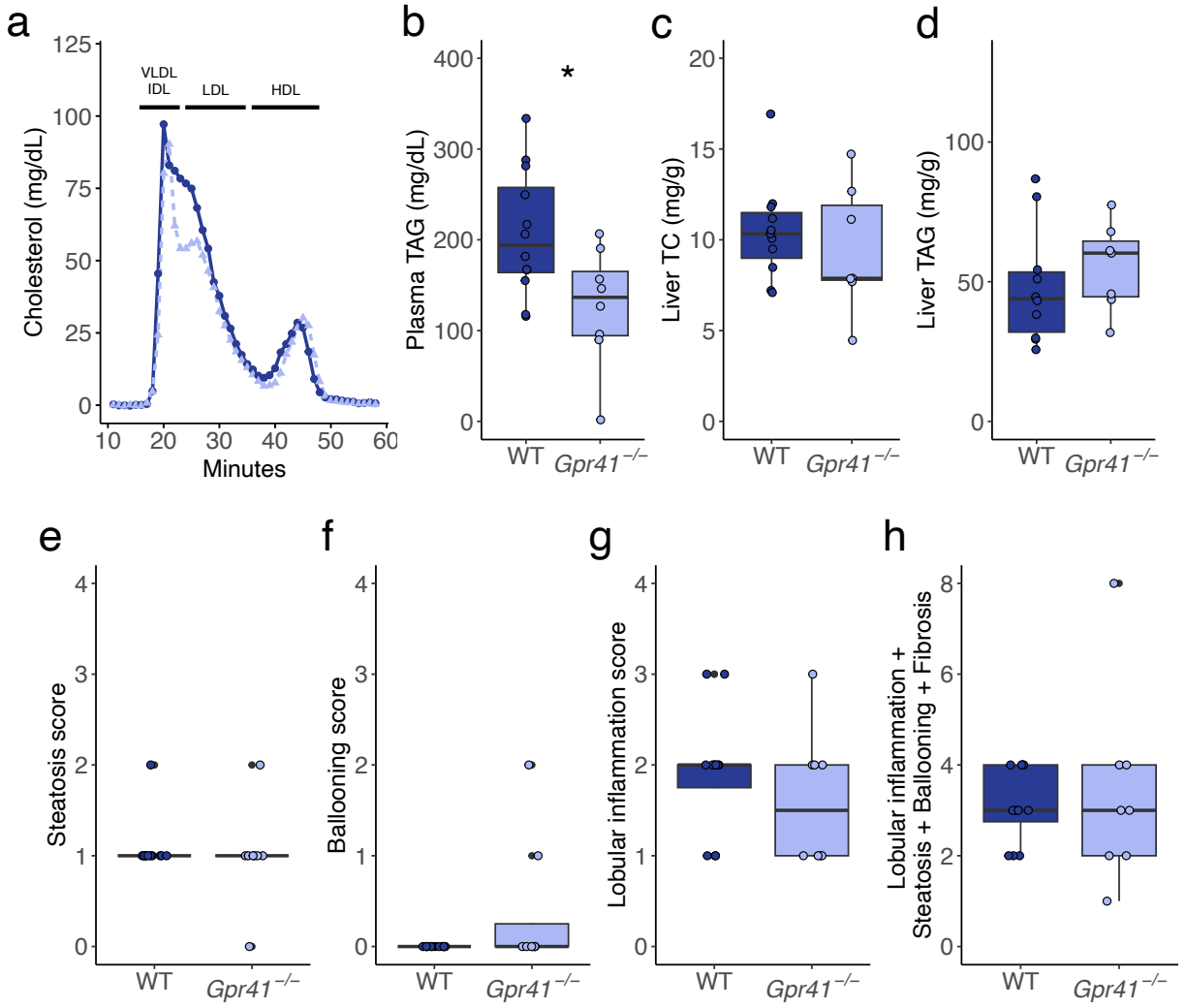

Figure 4.2. Plasma and liver metabolic phenotypes. (**a**) Cholesterol content of fast protein liquid chromatography (FPLC) fractions from pooled plasma samples from male WT (dark blue, circles, solid line) and *Gpr41*$^{-/-}$ (light blue, triangles, dotted line) mice. (**b**) Plasma levels of TAG. Cholesterol (**c**) and TAG (**d**) content in liver tissue. Histological scores of steatosis (**e**), ballooning (**f**), lobular inflammation (**g**), and a sum of all scores (**h**). Comparison of means was conducted via Student's T test for plasma and liver lipids (n = 6-12/group) and Wilcoxon rank-sum test for histology scores (n = 8-12/group). The level of significance is indicated with (*) $P < 0.05$. VLDL,

very-low density lipoprotein; IDL, intermediate density lipoprotein; LDL, low density lipoprotein; HDL, high density lipoprotein; TC, total cholesterol; TAG, triacylglycerol.

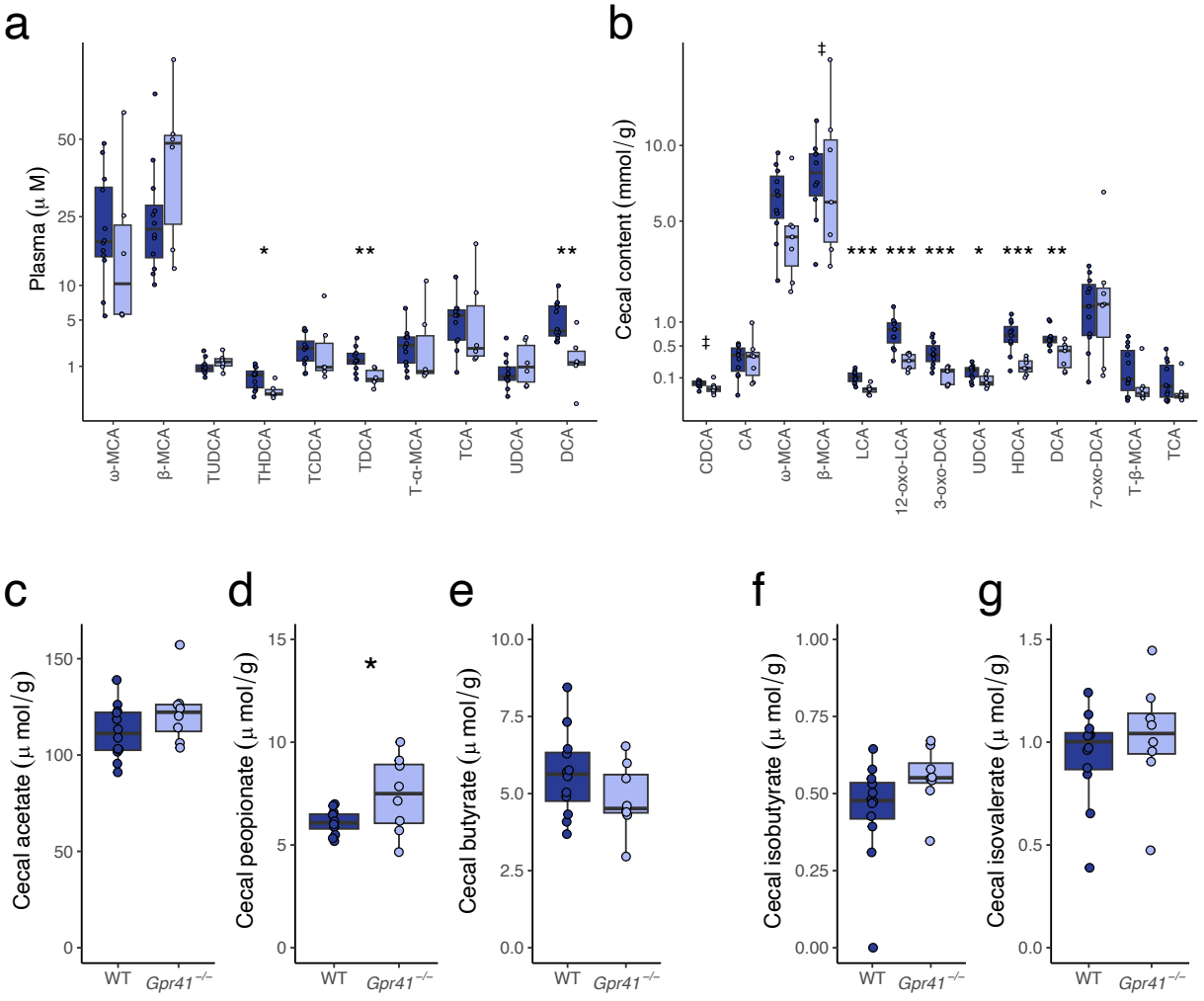

Figure 4.3. Plasma and cecal bile acid measurements and cecal levels of SCFAs. Concentrations of bile acids in the plasma (**a**) and cecal contents (**b**) from male WT and *Gpr41*$^{-/-}$ mice. Cecal levels of acetate (**c**), propionate (**d**) and butyrate (**e**), isobutyrate (**f**), and isovalerate (**g**). Comparisons of means was conducted via T-test between genotypes (n = 6-12/group). The level of significance is indicated with (‡) $P < 0.1$, (*) $P < 0.05$, (**) $P < 0.01$, (***) $P < 0.001$. 12-oxo-LCA, 12-oxo-lithocholic acid; 3-oxo-DCA, 3-oxo-deoxycholic acid; 7-oxo-DCA, 7-oxo-deoxycholic acid; β-MCA, β-Muricholic acid; CDCA, Chenodeoxycholic acid; CA, Cholic acid; DCA, Deoxycholic acid; HDCA, Hyodeoxycholic acid; LCA, Lithocholic acid; T-α-MCA, Tauro_a_Muricholic acid; T-β-MCA, Tauro-β-Muricholic acid; TCDCA, Taurochenodeoxycholic acid; TCA, Taurocholic

acid; TDCA, Taurodeoxycholic acid; THDCA, Taurohyodeoxycholic acid; TUDCA, Tauroursodeoxycholic Acid; UDCA, Ursodeoxycholic acid; ω-MCA, ω-Muricholic acid.

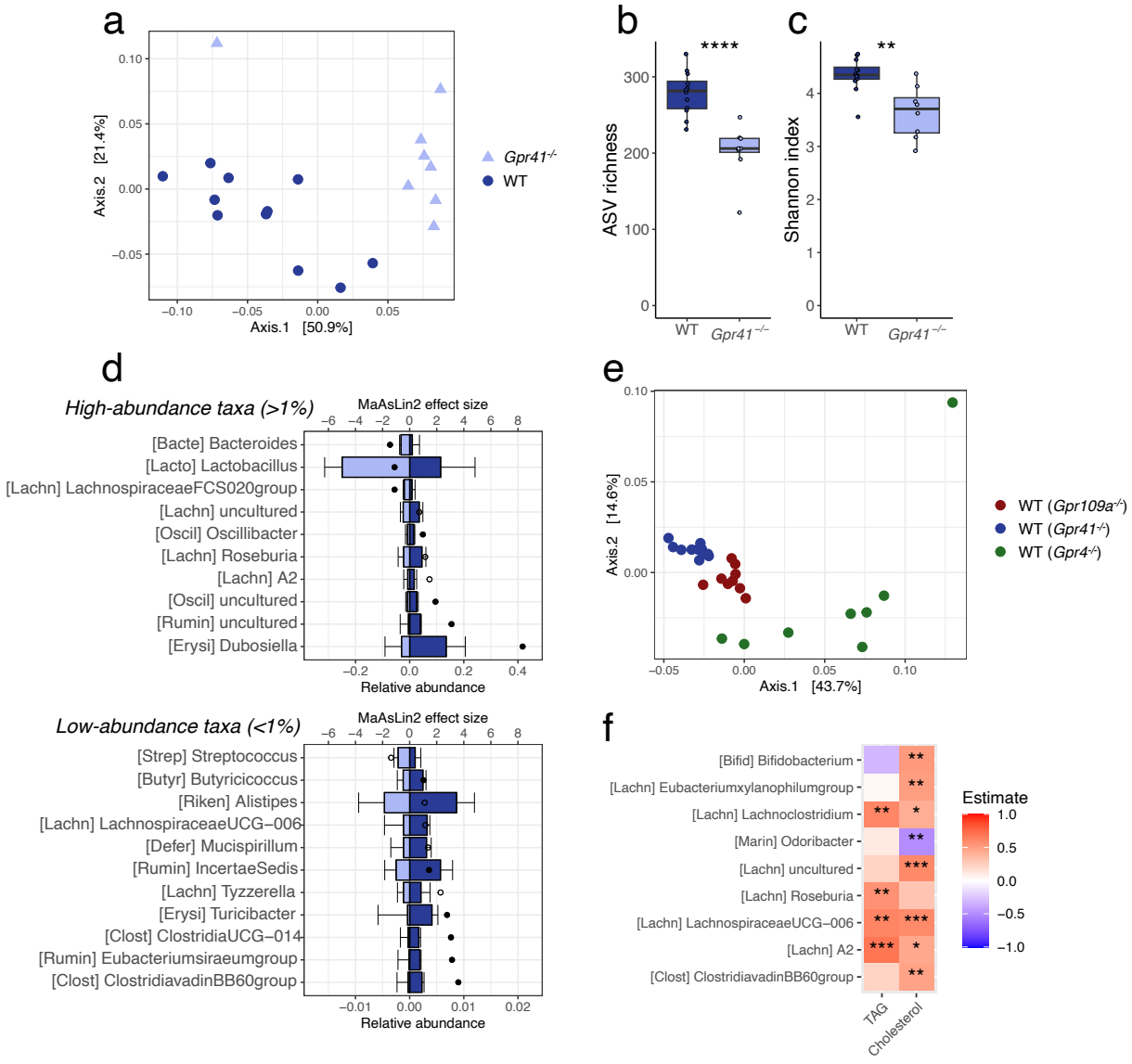

Figure 4.4. Characterization of cecal microbiota composition of WT and *Gpr41*$^{-/-}$ mice. (**a**) PCoA plot using weighted UniFrac distances of 16S rRNA ASV profiles from male WT and *Gpr41*$^{-/-}$ cecal content. ASV richness (**b**), and Shannon diversity index values (**c**). (**d**) MaAsLin2 effect sizes (top axis, dots) and relative abundances (bottom axis, bars) that were differentially abundant ($P < 0.05$). *High-abundance taxa* were those that averaged above 1% relative abundance across all mice, whereas *Low-abundance taxa* were those below 1% (0.01% minimum cutoff). The negative (left) direction indicates abundances in *Gpr41*$^{-/-}$ mice (light blue bar) while the positive

(right) direction indicates the abundance in WT mice (dark blue bar). MaAsLin2 effect sizes to the left of the origin denotes significantly (open dots = $P < 0.05$; solid dots = adjusted $P < 0.1$) greater abundance in *Gpr41*$^{-/-}$ mice, whereas effect sizes to the right of the origin indicates significantly greater abundance in WT mice. (**e**) Weighted UniFrac PCoA of 16S rRNA profiles from all male WT littermates belonging to the *Gpr41* (dark blue), and *Gpr43* (dark green), and *Gpr41* (dark red) groups. (**f**) Spearman correlations between taxa and plasma TAG and total cholesterol using all male WT mice. Comparisons of means for alpha diversity metrics were conducted via T-test between genotypes (n = 8-12/group). The level of significance is indicated with (‡) $P < 0.1$, (*) $P < 0.05$, (**) $P < 0.01$, (***) $P < 0.001$, (****) $P < 0.0001$.

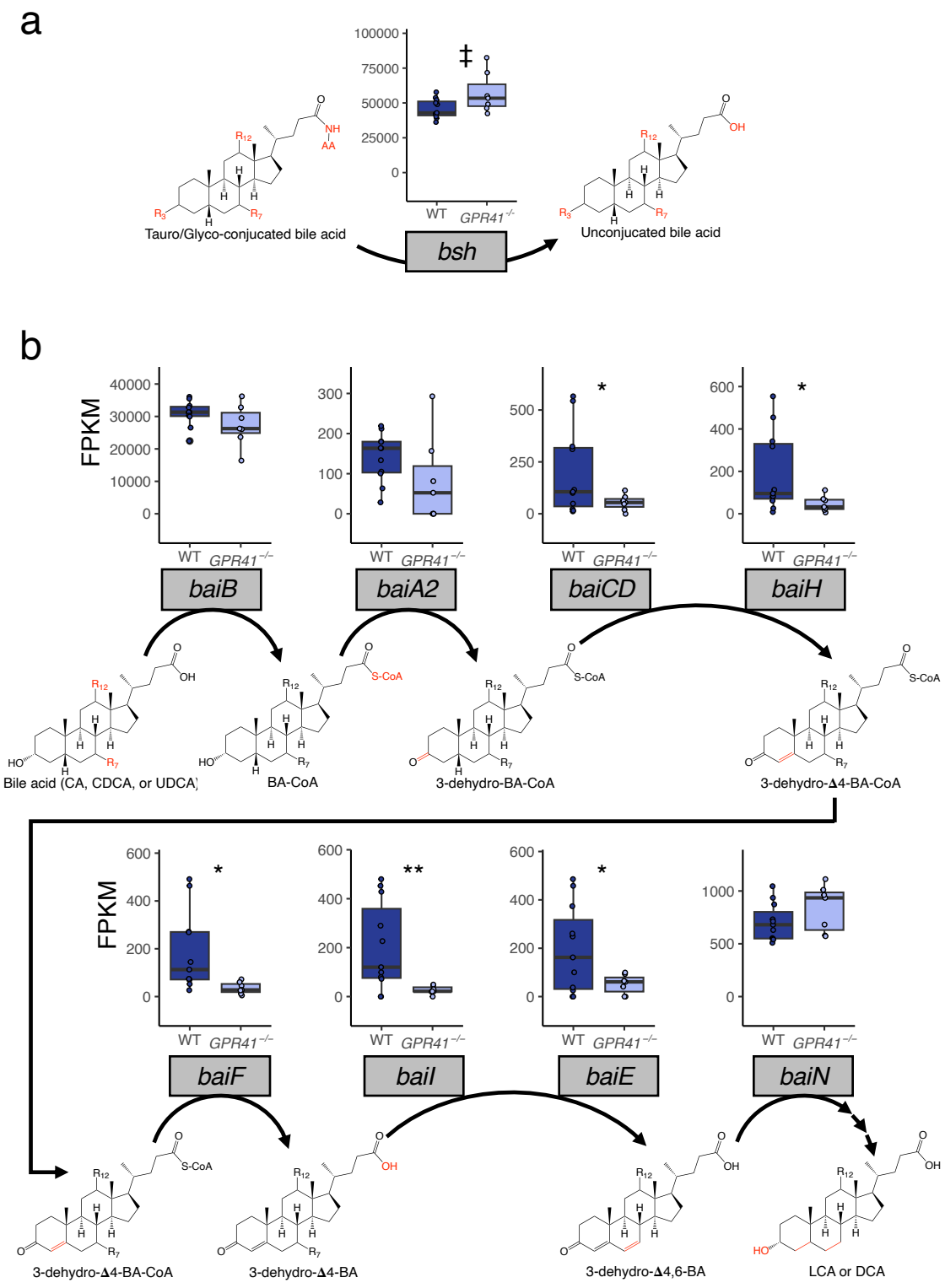

Figure 4.5. Abundance of Bile acid modifying genes in WT and *Gpr41*$^{-/-}$ mice. Fragment per kilobase million (FPKM) counts of *bsh* (**a**), the gene coding for protein that removes the amino

acid groups from conjugated bile acids, in the cecal metagenomes of male *Gpr41*$^{-/-}$ mice and their WT littermates. FPKM counts of the *bai* operon (**b**) which encodes the 7α-dehydroxylation pathway that converts CA to DCA, and CDCA or UDCA to LCA. Comparisons of means were conducted via T-test between genotypes (n = 7-11/group). The level of significance is indicated with (‡) $P < 0.1$, (*) $P < 0.05$, (**) $P < 0.01$.

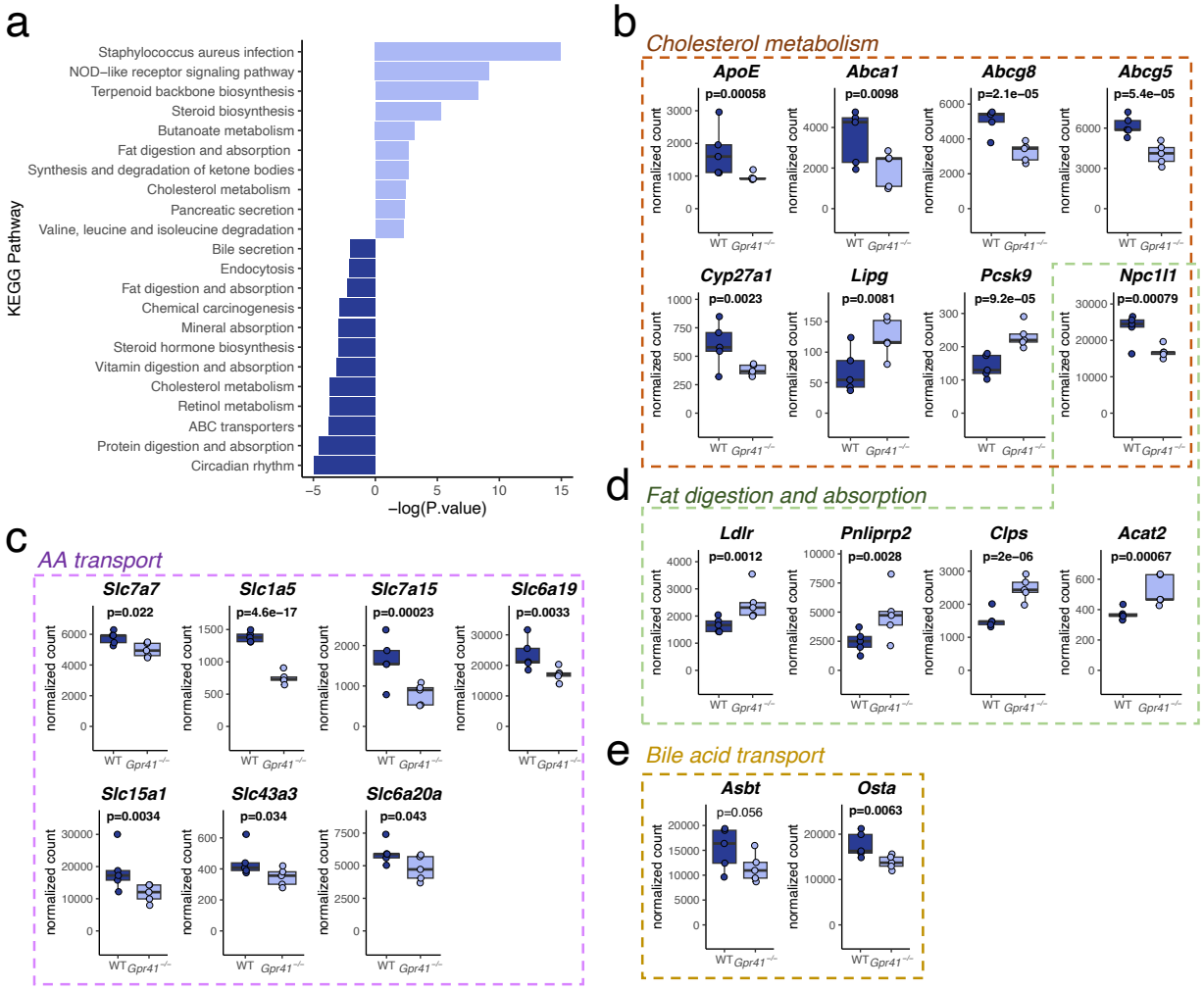

Figure 4.6. Transcriptomic analysis of ileum samples from WT and *Gpr41*$^{-/-}$ mice. **a** Significantly enriched KEGG pathways ($P < 0.05$) resulting from pathway enrichment analysis (Enrichr) of differentially expressed genes (DESeq2, $P < 0.05$). in the ileum of male *Gpr41*$^{-/-}$ mice and their WT littermates. Normalized expression (TPM) of individual genes involved in cholesterol metabolism (**b**), amino acid transport (**c**), fat digestion and absorption (**d**), and bile acid transport (**e**). Unadjusted *P* values of comparisons of means of individual genes were generated with DESeq2 package in R. Sample size = 5 per group.

SUPPLEMENTARY FIGURES AND TABLES

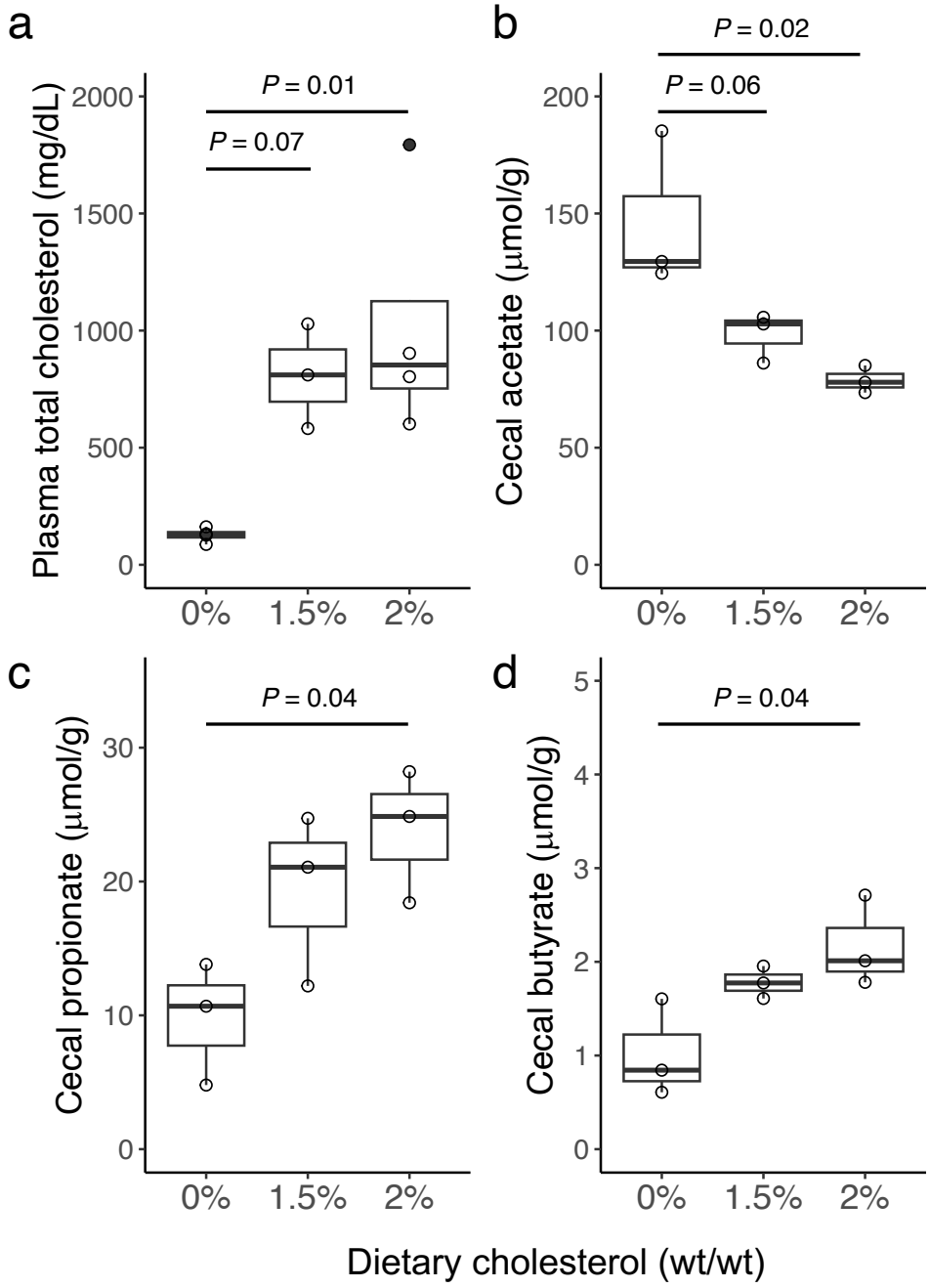

Supplemental Figure 4.1. Levels of plasma total cholesterol (**a**), and cecal levels of acetate (**b**), propionate (**c**) and butyrate (**d**) expressed in μmol per g of wet-weight fecal content of PCSK9-AAV infected mice fed a chow diet supplemented with 0, 1.5, or 2% cholesterol (wt/wt) for 6 weeks. One-way ANOVA followed by Tukey's Post Hoc test. Pairwise Tukey's test *P*-values are shown if they are less than 0.1. Sample size = 3-4 per group.

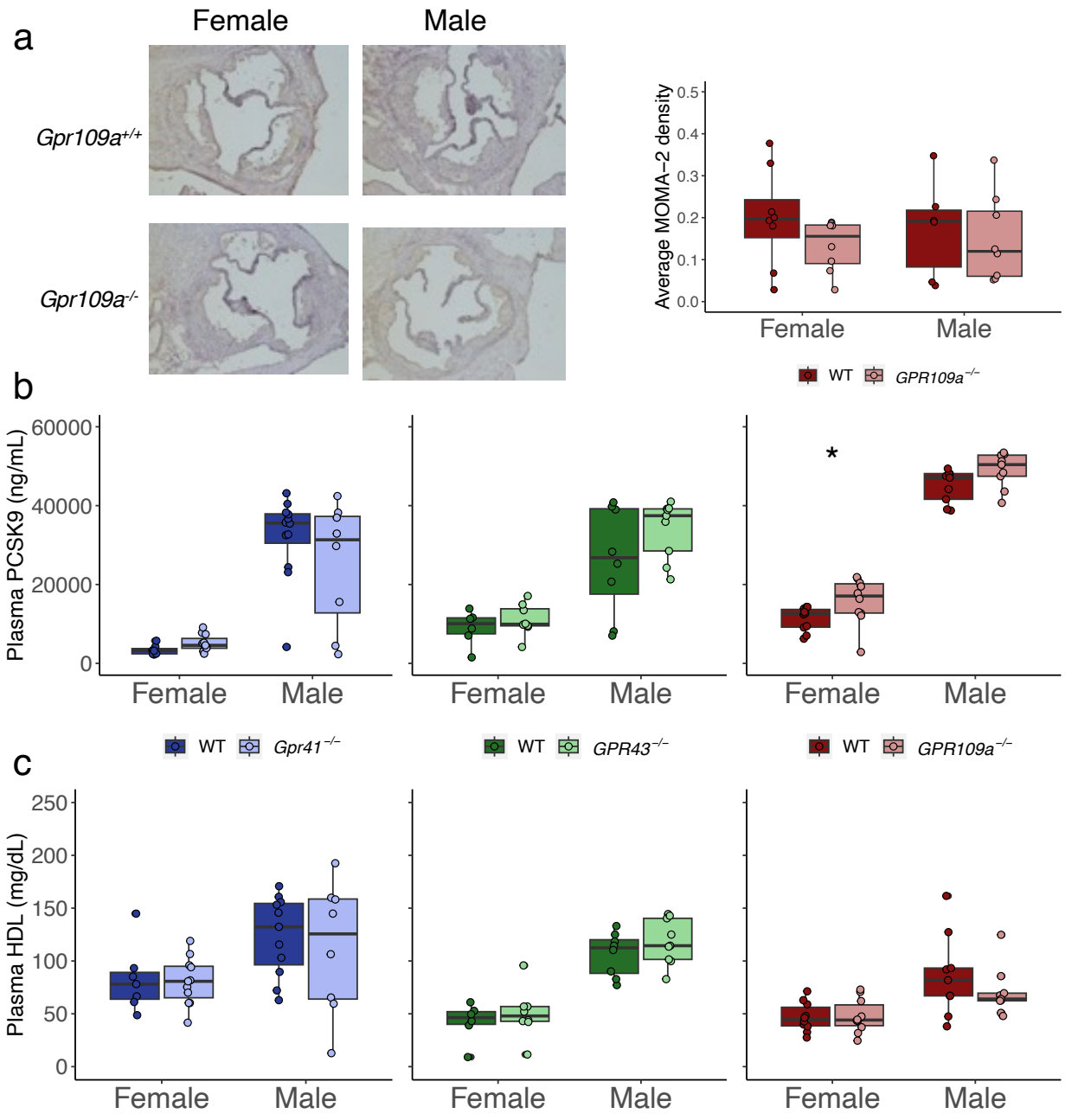

Supplemental Figure 4.2. **a** Measurement of macrophage infiltration via MOMA-2 staining of atherosclerotic lesion in male and female *Gpr109a*$^{-/-}$ and their WT littermates. Plasma PCSK9 levels (b) and HDL levels (c) in male and female Gpr-KO mice and their WT littermates. Comparisons of means were conducted via T-test *P* between genotypes (n = 7-11/group). The level of significance is indicated with (*) $P < 0.05$, (n = 6-12/group).

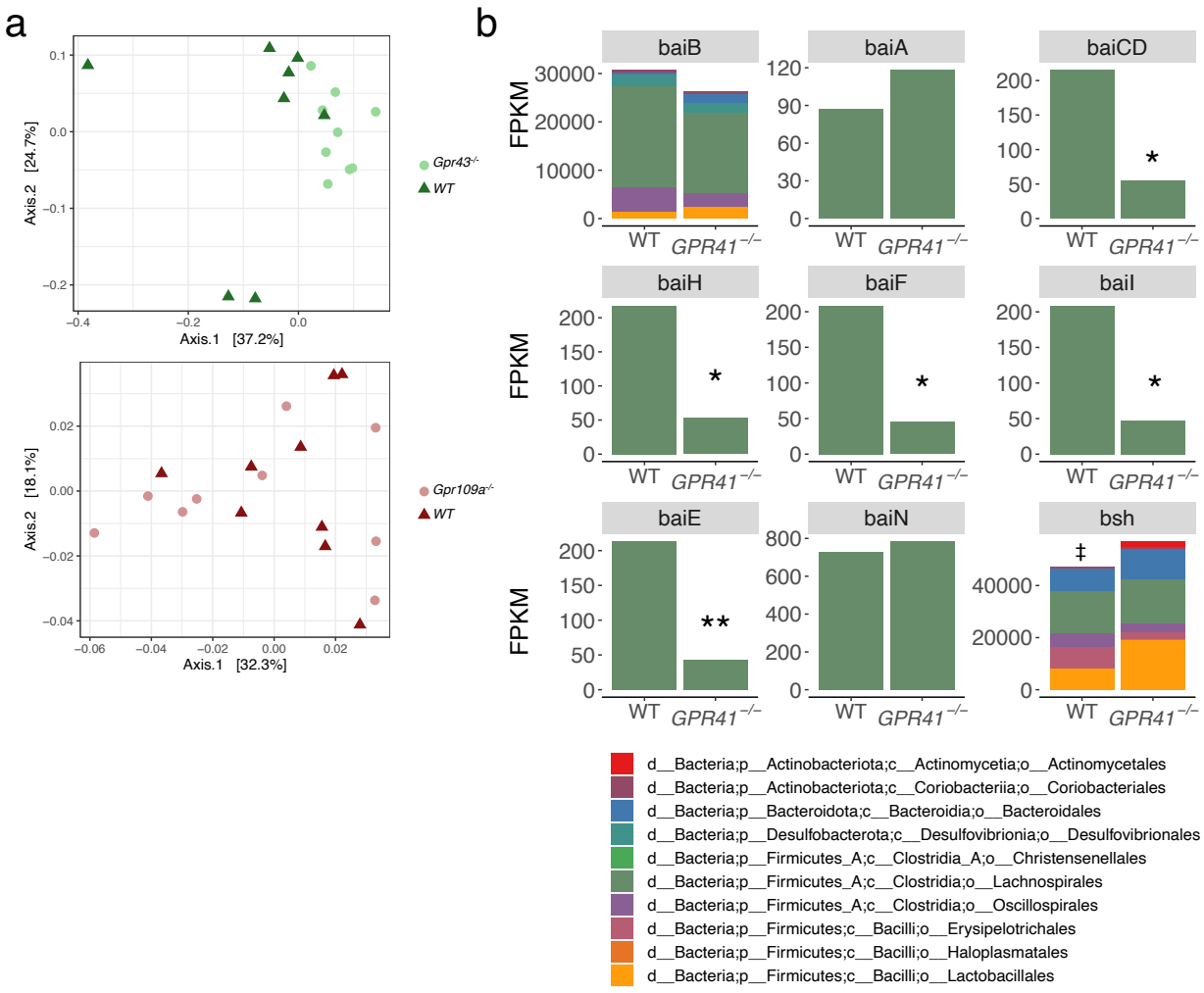

Supplemental Figure 4.3. a Weighted UniFrac PCoA plots of male *Gpr43*$^{-/-}$, and *Gpr109a*$^{-/-}$ mice and their WT littermates. **b** Average FPKM counts of *bsh* and genes in the *bai* operon in male *Gpr41*$^{-/-}$ and their WT littermates broken out by taxonomic contribution at the order level. Comparisons of means were conducted via T-test between genotypes (n = 7-11/group). The level of significance is indicated with (‡) $P < 0.1$, (*) $P < 0.05$, (**) $P < 0.01$.

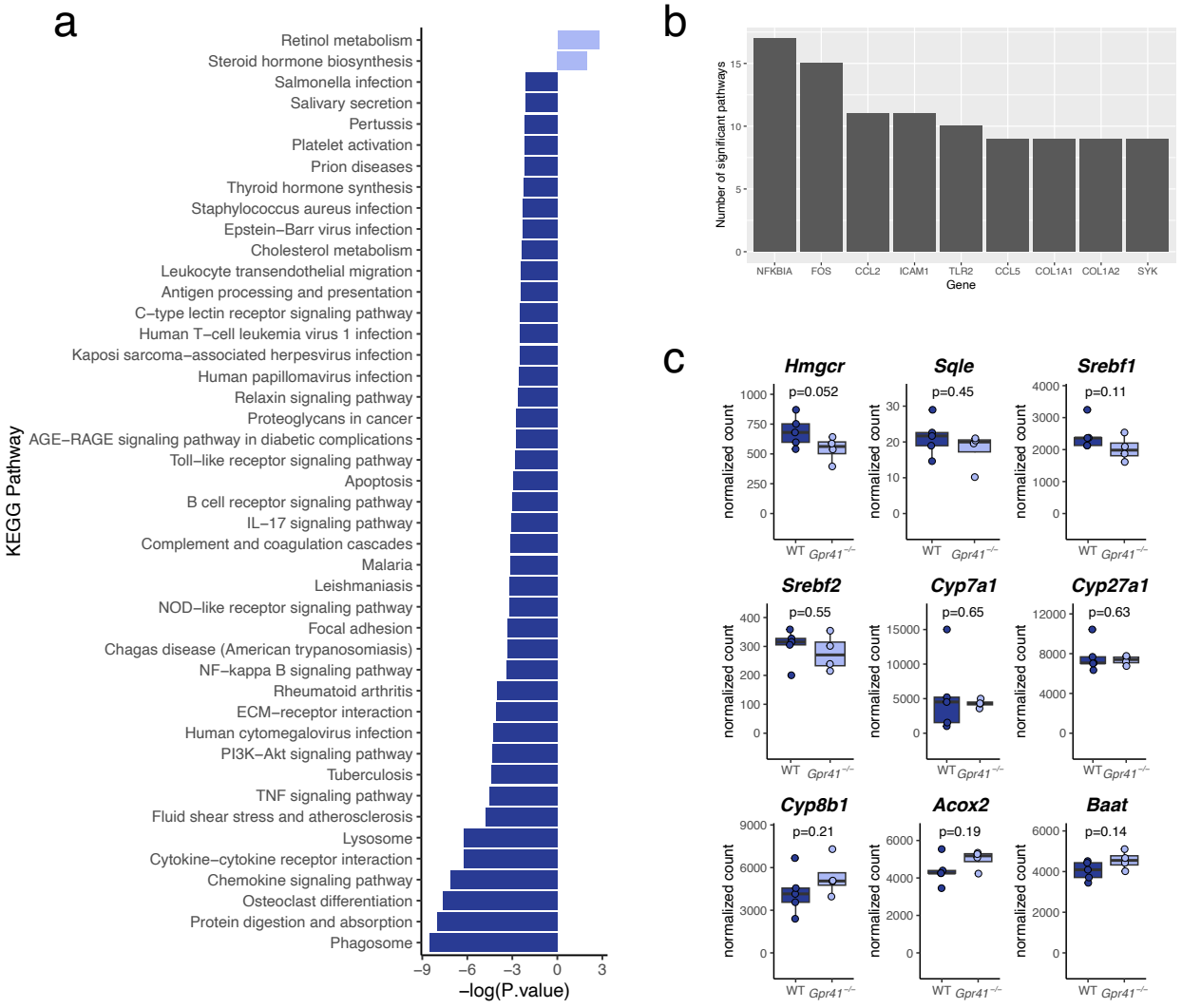

Supplemental Figure 4.4. Liver transcriptomic analysis. **a** Significantly enriched ($P < 0.05$) KEGG pathways resulting from Enrichr analysis of DEGs ($P < 0.05$). **b** The frequency in which individual DEGs appear within significantly enriched KEGG pathways. **c** Normalized expression (TPM) of individual genes involved cholesterol synthesis (*Hmgcr*, *Sqle*) and its regulation (*Srepf1*, *Srebf2*), as well as bile acid synthesis genes (*Cyp7a1*, *Cyp27a1*, *Cyp8b1*, *Acox2*, *Baat*). Unadjusted *P* values of comparisons of means of individual genes were generated with DESeq2 package in R. Sample size = 4-5 per group.

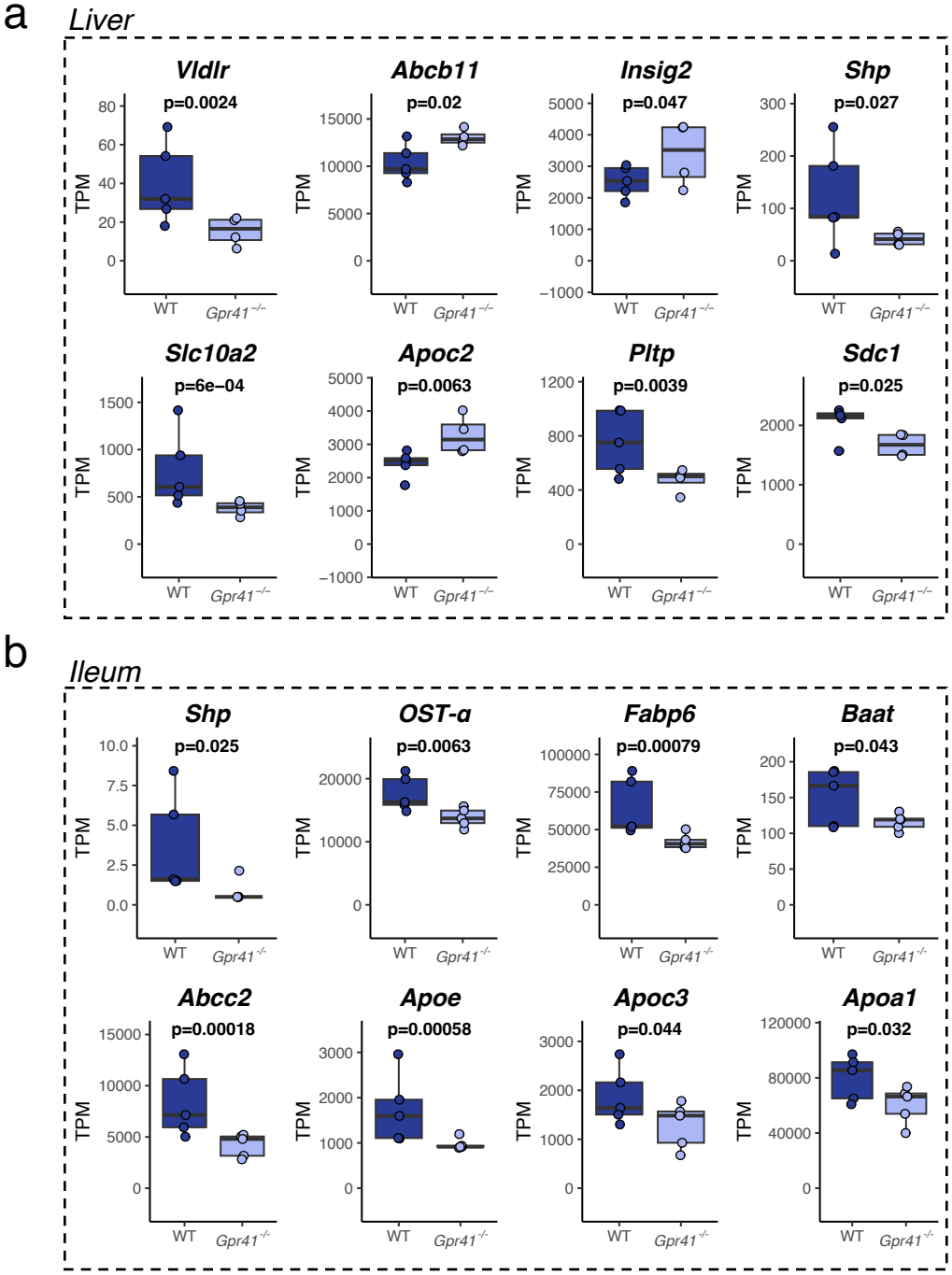

Supplemental Figure 4.5. Expression of known factor farnesoid X receptor (FXR) gene targets that were significantly different (unadjusted $P < 0.05$) in the liver (a) and the ileum (b). Unadjusted *P* values of comparisons of means of individual genes were generated with DESeq2 package in R. Sample size = 4-5 per group.

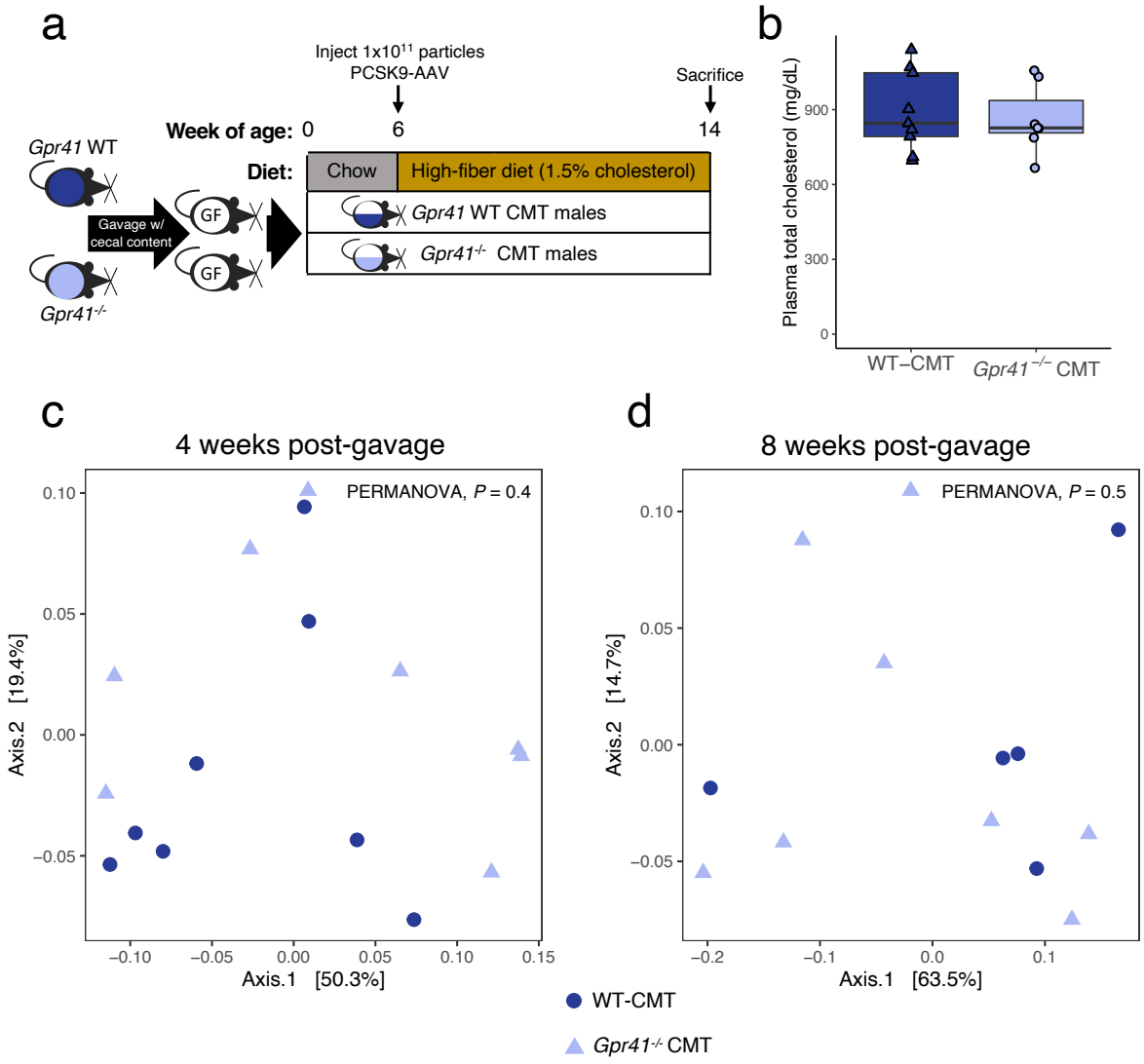

Supplemental Figure 4.6. a Cecal microbiota from WT and Gpr41$^{-/-}$ male mice were transplanted in the GF males which were subsequently injected with PCSK9-AAV and maintained on a high-fiber/high-cholesterol diet for 8 weeks. **b** Plasma levels of total cholesterol 8 weeks after injection. Weighted UniFrac PCoA plots of fecal bacterial communities collected 4 weeks post-injection (**c**) and cecal bacterial communities collected 8 weeks post-injection (**d**) as measured by 16S rRNA profiles. Comparison of means was conducted by a Students T-test. Cecal community structure dissimilarity was assessed by PERMANOVA. Sample size = 8 per group.

Supplemental Table 4.1. Score thresholds for hmmsearch of hidden Markov model (HMM) profiles of bile acid genes against MGBC genomes.

		hmmsearch score threshold	
Gene name	**KEGG ID**	**Original**	**Adjusted (50%)**
baiA	K15869	483*	241.5
baiB	K15868	493.53	246.8
baiCD	K15870	1418.3	709.2
baiE	K15872	335*	167.5
baiF	K15871	858.37	429.2
baiH	K15873	1525.1	762.6
baiI	K15874	247*	123.5
baiN	K07007	878*	439
bsh	K01442	350.3	175.2

*Extrapolated from hmmsearch score of HMM profile against *C. scindens* genome (ASM2089211v1).

CHAPTER 5: FUTURE DIRECTIONS

INTRODUCTION

The body of work presented here has shed some light on the relationships between SCFAs and cardiometabolic disease with a particular focus on gut microbiome variation and SCFA receptors. In Chapter 2, I investigated the role of gut microbiome variation in modifying the effects of dietary fiber on atherosclerosis and found that atheroprotection was linked to butyrate production. In Chapter 3, I show that the gut microbiome modulated the impact of a next-generation probiotic, *Anaerobutyricum soehngenii*, on insulin sensitivity in humanized gnotobiotic and described how this effect was linked to differential responses to propionate. Lastly, in Chapter 4, I examined the mechanism behind butyrate-induced atheroprotection by interrogating the roles of butyrate receptors Gpr41, Gpr43, and Gpr109a in an atherosclerosis model and found that Gpr41 is involved in cholesterol uptake and lipid metabolism. While these studies have helped to fill some of the gaps in this area of research, they have also led to more questions which deserve further attention. Some of the most intriguing questions are addressed below.

5.1 Can synthetic microbial communities replicate mechanisms of atheroprotection?

Our primary goal of Chapter 2 was to assess the effect of different microbiomes, with disparate short-chain fatty acid (SCFA) producing capabilities, to modulate atheroprotection of a fermentable fiber (FF) diet (Hutchison et al., 2023). We tested this by colonizing germ-free (GF) *Apoe*$^{-/-}$ mice with fecal microbiota from human donors (DonA, DonB, and DonC), which exhibit differing capacities to make SCFAs, particularly butyrate. We found that the microbiome did indeed modify the effects of fermentable fiber on atherosclerosis and observed that atheroprotection was observed only in DonA-colonized mice and was associated with elevated butyrate levels in the cecum (Fig. 2.2 and Fig. 2.3). Conversely, DonB-colonized mice, which did

not receive FF-induced atheroprotection, had lower levels of butyrate with FF feeding. The link between butyrate and atheroprotection had also been observed in previous studies (Aguilar et al., 2014; Kasahara et al., 2018) supporting the notion that the promotion of butyrate production is desirable for individuals predisposed to atherogenesis. In our study, we also observed that FF consumption increases the relative abundances of many butyrate production genera (*Clostridium*, *Oscillospira*, *Gemmiger*, *Faecalubacterium*, and *Ruminococcus*) only in DonA-colonized mice which received atheroprotection (Fig. 2.1). Even though these genera were present in the DonB- and DonC-colonized mice, they did not expand with FF feeding (Fig. 2.1). This is likely due to the mice harboring different species or strains of bacteria within each genus that respond differently to FF. This notion is supported by others who have noted that even strain-level variation can lead to significantly different physiology (Zeevi et al., 2019). I hypothesize that the species- and strain-level features within the atheroprotection-associated genera (*Clostridium*, *Oscillospira*, *Gemmiger*, *Faecalubacterium*, and *Ruminococcus*) are metabolically distinct between those present in the FF-responding mice (DonA) and FF-non-responding mice (DonB).

To test this, one could construct synthetic microbial communities by isolating as many microbes from DonA and DonB-colonized mice and assembling synthetic microbiomes (SyM) for colonization in GF Apoe$^{-/-}$ mice. An initial test could be done to see if the DnA-SyM and DonB-SyM-colonized mice recapitulate the atherogenic and/or SCFA responses to FF. This would also allow for the swapping of individual genera, strains, or collections of microbiota between DonA and DonB mice and observe their atherogenic response. For example, one could test the effect of FF on gnotobiotic Apoe$^{-/-}$ mice colonized with non-responding DonB-SyM compared to DonB-SyM in which the atheroprotection-associated genera are swapped with DonA's. Various iterations on this design could be done to test individual taxa or possibly even genes if the taxa in question

are tractable for genetic manipulation. Semi-complex communities, especially if they elicit disparate phenotypes in the host, are powerful tools to help elucidate microbiota-host interactions at a mechanistic level.

5.1 Does *Gpr109a* expression in macrophages modulate atherosclerosis?

Our investigation into the effect of the butyrate receptors Gpr41, Gpr43, and Gpr109a on atherosclerosis (Chapter 4) led to the observation that Gpr109a$^{-/-}$ males and females had reduced atherosclerotic lipid deposition than their wildtype (WT) counterparts (Fig. 4.1). Macrophages play a central role atherosclerosis through lipid uptake and foam-cell formation (Yu et al., 2013). Although we did not find evidence of differences in macrophage infiltration (Fig. 4.S2) in *Gpr109a*$^{-/-}$ mice, Gpr109a is known to affect macrophage function (Zandi-Nejad et al., 2013). Zandi-Nejad et al. found that Gpr109a activation with niacin reduced expression of proinflammatory cytokines *in vitro* (Zandi-Nejad et al., 2013). In contrast, niacin-induced Gpr109a activation is proinflammatory in skin cells and mediates the so-called "niacin flush", a rash often occuring with niacin treatment. Whether Gpr109a activation by butyrate in macrophages is pro- or anti-inflammatory remains an open question.

To test this, one could implement a series of experiments. First, transcriptomics of frozen descending aorta between *Gpr109a*$^{-/-}$ mice and their WT littermates could be analyzed to examine evidence of differences in immune status or macrophage function. These samples are currently stored in an ultra-low temperature freezer. Second, bone-marrow derived macrophages could be collected from hypercholesterolemic *Gpr109a*$^{-/-}$ mice and WT mice to examine butyrate's effect on cytokine production. A previous study suggests that butyrate induced anti-inflammatory spleen-derived macrophages in a *Gpr109a*$^{-/-}$-dependent manner (Singh et al., 2014), but whether

hypercholesterolemia modifies this effect is not known. Finally, our study in Chapter 4 was limited using whole-body knockout mice, therefore bone marrow transplantation from WT or *Gpr109a*$^{-/-}$ mice into *Apoe*$^{-/-}$ recipients would help to isolate the effect of bone-marrow derived cells (i.e. macrophages) in atherosclerosis.

5.3 Do deoxycholic acid and lithocholic acid affect plasma cholesterol levels?

The study described in Chapter 4 showed that male *Gpr41*$^{-/-}$ mice had reduced plasma LDL cholesterol than their WT littermates through downregulation of intestinal cholesterol transporter *Npc1l1* (Figs. 4.1, 4.2, 4.6). We also found that this coincided with reduced levels of the secondary bile acids lithocholic acid (LCA) and deoxycholic acid (DCA) in the cecum and DCA in the plasma. In agreement with this finding, we also observed distinct microbiomes between male WT and *Gpr41*$^{-/-}$ mice (Fig. 4.4) as well as a reduction in genes belonging to the microbial LCA/DCA synthesis pathway (*bai* operon) in the cecal metagenomes of *Gpr41*$^{-/-}$ mice (Fig. 4.5). This suggests that Gpr41 regulates membership and function of the microbiome, but we were unable to determine whether this was the causal factor mediating Gpr41's effect on plasma LDL cholesterol. We attempted to test the microbiome directly by transplanting cecal microbiota from *Gpr41*$^{-/-}$ mice or their WT littermates into hypercholesterolemic GF mice but found that the recipient microbiomes were indistinguishable after 4 weeks, suggesting that *Gpr41* deficiency is required to maintain the differences in microbiota membership. *Gpr41*-defficient mice exhibited signs of distorted signaling by factor farnesoid X receptor (FXR), a transcription factor that is activated by LCA and DCA and is a critical regulator of whole-body lipid metabolism. I hypothesize that the modified bile acid pools present in *Gpr41*$^{-/-}$ mice, specifically with respect to LCA and DCA, elicit altered lipid uptake. Therefore, an alternative strategy could be to test the role of DCA and LCA as

mediators in modulating plasma LDL cholesterol and intestinal *Npc1l1* expression in gnotobiotic mice colonized with bacteria with and without the capacity to produce DCA and LCA.

The *bai* operon is necessary for LCA and DCA production and only known to be present in a handful of organisms belonging to the Clostridioides, Lachnoclostridium and Eggerthella, bacterial families, including *Clostridium scindens* of Lachnospiraceae. For the proposed study, one could colonize mice with a core microbiota that lack the capacity to make LCA and DCA, with or without *C. scindens*. These mice would then be infected with proprotein convertase subtilisin/kexin type 9 carrying adeno-associated virus (PCSK9-AAV) and fed a high-cholesterol diet to induce hypercholesterolemia. Eight weeks later, plasma lipids and ileal *Npc1l1* expression could be measured along with FXR target genes. This experiment would help elucidate the connection between endogenously-produced DCA and LCA with cholesterol metabolism and possibly provide an explanations for the phenotypes that we observed in *Gpr41*$^{-/-}$ mice.

5.4 Does Gpr41 signaling directly control *Npc1l1* expression in the intestine?

One of the major questions we were left with after the experiments described in Chapter 4 was whether Grp41 regulates *Npc1l1* expression in the ileum directly through cellular signaling, or if it is indirectly regulated through modulation of the gut microbiome and it's metabolites, i.e. bile acids and SCFAs. The previous experimental proposal is meant to help answer the question of indirect regulation, but it is also important to test (to either confirm or rule out) direct regulation. To date, I am not aware of any studies that have investigated Gpr41's role in regulating expression of *Npc1l1*. I hypothesize that Gpr41 directly regulates *Npc1l1* expression and cholesterol absorption through cellular signaling, independent of gut microbiota. To test this, one could extract small-intestinal crypts from *Gpr41*$^{-/-}$ and WT mice to cultivate organoids and assay for cholesterol

uptake using labeled cholesterol as described by Kim and collogues (Kim et al., 2019). By toggling Gpr41 activation with and without SCFAs (a mixture of Gpr41's primary ligands butyrate and propionate) in the growth medium, one could answer whether cholesterol uptake and *Npc1l1* expression is regulated by Gpr41 in an activation-dependent manner. In concert with the previous experimental proposal, one could use these organoids to also test the effect to LCA and DCA on cholesterol uptake and *Npc1l1* expression using a similar design.

5.5 Does *Alistipes* induce adiposity and insulin resistance?

The study described in Appendix A shows that 15 groups of gnotobiotic mice, each colonized with different human fecal microbiota, exhibited a wide range of metabolic phenotypes including food intake, adiposity, and responses to oral glucose tolerance tests (oGTT) and insulin tolerance testes (ITT) (Fig. A.1). Correlations between these phenotypes and 16S rRNA gene amplicon profiles of recipient mice showed that the genus *Alistipes* was positively associated with adiposity and areas under the curve for oGTT and ITT (Fig. A.2). The literature is mixed as to whether *Alistipes* is protective or harmful (Parker et al., 2020) but our data supports the hypothesis that *Alistipes* promotes insulin resistance (IR) and adiposity. I propose two experiments to address this hypothesis: First, one could conduct metagenomic analysis of the cecal content of the humanized mice to validate the association with *Alistipes* and to gain a higher resolution of the taxonomy (species- and strain-level), and conduct transcriptomics on the intestinal and liver tissues to establish potential mechanisms of action. Second, to test if *Alistipes* is causal in promoting IR and adiposity, one could colonize GF mice with a community of core microbiota plus or minus *Alistipes* (preferably a strain isolated from the human subjects in question) and feed a Western style diet to promote glucose dysregulation. ITT and oGTT could be performed to test glycemic

control and NMR could be used to measure whole-body adiposity. If our hypothesis is correct, these experiments would establish a causal link between *Alistipes* and IR and could be used as a model to elucidate mechanisms of microbe-host interactions and glycose homeostasis.

CONCLUSION

In conclusion, the studies described in the previous chapters have shed light on the role of interpersonal variation within the microbiome on cardiometabolic diseases and brought forth new findings on the role of Gpr41 on lipid metabolism. The future studies proposed here would continue along these lines of research and answer new and exciting questions. The field has struggled for decades to define what a "healthy" microbiome looks like, perhaps because a healthy microbiome, as defined by the organisms that comprise it, does not exist. Instead, perhaps a more achievable goal is to define a healthy *functioning* microbiome—Does it attenuate inflammation? Does it help build a strong gut barrier? Does it produce useful metabolites and vitamins? Focusing on the interactions that determine these questions at a personalized and molecular level is curtail for the development of microbiome-targeted therapeutics. I hope that the studies described here have, in their own way, contributed to this aim.

REFERENCES

Aguilar, E. C., Leonel, A. J., Teixeira, L. G., Silva, A. R., Silva, J. F., Pelaez, J. M. N., Capettini, L. S. A., Lemos, V. S., Santos, R. A. S., & Alvarez-Leite, J. I. (2014). Butyrate impairs atherogenesis by reducing plaque inflammation and vulnerability and decreasing NFκB activation. *Nutrition, Metabolism and Cardiovascular Diseases*, *24*(6), 606–613. https://doi.org/10.1016/j.numecd.2014.01.002

Hutchison, E. R., Kasahara, K., Zhang, Q., Vivas, E. I., Cross, T.-W. L., & Rey, F. E. (2023). Dissecting the impact of dietary fiber type on atherosclerosis in mice colonized with different gut microbial communities. *Npj Biofilms and Microbiomes*, *9*(1), Article 1. https://doi.org/10.1038/s41522-023-00402-7

Kasahara, K., Krautkramer, K. A., Org, E., Romano, K. A., Kerby, R. L., Vivas, E. I., Mehrabian, M., Denu, J. M., Bäckhed, F., Lusis, A. J., & Rey, F. E. (2018). Interactions between Roseburia intestinalis and diet modulate atherogenesis in a murine model. *Nature Microbiology*, *3*(12), 1461. https://doi.org/10.1038/s41564-018-0272-x

Kim, Y.-C., Byun, S., Seok, S., Guo, G., Xu, H. E., Kemper, B., & Kemper, J. K. (2019). Small Heterodimer Partner and Fibroblast Growth Factor 19 Inhibit Expression of NPC1L1 in Mouse Intestine and Cholesterol Absorption. *Gastroenterology*, *156*(4), 1052–1065. https://doi.org/10.1053/j.gastro.2018.11.061

Parker, B. J., Wearsch, P. A., Veloo, A. C. M., & Rodriguez-Palacios, A. (2020). The Genus Alistipes: Gut Bacteria With Emerging Implications to Inflammation, Cancer, and Mental Health. *Frontiers in Immunology*, *11*. https://www.frontiersin.org/articles/10.3389/fimmu.2020.00906

Singh, N., Gurav, A., Sivaprakasam, S., Brady, E., Padia, R., Shi, H., Thangaraju, M., Prasad, P. D., Manicassamy, S., Munn, D. H., Lee, J. R., Offermanns, S., & Ganapathy, V. (2014).

Activation of Gpr109a, Receptor for Niacin and the Commensal Metabolite Butyrate, Suppresses Colonic Inflammation and Carcinogenesis. *Immunity*, *40*(1), 128–139. https://doi.org/10.1016/j.immuni.2013.12.007

Yu, X.-H., Fu, Y.-C., Zhang, D.-W., Yin, K., & Tang, C.-K. (2013). Foam cells in atherosclerosis. *Clinica Chimica Acta*, *424*, 245–252. https://doi.org/10.1016/j.cca.2013.06.006

Zandi-Nejad, K., Takakura, A., Jurewicz, M., Chandraker, A. K., Offermanns, S., Mount, D., & Abdi, R. (2013). The role of HCA2 (GPR109A) in regulating macrophage function. *The FASEB Journal*, *27*(11), 4366–4374. https://doi.org/10.1096/fj.12-223933

Zeevi, D., Korem, T., Godneva, A., Bar, N., Kurilshikov, A., Lotan-Pompan, M., Weinberger, A., Fu, J., Wijmenga, C., Zhernakova, A., & Segal, E. (2019). Structural variation in the gut microbiome associates with host health. *Nature*, *568*(7750), 43. https://doi.org/10.1038/s41586-019-1065-y

APPENDIX A: *Alistipes* is associated with glycemic dysregulation in a large cohort of humanized gnotobiotic mice

Evan R. Hutchison[+], *Kazuyuki Kasahara, Jean Debédat, Mariko S. Yokoyama, Karine Clément, Federico E. Rey*[*]

[+]Lead author

*Corresponding author

AUTHOR CONTRIBUTIONS

JD, KC, KK and FER conceived of the study. KK and ERH conducted the mouse experiments. ERH, KK, and MSY processed the samples and generated datasets. ERH analyzed the data. ERH and FER wrote the manuscript.

ABSTRACT

Insulin resistance (IR) is highly prevalent in the United States and is growing globally. IR contributes to metabolic diseases such as type 2 diabetes and cardiovascular disease. Recent research implicates the gut microbiome in the development and progression of IR but the exact dynamics underpinning this relationship are not fully understood. In this study, we used humanized gnotobiotic mouse models to investigate the role of the microbiome in metabolic health. We colonized the mice with fecal samples from 15 human donors who had previously undergone Roux-en-Y gastric bypass surgery. We characterized the glycemic control of recipient mice by conducting oral glucose tolerance tests (oGTT) and insulin tolerance tests (ITT) and measured metabolic phenotypes such as food consumption and adiposity. We found that donor microbiota had a strong influence over responses to oGTT and ITT and regulated adiposity and food consumption. We also found that *Alistipes*, *Ruminococcus*, and *Erysipelatoclostridium* were associated with exacerbated metabolic dysfunction across all individual mice. Our large cohort of donor groups enabled us to determine that only the *Alistipes* associations were robust to analysis at the donor-level. Together, this study offers a unique insight into the utility of humanized gnotobiotic mouse models using many donors to detect disease-microbiota interactions that may better reflect the biological dynamics of the human donors.

INTRODUCTION

Insulin resistance (IR) is a growing global health concern, with an estimated prevalence 44% young adults in the United States (Parcha et al., 2022). IR is a key contributor to the development of metabolic and diseases such as type 2 diabetes and cardiovascular disease (Bornfeldt & Tabas, 2011). Emerging research has implicated the gut microbiome, the diverse community of microorganisms residing in our intestines, in the development and progression of IR (Lee et al., 2020). The complex dynamics between the host and its microbiome play a crucial role in regulating IR at a mechanistic level. For example, the microbial metabolite butyrate, produced from fermentation of dietary fiber, is protective against IR progression by improving insulin signaling (Gao et al., 2009). On the other hand, imidazole propionate, a byproduct of microbial metabolism of histidine, impairs insulin signaling and exacerbates IR (Koh et al., 2018). Understanding these interactions is vital for the development of novel microbiome-targeting therapeutics aimed at improving insulin sensitivity.

Humanized gnotobiotic mouse models, which consist of germ-free (GF) mice colonized with fecal microbiota from humans, have proven to be a valuable tool for investigating the role of the microbiome in metabolic health (Faith et al., 2010) These models allow for controlled studies of host-microbe interactions, providing insights into the complex dynamics that govern the gut microbiome and IR. Here, we used fecal samples from 15 human donors who had previously undergone Roux-en-Y gastric bypass surgery to colonize groups of GF mice. We characterized the glycemic control of recipient mice by conduction oral glucose tolerance tests (oGTT) and insulin tolerance tests (ITT) and measured metabolic phenotypes such as food consumption and adiposity. We found that glycemic control and fat accumulation varied widely between mice colonized with different microbiota. We observed both positive and negative associations between multiple

genera and measures of IR at the level of individual mice. However, when we aggregated by donor group, only *Alistipes* retained it's strong correlation. Together, this study demonstrates utility of gnotobiotic mouse models combined with many human donors to detect robust microbe-disease interactions.

RESULTS

We transplanted human microbiota from 15 different human volunteers (Donor1-15) who had previously undergone Roux-en-Y Gastric Bypass (RYGB) surgery into groups of 4 week-old GF C57BL/6 mice (Fig. A.1a). These mice were maintained on a Western style diet *ad libitum*. Ten weeks after colonization, mice were subjected to an oral glucose tolerance test (oGTT). Blood glucose curves and oGTT area under the curve (AUC) varied across the different donor groups (Fig A.1b-c). oGTT AUCs ranged from the lowest at 24,658 (Donor13) to the highest at 44,850 (Donor10) (Fig. A.1c). Similarly, ITT glucose curves and AUCs ranged between donor groups with the lowest AUC at 7,627 (Donor4) and the highest at 17,756 (Donor7) (Fig. A.1d-e). Fasting blood levels, collected 30 minutes prior to the start of the oGTT, also differed by donor group, with Donor13-colonized mice having an average of 149 mg/dL and Donor8-colonized mice having 245 mg/dL (Fig. A.1g). Fat mass, as measured by nuclear magnetic resonance (NMR) of mouse body composition was collected at sacrifice, ranged from 4.2 g (Donor13), to 13.0 g (Donor14) (Fig. A.1f). Interestingly, Donor13-colonized were consistently least harmed in each metabolic phenotype, suggesting that these mice were protected by the donor microbiota.

We next examined the microbial community structures of the recipient mice by analyzing their cecal 16S rRNA amplicon profiles. We found that engraftment was relatively consistent between mice within each donor group, as most members of each group clustered together after

principal coordinate analysis (PCoA) by unweighted UniFrac distances Fig. A.2a). We also observed that among the 120 genus-level features detected at above a within-group average 0.1% relative abundance cutoff, 17 were detected in all donor groups: *Lachnoclostridium*, *Blautia*, *Bacteroides*, *Butyricimonas*, *Alistipes*, *Incertae* (*Sedis*), UBA1819, *Oscillibacter*, *Flavonifactor*, *Colidextribacter*, *Butyricicoccus*, *Bilophila*, *Sutterella*, *Enterococcus*, *Lactococcus*, [*Clostridium*] *innocuum* group, and *Hungatella* (Fig. A.2b). Among these "Core taxa", *Bacteroidies spp*. was consistently the highest relative abundance genus across all donor groups (Fig. A.2b).

Next, we ran Spearman correlations between above-threshold genus-level taxa and the metabolic phenotypes using all mice regardless of donor group (Fig. A.2c). We included the following phenotypes: daily food consumption, NMR fat mass, NMR lean mass, food conversion to fat (ratio of fat mass to daily consumption), oGTT AUC, and ITT AUC. We found that a number of genera had significant correlations ($P < 0.05$) with one or more phenotypes. *Alitipes* and *Ruminococcus torquez* group was strongly positively associated with multiple detrimental phenotypes including NMR fat mass, food conversion to fat, oGTT AUC, and ITT AUC while *Erysipelatoclostridium* had the opposite associations (Fig. A.2c). We next tested whether these associations remained after aggregating by donor group. To do this we averaged the taxanomic relative abundances and phenotype data within each donor group and reran Spearman correlations. We found that the significant associations remained between *Alistipes* versus oGTT, fat mass, and food conversion to fat, as well as a trending positive association with ITT at the donor-level (Fig. A.2d). However, the associations with *Ruminococcus torquez* group and *Erysipelatoclostridium* were no longer significant at the donor-level (Fig. A.3). These results suggest that *Alistipes* exacerbates the effects of Western-diet feeding on glycemic dysfunction any may reflect biological dynamics present in the human donors.

DISCUSSION

In the present study, we colonized GF mice with fecal microbiota from 15 different human donors and assessed glucose homeostasis and metabolic phenotypes of the recipient mice. We found that the recipients of each donor group exhibited disparate levels glycemic control, and metabolic phenotypes including fat mass and food consumption. This is consistent with previous findings that transplantation of human microbiota into GF mice can modulate host physiology (Hutchison et al., 2023; Murga-Garrido et al., 2021; Turnbaugh et al., 2009). Humanized gnotobiotic mouse studies often lack the power to make generalizable interpretations about host-microbiota associations because they only include a small number of human donors. If we are concerned with the connections between phenotypes and microbiota in *humans*, then it is logical to consider the number of mice within each humanized recipient group as technical replicates and the number of human donors as biological replicates. Therefore, the more human donor groups that are included, the greater the statistical power to detect associations. The number of mice (i.e. technical replication) is still very important as it reduced the error and increases confidence in the statics. However, increasing the number of mice may lead to spurious associations if the associations are conducted at the level of the individual mice. By testing whether any associations remain at the group level can minimize the risk of interpreting false-positive results.

Here, we correlated the cecal 16S rRNA profiles if individual mouse with mouse phenotype data and detected several genera that were significantly associated with multiple metabolic phenotypes. Namely, *Alistipes* and *Ruminoccocus torques* group were positively associated with IR exacerbation, while *Erysipelatoclostridium* had the opposite association However, when we aggregated the microbial and phenotypic data by donor group and reran the correlation analysis,

only *Alistipes* remained strongly correlated. We conclude that this association is robust and may represent a generalizable effect of *Alistpes* in mice on a Western diet. Further study is needed to prove this and show causation. Interestingly, *Alistipes* was found to predict T2D remission in gastric bypass patients in a previous study (Davies et al., 2020). This discrepancy in *Alitipes's* harmful versus beneficial effect may be due to differences at the species or strain level. Metagenomic profiling of our mice is needed to elucidate associations at the lower taxonomic and functional levels.

Importantly, as in all humanized gnotobiotic mouse studies, the recipient mouse is never a perfect representation of the human donor (Park & Im, 2020). Not only is the physiology between humans and mice different, so are the microbes that colonize them. Nonetheless, humanized gnotobiotic animal models are a powerful toll that can uncover novel mechanisms of host-microbe interactions.

Together, this study offers unique insight into the utility of humanized gnotobiotic mouse models at detecting host microbiota interactions. Our use of a large number of human donors has shed some light on the variability of glycemic control phenotypes among humanized gnotobiotic mice and identified potentially causal taxa that mediate this variation.

METHODS

Germ-free animals

All animals used in this study were handled in accordance with the University of Wisconsin-Madison's animal welfare policies and all experiments were conduction under an Animal Care and Use Committee-approved protocol. GF C57BL/6 mice were housed in sterile isolators and maintained on autoclaved chow (LabDiet 5021; LabDiet, St. Louis, MO) and sterile water *ad*

libitum. GF cages contained Alpha-dri® (Shepherd Specialty Papers, Kalamazoo, MI) bedding along with paper huts (Bio-Huts, Bio-Serv, Flemington, NJ) and ALPHA-twist™ (Shepherd Specialty Papers) for enrichment. Monthly tests were conducted in each isolator to confirm GF status of the mice. These included a growth test of feces in rich media for 7 days at 37 °C and checking for amplification of the 16S rRNA gene using universal primers.

Human donor samples

Fecal samples were collected from human participants of a previous study (Debédat et al., 2022) examining the effect of gut microbes on glycemic control in patients that had previously undergone Roux-en-Y Gastric Bypass (RYGB) surgery. All subjects provided written informed consent as participants of multiple studies registered on https:// clinicaltrials.gov (P050318 Les Comités de Protéction des Personnes (CPP) approval: 24 November 2006, NCT01655017, NCT01454232).

Colonization of GF mice with human fecal microbiota

Groups of male GF C57BL/6J mice (n = 9-10) were moved from isolators to an Allentown Sentry SPP IVC rack system (Allentown Inc., Allentown, NJ) at 4 weeks of age and place on an irradiated HFD (Supp. Table 2, TD.08811; Envigo, Madison, WI). Human fecal samples were prepared in a slurry as described in Debédat et al. Each mouse was gavaged with 100 µL of fecal slurry. Mice were gavaged for a second time one week later. All mice within a single donor group were housed together and maintained on the HFD until sacrifice.

Euthanasia

All mice were fasted for 4 hours prior to euthanasia. Prior to sacrifice, body weight and fat vs lean mass were measured via nuclear magnetic resonance (NMR) machine fitted for mice (LF90 Body Composition Analyzer, Bruker Corporation, Billerica, MA). Upon sacrifice, mice were anesthetized using isoflurane and blood was collected via heart puncture. Mice were then immediately euthanized via cervical dislocation and various tissues including epididymal fat pads, the small intestine, cecal content, colon, liver were dissected and flash-frozen using liquid nitrogen.

OGTT

Four weeks after treatment initiation mice were placed in fresh cages fasted for 4 hours. Baseline blood glucose measurements were taken at 30 minutes before (-30 min) and just prior to starting the oGTT. (0 min baseline) using a Accu-Chek Performa glucometer (Roche, Indianapolis, IN) a drop of blood from a tail snip. After the 0 min baseline measurement mice were immediately dosed with 2 g of glucose per Kg of body weight. Subsequent blood glucose measurements were taken 15, 30, 60 and 90 minutes after the baseline measurement. Plasma samples were collected at baseline as well as the 30-minute and 60-minute time points for insulin measurements.

ITT

One week after the OGTT mice were place in new cages and fasted for 4 hours. A baseline blood glucose measurement (0 min) was taken as described above and freshly prepared insulin (Gibco, ThermoFisher Scientific, Waltham, MA) was immediately dosed at 0.75 IU per Kg of body weight via IP injection. Subsequent blood glucose measurements were taken 15, 30, 60 and 90 minutes after the baseline measurement.

16S rRNA gene sequencing

DNA and microbiome characterization from human fecal slurries, mouse cecal content, and mouse feces was extracted using a phenol:chloroform plus bead-beating protocol followed by 16S rRNA gene amplicon sequencing as previously described (Hutchison et al., 2023). Briefly, fecal/cecal mixed by bead-beating twice for 3 minutes in the presence of phenol:cholraphorm:isoamyl. alcohol (UltraPure™ [25:24:1, v/v], ThermoFisher Scientific) and SDS. The aqueous phase was collected and DNA was precipitated by the addition of 1 M sodium acetate and 100% isopropanol. The DNA was then cleaned with the Neucleospin cleanup kit (Macherey-Nagel, Düren, Nordrhein-Westfalen, Germany) and the purified DNA was subjected to 16S rRNA gene amplicon sequencing. 16S rRNA V3-V4 amplicon sequencing was conducted at the University of Minnesota Genomics Center (Minneapolis, MN). DADA2 (Callahan et al., 2016) quality control and clean-up was conducted on demultilexed reads with Qiime2 (Bolyen et al., 2019) (version 2022.2). Taxonomy was classified using the SILVA database (Quast et al., 2013) (version 132).

Microbiome analysis

The phyloseq (version 1.40.0) package in R was used to generate UniFrac distance matrices. The pairwiseAdonis (version 0.4) R package with 9999 permutations was used to conduct PERMANOVA tests to compare ASV profiles between treatment groups within each donor group. Any genus-level features were that have group-level averages less that 0.1% were removed from further analysis.

Statistics

Spearman correlation analysis was conducted using the cor.test function as part of the stats package (version 4.2.0) in R. Only taxa that were detected (relative abundance > 0) in at least 50% of all mice were included in the analysis. All box and whisker plots represent the interquartile range (IR), median, and 1.5 times the IR overlayed with individual data points from each mouse. Line plots depict the mean of each group at each timepoint with error bars representing the standard error.

DATA AVAILABILITY

The data from this study is available upon request.

REFERENCES

Bolyen, E., Rideout, J. R., Dillon, M. R., Bokulich, N. A., Abnet, C. C., Al-Ghalith, G. A., Alexander, H., Alm, E. J., Arumugam, M., Asnicar, F., Bai, Y., Bisanz, J. E., Bittinger, K., Brejnrod, A., Brislawn, C. J., Brown, C. T., Callahan, B. J., Caraballo-Rodríguez, A. M., Chase, J., … Caporaso, J. G. (2019). Reproducible, interactive, scalable and extensible microbiome data science using QIIME 2. *Nature Biotechnology*, *37*(8), Article 8. https://doi.org/10.1038/s41587-019-0209-9

Bornfeldt, K. E., & Tabas, I. (2011). Insulin Resistance, Hyperglycemia, and Atherosclerosis. *Cell Metabolism*, *14*(5), 575–585. https://doi.org/10.1016/j.cmet.2011.07.015

Callahan, B. J., McMurdie, P. J., Rosen, M. J., Han, A. W., Johnson, A. J. A., & Holmes, S. P. (2016). DADA2: High resolution sample inference from Illumina amplicon data. *Nature Methods*, *13*(7), 581–583. https://doi.org/10.1038/nmeth.3869

Davies, N., O'Sullivan, J. M., Plank, L. D., & Murphy, R. (2020). Gut Microbial Predictors of Type 2 Diabetes Remission Following Bariatric Surgery. *Obesity Surgery*, *30*(9), 3536–3548. https://doi.org/10.1007/s11695-020-04684-0

Debédat, J., Le Roy, T., Voland, L., Belda, E., Alili, R., Adriouch, S., Bel Lassen, P., Kasahara, K., Hutchison, E., Genser, L., Torres, L., Gamblin, C., Rouault, C., Zucker, J.-D., Kapel, N., Poitou, C., Marcelin, G., Rey, F. E., Aron-Wisnewsky, J., & Clément, K. (2022). The human gut microbiota contributes to type-2 diabetes non-resolution 5-years after Roux-en-Y gastric bypass. *Gut Microbes*, *14*(1), 2050635. https://doi.org/10.1080/19490976.2022.2050635

Faith, J. J., Rey, F. E., O'Donnell, D., Karlsson, M., McNulty, N. P., Kallstrom, G., Goodman, A. L., & Gordon, J. I. (2010). Creating and characterizing communities of human gut microbes

in gnotobiotic mice. *The ISME Journal*, *4*, 1094–1098. https://doi.org/10.1038/ismej.2010.110

Gao, Z., Yin, J., Zhang, J., Ward, R. E., Martin, R. J., Lefevre, M., Cefalu, W. T., & Ye, J. (2009). Butyrate Improves Insulin Sensitivity and Increases Energy Expenditure in Mice. *Diabetes*, *58*(7), 1509–1517. https://doi.org/10.2337/db08-1637

Hutchison, E. R., Kasahara, K., Zhang, Q., Vivas, E. I., Cross, T.-W. L., & Rey, F. E. (2023). Dissecting the impact of dietary fiber type on atherosclerosis in mice colonized with different gut microbial communities. *Npj Biofilms and Microbiomes*, *9*(1), Article 1. https://doi.org/10.1038/s41522-023-00402-7

Koh, A., Molinaro, A., Ståhlman, M., Khan, M. T., Schmidt, C., Mannerås-Holm, L., Wu, H., Carreras, A., Jeong, H., Olofsson, L. E., Bergh, P.-O., Gerdes, V., Hartstra, A., De Brauw, M., Perkins, R., Nieuwdorp, M., Bergström, G., & Bäckhed, F. (2018). Microbially Produced Imidazole Propionate Impairs Insulin Signaling through mTORC1. *Cell*, *175*(4), 947-961.e17. https://doi.org/10.1016/j.cell.2018.09.055

Lee, C. J., Sears, C. L., & Maruthur, N. (2020). Gut microbiome and its role in obesity and insulin resistance. *Annals of the New York Academy of Sciences*, *1461*(1), 37–52. https://doi.org/10.1111/nyas.14107

Murga-Garrido, S. M., Hong, Q., Cross, T.-W. L., Hutchison, E. R., Han, J., Thomas, S. P., Vivas, E. I., Denu, J., Ceschin, D. G., Tang, Z.-Z., & Rey, F. E. (2021). Gut microbiome variation modulates the effects of dietary fiber on host metabolism. *Microbiome*, *9*(1), 117. https://doi.org/10.1186/s40168-021-01061-6

Parcha, V., Heindl, B., Kalra, R., Li, P., Gower, B., Arora, G., & Arora, P. (2022). Insulin Resistance and Cardiometabolic Risk Profile Among Nondiabetic American Young

Adults: Insights From NHANES. *The Journal of Clinical Endocrinology & Metabolism*, *107*(1), e25–e37. https://doi.org/10.1210/clinem/dgab645

Park, J. C., & Im, S.-H. (2020). Of men in mice: The development and application of a humanized gnotobiotic mouse model for microbiome therapeutics. *Experimental & Molecular Medicine*, *52*(9), Article 9. https://doi.org/10.1038/s12276-020-0473-2

Quast, C., Pruesse, E., Yilmaz, P., Gerken, J., Schweer, T., Yarza, P., Peplies, J., & Glöckner, F. O. (2013). The SILVA ribosomal RNA gene database project: Improved data processing and web-based tools. *Nucleic Acids Research*, *41*(D1), D590–D596. https://doi.org/10.1093/nar/gks1219

Turnbaugh, P. J., Ridaura, V. K., Faith, J. J., Rey, F. E., Knight, R., & Gordon, J. I. (2009). The Effect of Diet on the Human Gut Microbiome: A Metagenomic Analysis in Humanized Gnotobiotic Mice. *Science Translational Medicine*, *1*(6), 6ra14-6ra14. https://doi.org/10.1126/scitranslmed.3000322

FIGURES

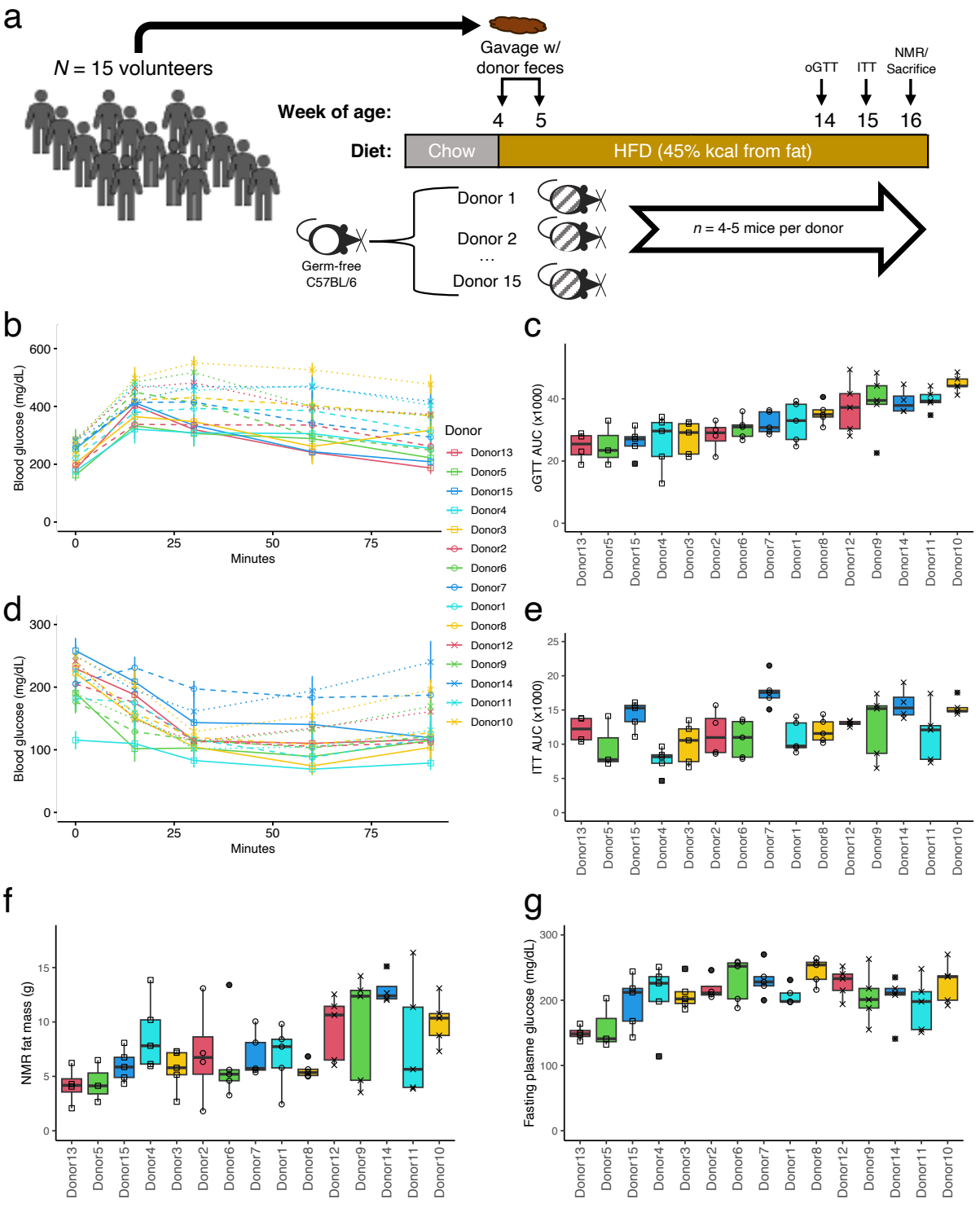

Figure A.1. Groups of humanized gnotobiotic mice exhibit disparate metabolic phenotypes. Germ-free mice were colonized with fecal microbiota from one of 15 different human donors (**a**) and fed a Western style diet. Blood glucose curves and areas under the curve for oGTT (**b, c**) and

ITT (**d**, **e**) by donor group. Fat mass as measured by nuclear magnetic resonance (**f**) and fasting blood glucose (**g**) measured 30 minutes prior to the oGTT. Sample size = 4-5 mice per group.

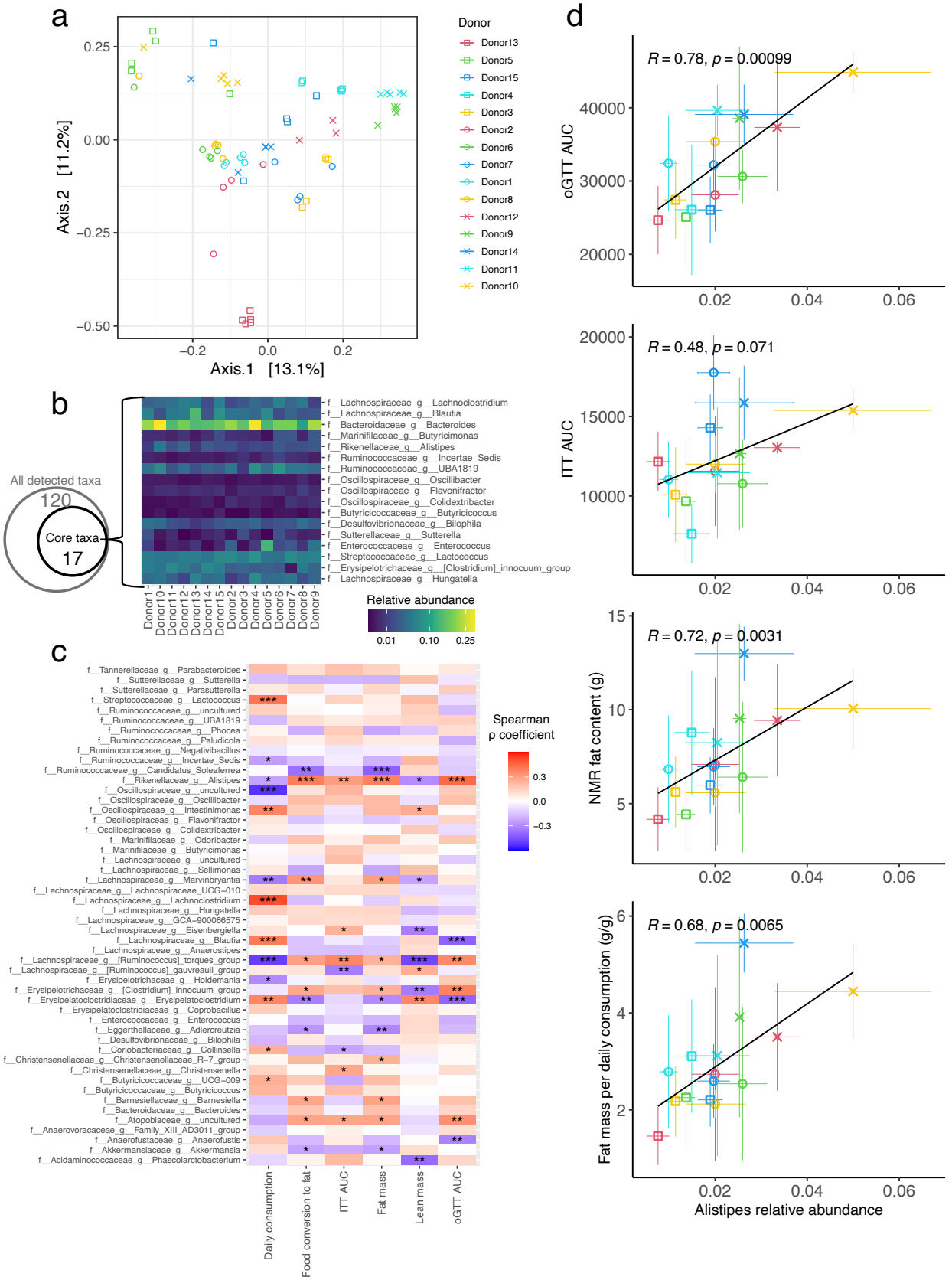
a
Axis.2 [11.2%]
Axis.1 [13.1%]
Donor
Donor13
Donor5
Donor15
Donor4
Donor3
Donor2
Donor6
Donor7
Donor1
Donor8
Donor12
Donor9
Donor14
Donor11
Donor10
b
All detected taxa
120
Core taxa
17
f__Lachnospiraceae_g__Lachnoclostridium
f__Lachnospiraceae_g__Blautia
f__Bacteroidaceae_g__Bacteroides
f__Marinifilaceae_g__Butyricimonas
f__Rikenellaceae_g__Alistipes
f__Ruminococcaceae_g__Incertae_Sedis
f__Ruminococcaceae_g__UBA1819
f__Oscillospiraceae_g__Oscillibacter
f__Oscillospiraceae_g__Flavonifractor
f__Oscillospiraceae_g__Colidextribacter
f__Butyricicoccaceae_g__Butyricicoccus
f__Desulfovibrionaceae_g__Bilophila
f__Sutterellaceae_g__Sutterella
f__Enterococcaceae_g__Enterococcus
f__Streptococcaceae_g__Lactococcus
f__Erysipelotrichaceae_g__[Clostridium]_innocuum_group
f__Lachnospiraceae_g__Hungatella
Donor1 Donor10 Donor11 Donor12 Donor13 Donor14 Donor15 Donor2 Donor3 Donor4 Donor5 Donor6 Donor7 Donor8 Donor9
Relative abundance
0.01 0.10 0.25
c
Spearman ρ coefficient
0.3
0.0
−0.3
Daily consumption
Food conversion to fat
ITT AUC
Fat mass
Lean mass
oGTT AUC
d
R = 0.78, p = 0.00099
oGTT AUC
R = 0.48, p = 0.071
ITT AUC
R = 0.72, p = 0.0031
NMR fat content (g)
R = 0.68, p = 0.0065
Fat mass per daily consumption (g/g)
Alistipes relative abundance

Figure A.2. Cecal bacterial taxa are associated with IR in humanized gnotobiotic mice. PCoA plot (**a**) of cecal 16S rRNA profiles of using unweighted UniFrac distances. **b** *Left* - Venn-diagram comparing the number of genus-level features detected in at least one donor group ("All taxa") versus those that were detected in all donor groups ("Core taxa"). The threshold for detection was set at a within-group average of 0.1% relative abundance. *Right* – heatmap of average relative abundances of all Core taxa by donor group. **c** Spearman correlations between metabolic phenotypes and genus-level cecal 16S rRNA features. Sample size = 4-5/group. Levels of significance are indicated by $*P < 0.05$, $**P < 0.01$, $***P < 0.001$. **d** Scatterplots of cecal relative abundance of *Alistipes* versus metabolic phenotypes by group with Spearman ϱ coefficients (R) and correlation P-values. Calculations were run using mean-aggregates of all mice within each donor group (points). Error bars show the SEM of individual mice within each donor group. Sample size = 15.

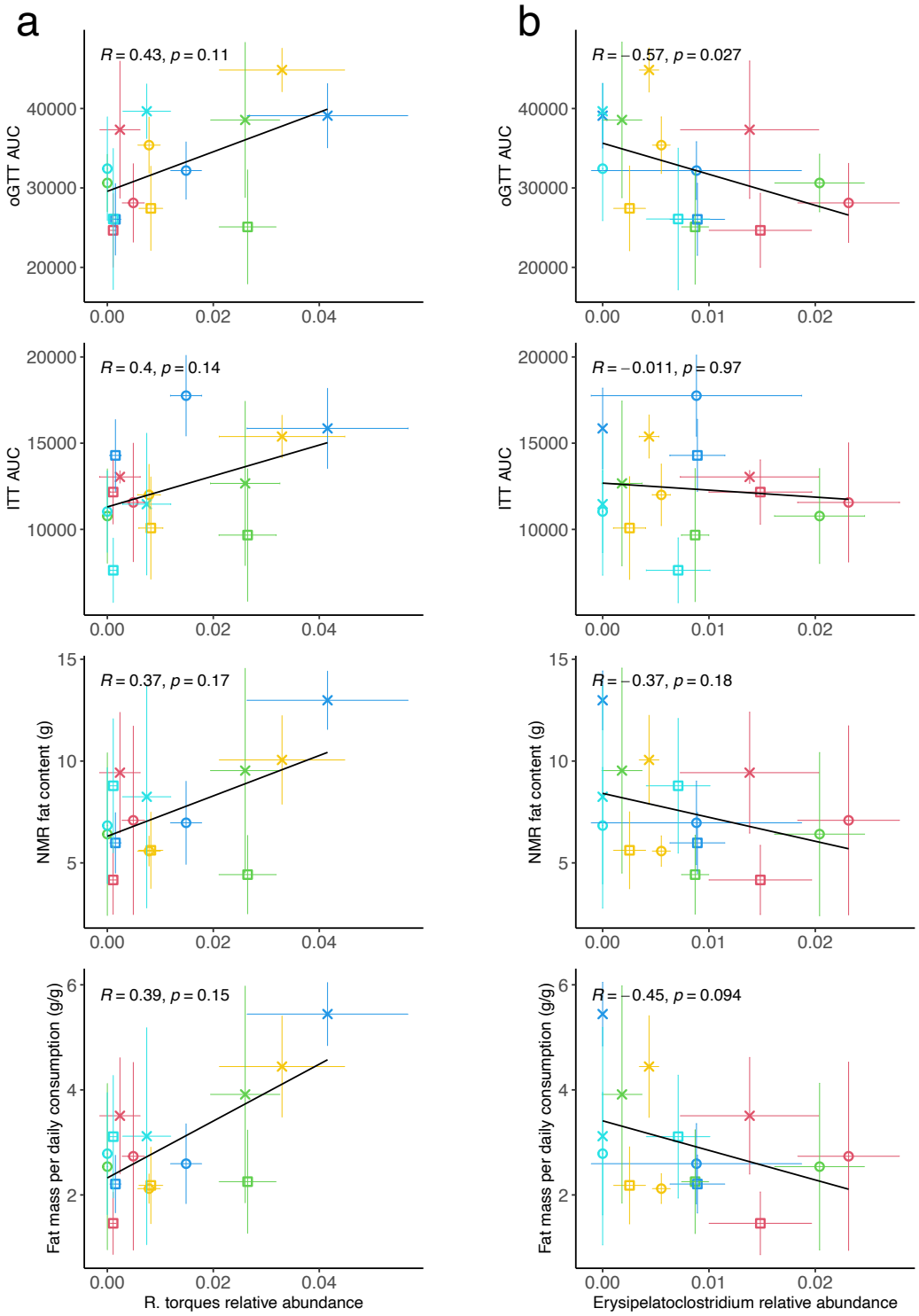

Figure A.3. Correlations of *Rumminococcus torquez* group and *Erysipelatoclostridium* with IR phenotypes are not robust to the donor-level. Scatterplots of cecal relative abundance of

Rumminococcus torquez group (**a**) and *Erysipelatoclostridium* (**b**) versus metabolic phenotypes by group with Spearman ϱ coefficients (*R*) and correlation *P*-values. Calculations were run using mean-aggregates of all mice within each donor group (points). Error bars show the SEM of individual mice within each donor group. Sample size = 15.

APPENDIX B: List of publications produced as a graduate student at the University of Wisconsin-Madison not included in this thesis

Cao, Y., Aquino-Martinez, R., **Hutchison, E.**, Allayee, H., Lusis, A. J., & Rey, F. E. (2022). Role of gut microbe-derived metabolites in cardiometabolic diseases: Systems based approach. *Molecular Metabolism*, *64*, 101557. https://doi.org/10.1016/j.molmet.2022.101557

Debédat, J., Le Roy, T., Voland, L., Belda, E., Alili, R., Adriouch, S., Bel Lassen, P., Kasahara, K., **Hutchison, E**., Genser, L., Torres, L., Gamblin, C., Rouault, C., Zucker, J.-D., Kapel, N., Poitou, C., Marcelin, G., Rey, F. E., Aron-Wisnewsky, J., & Clément, K. (2022). The human gut microbiota contributes to type-2 diabetes non-resolution 5-years after Roux-en-Y gastric bypass. *Gut Microbes*, *14*(1), 2050635. https://doi.org/10.1080/19490976.2022.2050635

Murga-Garrido, S. M., Hong, Q., Cross, T.-W. L., **Hutchison, E. R**., Han, J., Thomas, S. P., Vivas, E. I., Denu, J., Ceschin, D. G., Tang, Z.-Z., & Rey, F. E. (2021). Gut microbiome variation modulates the effects of dietary fiber on host metabolism. *Microbiome*, *9*(1), 117. https://doi.org/10.1186/s40168-021-01061-6Cao, Y., Aquino-Martinez, R., Hutchison, E., Allayee, H., Lusis, A. J., & Rey, F. E. (2022). Role of gut microbe-derived metabolites in cardiometabolic diseases: Systems based approach. Molecular Metabolism, 64, 101557. https://doi.org/10.1016/j.molmet.2022.101557